
Structural and biochemical investigations of the eukaryotic DNA double-strand break repair complex Mre11-Rad50-Nbs1

Florian Ulrich Seifert

Dissertation
der Fakultät für Biologie
der Ludwig-Maximilians-Universität
München

vorgelegt von
Florian Ulrich Seifert
aus Biberach an der Riss

München, den 07. Juli 2015

- | | |
|---------------|------------------------------|
| 1. Gutachter: | Prof. Dr. Heinrich Leonhardt |
| 2. Gutachter: | Prof. Dr. Heinrich Jung |
| Gast: | Prof. Dr. Karl-Peter Hopfner |

Tag der Abgabe: 07.07.2015

Tag der mündlichen Prüfung: 26.10.2015

This work has been prepared from November 2011 to June 2015 in the laboratory of Prof. Dr. Karl-Peter Hopfner at the Gene Center and Department of Biochemistry, LMU München, Germany.

Parts of this work have been published in the following publications:

Seifert FU, Lammens K, Hopfner KP.

“Structure of the catalytic domain of Mre11 from *Chaetomium thermophilum*.”

Acta Cryst. 2015 Jun 1. F71, 752-757 doi:10.1107/S2053230X15007566

Rojowska A, Lammens K, Seifert FU, Drenth J, Feldmann H, Hopfner KP.

“Structure of the Rad50 DNA double-strand break repair protein in complex with DNA.”

EMBO J. 2014 Dec 1;33(23):2847-59. doi: 10.15252/emboj.201488889. Epub 2014 Oct 27.

Schiller CB*, Seifert FU*, Linke-Winnebeck C*, Hopfner KP.

“Structural studies of DNA end detection and resection in homologous recombination.”

Cold Spring Harb Perspect Biol. 2014 Jul 31;6(10):a017962. doi: 10.1101/cshperspect.a017962.

* These authors contributed equally to this work.

Parts of the present thesis will be submitted for publication:

Seifert FU, Lammens K, Stoehr G, Keßler B, Hopfner KP.

“Structural mechanism of ATP-dependent DNA binding by eukaryotic Rad50.”

Manuscript in preparation

Parts of this thesis have been presented at the following conference:

Poster presentation at the conference of the German Society for DNA Repair (DGDR) in Mainz, Germany.

Table of Contents

Summary.....	1
Zusammenfassung.....	2
1. Introduction	3
1.1 DNA damages	3
1.2 DNA double-strand breaks.....	5
1.3 DNA double-strand break repair pathways.....	6
1.3.1 Canonical and alternative non-homologous end joining (NHEJ)	7
1.3.2 Homologous recombination (HR)	7
1.4 Mre11-Rad50-Nbs1 complex.....	9
1.4.1 Biochemical functions of the MRN complex	10
1.4.2 Structural insights into the Mre11-Rad50-Nbs1 complex	13
1.4.2.1 The Mre11 subunit.....	13
1.4.2.2 The Rad50 subunit	15
1.4.2.3 The Nbs1 subunit	17
1.4.2.4 Eukaryotic crystal structure of Mre11-Nbs1.....	18
1.4.2.5 Bacterial and archaeal Mre11-Rad50 crystal structures.....	18
1.4.3 The MRN complex in DNA end metabolism	19
1.5 MRN mutations in human diseases	21
1.6 Aims of this work.....	23
2. Results.....	25
2.1 Structure of the catalytic domain of Mre11 from <i>Chaetomium thermophilum</i> ...25	
2.2 Structural mechanism of ATP-dependent DNA binding and DNA end bridging by eukaryotic Rad50.....	35
2.3 Structure of the Rad50 DNA double-strand break repair protein in complex with DNA	93
2.4 Structural Studies of DNA End Detection and Resection in Homologous Recombination	119
3. Discussion	147

Table of Contents

3.1	Eukaryotic CtMre11 ^{CD} and CtMre11 ^{RBD} -CtRad50 ^{NBD} crystal structures	148
3.1.1	Crystal structure of the catalytic domain of CtMre11	148
3.1.2	Crystal structure of dimeric CtMre11 ^{RBD} -CtRad50 ^{NBD}	149
3.1.3	Comparison between CtRad50 ^{NBD} and prokaryotic Rad50 ^{NBD} structures.....	151
3.1.4	The C-terminal CtMre11 Rad50-binding domain.....	151
3.2	Eukaryotic MR(N) and ATP-dependent conformational changes	152
3.2.1	Eukaryotic MR(N) model	152
3.2.2	ATP-dependent conformational changes of eukaryotic MR(N)	154
3.3	Structure of CtRad50 ^{NBD} -DNA and comparison with DNA-free CtRad50 ^{NBD} and TmRad50 ^{NBD} -DNA crystal structures	155
3.3.1	The CtRad50 ^{NBD} -DNA crystal structure	155
3.3.2	Comparison between CtRad50 ^{NBD} -DNA and DNA-free CtRad50 ^{NBD}	156
3.3.3	Comparison with the TmRad50 ^{NBD} -DNA structure.....	157
3.4	Plate survival assay with <i>Saccharomyces cerevisiae</i> Rad50 mutants	157
3.5	Model of the ATP-dependent conformations of the eukaryotic MRN complex.....	158
3.6	Outlook.....	159
4.	Appendix	161
4.1	References	161
4.2	Abbreviations	172
4.3	Contributions.....	176
4.4	Declaration	178
4.5	Acknowledgements	179
4.6	Curriculum vitae.....	180
4.7	Publications	181

Summary

In all living organisms DNA double-strand breaks (DSBs) are among the most threatening DNA lesions leading to genome instability and cancer development in humans. Unrecognized or unrepaired DSBs can lead to chromosomal aberrations resulting in apoptosis or mutations, which cause carcinogenesis. The two major pathways to repair DSBs are non-homologous end joining (NHEJ) and homologous recombination (HR). During NHEJ the two DNA breaks are ligated together, which can result in the loss of genetic information when the DNA ends have been processed. In contrast, HR is a more error-free pathway to repair DNA DSBs by using the sequence information of a sister chromatid to restore the lost genetic information. In NHEJ and HR the Mre11-Rad50-Nbs1 (MRN) complex plays an important role as DSB sensor, repair complex and signaling machinery by recruiting the ATM (ataxia-telangiectasia mutated) kinase, which activates the cell-cycle checkpoint. Mutations in *MRE11*, *RAD50* or *NBS1* genes are found in diseases like Nijmegen breakage syndrome (NBS), NBS-like disorder (NBSLD) and ataxia-telangiectasia-like disorder (ATLD) where defects in checkpoint signaling and chromosomal fragility are detected. After extended investigations of the NHEJ and HR repair pathways, high resolution crystal structures of the eukaryotic Rad50 in complex with DNA and the Rad50 interaction domain of Mre11 were missing when this project started. Recently published studies reveal the structural change of a prokaryotic MR complex after ATP binding and the binding mode of bacterial Rad50 to DNA. The aim of this work was to investigate the eukaryotic MRN complex from *Chaetomium thermophilum* (Ct) on structural and biochemical level. After optimizing the purification of MR(N) subcomplexes, the crystal structures of the dimeric CtMre11 catalytic domain and of the ATP γ S-bound dimeric CtRad50 nucleotide-binding domain (NBD) in complex with the C-terminal Rad50-binding domain (RBD) of Mre11 were solved. This led to the structural model of the ATP-bound eukaryotic MR complex. Further, the structure of the DNA-bound CtRad50^{NBD} dimer was determined and the mode of binding was further investigated by *in vitro* and *in vivo* experiments. These new findings explain the ATP-dependent DNA binding of eukaryotic Rad50 and indicate an important tethering function during DNA repair. For future perspectives, the presented results enable a more detailed structural and biochemical knowledge about DNA damage repair, telomere and genome maintenance.

Zusammenfassung

In allen lebenden Organismen gehören DNA-Doppelstrangbrüche (DSBs) zu den gefährlichsten Schäden, da sie zu Genominstabilität und Krebsentstehung im Menschen führen können. Unerkannte oder nicht reparierte DSBs können Chromosomen verändern und dadurch Apoptose einleiten oder Mutationen verursachen, die die Tumorentwicklung fördern. Die zwei wichtigsten Mechanismen DSBs zu reparieren sind die nicht-homologe Endverknüpfung (engl.: *non-homologous end-joining*; NHEJ) und homologe Rekombination (HR). Während NHEJ werden die DNA-Brüche verbunden, was zum Verlust genetischer Information führen kann, wenn die Enden prozessiert wurden. HR ist dagegen größtenteils fehlerfrei, da die Sequenzinformation eines Schwesterchromatides genutzt wird, um die verlorene genetische Information wiederherzustellen. In NHEJ und HR spielt der Mre11-Rad50-Nbs1-Komplex (MRN-Komplex) eine wichtige Rolle als DSB-Sensor, Reparaturkomplex und Signalmaschinerie, da er die ATM-Kinase rekrutiert, die den Zellzykluskontrollpunkt aktiviert. Mutationen im *MRE11*-, *RAD50*- oder *NBS1*-Gen werden in Krankheiten gefunden, in denen fehlerhafte Zellzykluskontrolle und Chromosomeninstabilität vorkommen. Trotz ausführlicher Untersuchungen der NHEJ- und HR-Reparaturmechanismen gab es bisher noch keine hochauflösende Kristallstruktur von eukaryotischem Rad50 alleine und im Komplex mit DNA oder der Rad50-interagierenden Domäne von Mre11. Veröffentlichte Studien zeigen strukturelle Änderungen des prokaryotischen MR-Komplexes nach ATP-Bindung und die Interaktion von bakteriellem Rad50 mit DNA.

Das Ziel dieser Arbeit war die strukturelle und biochemische Untersuchung des eukaryotischen MRN-Komplexes von *Chaetomium thermophilum* (Ct). Dabei wurde die Strukturen der dimerisierten katalytischen Einheit von Mre11 gelöst und der ATP γ S-gebundenen dimerischen Rad50 Nukleotid-bindenden Domäne (NBD) im Komplex mit der C-terminalen Rad50-bindenden Domäne von Mre11 gelöst. Dies führte zu dem strukturellen Modell des ATP-gebundene eukaryotischen MR-Komplexes. Des Weiteren wurde die Struktur von DNA-gebundenem CtRad50^{NBD}-dimer gelöst und der Bindungsmodus mittels *in vitro* und *in vivo* Experimenten untersucht. Diese neuen Ergebnisse erklären die ATP-abhängige DNA-Bindung von eukaryotischem Rad50 und deuten auf eine wichtige Funktion während der DNA-Reparatur hin. Diese Resultate liefern ein detaillierteres Wissen über DNA-Reparatur für zukünftige Forschungsprojekte.

1. Introduction

1.1 DNA damages

Deoxyribonucleic acid (DNA) stores the genetic information of all living organisms. For these organisms DNA damage represents a considerable threat for genome stability potentially leading to cell death and mutations, which further can cause abnormal cell growth and cancer development in humans. Different DNA damaging agents can cause changes in the structure of the DNA. Their sources and repair pathways have been studied intensively during last decades (Figure 1).

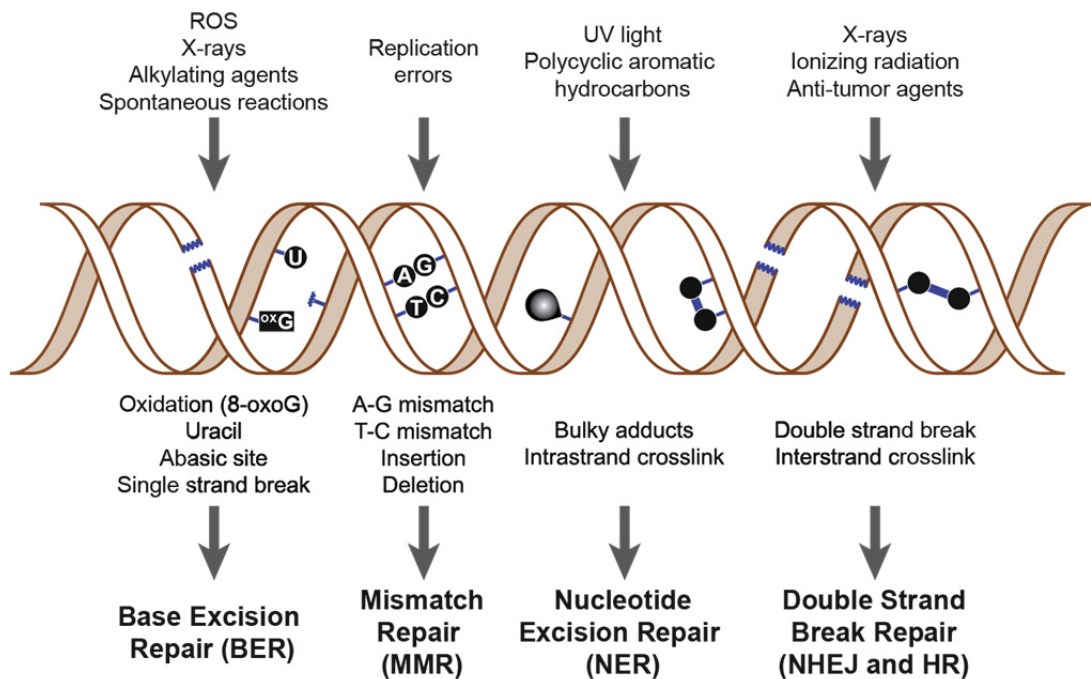


Figure 1: DNA damage and repair pathways. The sources for DNA damage, the resulting lesions and the corresponding repair pathways are illustrated. Figure adapted from (Dexheimer 2013).

Modifications that do not change the overall structure of the DNA or disturb base-pairing can be repaired by direct DNA damage reversal (DDR). Alkylating agents for example can lead to methyl phosphotriesters or O6-methylguanine in the DNA. The latter modification can lead to G:C → A:T transition after replication, but during DDR the

DNA modification is removed without incising the DNA sugar-phosphate backbone or without removing a base (Eker *et al.* 2009).

Endogenous metabolism also leads to more complex base modifications like deamination, alkylation or oxidation. By reactive oxygen species (ROS) for instance guanine can be oxidized to 8-oxo-7,8-dihydroguanine (8-OxoG). These base modifications are repaired by the base excision repair (BER) pathway. Thereby the damaged base is removed after recognition by a DNA glycosylase and an abasic site is generated (Hoeijmakers 2001). This abasic site can also arise by spontaneous hydrolysis in the cell and it is estimated that in a human cell approximately 9,000 abasic sites occur per day (Nakamura *et al.* 1998, Kunkel 1999). In BER the abasic site is incised, the sugar residue removed and the gap is filled by a DNA polymerase. The remaining nick is sealed by a DNA ligase (Kim and Wilson 2012). DNA single-strand breaks (SSBs), which occur after DNA incision during BER, are also results of oxidative attacks by ROS or of abortive DNA topoisomerase I activity. The latter SSBs are recognized and bound by poly (ADP-ribose) polymerase (PARP). After PARP activation and recruitment of additional factors the repair pathway enters BER at the state that follows the abasic site formation and DNA cleavage (Hoeijmakers 2001, Caldecott 2014). DDR and BER function predominantly at the repair of DNA damage lesions with largely unaltered DNA structures.

More severe DNA lesions like base cross-links or bulky adducts distort the DNA helix or block transcription and thus require more substantial repair mechanisms. Ultraviolet (UV) light induces for instance thymine dimers, cyclobutane-pyrimidine dimers or 6-4 pyrimidine-pyrimidone photoproducts. ROS are able to generate cyclopurines and the chemotherapeutic drug cisplatin for example also induces intra-strand cross-links. Nucleotide excision repair (NER) is the major pathway repairing these lesions. It is subdivided into global genomic NER (GG-NER) and transcription-coupled NER (TC-NER), which is associated to RNA polymerase stalling. After recognition of the DNA lesion, the sugar phosphate is incised 3' and 5' of the damaged site and a 22–30 bp long single-stranded DNA fragment is excised. The gap is filled by DNA polymerases and subsequently ligated (Reardon and Sancar 2003, Marteijn *et al.* 2014).

Another form of DNA damage occurs during the replication of highly repetitive sequences that can lead to DNA polymerase slippage and the formation of insertion or deletion loops. These loops as well as mispaired nucleotides are repaired by mismatch

repair (MMR). Mismatch recognition precedes the recruitment of other MMR factors. Then the newly synthesized DNA strand is identified and after degradation of this strand towards the mismatch the DNA is resynthesized (Hoeijmakers 2001). Of note, repair mechanisms represent very complex, partly overlapping repair pathways and common factors therein.

1.2 DNA double-strand breaks

Among the most dangerous DNA damage lesions are DNA double-strand breaks (DSBs) in which, simultaneously, the sugar-phosphate backbone on both DNA strands contains breaks within a short distance. Already one single DSB seems to be sufficient to activate cell-cycle arrest and to induce cell death (Bennett *et al.* 1996, Huang *et al.* 1996). DSBs can be introduced endogenously by intracellular metabolism products like ROS or by replication stress. Thereby un- or misrepaired DNA adducts cause replication fork stalling, which may be processed into DSBs. Repair intermediates like gaps, nicks or SSBs can also be converted into DSBs when replicated by a DNA polymerase (Ciccia and Elledge 2010, Ghosal and Chen 2013, Zeman and Cimprich 2014). Further, exogenous DNA-damaging agents like genotoxic chemicals or ionizing radiation can cause DSBs. Genotoxic chemicals can inhibit topoisomerases, which directly lead to DSBs or indirectly when replication forks collide. Antitumor drugs like camptothecin (CPT) inhibit topoisomerase I, which results in an increase of TopI-bound SSBs, leading to DSBs when replication forks collapse (Pommier *et al.* 2003). Moreover the anticancer drug etoposide inhibits topoisomerase II and prevents the ligation of the introduced DSB (Bromberg *et al.* 2003, Degraasi *et al.* 2004). In tumor treatment the aim of inducing DSBs is to induce apoptosis in highly proliferating cancer cells.

Highly energetic ionizing radiation (IR) can have different sources. IR appears as gamma radiation during decay of atomic nuclei, as X-rays in medical procedures, or as cosmic radiation. IR can cause direct DNA damage by energy transfer or indirectly by generating ROS (Mahaney *et al.* 2009). For instance two IR-induced SSBs in close proximity and on each DNA strand can lead to a DSB. Moreover a ROS induced SSB can cause a DSB when a replication fork passes this break (Sutherland *et al.* 2000, Aguilera and Gomez-Gonzalez 2008, Cadet *et al.* 2012, Mehta and Haber 2014).

On the other hand, programmed DSBs are induced specifically by endonucleases, for example during recombination of homologous chromosomes in meiotic cells. This leads to genetic diversity, which is fundamental for evolution (Lam and Keeney 2015). During immune system development DSBs are created in class switch and V(D)J recombination to generate antibody diversity (Gapud and Sleckman 2011, Xu *et al.* 2012). Moreover, in *Saccharomyces cerevisiae*, DSBs are also introduced for yeast mating type switching (Haber 2012). Un- or misrepaired DSBs can result in apoptosis or gross chromosomal aberrations, which can lead to carcinogenesis in humans (Myung *et al.* 2001a, Myung *et al.* 2001b, Hanahan and Weinberg 2011). To repair DSBs several mechanisms have been developed during evolution to maintain genome integrity.

1.3 DNA double-strand break repair pathways

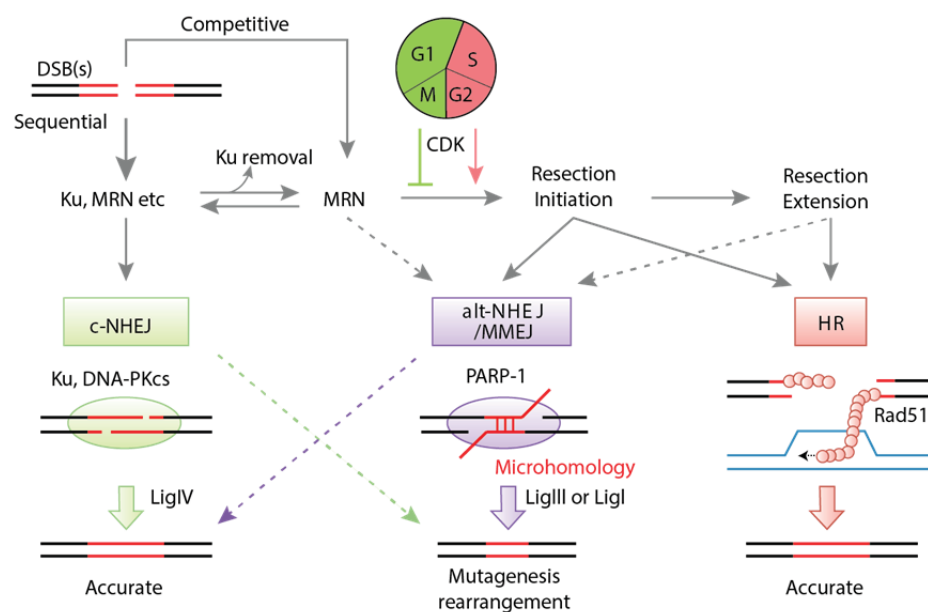


Figure 2: Model of different DSB repair pathways. DSBs can be repaired by canonical non-homologous end joining (c-NHEJ), alternative NHEJ (alt-NHEJ) or microhomology-mediated end joining, and homologous recombination (HR). Important factors are illustrated. Figure adapted from (Chiruvella *et al.* 2013).

The non-homologous end joining (NHEJ) pathway and homologous recombination (HR) are the two major pathways to repair double stranded DNA (dsDNA) lesions (Figure 2). If these DNA damage response pathways are inaccurate, DSBs can lead to genome instability, which threatens genome integrity in daughter cells and might cause cancer development (Pardo *et al.* 2009).

1.3.1 Canonical and alternative non-homologous end joining (NHEJ)

One major DSB repair pathway is non-homologous end joining (NHEJ), which is template independent and thus can take place during the whole cell cycle. Nevertheless, in mammals NHEJ seems to be the major pathway outside of S phase which indicates a cell cycle dependent regulation (Ferretti *et al.* 2013). In canonical NHEJ (c-NHEJ), basically two DNA ends are detected and bound by the Ku complex and the DNA ends are ligated by Ligase IV. At other subclasses of NHEJ, called alternative NHEJ (alt-NHEJ) or microhomology-mediated end joining (MMEJ), DNA ends are processed more substantially until complementary sequences are generated. These sequences anneal with each other and the break can be filled up and ligated. This repair process may result in the loss of genetic information due to nucleolytic degradation of the DNA ends (Figure 2) (Thompson 2012, Chiruvella *et al.* 2013).

1.3.2 Homologous recombination (HR)

The more accurate DSB repair mechanism is the homologous recombination (HR) pathway. HR or homology directed repair (HDR) are present in all kingdoms of life to maintain genome stability and to guarantee genetic diversity. HR initiation is triggered by unprotected dsDNA ends, which occur for example at collapsed replication forks or normal DSBs. In contrast to NHEJ, HR is restricted to S and G2 phase of the cell cycle and requires a sister chromatid or a homologous chromosome as a template to repair the DSB. In HR the DNA ends are processed extensively in various steps (Symington 2014). First, DSB sensors recognize the DNA ends and initiate resection. If the DNA ends do not represent a clean cut but modified DNA ends or ends that are blocked by end-binding proteins like Ku, the ends have to be freed for HR. To clean the DNA ends, the Mre11-Rad50-Nbs1 (MRN) complex together with CtIP (CtBP-interacting protein) endonucleolytically cut the DNA and process the dsDNA towards the break and thereby free the DNA break (Garcia *et al.* 2011, Cannavo and Cejka 2014).

MRN is denoted Mre11-Rad50-Xrs2 (MRX) in *S. cerevisiae* and CtIP is denoted Sae2 in *S. cerevisiae* and Ctp1 in *Schizosaccharomyces pombe*. For clarity reasons the terms “MRN” and “CtIP” will be used throughout this thesis.

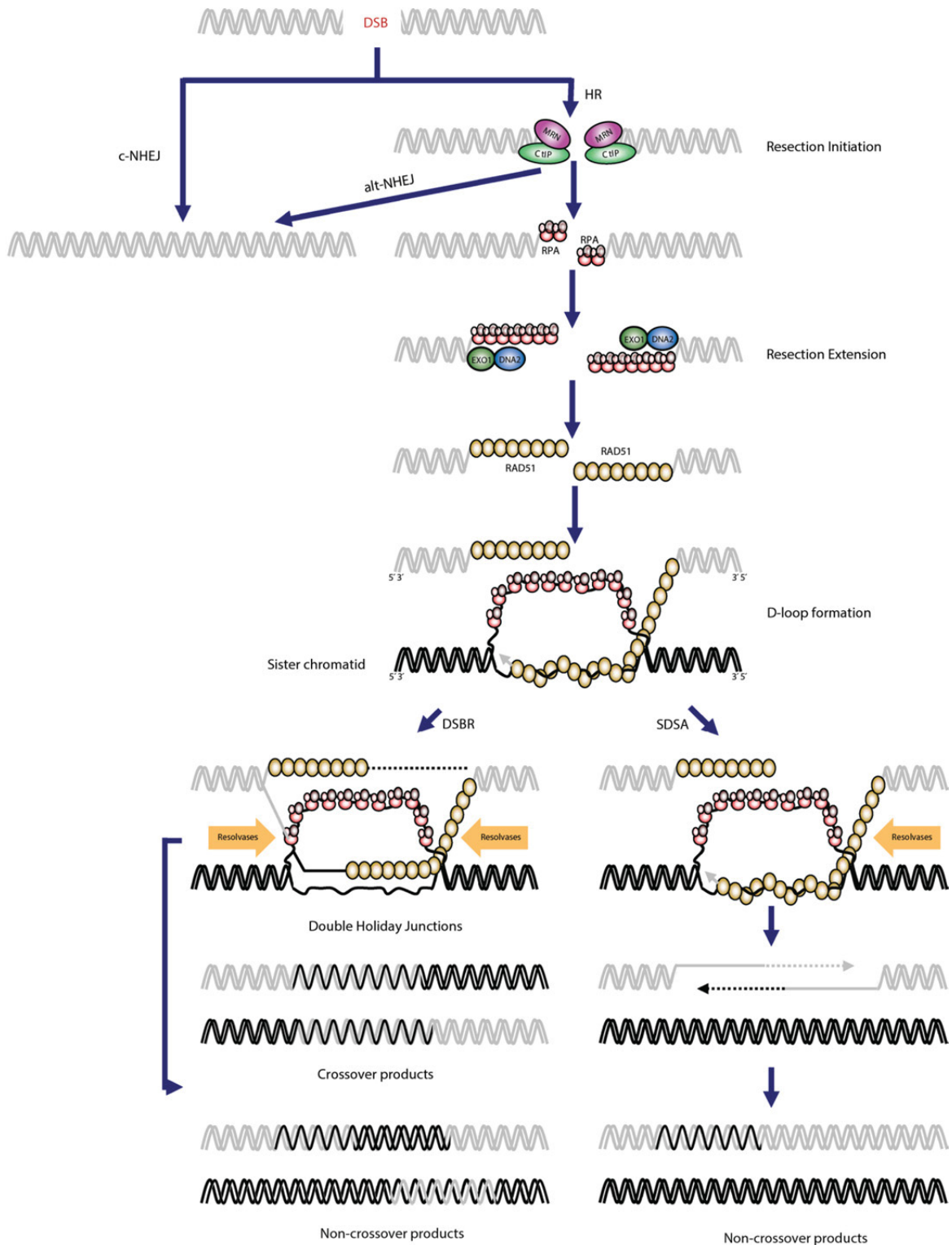


Figure 3: Model of NHEJ and HR pathways in DSB repair. DSBs can be repaired by c-NHEJ or after short-range resection by alt-NHEJ/MMEJ and HR. Alt-NHEJ and HR have a common initial resection step to process DSBs. Long-range resection then guides the repair process towards HR. Important steps during HR are RPA binding to single-stranded DNA (ssDNA), Rad51 filament formation, D-loop formation and DNA synthesis. Resolution via double-strand break repair (DSBR) or synthesis-dependent strand annealing (SDSA) results in crossover or non-crossover products. Figure adapted from (Liu and Huang 2014).

Since MMEJ and HR share common initial factors, MMEJ is still able to occur after short-range resection (Figure 2 and Figure 3) (Chiruvella *et al.* 2013, Truong *et al.* 2013). The followed long-range resection in 5'–3' direction then guides the pathway towards HR. Long-range resection is performed by nucleases and helicases like EXO1, DNA2 and BLM. Replication protein A (RPA) binds to the generated 3' single-stranded DNA (ssDNA) and subsequently is replaced by the strand exchange protein Rad51 (denoted RecA in *E. coli*). The formed Rad51-ssDNA filament searches for, and invades into the homologue DNA strand. Thereby a D-loop is formed by pairing of the ssDNA filament with the homologous sequence on the template strand. By using the 3' tail as a primer and the homologous DNA strand as template, the DNA polymerases Pol δ and Pol ϵ extend the 3' end in 5' to 3' direction. After Holiday junction formation and resolution, or D-loop cleavage the DNA break is repaired (Figure 3). If a second DNA end is not present, for instance at collapsed replication forks, break-induced replication (BIR) occurs to copy the sequence from the homologous region to the telomere. At DSBs with flanking direct repeats, single-strand annealing (SSA) can take place when the resected complementary strands are exposed. SSA always leads to sequence deletion and therefore is highly mutagenic (Mehta and Haber 2014). One crucial factor in DSB detection and the pathway choice between NHEJ and HR is the MRN complex.

1.4 Mre11-Rad50-Nbs1 complex

The MRN complex consists of Mre11 (meiotic recombination 11) and Rad50 (radiation 50), whose homologs are found in all kingdoms of life, plus the solely in eukaryotes present Nbs1 (Nijmegen breakage syndrome 1) subunit (Game and Mortimer 1974, Ajimura *et al.* 1993, Sharples and Leach 1995, Carney *et al.* 1998, Varon *et al.* 1998, Hopfner *et al.* 2000a). The Mre11-Rad50 core complex is even found in viruses, for instance the bacteriophage T4 (Herdendorf *et al.* 2011) and in some organisms, homologs of Mre11 and Rad50 are fused together into one peptide chain (Yoshida *et al.* 2011). In bacteriophage T4, the MR homolog (denoted gp46/gp47; gene products 46/47) plays a crucial role during late stages of infection, at the beginning of recombination-dependent replication (Kreuzer and Brister 2010, Almond *et al.* 2013). The bacterial homolog of MR (SbcCD; suppressor of recBC mutations CD) functions in the wake of replication forks by degrading hairpin structures and together with RecA (recombination protein A) prevents

inverted chromosome duplication in the cell (Zahra *et al.* 2007, Eykelenboom *et al.* 2008, Darmon *et al.* 2010). After recruitment to DSBs archaeal and eukaryotic MR(N) repairs DSBs caused by genotoxic chemicals, ionizing radiation or at stalled replication forks (Costanzo *et al.* 2001, Trenz *et al.* 2006, Frols *et al.* 2007, Quaiser *et al.* 2008, Delmas *et al.* 2013, Mehta and Haber 2014). Further, eukaryotic MRN is important for the maintenance of replicated telomeres and the processing of DNA ends that are blocked by DNA hairpins or bound proteins like Ku or Spo11, which is important for meiotic recombination (Lobachev *et al.* 2002, Neale *et al.* 2005, Bonetti *et al.* 2009, Bonetti *et al.* 2010). For the processing of blocked DNA ends an endonucleolytic cut away from the break is necessary to free the DNA end. This process is triggered by CtIP (Sae2/Ctp1) (Connelly *et al.* 2003, Bonetti *et al.* 2009, Mimitou and Symington 2010, Langerak *et al.* 2011, Cannavo and Cejka 2014).

As a key player in DSB repair MRN is involved in DSB sensing, binding as well as the resection of the DNA end. In addition, MRN functions as a recruitment platform for other DNA repair factors and as a DNA damage signal transducer by activation of the ATM (ataxia-telangiectasia mutated) checkpoint kinase (Assenmacher and Hopfner 2004, Williams *et al.* 2010). In mice complete deletion of either *Mre11*, *Rad50* or *Nbs1* results in lethality during embryogenesis (Xiao and Weaver 1997, Luo *et al.* 1999, Zhu *et al.* 2001, Buis *et al.* 2008). In humans, hypomorphic mutations in MRN genes are associated with different diseases, which are discussed below (Chapter 1.5).

1.4.1 Biochemical functions of the MRN complex

Biochemical *in vitro* studies with MR(N) proteins from bacteria, archaea, yeast and humans revealed Mn^{2+} -dependent nuclease activities of the Mre11 subunit. It possesses 3'–5' dsDNA exonuclease activity, ssDNA endonuclease activity and dsDNA endonuclease activity, in which only one DNA strand of the DNA duplex is incised (Connelly *et al.* 1997, Furuse *et al.* 1998, Paull and Gellert 1998, Trujillo *et al.* 1998, Connelly *et al.* 1999, Hopfner *et al.* 2000a, Herdendorf *et al.* 2011, Cannavo and Cejka 2014). *E. coli* MR is also able to introduce a DSB by nicking both strands of the DNA duplex to remove protein from a DNA end (Connelly *et al.* 2003). The processive exonuclease activity of Mre11 on 3' dsDNA as well as the dsDNA endonuclease are influenced by ATP binding to the Rad50 ATPase (Majka *et al.* 2012). Thereby, inhibited

ATP hydrolysis negatively regulates the dsDNA exo- and endonuclease (Connelly *et al.* 1997, Hopfner *et al.* 2001, Trujillo and Sung 2001, Herdendorf *et al.* 2011, Lim *et al.* 2011, Cannavo and Cejka 2014, Deshpande *et al.* 2014), whereas it was reported that the ssDNA endonuclease of MR from *E. coli* and bacteriophage T4 is ATP-independent (Connelly and Leach 1996, Herdendorf *et al.* 2011). A recent study with yeast MRN (MRX) and CtIP (Sae2), which promotes the Mre11 dsDNA endonuclease, shows that ATP is essential for the endonuclease activity and the results indicate increased exonuclease activity when ATP is absent. Interestingly, the MRN-CtIP (denoted MRX-Sae2 in *S. cerevisiae*) interaction always leads to the incision of the 5' DNA strand, resulting in a single-stranded 3' strand (Cannavo and Cejka 2014). MR(N) is also able to open hairpin DNA and to process it in an ATP-dependent manner (Paull and Gellert 1998, Connelly *et al.* 1999, Trujillo and Sung 2001). Covalently bound proteins to DNA ends, e.g. Spo11, can be removed by MR(N) (Connelly *et al.* 2003, Hartsuiker *et al.* 2009).

Despite extensive research since the first archaeal Rad50 structure was solved in 2000 (Hopfner *et al.* 2000b), detailed knowledge about the mechanism of eukaryotic MRN in DSB sensing and processing are still missing. Until now many biochemical DNA binding studies with MR(N) homologs revealed relatively weak affinity to DNA ends compared to other DSB sensors like the Ku complex (Blier *et al.* 1993, Walker *et al.* 2001, Lee *et al.* 2003a, Möckel *et al.* 2012). However, picomolare DNA binding affinities have been measured in single molecule fluorescence energy transfer (Förster resonance energy transfer, FRET) experiments of human MRN (Cannon *et al.* 2013). It is unclear whether this difference may be explained by different experimental set-ups or because *in vitro* MR(N) can form large higher-order molecular assemblies, which influence the DNA binding affinity (de Jager *et al.* 2001). This could also explain the necessity of the Rad50 coiled-coils (CCs), to form multimers that increase the affinity to DNA (Lee *et al.* 2013). Beside the CC domain, Rad50 comprises a ABC (ATP-binding cassette)-type ATPase domain that binds and hydrolyses ATP. The ATPase domain is formed by an N-terminal Walker A, C-terminal Walker B and a signature motif (Walker *et al.* 1982, Hopfner *et al.* 2000b). If the ATP-free or -bound state is the predominant state *in vivo* and whether so far unknown factors play a role in regulating the ATPase activity, have to be studied in the future. By generating mutants that are deficient in either ATP binding or hydrolysis, different functions have been identified in the past. Stabilizing Rad50 in ATP-bound or

ATP-free state showed severe differences in the MRN activity, especially in the control of the nuclease activity. Stabilizing the Rad50 dimer conformation for instance by non-hydrolysable ATP analogs, decreases the dsDNA exonuclease activity of MR(N). In contrast, ATP hydrolysis or inhibition of the ATP-dependent Rad50 dimerization stimulate the exonucleolytic processing of dsDNA (Hopfner *et al.* 2001, Trujillo and Sung 2001, Lim *et al.* 2011, Majka *et al.* 2012, Cannavo and Cejka 2014, Deshpande *et al.* 2014). Interestingly, the dsDNA endonuclease activity also requires ATP binding and hydrolysis, and is reduced when the non-hydrolysable ATP analog ATP γ S is present but also when ATP is absent at all (Trujillo and Sung 2001, Cannavo and Cejka 2014). The ssDNA endonuclease activity seems to be largely independent of the ATP-state (Connelly and Leach 1996, Herdendorf *et al.* 2011). Furthermore, Rad50 ATPase activity also plays a crucial role during hairpin or dsDNA unwinding and influences DNA tethering during end-joining (Paull and Gellert 1999, Cannon *et al.* 2013, Deshpande *et al.* 2014).

The eukaryotic Nbs1 subunit has no catalytic activity within the MRN complex but regulatory functions. Nbs1 stimulates DNA binding of MRN, DNA unwinding and hairpin processing (Paull and Gellert 1999, Trujillo *et al.* 2003). Upon DSB formation Nbs1 is necessary for the recruitment and the activation of the checkpoint kinase ATM, which phosphorylates Nbs1. Although *in vitro* MR can interact with ATM, the Nbs1 C-terminus is important for the activation of ATM. In particular, in *Xenopus* egg extract with depleted Nbs1, the last 147 amino acids of Nbs1 are able to restore ATM activation. In a mouse model it was shown that the Nbs1 C-terminus plays a role in signaling of apoptosis and cell cycle arrest (Gatei *et al.* 2000, Lee *et al.* 2003b, Nakada *et al.* 2003, Lee and Paull 2004, Falck *et al.* 2005, Lee and Paull 2005, You *et al.* 2005, Berkovich *et al.* 2007, Stracker *et al.* 2007). Besides the signaling function, Nbs1 builds a platform to recruit other DNA repair factors like DNA2, MDC1 (mediator of DNA damage checkpoint protein 1), BRCA1 (breast cancer 1) or CtIP to DSBs (Wang *et al.* 2000, Kobayashi *et al.* 2002, Chapman and Jackson 2008, Chen *et al.* 2008, Melander *et al.* 2008, Spycher *et al.* 2008, Wu *et al.* 2008, Wawrousek *et al.* 2010, Nimonkar *et al.* 2011). Within the MRN complex Nbs1 is responsible for the nuclear localization of the complex and ionizing radiation-induced MR foci do not form in the nucleus when Nbs1 is not present (Carney *et al.* 1998, Desai-Mehta *et al.* 2001, Tsukamoto *et al.* 2005). A *S. cerevisiae* mutation in the *MRE11* gene, which destabilized the Mre11-Nbs1 (MN) interaction (denoted Mre11-Xrs2 in *S. cerevisiae*), resulted in an *mre11* knockout

phenotype on DNA damage repair. This phenotype was rescued by fusing a nuclear localization signal (NLS) to the Mre11 protein, because the reduced MN interaction leads to no detectable Mre11 in the nucleus (Schiller *et al.* 2012). A crystal structure of *S. pombe* Nbs1 in complex with CtIP (denoted Ctp1 in *S. pombe*) revealed that the very N-terminal FHA (forkhead associated) domain interacts with a phosphorylated threonine, which is probably important for the recruitment to DSB sites and thus for DNA damage repair (Williams *et al.* 2009). In yeast, very recent studies with CtIP and MRN (denoted Sae2 and MRX, respectively in *S. cerevisiae*) indicate that CtIP is also important for the removal of MRN from DSBs after recognition and repair initiation (Chen *et al.* 2015).

Although many MRN enzymatic functions are executed by one subunit, its regulation can take place by other subunits. Thus, all functional and regulatory aspects have to be considered in respect to the whole assembly, which represents a very complex system.

1.4.2 Structural insights into the Mre11-Rad50-Nbs1 complex

In the past, structural studies about the MRN complex from different organisms have led to numerous models for the molecular architecture of the MRN complex.

1.4.2.1 The Mre11 subunit

Mre11 can be considered as the core of the MRN complex, because of its interaction with the Rad50 and Nbs1 subunits. The highly conserved architecture of the dimer conformation and the N-terminal nuclease domain becomes evident by Mre11 crystal structures from bacteria, archaea and eukaryotes (Figure 4) (Hopfner *et al.* 2001, Arthur *et al.* 2004, Williams *et al.* 2008, Das *et al.* 2010, Lammens *et al.* 2011, Lim *et al.* 2011, Limbo *et al.* 2012, Möckel *et al.* 2012, Schiller *et al.* 2012, Liu *et al.* 2014). In yeast, mutating the dimer interface phenocopies a *mre11* knock-out on DNA damage repair and shows the functional importance of the Mre11 dimer. *In vitro*, monomeric *P. furiosus* Mre11 has decreased DNA affinity, but the nuclease activity seems unaltered (Williams *et al.* 2008, Schiller *et al.* 2012). Mre11 contains a highly conserved phosphodiesterase domain at the N-terminus and a capping domain afterwards (Figure 4). The enzymatic active site of Mre11 is formed by two coordinated manganese ions in the phosphodiesterase domain (Trujillo *et al.* 1998, Hopfner *et al.* 2001).

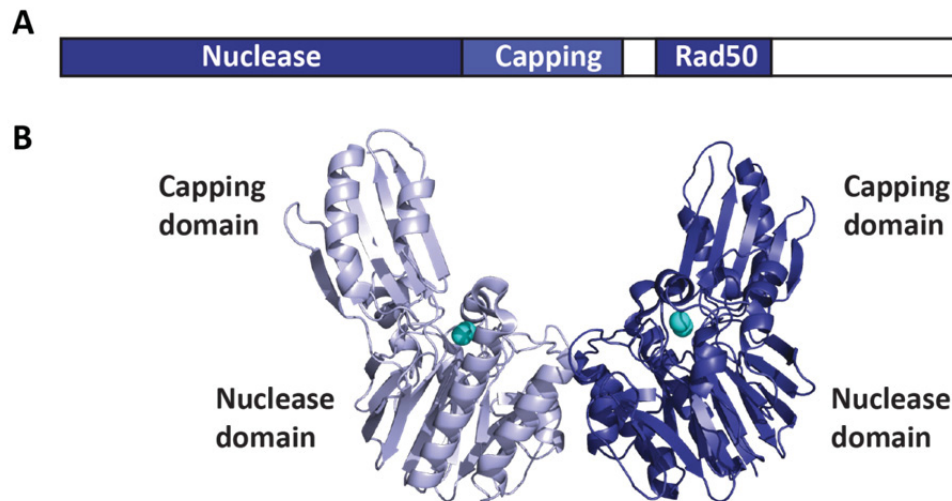


Figure 4: (A) Domain model of Mre11 protein. Nuclease domain, capping and Rad50-binding domains of Mre11 are highlighted in blue. (B) Crystal structure of dimeric *Pyrococcus furiosus* Mre11 nuclease and capping domain (PDB code: 1HI7). Mre11 protomers are colored in light and deep blue. Manganese ions in the active sites are depicted as spheres (cyan).

In vitro, dimeric Mre11 can bridge two DNA ends, which could be essential considering its function in end-joining pathways or HR (Figure 5A) (Chen *et al.* 2001, Williams *et al.* 2008, Reis *et al.* 2012, Ghodke and Muniyappa 2013). In eukaryotes, it has been shown that further DNA-binding sites are present in the Mre11 C-terminus. They are crucial for DSB repair, but also for the formation and processing of DSBs in meiotic recombination (Furuse *et al.* 1998, Usui *et al.* 1998). Another interesting motif has been observed in homologs of metazoan Mre11, where a glycine/arginine-rich motif facilitates DNA binding, nucleolytic processing *in vitro* and recruitment to DSBs *in vivo* (Dery *et al.* 2008). A superimposition of so far published crystal structures shows that the Mre11 dimer is not rigid and adopts different angles between the two protomers (Figure 5B). A variation of the angle between the two protomers can also be observed within structures of the same organism. The structures of *S. pombe* Mre11 show very different dimer conformations with and without Nbs1 (Schiller *et al.* 2012). The dimer flexibility of Mre11 might also be influenced by Rad50, DNA or Nbs1 binding and thus might have important functional aspects that have to be analyzed in future experiments. The crystal structure of human Mre11 represents an unusual dimer interface, which is stabilized by a disulfide bond and thereby decreases flexibility (Park *et al.* 2011). Previously, it has been shown that Mre11 contains a conserved metal binding site and the coordinating histidines explain the preference for manganese over magnesium for the 3′–5′ exonuclease activity

(Hopfner *et al.* 2001). However, in *P. furiosus* Mre11 the magnesium-dependent endonuclease promotes resection of the 5' strand (Hopkins and Paull 2008). The structural mechanism of this enzymatic reaction has to be analyzed in future studies and although the interaction between Mre11 and DNA has been characterized (Williams *et al.* 2008), a detailed structure of the active site during endonucleolytic DNA processing is still missing.

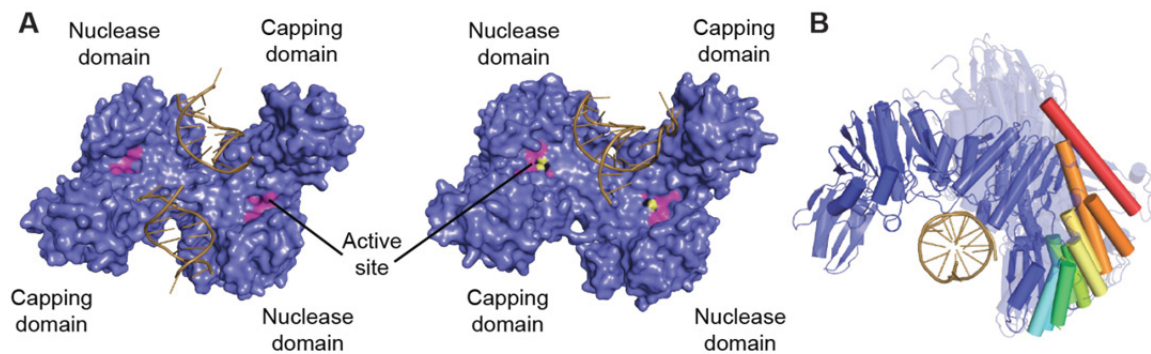


Figure 5: Crystal structures of Mre11-DNA complex. (A) Crystal structure of Mre11 (blue) bound to two dsDNA ends (left) and synaptic DNA (right) are depicted. (B) Comparison of different published Mre11 structures reveals a movement of the capping domain. Dimeric crystal structures are aligned onto the left monomer of *P. furiosus* Mre11 (blue). For clarity, the overlaid monomers are not depicted, the right monomers are transparent, and the first α -helix from the capping domain is marked from blue to red to highlight the differences. DNA (sand) indicates the accessible nuclease active site. The PDB codes are 1S8E (Arthur *et al.* 2004), 3DSD, 3DSC (Williams *et al.* 2008), 2Q8U (Das *et al.* 2010), 3AUZ, 3AV0 (Lim *et al.* 2011), 4HD0 (Limbo *et al.* 2012), 3THO, 3THN (Möckel *et al.* 2012), 3QG5 (Lammens *et al.* 2011), 1II7 (Hopfner *et al.* 2001), 4FBQ, 4FBW, 4FBK, and 4FCX (Schiller *et al.* 2012). Adapted from (Schiller *et al.* 2014).

1.4.2.2 The Rad50 subunit

In bacteria and archaea, the Mre11 C-terminal end forms two or three helices, which bind to the Rad50 subunit (Lammens *et al.* 2011, Lim *et al.* 2011, Möckel *et al.* 2012). Rad50 is a member of the structural maintenance of chromosomes (SMC) family. First structural investigations of *P. furiosus* Rad50 revealed a globular N- and C-terminal domain, which together form a nucleotide binding domain (NBD). Out of the NBD protrude very long CCs (coiled-coils), which fold back on themselves and enable the interaction between the N- and C-terminus (Figure 6A, B) (Hopfner *et al.* 2000b). Between the different domains of life the lengths of the CCs can vary extremely and seem to increase with the complexity of the kingdom (Schiller *et al.* 2014). The CCs contain a highly conserved CXXC motif at the apex, which forms the zinc-binding hook. For dimerization one zinc

ion is coordinated by four cysteines, two from each CXXC motif of one CC (Hopfner *et al.* 2002). The Zn-mediated interactions between two CCs enable intra- as well as inter-complex interactions. Electron microscopy and atomic force microscopy (AFM) studies revealed inter-complex interactions, which in principle enable the tethering of two DNA molecules (de Jager *et al.* 2001, Hopfner *et al.* 2002, Moreno-Herrero *et al.* 2005). These results might explain how a sister chromatid is kept in close spatial proximity during HR. The globular domain of Rad50 forms the NBD, which can dimerize upon binding of two ATP nucleotides and Mg^{2+} ions. Monomeric Rad50 consists of interacting N- and C-terminal regions of the polypeptide chain. The NBD structure can be separated into lobe I and lobe II (Figure 6B). The ATP binding site is characterized by the N-terminal Walker A motif and the C-terminal Walker B motif plus the signature motif interacting in trans. One ATP- Mg^{2+} molecule is trapped between lobe I of one Rad50 protomer and lobe II of the other protomer (Figure 6C) (Hopfner *et al.* 2000b).

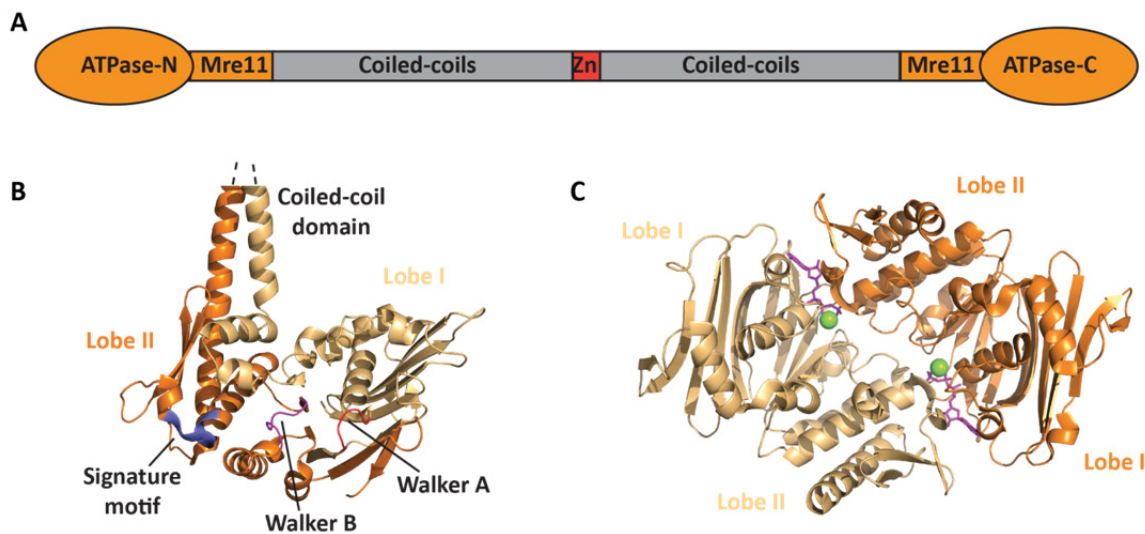


Figure 6: (A) Domain model of Rad50 protein. N- and C-terminal ATPase domains of Rad50 (ATPase-N; ATPase-C) as well as the Mre11-interacting domains are marked (orange). The Coiled-coil domains (grey) and the zinc-hook (Zn, red) are depicted. (B) Crystal structure of monomeric *P. furiosus* Rad50 with protruding coiled-coils. Lobe I and lobe II are highlighted in light and dark orange. Walker A (red), Walker B (magenta) and Signature (blue) motifs are marked (PDB code: 1H18). (C) Crystal structure of first Rad50 dimer from *P. furiosus* (PDB code: 1F2U). Rad50 protomers are highlighted in light orange and orange. ATP (magenta) and Magnesium (green) are depicted.

Studies with bacterial Rad50 revealed a structural rearrangement within the Rad50 protomer upon ATP binding. Thereby, the beta-sheets in lobe I move in respect to each other, which also leads to a different orientation of the CCs. Further, areas close to the

ATP binding motif undergo structural movements upon nucleotide binding and a positively charged region emerges in the dimer groove in *Thermotoga maritima* (Lammens *et al.* 2011, Williams *et al.* 2011, Möckel *et al.* 2012). *In vitro* studies with prokaryotic Rad50 showed that the affinity of Rad50 to DNA is stimulated by ATP (Lim *et al.* 2011, Möckel *et al.* 2012). Since Mre11 and Rad50 are able to bind DNA, the ATP-bound state probably regulates which subunit is accessible.

1.4.2.3 The Nbs1 subunit

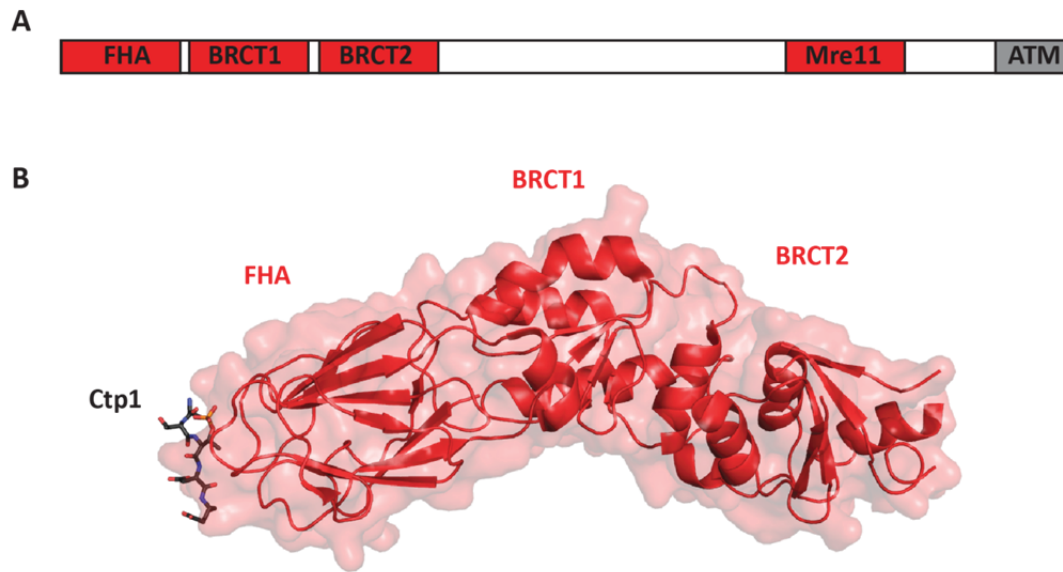


Figure 7: (A) Domain model of Nbs1 protein. The N-terminal FHA, BRCT1 and BRCT2 domains are highlighted and the predicted C-terminal Mre11- and ATM-interacting regions are marked. (B) Crystal structure of N-terminal FHA, BRCT1 and BRCT2 domains (red) in complex with a phosphorylated peptide of CtIP (denoted Ctp1 in *S. pombe*) (black). The PDB entry is 3HUF.

Secondary structure predictions of Nbs1 reveal large unstructured regions and crystal structures of N-terminal Nbs1 from *S. pombe* have been solved. The Nbs1 amino terminus comprises the FHA, BRCT1 (BRCA1 C-terminus 1) and BRCT2 domains (Lloyd *et al.* 2009). Another crystal structure explains the mode of binding of phosphorylated *S. pombe* CtIP (denoted Ctp1) to the FHA domain of Nbs1 (Figure 7) (Williams *et al.* 2009). Via the N-terminal region Nbs1 functions as a recruitment platform for other DSB repair factors. The Mre11-interacting region and ATM-binding domains are located in the C-terminal part of the Nbs1 polypeptide. The conserved ATM-interacting carboxy terminus is characterized by a FXF/Y motif and a cluster of acidic amino acids. As already mentioned, in *Xenopus* the C-terminal part of Nbs1 is sufficient

to activate ATM (Falck *et al.* 2005, You *et al.* 2005). Whether the relatively large unstructured and probably flexible regions in Nbs1 function as a tether for the recruitment of other repair factors has to be studied. Additional structural information about Nbs1 is gained by *S. pombe* Mre11 crystal structures bound to the C-terminal Mre11 interacting region of Nbs1 (Schiller *et al.* 2012).

1.4.2.4 Eukaryotic crystal structure of Mre11-Nbs1

The only structural information about interactions between the subunits within the eukaryotic MRN complex comes from *S. pombe* MN crystal structures. It has been shown that a conserved motif in the C-terminal region of Nbs1 interacts with Mre11. Interestingly, Nbs1-free Mre11 adopts a different conformation than Nbs1-bound Mre11 and the eukaryotic specific insertion loops become structured upon complex formation. Nbs1 binds asymmetrically to the Mre11 dimer. Thereby, one Nbs1 peptide binds to the outer side of each Mre11 protomer but only one peptide bridges the Mre11 dimer interface. The latter interaction is characterized by a conserved NFKxFxK motif, which leads to the mentioned ordering of the eukaryote specific insertion loops and probably stabilizes the Mre11 dimer (Schiller *et al.* 2012).

1.4.2.5 Bacterial and archaeal Mre11-Rad50 crystal structures

The bacterial and archaeal MR complex contains a globular head domain consisting of the Mre11 nuclease domain and the NBD of Rad50 (Rad50^{NBD}) (Connelly *et al.* 1998, Anderson *et al.* 2001, de Jager *et al.* 2001). Thereby, the center of the head module is formed by the dimerized Mre11 nuclease (Hopfner *et al.* 2001, Williams *et al.* 2008, Das *et al.* 2010, Park *et al.* 2011). Each Mre11 protomer interacts with one Rad50 where the CCs protrude out of the Rad50^{NBD}. This head complex forms a conserved heterotetrameric M₂R₂ structure. In ATP-bound state, the Rad50^{NBD} protomers dimerize and decrease the accessibility of the Mre11 active site, which becomes more accessible upon ATP hydrolysis (Figure 8). Whereas the C-terminal Rad50-binding domain of Mre11 (Mre11^{RBD}) consists of a helix-loop-helix motif in bacteria, there is no detailed structural information about the eukaryotic interface between Mre11 and Rad50 so far (de Jager *et al.* 2001, Hopfner *et al.* 2001, Lammens *et al.* 2011, Lim *et al.* 2011, Limbo *et al.* 2012, Möckel *et al.* 2012).

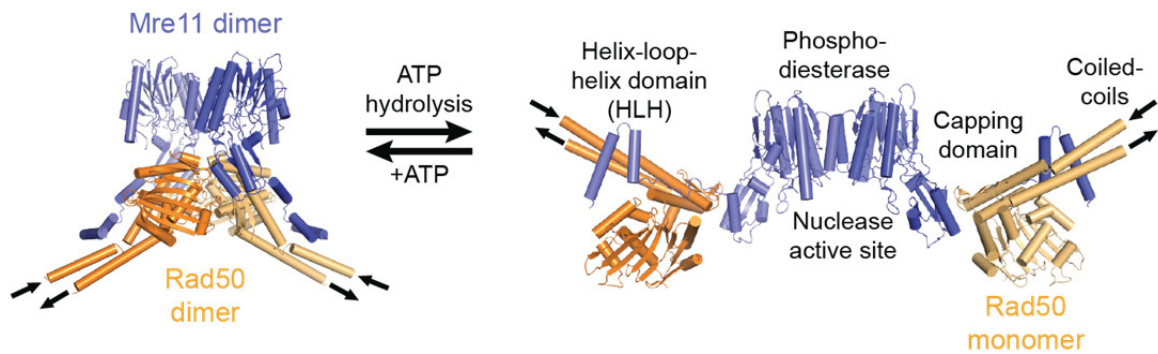


Figure 8: ATP-dependent movement of the bacterial Mre11-Rad50 complex. Structures of *T. maritima* MR in nucleotide-bound (left) and nucleotide-free (right) state are depicted. Figure adapted from (Schiller *et al.* 2014).

1.4.3 The MRN complex in DNA end metabolism

MRN possesses multiple functions and is involved in DSB recognition, DSB repair initiation, DSB processing, DNA tethering and activation of the cell cycle checkpoint. It plays an important role in the choice between DSB repair pathways where end resection is needed (HR, alt-NHEJ; MMEJ) and c-NHEJ (Chiruvella *et al.* 2013, Truong *et al.* 2013). Additionally, MRN is involved in processes like meiotic recombination and telomere maintenance (Mimitou and Symington 2009).

The MRN complex in HR

During HR in mitotic cells MRN functions as a DSB sensor by being among the first complexes that are recruited to DSBs and initiate the HR pathway (Lisby *et al.* 2004). The MRN complex and especially the endonuclease activity of Mre11 are important for the initial resection of the 5' DNA end preceding HR (Williams *et al.* 2008). At unclean DNA ends, which might comprise phosphor 3'-ends or hairpin structures but also bound proteins, the ends can be freed by MRN. Thereby, the endonucleolytic cut is triggered by CtIP and the DNA is processed towards the break to generate a clean and free ssDNA end. Recruitment of Exo1 and the Sgs1-Dna2 complex as well as other nucleases and helicases enables the long-range resection of several hundred bases to generate 3' ssDNA, to which RPA can bind (Shim *et al.* 2010, Garcia *et al.* 2011, Cannavo and Cejka 2014). Besides initiation of DNA end resection in HR, MRN functions as a scaffolding factor to tether two DNA molecules by inter-complex interactions (de Jager *et al.* 2001, Hopfner *et al.* 2002, Moreno-Herrero *et al.* 2005). Upon DSB sensing MRN transduces the signal to the ATM kinase, which leads to downstream signaling. ATM phosphorylates various

repair and checkpoint factors like Nbs1, H2AX histone, SMC1, checkpoint kinases Chk1, Chk2 and transcription regulator p53. This leads to the formation of repair foci and cell cycle checkpoint activation to enable DNA repair (Paull 2015).

The MRN complex in meiotic recombination

In meiotic recombination DSBs are induced by the Spo11 (sporulation 11) protein that covalently binds to the DNA end and has to be removed in advance of the recombination process. Studies in yeast showed that the MRN complex is needed for the removal of Spo11. Since Spo11 forms a covalent bond with the 5' DNA end, the polarity could explain the preferential processing by MRN of this strand. Reported mutations in the *RAD50* gene represent a separation-of-function phenotype (*rad50S*) by being able to repair DNA damage but showing accumulation of unresected Spo11-bound DSBs, which leads to a defect in meiotic recombination and no spore formation in yeast (Alani *et al.* 1990, Mimitou and Symington 2009).

The MRN complex in telomere maintenance

Newly replicated chromosomes represent a one-sided DSB on the leading strand. Telomeres are special DNA-protein structures at the ends of eukaryotic chromosomes to protect them from recognition by the DNA damage repair machinery and to prevent degradation, fusion or recombination (Faure *et al.* 2010). The MRN complex plays an important role in telomere maintenance and thereby also ensures genome integrity. MRN together with CtIP is necessary for the resection of the C-rich 5' DNA end to generate the 3' G-strand which is important for telomere elongation and t-loop formation in mammals (Bonetti *et al.* 2014). MRN senses dysfunctional telomeres and in *S. cerevisiae* MRN recruits Tel1, which is the ATM homolog, to stimulate telomere lengthening by the telomerase (Goudsouzian *et al.* 2006, Hector *et al.* 2007, Deng *et al.* 2009, Hirano *et al.* 2009, Stracker and Petrini 2011). Deletion of MRN (*MRX*) genes or complex disrupting mutations lead to telomere shortening in yeast cells (Kironmai and Muniyappa 1997, Boulton and Jackson 1998, Schiller *et al.* 2012).

MRN in NHEJ

Since the Ku complex shows high affinity to DNA ends and forms a ring structure around dsDNA it seems to be the predominant factor for c-NHEJ (Blier *et al.* 1993, Walker *et al.* 2001). However, MRN depletion leads to a reduced end-joining efficiency in c-NHEJ as well as alt-NHEJ/MMEJ (Rass *et al.* 2009, Xie *et al.* 2009). Interestingly, the Rad50 ATPase activity, but not the Mre11 nuclease activity, is important for c-NHEJ (Zhang and Paull 2005). The repair process is guided towards alt-NHEJ by the MRN complex together with CtIP. Thereby the Mre11 nuclease activity is important for the initial short-range resection and the release of proteins bound to DNA ends, like Ku. For alt-NHEJ the factors that are important for the short-range resection, also play a role in the initial resection process during HR (Figure 2) (Langerak *et al.* 2011, Chiruvella *et al.* 2013, Truong *et al.* 2013).

1.5 MRN mutations in human diseases

In mice deletions of *Mre11*, *Rad50* and *Nbs1* are lethal during embryogenesis (Luo *et al.* 1999, Zhu *et al.* 2001, Buis *et al.* 2008). In human, hypomorphic mutations of the *MRE11*, *RAD50* or *NBS1* genes are in relation to different disease like Nijmegen breakage syndrome (NBS), NBS-like disorder (NBSLD) and ataxia-telangiectasia-like disorder (ATLD) (Figure 9). Cells from these patients and cells from patients with Ataxia telangiectasia (A-T) disease, which results by ATM disruption, show similar phenotypes, and thus indicate the functional connection between ATM and MRN (Reynolds and Stewart 2013). As common characteristics, patient cells carrying MRN mutations comprise higher sensitivity to DSB inducing agents like ionizing radiation and show spontaneous chromosome instability (Taylor *et al.* 1975, Taylor *et al.* 2004). A-T patients develop cerebellar neurodegeneration, which leads to gait ataxia (loss of balance), dysarthria (speaking problems), oculomotor apraxia (abnormal eye movement), dyssynergia (loss of smooth muscle movements) and have a higher risk to develop cancer. On the other hand, some A-T patients show mild neurological and clinical characteristics (Taylor *et al.* 2004, Uchisaka *et al.* 2009, Reynolds and Stewart 2013). ATLD patients exhibit similar phenotypes like A-T patients, including cerebellar atrophy, except that no telangiectasia has been reported so far and just two siblings out of 18 reported ATLD cases, developed lung cancer (Uchisaka *et al.* 2009). Over 90 % of all NBS patients carry

a mutation in the *NBS1* gene that leads to the expression of an approx. 26 kDa N-terminal (Nbs1p26) and a 70 kDa C-terminal fragment (Nbs1p70). Nbs1p26 contains the FHA and BRCT1 domains and Nbs1p70 contains the BRCT2, Mre11- and ATM-interacting domains (Maser *et al.* 2001, Digweed and Sperling 2004, Williams *et al.* 2009). NBS and A-T patients comprise immunodeficiency and a higher cancer predisposition. Cells from these patients are more sensitive to ionizing radiation and show altered cell cycle checkpoints as well as translocations between chromosome 7 and 14. In contrast to A-T and ATLD patients, NBS patients exhibit microcephaly combined with mental retardation and no neurodegeneration. NBS patients do not present ataxia, telangiectasia, dysarthria or abnormal eye movements (Taylor *et al.* 2004, Reynolds and Stewart 2013). So far, one patient with mutations on both *RAD50* alleles has been described as NBS-like disorder (NBSLD) because of similar clinical characteristics. The mutations lead to the expression of Rad50 protein with elongated C-terminus (Waltes *et al.* 2009). Two patients with mutations in *MRE11* genes showed NBSLD symptoms like microcephaly and chromosomal instability (Matsumoto *et al.* 2011).

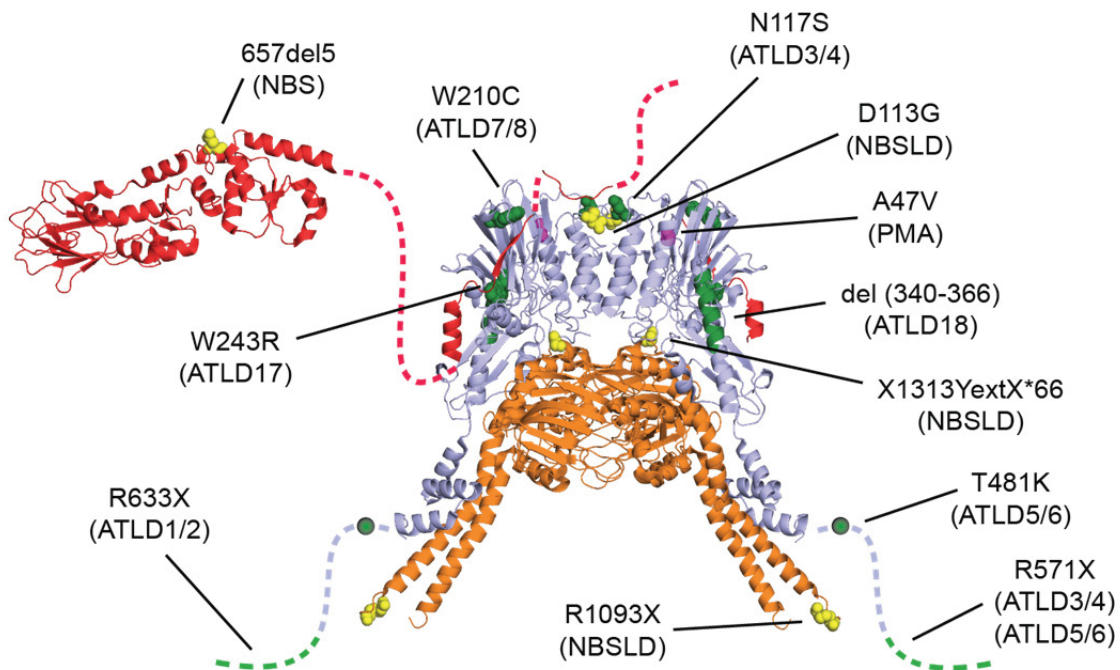


Figure 9: Model of the MRN complex and human disease. The model consists of *S. pombe* MN, Nbs1 and *Methanocaldococcus jannaschii* MR without Mre11 catalytic domain. PDB codes are 4FBW (Schiller *et al.* 2012), 3HUE (Williams *et al.* 2009), and 3AVO (Lim *et al.* 2011). MRN mutations that are found in human disorders are mapped onto a MRN model (Mre11: blue; Rad50: orange; Nbs1: red). NBS/-LD, ATLD and PMA mutations are highlighted in yellow, green and lilac, respectively. Figure is adapted from (Schiller *et al.* 2014).

It was discussed that in A-T/ATLD cells the MRN-ATM pathway is so severely damaged, that DSBs appearing during development are not recognized but with increasing lifespan accumulate to a level where ATM-independent apoptosis is induced, which leads to degeneration of neurons. Malfunctioning ATM control might also lead to re-entry of the cell-cycle of developed neurons, which then are committed to cell death. In NBS/NBSLD small amounts of partially functional MRN, which is able to activate ATM, are probably present. But after recognition of DSBs and ATM-activation, the inaccurate DSB repair leads to apoptosis during development of the nervous system, and thus to microcephaly (Reynolds and Stewart 2013). Recently, another *MRE11* mutation has been found in a PMA (progressive myoclonic ataxia) patient, which might destabilize the interaction between Mre11 and Nbs1 (Figure 9) (Miyamoto *et al.* 2014).

1.6 Aims of this work

The MRN complex plays an important role in many DNA repair processes to ensure genome integrity. During extensive research in the past, many structural and biochemical characteristics of the MRN complex were determined. Most of the structural work was performed with bacterial or archaeal MR homologs and many biochemical experiments with eukaryotic MRN confirmed studies about prokaryotic MR. Nevertheless, it is indispensable to gain knowledge about the architecture of the eukaryotic MRN complex. Also considering experimental approaches in eukaryotic organisms, high resolution structures of the MRN complex are needed. When the work for this thesis was started, crystal structures of eukaryotic Rad50 and Rad50 interacting with Mre11 or dsDNA were still missing.

The aims of this work were to characterize the architecture of the eukaryotic MRN complex from *Chaetomium thermophilum* (CtMRN) and to investigate the DNA binding of the Rad50 subunit. For crystallization of CtMR(N) various subcomplexes had to be purified and crystallization trials had to be performed. To gain structural information about CtMR(N) the structure of the CtMre11 catalytic domain had to be solved (Chapter 2.1). For a model of the MR(N) complex and to characterize the structural architecture of eukaryotic Rad50, the crystal structure of dimeric CtRad50^{NBD} in complex with the CtMre11^{RBD} or dsDNA had to be determined. Besides crystallization, the MR(N) complex from *C. thermophilum* had to be characterized biochemically using small angle

X-ray scattering (SAXS) analysis. Thereby, the ATP-dependent conformational rearrangements of MR(N) and the DNA-binding mode had to be investigated (Chapter 2.2). To analyze the role of Rad50 during DSB repair, *in vivo* plate survival assays with yeast Rad50 mutants and *in vitro* DNA binding assays had to be performed (Chapter 2.2 and Chapter 2.3).

2. Results

2.1 Structure of the catalytic domain of Mre11 from *Chaetomium thermophilum*



Structure of the catalytic domain of Mre11 from *Chaetomium thermophilum*

Florian Ulrich Seifert, Katja Lammens and Karl-Peter Hopfner

Acta Cryst. (2015). **F71**, 752–757



IUCr Journals

CRYSTALLOGRAPHY JOURNALS ONLINE

Copyright © International Union of Crystallography

Author(s) of this paper may load this reprint on their own web site or institutional repository provided that this cover page is retained. Republication of this article or its storage in electronic databases other than as specified above is not permitted without prior permission in writing from the IUCr.

For further information see <http://journals.iucr.org/services/authorrights.html>



Structure of the catalytic domain of Mre11 from *Chaetomium thermophilum*

Florian Ulrich Seifert, Katja Lammens and Karl-Peter Hopfner*

Gene Center and Department of Biochemistry, Ludwig-Maximilians-University Munich, Feodor-Lynen-Strasse 25, 81377 Munich, Germany. *Correspondence e-mail: hopfner@genzentrum.lmu.de

Received 12 March 2015

Accepted 16 April 2015

Edited by N. Sträter, University of Leipzig, Germany

Keywords: Mre11 nuclease; MRN complex.

PDB reference: Mre11 catalytic domain, 4yke

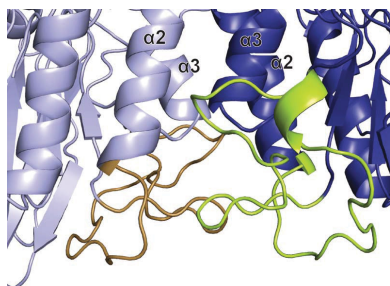
Supporting information: this article has supporting information at journals.iucr.org/f

Together with the Rad50 ATPase, the Mre11 nuclease forms an evolutionarily conserved protein complex that plays a central role in the repair of DNA double-strand breaks (DSBs). Mre11–Rad50 detects and processes DNA ends, and has functions in the tethering as well as the signalling of DSBs. The Mre11 dimer can bind one or two DNA ends or hairpins, and processes DNA endonucleolytically as well as exonucleolytically in the 3′-to-5′ direction. Here, the crystal structure of the Mre11 catalytic domain dimer from *Chaetomium thermophilum* (CtMre11^{CD}) is reported. CtMre11^{CD} crystals diffracted to 2.8 Å resolution and revealed previously undefined features within the dimer interface, in particular fully ordered eukaryote-specific insertion loops that considerably expand the dimer interface. Furthermore, comparison with other eukaryotic Mre11 structures reveals differences in the conformations of the dimer and the capping domain. In summary, the results reported here provide new insights into the architecture of the eukaryotic Mre11 dimer.

1. Introduction

Double-strand breaks (DSBs), which occur through exposure to genotoxic chemicals, ionizing radiation or reactive oxygen species or during replication-fork blockage (Costanzo *et al.*, 2001; Sutherland *et al.*, 2000; Aguilera & Gómez-González, 2008; Cadet *et al.*, 2012; Mehta & Haber, 2014), are one of the most threatening forms of DNA damage. On the other hand, DSBs are enzymatically introduced in a programmed fashion during meiosis and V(D)J or class-switch recombination during immunoglobulin development (Lam & Keeney, 2014; Gapud & Sleckman, 2011; Xu *et al.*, 2012). To prevent chromosomal rearrangements and genome instability, organisms in all kingdoms of life have developed different DSB-repair pathways (Hanahan & Weinberg, 2011; Myung, Chen *et al.*, 2001; Myung, Datta *et al.*, 2001).

DSBs are repaired by principal pathways such as non-homologous end joining (NHEJ) and homology-directed repair or homologous recombination (HR), or alternative pathways such as microhomology-mediated end joining (MMEJ) (Chiruvella *et al.*, 2013; Chapman *et al.*, 2012). In eukaryotes, the Mre11–Rad50–Nbs1 (MRN) complex plays a key role in the early steps of DSB repair, and its function in the initial detection and processing of DNA ends is important for the choice between resection-dependent (HR, MMEJ) and resection-independent (NHEJ) pathways (Lisby *et al.*, 2004; Truong *et al.*, 2013; Chiruvella *et al.*, 2013; Shibata *et al.*, 2014). MRN consists of a dimer of Mre11, two Rad50s and, in eukaryotes, Nbs1 (Lammens *et al.*, 2011; Schiller *et al.*, 2012; Möckel *et al.*, 2012; Lim *et al.*, 2011; Arthur *et al.*, 2004; Das *et al.*, 2010; Limbo *et al.*, 2012). The Mre11 nuclease forms the enzymatically active centre of the complex. *In vitro*, Mre11 is



© 2015 International Union of Crystallography

Table 1
Crystallization.

Method	Hanging-drop vapour diffusion
Plate type	24-well plates (Crystalgen SuperClear Plates, pregreased; Jena Bioscience)
Temperature (K)	292
Protein concentration (mg ml ⁻¹)	7.0
Buffer composition of protein solution	200 mM NaCl, 25 mM Tris pH 8.0
Composition of reservoir solution	200 mM ammonium citrate tribasic pH 6.8–7.0, 18% (w/v) PEG 3350
Volume and ratio of drop	3 µl; 2:1 protein:reservoir
Volume of reservoir (µl)	500

able to process DNA exonucleolytically in the 3'-to-5' direction and cuts ssDNA endonucleolytically (Trujillo *et al.*, 1998; Hopfner *et al.*, 2001). To date, Mre11 has been found as a dimer in all available crystal structures. Although comparison of these structures reveals a highly conserved overall shape of the protein, consisting of an N-terminal phosphodiesterase domain followed by a capping domain, the dimer angle between the Mre11 protomers can adopt remarkably different conformations (Schiller *et al.*, 2014). In eukaryotes, the dimer angle is stabilized by latching loops that provide a critical interaction site for Nbs1 with Mre11 (Schiller *et al.*, 2012; Park *et al.*, 2011). However, a substantial portion of the functionally important, eukaryote-specific latching loops remained disordered in previously determined structures (Schiller *et al.*, 2012; Park *et al.*, 2011). Here, we present the crystal structure of the Mre11 catalytic domain dimer from the thermophilic eukaryote *Chaetomium thermophilum* (CtMre11^{CD}) at 2.8 Å resolution. We find interpretable electron density for the entire latching loops, revealing an unexpected expansion of the Mre11 dimer interface by this functionally critical region.

2. Materials and methods

2.1. Protein expression and purification

For co-expression, open reading frames for the components of the MRN head complex (MRN^{HC}) were cloned into two different expression vectors. The Mre11 sequence coding for amino acids 1–537 was cloned into pET-21b vector (Novagen) with NdeI and NotI, and a C-terminal His₆ tag from the vector was fused to the polypeptide chain. Three constructs coding for the Rad50 N- and C-termini (amino acids 1–224 and 1103–1315, respectively) as well as Nbs1 (amino acids 565–714) were first cloned into a modified polycistronic pET-29 vector with NdeI/NotI and then combined with AarI/AscI into a single vector. After co-transformation and induction at an OD₆₀₀ of 0.8 with IPTG (0.3 mM final concentration), expression in *Escherichia coli* Rosetta (DE3) cells took place overnight at 18° C. After cell resuspension in lysis buffer (300 mM NaCl, 25 mM Tris pH 8.0) plus 10 mM imidazole and disruption by sonication, cell debris was removed by centrifugation. The supernatant was incubated with nickel-NTA (Qiagen) for 2 h at 7° C. The nickel-NTA column was washed with 10 column volumes (CVs) of lysis buffer and 5 CVs each of lysis buffer containing 20 and then 50 mM imidazole. The protein complex

Table 2
Data collection and processing.

Values in parentheses are for the outer shell.

Diffraction source	Beamline X06SA, SLS
Wavelength (Å)	0.979600
Temperature (K)	199.4
Detector	MAR Mosaic 225 CCD
Crystal-to-detector distance (mm)	270.00
Rotation range per image (°)	1.0
Total rotation range (°)	180
Exposure time per image (s)	1.0
Space group	<i>P</i> 2 ₁ 2 ₁ 2 ₁
<i>a</i> , <i>b</i> , <i>c</i> (Å)	56.7, 56.6, 304.6
α , β , γ (°)	90, 90, 90
Mosaicity (°)	0.245
Resolution range (Å)	50.00–2.78 (2.95–2.78)
Total No. of reflections	168505 (22412)
No. of unique reflections	25153 (3657)
Completeness (%)	98.1 (89.5)
Multiplicity	6.7 (6.13)
$\langle I/\sigma(I) \rangle$	11.18 (1.81)
CC _{1/2}	99.6 (74.5)
<i>R</i> _{meas}	0.136 (0.962)
Overall <i>B</i> factor from Wilson plot (Å ²)	65.1

was eluted with lysis buffer containing 250 mM imidazole. Subsequently, size-exclusion chromatography (Superdex 200 26/60, GE Healthcare) was performed (buffer: 200 mM NaCl, 25 mM Tris pH 8.0); the purified protein was concentrated to 7.0 mg ml⁻¹ and aliquots were frozen in liquid nitrogen.

2.2. Crystallization

Crystallization trials with the MRN^{HC} protein were performed by hanging-drop vapour diffusion (Table 1). Small plate-shaped crystals appeared after three months, and after a further month these were transferred into reservoir solution containing 10% (v/v) 2,3-butanediol for cryoprotection. The crystals were flash-cooled and stored in liquid nitrogen.

2.3. Data collection and processing

Data were collected on the X06SA beamline at the Swiss Light Source (SLS), Villigen, Switzerland. The data were indexed and integrated with *XDS* (Kabsch, 2010*a,b*). Data-collection statistics are shown in Table 2.

2.4. Structure solution and refinement

The *L*-test from *POINTLESS* indicated the presence of twinning and further analysis with *phenix.xtriage* identified the twin operator as *k*, *h*, $-l$ (Adams *et al.*, 2010; Winn *et al.*, 2011; Evans, 2006, 2011). The structure of the *C. thermophilum* Mre11 catalytic domain (CtMre11^{CD}; amino acids 4–412) was solved by molecular replacement with *Phaser* (McCoy *et al.*, 2007). The search model was the structure of monomeric *Schizosaccharomyces pombe* Mre11 (PDB entry 4fbq; Schiller *et al.*, 2012), which was co-crystallized with an Nbs1 construct. The structure was refined with *PHENIX*, accounting for twinning (Adams *et al.*, 2010), in combination with manual model building using *Coot* (Emsley & Cowtan, 2004; Emsley *et al.*, 2010). An initial round of rigid-body refinement was followed by restrained refinement with TLS refinement. The

$F_o - F_c$ map revealed density for two manganese ions in the active site, and water molecules were added manually. Structure factors and atomic coordinates of CtMre11^{CD} have been deposited in the Protein Data Bank with accession code 4yke and refinement statistics are reported in Table 3.

3. Results and discussion

We crystallized the catalytic domain of CtMre11 (CtMre11^{CD}; amino acids 4–412) and determined the structure by molecular replacement using *S. pombe* Mre11 (SpMre11^{CD}) as the search model (PDB entry 4fbq; Schiller *et al.*, 2012). The crystallization screen contained the MRN head complex (MRN^{HC}) and, presumably owing to proteolysis, CtMre11^{CD} crystals formed. CtMre11^{CD} contains an N-terminal nuclease domain, which is characterized by a phosphodiesterase motif, and a C-terminal capping domain (amino acids 300–412; Fig. 1*a*). The asymmetric unit consists of two Mre11 protomers that together form the characteristic, previously observed Mre11 dimer mediated by interactions between α -helices $\alpha 2$ and $\alpha 3$ (Hopfner *et al.*, 2001; Schiller *et al.*, 2012; Fig. 1 and Supplementary Fig. S1). The interface between these two helices consists of mainly hydrophobic residues: Tyr70, Met73, Leu139 and Val142. The dimer interface is extended by Arg66, which forms hydrogen bonds to Asn62, Ser129 and Leu134 from the other protomer (Fig. 2*a*). The two manganese ions that are present in the nuclease domains of both CtMre11^{CD} protomers are coordinated in a similar fashion by the absolutely conserved residues Asp17, His19, Asp57, Asn124, His213, His241 and His243 (Schiller *et al.*, 2012; Fig. 2*b*).

Table 3

Structure refinement.

Values in parentheses are for the outer shell.

Resolution range (Å)	49.52–2.78 (2.89–2.78)
Completeness (%)	98.2
No. of reflections, working set	25153 (2253)
No. of reflections, test set	1251 (110)
Final R_{work} (%)	19.8 (30.8)
Final R_{free} (%)	23.1 (40.1)
No. of non-H atoms	
Protein	6548
Manganese	4
Water	60
Total	6612
R.m.s. deviations	
Bonds (Å)	0.003
Angles (°)	0.683
Average B factors (Å ²)	
Protein	83.9
Manganese	60.0
Water	45.0
Ramachandran plot	
Favoured regions (%)	96
Additionally allowed (%)	4
Outliers (%)	0

Structural comparison of the individual Mre11 protomers of CtMre11^{CD} with *Homo sapiens* Mre11^{CD} (HsMre11^{CD}) and SpMre11^{CD} reveals that they have similar structures, consistent with their high sequence identities of 46 and 61%, respectively (Schiller *et al.*, 2012; Park *et al.*, 2011; Sievers *et al.*, 2011; Goujon *et al.*, 2010). CtMre11^{CD} largely adopts the conformation of SpMre11^{CD}, but is even more compact than either Nbs1-bound or unbound SpMre11^{CD} owing to an

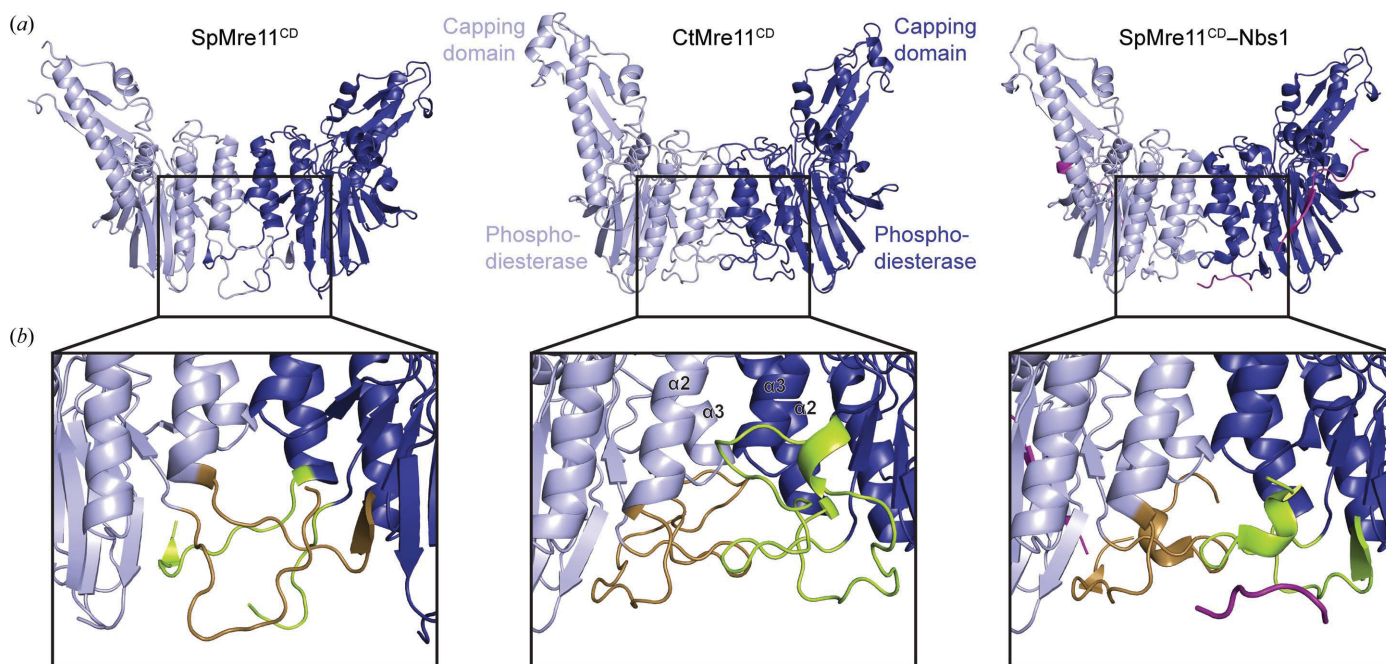


Figure 1

Crystal structure of CtMre11^{CD} and comparison with Nbs1-bound and unbound SpMre11^{CD} structures (SpMre11^{CD} and SpMre11^{CD}-Nbs1, respectively). (*a*) Structures of the dimer of the catalytic domains of SpMre11^{CD}, CtMre11^{CD} and SpMre11^{CD} in complex with the Nbs1 peptide (purple; SpMre11^{CD}-Nbs1; PDB entries 4fcx, 4yke and 4fbw, respectively). The models are displayed in ribbon representation. Mre11 protomers are highlighted in light and deep blue. (*b*) Details of the Mre11 dimer interface and the eukaryotic insertion loops (lime and brown). The conformation of the CtMre11^{CD} insertion loops is similar to the conformation of the loops in the SpMre11^{CD}-Nbs1 structure.

approximately 5 Å movement of the capping domain towards the nuclease active site (Fig. 2c). In contrast, the conformation of the Mre11^{CD} dimer displays greater variation between the eukaryotic Mre11 structures. CtMre11^{CD} and SpMre11^{CD} adopt similar conformations yet differ with respect to the human Mre11^{CD} dimer, in which a significantly different interface between the two nuclease domains is stabilized by a disulfide bond. This disulfide bond is absent in the *S. pombe*

structures and the presented CtMre11 structure (Park *et al.*, 2011; Schiller *et al.*, 2012).

Interestingly, comparison with SpMre11^{CD} and the SpMre11^{CD}–Nbs1 complex reveals that CtMre11^{CD} has fully ordered insertion loops even in the absence of Nbs1, and we are now able to model the entire eukaryote-specific loop insertion that plays a critical role in the interaction with Nbs1 and in damage signalling (Figs. 1 and 2d). In the case of

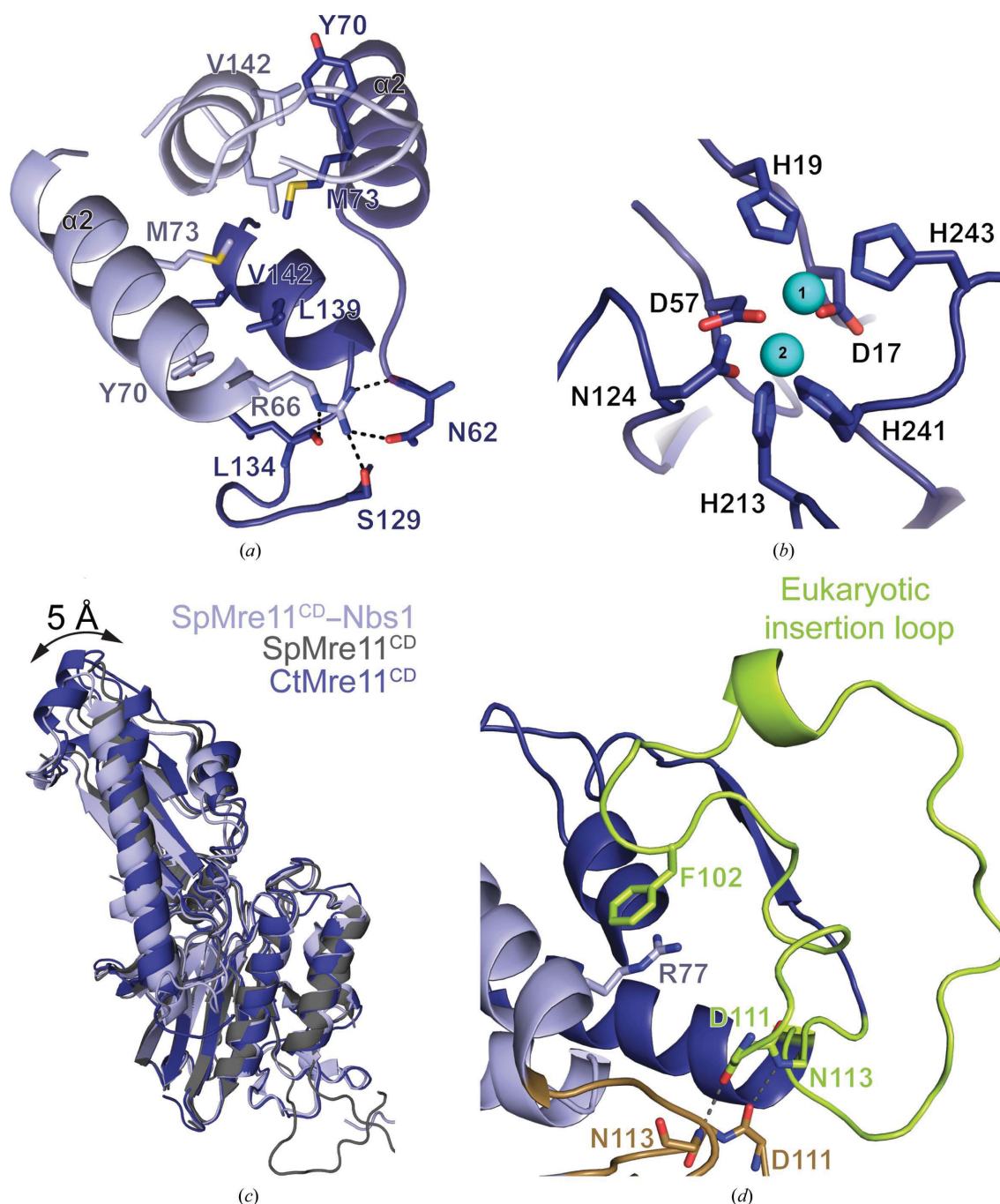


Figure 2

Details of the Mre11^{CD} crystal structure from *C. thermophilum*. (a) Detailed view of the CtMre11^{CD} dimer interface consisting of α -helices $\alpha 2$ and $\alpha 3$ from each protomer. (b) CtMre11^{CD} nuclease active site with two coordinated manganese ions (cyan). (c) Overlay of SpMre11^{CD} (grey), SpMre11^{CD}–Nbs1 (light blue) and CtMre11^{CD} (deep blue) by alignment of the nuclease domains onto the nuclease domain of CtMre11^{CD} indicates the movement of the capping domain by up to 5 Å. (d) Fully modelled eukaryotic insertion loop (lime and brown). The interaction between Arg77 and Phe102 is highlighted. Selected residues are depicted as colour-coded sticks and annotated. Hydrogen bonds in (a) and (d) are highlighted as dashed lines.

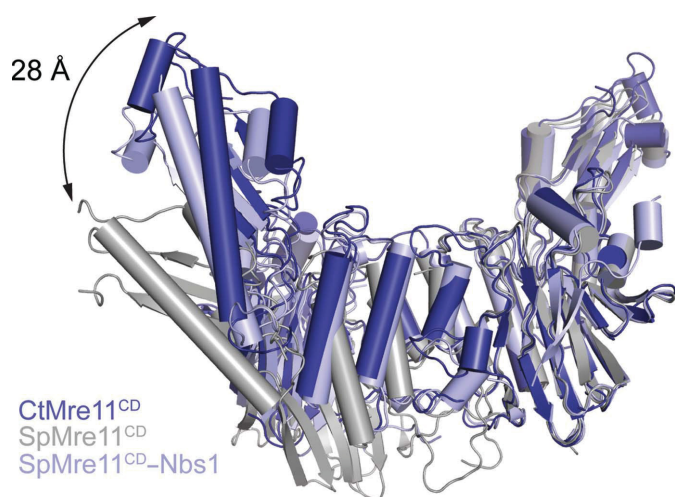


Figure 3

Overlay of CtMre11^{CD}, SpMre11^{CD} and SpMre11^{CD}-Nbs1. Structures of SpMre11^{CD} (grey) and SpMre11^{CD}-Nbs1 (light blue) dimers are aligned via one of the two CtMre11^{CD} (dark blue) protomers to show the variability of the dimer interface and dimer angle. The distance between the capping domains of CtMre11^{CD} and SpMre11^{CD} reaches 28 Å.

SpMre11^{CD}, Nbs1 binding partially orders the insertion loops, resulting in a more compact Mre11 dimer (Schiller *et al.*, 2012; Fig. 1*b*). Indeed, the dimeric conformation of CtMre11^{CD} with fully ordered insertion loops is very similar to that of SpMre11^{CD} bound to Nbs1, but is quite distinct from the more open SpMre11^{CD} dimer conformation in the absence of Nbs1 (Fig. 3). The Nbs1-binding site bridging the SpMre11 dimer is occupied in the presented structure by symmetry-related molecules that may stabilize the insertion loops. This dimeric structure of Mre11 enables each nuclease active site to bind a dsDNA substrate and thus allows the bridging of two DNA ends (Williams *et al.*, 2008). Interestingly, the insertion loops extend the Mre11 dimer interface through reaching across the lateral CtMre11^{CD} dimer interface. Notably, the conserved phenylalanine (Phe102 in *C. thermophilum*) stacks with and stabilizes Arg77, a critical residue in stabilizing the Mre11 dimer interface (Schiller *et al.*, 2012), of the opposing protomer (Fig. 2*d*). As a result, the 1490 Å² Mre11–Mre11 interface of CtMre11^{CD} is twice as large as that of Mre11 from the thermophilic archaeon *Pyrococcus furiosus* (Krissinel & Henrick, 2007), in which the insertion loops are absent.

In summary, this structure of CtMre11^{CD} fully defines the eukaryotic insertion loops and shows that these loops expand the Mre11 dimer interface (Hopfner *et al.*, 2001). Furthermore, our results show considerable flexibility not only between the Mre11 protomers but also between the phosphodiesterase domain and the capping domain.

Acknowledgements

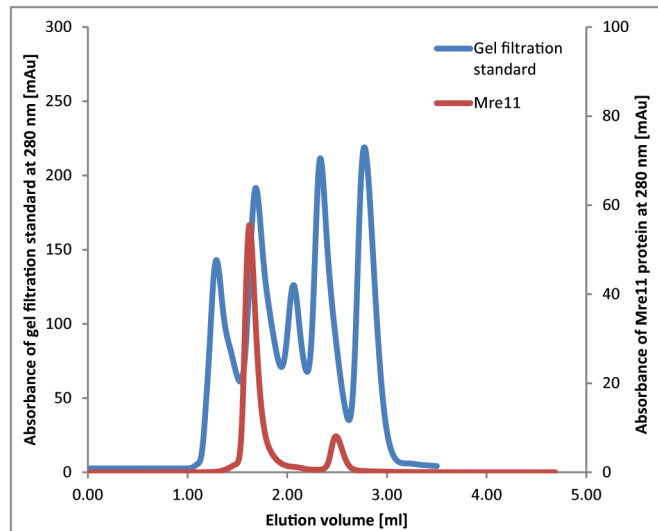
We thank Brigitte Kessler for help with cloning and protein purification and Robert Byrne for comments on the manuscript, as well as the staff of the Swiss Light Source, Villigen, Switzerland for technical support. This work was funded by the German Research Council projects GRK1721 and SFB684, the Center for Integrated Protein Sciences Munich

and the European Research Council Advanced Grant ATMMACHINE to K-PH.

References

- Adams, P. D. *et al.* (2010). *Acta Cryst.* **D66**, 213–221.
- Aguilera, A. & Gómez-González, B. (2008). *Nature Rev. Genet.* **9**, 204–217.
- Arthur, L. M., Gustausson, K., Hopfner, K.-P., Carson, C. T., Stracker, T. H., Karcher, A., Felton, D., Weitzman, M. D., Tainer, J. & Carney, J. P. (2004). *Nucleic Acids Res.* **32**, 1886–1893.
- Cadet, J., Ravanat, J. L., TavernaPorro, M., Menoni, H. & Angelov, D. (2012). *Cancer Lett.* **327**, 5–15.
- Chapman, J. R., Taylor, M. R. G. & Boulton, S. J. (2012). *Mol. Cell*, **47**, 497–510.
- Chiruvella, K. K., Liang, Z. & Wilson, T. E. (2013). *Cold Spring Harb. Perspect. Biol.* **5**, a012757.
- Costanzo, V., Robertson, K., Bibikova, M., Kim, E., Grieco, D., Gottesman, M., Carroll, D. & Gautier, J. (2001). *Mol. Cell*, **8**, 137–147.
- Das, D. *et al.* (2010). *J. Mol. Biol.* **397**, 647–663.
- Emsley, P. & Cowtan, K. (2004). *Acta Cryst.* **D60**, 2126–2132.
- Emsley, P., Lohkamp, B., Scott, W. G. & Cowtan, K. (2010). *Acta Cryst.* **D66**, 486–501.
- Evans, P. (2006). *Acta Cryst.* **D62**, 72–82.
- Evans, P. R. (2011). *Acta Cryst.* **D67**, 282–292.
- Gapud, E. J. & Sleckman, B. P. (2011). *Cell Cycle*, **10**, 1928–1935.
- Goujon, M., McWilliam, H., Li, W., Valentin, F., Squizzato, S., Paern, J. & Lopez, R. (2010). *Nucleic Acids Res.* **38**, W695–W699.
- Hanahan, D. & Weinberg, R. A. (2011). *Cell*, **144**, 646–674.
- Hopfner, K. P., Karcher, A., Craig, L., Woo, T. T., Carney, J. P. & Tainer, J. A. (2001). *Cell*, **105**, 473–485.
- Kabsch, W. (2010*a*). *Acta Cryst.* **D66**, 125–132.
- Kabsch, W. (2010*b*). *Acta Cryst.* **D66**, 133–144.
- Krissinel, E. & Henrick, K. (2007). *J. Mol. Biol.* **372**, 774–797.
- Lam, I. & Keeney, S. (2014). *Cold Spring Harb. Perspect. Biol.* **7**, a016634.
- Lammens, K., Bemeleit, D. J., Möckel, C., Clausing, E., Schele, A., Hartung, S., Schiller, C. B., Lucas, M., Angermüller, C., Söding, J., Strässer, K. & Hopfner, K. P. (2011). *Cell*, **145**, 54–66.
- Lim, H. S., Kim, J. S., Park, Y. B., Gwon, G. H. & Cho, Y. (2011). *Genes Dev.* **25**, 1091–1104.
- Limbo, O., Moiani, D., Kertokallio, A., Wyman, C., Tainer, J. A. & Russell, P. (2012). *Nucleic Acids Res.* **40**, 11435–11449.
- Lisby, M., Barlow, J. H., Burgess, R. C. & Rothstein, R. (2004). *Cell*, **118**, 699–713.
- McCoy, A. J., Grosse-Kunstleve, R. W., Adams, P. D., Winn, M. D., Storoni, L. C. & Read, R. J. (2007). *J. Appl. Cryst.* **40**, 658–674.
- Mehta, A. & Haber, J. E. (2014). *Cold Spring Harb. Perspect. Biol.* **6**, a016428.
- Möckel, C., Lammens, K., Schele, A. & Hopfner, K.-P. (2012). *Nucleic Acids Res.* **40**, 914–927.
- Myung, K., Chen, C. & Kolodner, R. D. (2001). *Nature (London)*, **411**, 1073–1076.
- Myung, K., Datta, A. & Kolodner, R. D. (2001). *Cell*, **104**, 397–408.
- Park, Y. B., Chae, J., Kim, Y. C. & Cho, Y. (2011). *Structure*, **19**, 1591–1602.
- Schiller, C. B., Lammens, K., Guerini, I., Coords, B., Feldmann, H., Schlauderer, F., Möckel, C., Schele, A., Strässer, K., Jackson, S. P. & Hopfner, K.-P. (2012). *Nature Struct. Mol. Biol.* **19**, 693–700.
- Schiller, C. B., Seifert, F. U., Linke-Winnebeck, C. & Hopfner, K.-P. (2014). *Cold Spring Harb. Perspect. Biol.* **6**, a017962.
- Shibata, A. *et al.* (2014). *Mol. Cell*, **53**, 7–18.
- Sievers, F., Wilm, A., Dineen, D., Gibson, T. J., Karplus, K., Li, W., Lopez, R., McWilliam, H., Remmert, M., Söding, J., Thompson, J. D. & Higgins, D. G. (2011). *Mol. Syst. Biol.* **7**, 539.
- Sutherland, B. M., Bennett, P. V., Sidorkina, O. & Laval, J. (2000). *Proc. Natl Acad. Sci. USA*, **97**, 103–108.

- Trujillo, K. M., Yuan, S.-S. F., Lee, E.-Y. P. & Sung, P. (1998). *J. Biol. Chem.* **273**, 21447–21450.
- Truong, L. N., Li, Y., Shi, L. Z., Hwang, P. Y.-H., He, J., Wang, H., Razavian, N., Berns, M. W. & Wu, X. (2013). *Proc. Natl Acad. Sci. USA*, **110**, 7720–7725.
- Williams, R. S., Moncalian, G., Williams, J. S., Yamada, Y., Limbo, O., Shin, D. S., Grocock, L. M., Cahill, D., Hitomi, C., Guenther, G., Moiani, D., Carney, J. P., Russell, P. & Tainer, J. A. (2008). *Cell*, **135**, 97–109.
- Winn, M. D. *et al.* (2011). *Acta Cryst. D* **67**, 235–242.
- Xu, Z., Zan, H., Pone, E. J., Mai, T. & Casali, P. (2012). *Nature Rev. Immunol.* **12**, 517–531.



Supplementary Figure S1: Elution profile of CtMre11CD and gel filtration standard (Bio-Rad) on analytical size exclusion chromatography column (S200 increase 5/150 GL). CtMre11CD (red) compared to gel filtration standard (blue): 1st peak (670 kDa), 2nd peak (158 kDa), 3rd peak (44 kDa), 4th peak (17 kDa), 5th peak (1.35 kDa). The catalytic domain of CtMre11 elutes at approximately the volume of a globular protein with a molecular weight of 158 kDa. These data show that Mre11 forms a defined multimer, given its non-globular shape presumably a dimer.

2.2 Structural mechanism of ATP-dependent DNA binding and DNA end bridging by eukaryotic Rad50

(Manuscript in preparation)

Structural mechanism of ATP-dependent DNA binding by eukaryotic Rad50

Florian Ulrich Seifert¹, Katja Lammens¹, Gabriele Stoehr¹, Brigitte Keßler¹, Karl-Peter Hopfner^{1,2*}

¹Department of Biochemistry and Gene Center, Ludwig-Maximilians-University, Munich

²Center for Integrated Protein Sciences, Munich

*Correspondence to: Prof. Dr. Karl-Peter Hopfner
Gene Center
Feodor-Lynen-Str. 25
81377 Munich, Germany
Tel. +49 (0)89 2180 76953
Fax. +49 (0)89 2180 76999
email: hopfner@genzentrum.lmu.de
www.hopfner.genzentrum.lmu.de

Summary

The Mre11-Rad50-Nbs1 (MRN) complex is a central factor in the repair of DNA double-strand breaks (DSBs). The ATP-dependent mechanisms of how MRN detects and endonucleolytically processes DNA ends for the repair by microhomology-mediated end joining or further resection in homologous recombination are still unclear. Here we report the crystal structures of the ATP γ S bound dimer of the Rad50^{NBD} (nucleotide-binding domain) from the thermophilic eukaryote *Chaetomium thermophilum* (Ct) in complex with either DNA or CtMre11^{RBD} (Rad50-binding domain) along with biochemical studies. Our analyses provide a structural framework for the architecture of the eukaryotic Mre11-Rad50 complex and clarify how MRN binds internal DNA as well as cohesive ends with 3' tails in an ATP-dependent fashion.

Introduction

DNA double-strand breaks (DSBs) threaten genome stability in all kingdoms of life. They arise during replication fork collapse and can be results of ionizing radiation, reactive oxygen species (ROS) or genotoxic chemicals (Sutherland *et al.* 2000 , Costanzo *et al.* 2001, Pommier *et al.* 2003, Mahaney *et al.* 2009). Un- or misrepaired DSBs can result in cell death or gross chromosomal aberrations and DSB induced genome instability is a hallmark of cancer (Hanahan and Weinberg 2011). DSBs are also enzymatically generated physiological intermediates in meiotic recombination, V(D)J and class switch recombination as well as yeast mating type switching (Gapud and Sleckman 2011, Haber 2012, Xu *et al.* 2012, Lam and Keeney 2015). All kingdoms of life require mechanisms to sensitively detect and repair DSBs in order to maintain the integrity of the genome.

Several pathways can repair DSBs. In canonical non-homologous end joining (c-NHEJ), the DNA ends are ligated directly in a reaction that depends on Ku and Ligase IV. However, a Ku and Ligase IV independent end-joining pathway also exists and is denoted alternative NHEJ (alt-NHEJ). Hereby, the DNA ends often undergo limited processing by endo/exonucleases and are joined at microhomologies (denoted also microhomology-mediated end joining, MMEJ). These template-independent end-joining reactions are

error-prone and can result in loss of genetic information or chromosomal alterations (Chiruvella *et al.* 2013).

The template-dependent homologous recombination (HR) repairs DNA ends in a typically error-free manner, but is limited to S and G2 phases of the cell cycle. HR shares the initial DNA processing steps with MMEJ, but in HR the DNA ends are further resected to several hundred bases long 3' single-strand tails. These tails are paired with homologous regions of the sister chromatid (or the homologous chromosome in meiosis) and are extended by DNA polymerases, thereby restoring the disrupted genetic information. The choice between NHEJ and HR is regulated in a cell cycle dependent manner (Chiruvella *et al.* 2013, Symington 2014).

The Mre11-Rad50-Nbs1 complex and its archaeal Mre11-Rad50, bacterial SbcC-SbcD and bacteriophage gp46-gp47 homologs, collectively denoted MRN or MR, are central factors in the cellular processes surrounding DSBs, hairpin structures, DNA ends and telomeres (Schiller *et al.* 2014). MRN is implicated in both end-joining and HR and among the first repair factors at DSBs in eukaryotic cells (Lisby *et al.* 2004, Mladenov and Iliakis 2011). MRN is an ATP-dependent endo/exonuclease that processes DNA ends in HR and MMEJ. It displays 3'–5' dsDNA exonuclease activity, hairpin opening activity, ssDNA endonuclease activity and an ATP-dependent dsDNA endonuclease activity (Paull and Gellert 1998, Connelly *et al.* 1999, Hopfner *et al.* 2000a, Trujillo and Sung 2001, Truong *et al.* 2013, Cannavo and Cejka 2014). In the latter, MRN cleaves the 5' strand near or at some distance from the DSB in a reaction that also requires the Sae2/CtIP protein in eukaryotes (Cannavo and Cejka 2014). The nuclease activity of MRN helps to remove Ku from DNA ends, can clear “dirty” DNA ends and generates initial 3' overhangs for MMEJ or further resection in HR (Garcia *et al.* 2011a, Langerak *et al.* 2011, Truong *et al.* 2013, Cannavo and Cejka 2014). MRN also recruits other repair factors to DSBs and helps eliciting the DNA damage response by activating the ataxia telangiectasia mutated (ATM) kinase (Lisby *et al.* 2004, Berkovich *et al.* 2007, Limbo *et al.* 2007, Mimitou and Symington 2008, Deshpande *et al.* 2014). Hypomorphic mutations in human MRN result in genetic instability and cause ataxia telangiectasia like disorder (ATLD), Nijmegen breakage syndrome (NBS), NBS like disorder (NBSLD) and progressive myoclonic ataxia (PMA) that are characterized to various extents by cancer predisposition, immune deficiency and neurological disorders (Carney *et al.* 1998, Varon

et al. 1998, Stewart *et al.* 1999, Waltes *et al.* 2009, Matsumoto *et al.* 2011, Miyamoto *et al.* 2014).

The MRN complex consists of two subunits of the endo/exonuclease Mre11, two subunits of the ATPase Rad50, plus the Nbs1 subunit (Lammens *et al.* 2011, Lim *et al.* 2011, Möckel *et al.* 2012, Schiller *et al.* 2012). Nbs1 (denoted Xrs2 in *Saccharomyces cerevisiae*) is only found in eukaryotes and is important for ATM activation, nuclear localization of MRN and recruitment of other repair factors (Desai-Mehta *et al.* 2001, You *et al.* 2005, Limbo *et al.* 2007, Chen *et al.* 2008, Mimitou and Symington 2008). Mre11 together with the Rad50 nucleotide-binding domains (NBDs) and the Mre11-interacting motif of Nbs1 forms the globular catalytic domain of MRN that binds and processes DNA in an ATP-dependent fashion. Rad50 further possesses a 15–50 nm long coiled-coil domain with a terminal Zn-hook dimerization motif (Schiller *et al.* 2014). The precise mechanistic functions of the coiled-coil domains are still unclear, but they are important for functions of the complex in NHEJ, ATM activation and DNA end processing (Hohl *et al.* 2011, Lee *et al.* 2013, Roset *et al.* 2014).

Structural studies revealed that ATP induces large conformational changes in the MR complex. While the Mre11 nuclease sites are accessible for dsDNA in the ATP-free form, ATP binding engages the two Rad50 NBDs and the resulting ATP-bound NBD dimer blocks the Mre11 DNA-binding cleft (Lim *et al.* 2011, Möckel *et al.* 2012). Mutational analyses showed that ATP binding but not hydrolysis by Rad50 is important for checkpoint activation, DNA tethering and telomere maintenance, whereas both ATP binding and ATP hydrolysis are required for DSB repair and DNA processing (Lee *et al.* 2013, Deshpande *et al.* 2014, Rojowska *et al.* 2014). These data suggest that the ATP-bound form of Rad50 functions in DNA tethering and ATM activation, while a full ATP binding and hydrolysis cycle is critical for efficient DNA processing.

The mechanism for the ATP-dependent DNA binding and DNA tethering by Rad50 is still unclear. We recently identified a DNA-binding motif on bacterial Rad50 (Rojowska *et al.* 2014), however it remained unresolved how ATP promotes a high affinity DNA binding conformation. Here we report the crystal structure of the *Chaetomium thermophilum* CtRad50^{NBD} dimer in complexes with ATP γ S and DNA or the Rad50-binding domain of Mre11 (Mre11^{RBD}). Although the general architecture of Mre11-Rad50 is similar to that of prokaryotic homologs, we also observe some notable

differences, including a substantially enlarged Mre11-Rad50 interaction interface. Most importantly, we present the crystal structure of CtRad50^{NBD} in complex with ATP γ S and dsDNA. This structure clarifies how Rad50 binds to DNA in an ATP-dependent fashion and shows that Rad50 dimers recognize approximately 18 base pairs of dsDNA across the NBD dimer interface. Interestingly, fluorescence anisotropy measurements further show that Rad50 not only binds dsDNA of sufficient length but can also efficiently bind shorter DNA molecules if they have cohesive 3' tails. Functional studies indicate that the presented DNA binding conformation is also critical for the DNA repair functions of Rad50. This suggests that the observed DNA interaction is not only a critical form in DNA signaling and tethering, but also an important intermediate in DNA end processing. Together, our studies establish a framework for the architecture and ATP-dependent dynamics of the eukaryotic Mre11-Rad50 catalytic head module and reveal how Rad50 binds dsDNA and bridges DNA ends in an ATP-dependent manner.

Results

Structure of *C. thermophilum* Rad50^{NBD} in complex with ATP γ S:Mg²⁺ and the Rad50-binding domain of Mre11

To obtain the structure of a eukaryotic Rad50 protein and its complex with Mre11^{RBD}, we co-purified CtRad50^{NBD} with the putative Rad50-binding domain of Mre11 (suppl. Fig. S1). Crystals containing a Rad50^{NBD} dimer bound to two Mre11^{RBD}s (residues 438–531) and two ATP γ S:Mg²⁺ molecules in the asymmetric unit diffracted to 3.0 Å and we obtained experimental phases by a single-wavelength anomalous diffraction experiment with selenomethionine-derivatized protein. Data collection and refinement statistics are summarized in supplementary Table S1.

Two CtRad50^{NBD}s assemble into a dimer with two ATP γ S:Mg²⁺ molecules sandwiched in the dimer interface (Fig. 1A). Each of the two ATP γ S:Mg²⁺ molecules is bound to opposing Walker A, Walker B and signature motifs in a generally symmetric dimer conformation (Fig. 1B) (Hopfner *et al.* 2000b). In general, our structure represents a pre-hydrolysis state (see also below for the DNA complex) with a tight coordination of the three phosphates by residues from Walker A and signature motifs, a tightly coordinated

Mg²⁺ ion and a formed catalytic “dyad” between Glu1238 (Walker B motif) and His1275 (His-switch) (Zaitseva *et al.* 2005).

The two protruding coiled-coil domains each bind one helical Mre11^{RBD} on the “outside” face of the Rad50^{NBD} dimer. Mre11^{RBD} is a five-membered helical bundle that predominantly interacts with the C-terminal α -helix of the antiparallel Rad50 coiled-coil domain (Fig. 1C). Hereby, the first three α -helices of Mre11^{RBD} bind approximately nine turns of the C-terminal (α H) and three turns of the N-terminal (α G) α -helix of the coiled-coil. The short fourth helix caps the RBD, while the fifth helix forms a “spine” that protrudes backwards to the lobe I of Rad50^{NBD}. The structure of eukaryotic Mre11^{RBD}-Rad50^{NBD} generally resembles that of its prokaryotic homologs but it reveals notable differences and extensions that are described in more detail in the following section.

Comparison to prokaryotic Mre11-Rad50

Compared to the previously determined structures of prokaryotic Rad50 and Mre11, CtRad50^{NBD} and CtMre11^{RBD} contain a number of structural insertions (Fig. 2, suppl. Fig. S2). The perhaps most notable and unexpected of these elements is the substantially enlarged Rad50-binding domain of Mre11. RBDs of bacterial SbcD (*Thermotoga maritima*) and archaeal Mre11 (*Methanocaldococcus jannaschii*) correspond to α -helices 1–2 or 1–3 of the RBD of CtMre11. Of note, the location of the CtMre11^{RBD} helix α 5, pointing towards the Rad50^{NBD} suggests that the remaining C-terminal polypeptide chain of eukaryotic Mre11 (about 100-200 additional amino acids depending on the species) is situated in the vicinity of the globular “head” of MRN, consistent with findings that identify the C-terminal region as important for stable DNA and Xrs2 binding as well as for meiotic recombination (Furuse *et al.* 1998, Usui *et al.* 1998, Bhattacharyya *et al.* 2008). Another indication for the importance of the conformation of the Mre11^{RBD} domain is the fact that a mutation in this domain (T481→K in human; Q489 in *C. thermophilum*) was found in a patient with AT-like disease (ATLD5/6) (Delia *et al.* 2004).

A noteworthy insertion is insertion II that is located in close proximity to the ATP-coordinating residues 62–68 (suppl. Fig. S2). This element forms a short α -helix at the Rad50-Rad50 interface in the ATP-bound state. Interestingly, the regions around

insertions I and II harbor three Rad50S mutations (Ser14→Pro, Arg20→Met and Val63→Glu in *S. cerevisiae*), suggesting that these insertions could play a role in the regulation of MRN activity by CtIP/Sae2 (Alani *et al.* 1990, Cannavo and Cejka 2014). Compared to prokaryotic Rad50, the CtRad50 dimer groove is enlarged by β -hairpin insertion III on top of lobe I and by insertion IV, a β -hairpin (β 8 and β 9) that binds along the coiled-coil.

Opposite from insertion II is another notable feature of eukaryotic Rad50 that concerns the ATP-binding site. The adenine moiety is bound by the opposing protomer at a rather hydrophobic face formed by Met1194 and Met1201. These methionines are part of an intriguing eukaryote-specific sulfur rich cluster that consists of two to four methionines (166, 1194, 1201 and 1203) plus a highly conserved cysteine (Cys1207) in the eukaryotic signature motif (suppl. Fig 2). A sulfur rich cluster at the ATP-binding site has been shown to regulate the ATPase activity of the ATP synthase in response to ROS (Buchert *et al.* 2012). Considering that ATM is directly activated by ROS (Guo *et al.* 2010), the unusual clustering of sulfur containing residues at the ATP-binding site of eukaryotic Rad50 raises the question as to whether MRN is also subject to regulation by ROS.

In summary, our structure defines notable features and expansions of eukaryotic Rad50 as compared to its simpler prokaryotic homologs and provides a framework to rationalize many functional and disease related mutations in Mre11^{RBD} and Rad50^{NBD} (see discussion).

Architecture and dynamics of the eukaryotic Mre11-Rad50 head complex

The structure of CtMre11^{RBD}-Rad50^{NBD} reported here together with a structure of the catalytic domain dimer of CtMre11 (CtMre11^{CD}) (Seifert *et al.* 2015) enabled us to address the architecture and dynamics of the eukaryotic Mre11-Rad50 head module by chemical cross-linking and mass spectrometry (CXMS) experiments as well as small angle X-ray scattering (SAXS). We superimposed the crystal structures of CtMre11^{CD} and CtMre11^{RBD}-Rad50^{NBD} onto the crystal structure of archaeal Mre11-Rad50^{NBD} (PDB code 3AVO). This rigid-body superposition led to a very reasonable fit between the Mre11 dimer and the Rad50 dimer (Fig. 3A). In this modeled complex, the C-terminus of the Mre11 capping domain (Ala-412) and the N-terminus of Mre11^{RBD} (Ser-438) are

approximately 10 Å apart, a distance that could be easily spanned by the 25 amino acids that connect these modules in the primary structure.

To validate this model, we cross-linked the MRN head complex (MRN^{hc}) with the lysine-specific cross-linker disuccinimidyl suberate (DSS) in the presence and absence of ATP γ S:Mg²⁺ and identified cross-linked peptides by mass spectrometry (suppl. Fig. S3) (Tosi *et al.* 2013, Leitner *et al.* 2014). Cross-links were found between all three different polypeptide chains (Fig. 3B): 91 specific non-redundant cross-links in the presence and 149 non-redundant cross-links in the absence of ATP γ S:Mg²⁺ (suppl. Table S3). The C-terminal part of the Nbs1 construct used here cross-links to many regions of the Rad50^{NBD} and Mre11 and is probably flexible. Next, we mapped cross-links between Mre11 and Rad50 onto the model for the closed complex. In the presence of ATP γ S, we identified 15 cross-links between Mre11 and Rad50. All cross-links except two identified in the presence of ATP γ S:Mg²⁺ map with a lysine C $_{\alpha}$ -lysine C $_{\alpha}$ distance of 15-41 Å, validating the docked model (Fig. 3C). In the absence of ATP γ S, we identified 35 cross-links between Rad50 and Mre11. The increased amount of cross-links could be the result of an increased flexibility between Mre11 and Rad50 or the presence of additional conformational states. In support of these possibilities, we also find a much broader distance distribution of these cross-links when mapped onto the model for the closed conformation, with many cross-links mapping to C $_{\alpha}$ -lysine C $_{\alpha}$ distance of >41Å.

To further analyze ATP-dependent structural dynamics, we performed SAXS analyses. Both the maximum distances (Dmax) as well as the mean distances in the particle become substantially smaller in the presence of ATP γ S (Fig. 3D). These data reveal that the eukaryotic Mre11-Rad50 head complex likely adopts a more closed state in the presence of ATP, which is consistent with the CXMS data (Fig. 3B, C) and the structural dynamics observed for bacterial and archaeal MR complexes (Lammens *et al.* 2011, Williams *et al.* 2011, Möckel *et al.* 2012, Deshpande *et al.* 2014).

Altogether, these analyses show that also the eukaryotic Mre11-Rad50 head module undergoes ATP-dependent structural transitions and adopts a more compact state in the presence of ATP, consistent with the model that a Rad50 dimer binds into the active site groove of the Mre11 dimer.

Structural basis for ATP-dependent DNA binding by Rad50

To establish a framework for DNA binding to eukaryotic Rad50 and to reveal how ATP promotes DNA binding to Rad50 proteins, we crystallized CtRad50^{NBD} in the presence of 22mer dsDNA and ATP γ S:Mg²⁺. Crystals in space group P2₁2₁2₁ diffracted X-rays to 2.5 Å resolution and we determined the structure by molecular replacement using CtRad50^{NBD} as a search model. The asymmetric unit contained one Rad50 dimer bound to two ATP γ S:Mg²⁺ molecules and 15 bp dsDNA. Although stoichiometric amounts of Mre11 were also present in the crystallization drops, Mre11 was not part of the crystals. Data collection, refinement and model statistics are summarized in suppl. Table S1.

dsDNA is well defined in the electron density and forms a quasi-continuous, undulating mainly B-form DNA double-helix in the crystal lattice (Fig. 4A, suppl. Fig. S4A, B). The asymmetric unit accommodates only 15 of the 22 base pairs, so either Mre11 in the crystallization drops partially degraded the DNA during the relatively long crystallization time (4 months) or, alternatively, the DNA molecules are shifted between adjacent asymmetric units. In either case, although density for the DNA backbone and bases is for the most part well defined, we refrained from assigning a defined sequence to the bound DNA.

The DNA duplex is situated in the positively charged groove between the two coiled-coils of the Rad50 dimer (Fig. 4B, suppl. Fig. S4C–E). Each of the two strands binds both sides of the Rad50 dimer, resulting in a symmetric interaction of the DNA minor groove along the dimer interface. The observed DNA-binding mode explains the up to now unclear dependency of Rad50 DNA binding on the presence of ATP: the ATP-driven reorientation of lobes I and II and dimer formation of two Rad50^{NBD}s positions and assembles eight DNA binding motifs (four on each side of the dimer) to recognize an approximately 18 base pair long DNA duplex via both backbone strands.

Details of ATP-dependent DNA binding of the Rad50 dimer

The Rad50^{NBD} dimer binds in total 12 bases within an 18bp duplex, six on each of the two halves of the 2-fold symmetric DNA-binding site. These six bases, three for each of the two strands per NBD, are bound via four DNA-binding motifs (I–IV) (Fig. 5A–C). Hereby, the DNA is recognized through the minor groove backbone, consistent with a

sequence independent mode of DNA binding. Motifs I–III are located on lobe I, while motif IV is located on lobe II. Together, these motifs clamp the DNA between the opposing Rad50 protomers on each of the two halves of the dimer. For the further discussion, we will denote the strand polarity as the direction from the center towards the outside of the Rad50 dimer, i.e. a 3'→5' strand on one side of the Rad50 dimer becomes the 5'→3' strand on the other side and vice versa.

Motif I is the top strand of the peripheral β -sheet ($\beta 6$) of the ABC (ATP-binding cassette) fold and binds the 5'→3' strand via interactions between the backbone of two consecutive bases to the main chain oxygen atoms of Thr110 and Gln113 as well as the main chain nitrogen atom of Thr113 (Fig. 5A–C). Motif II, the previously identified strand-loop-helix motif (Rojowska *et al.* 2014), contributes to the DNA interaction by providing charge complementarity and through interactions of Arg132 with the major groove and/or DNA backbone, but intriguingly appears to have a minor role in overall DNA recognition compared to what was previously found for bacterial Rad50 (see discussion).

The 3'→5' strand is bound across the Rad50^{NBD} dimer interface by motifs III and IV. Motif III is situated in the central cavity of the DNA binding groove and connects the two main ATP-binding elements, the helix αA (following the P-loop/Walker A motif) and the adenine recognition loop (aa 64–68) (Fig. 5A–C). As such, this loop could play an important role in coupling DNA binding and ATP binding or hydrolysis. Motif III binds a DNA backbone phosphate via main chain and side chain interactions of Asn58 and by inserting Arg61 into the minor groove. The two preceding phosphates are recognized by Arg1204 as well as Motif IV from the opposing NBD. Motif IV is located at the N-terminal turn of αF , which connects the nucleotide-binding and coiled-coil domains. Arg1204 is situated in the Rad50 dimer interface and besides directly binding to the phosphate backbone it also stacks with Asn58 on motif III and could thereby more broadly facilitate DNA binding.

In summary, both strands of the dsDNA are recognized in a fashion that predominantly involves hydrogen bonds between the DNA backbone and the protein main chain in conjunction with three arginine fingers that reach into the minor groove or directly bind the DNA backbone at the Rad50 dimer interface. The interactions with Arg1204 and motifs III and IV can only form in the tightly engaged, ATP-bound Rad50^{NBD} dimer and

the observed DNA-binding mode provides a mechanistic basis for the ATP-dependent recognition of DNA by Rad50.

Functional analysis of Rad50 DNA interaction in *S. cerevisiae*

To test the relevance of the observed ATP-dependent DNA interaction of Rad50 in a functional context *in vivo*, we analyzed the capability of *rad50* mutants to rescue the camptothecin (abortive topoisomerase I) sensitivity of a $\Delta rad50$ strain. Some previously designed mutants in the DNA binding groove of Rad50 on the basis of the DNA complex of *Thermotoga maritima* (Tm) Rad50 did not reduce the activity of Rad50 in the repair of camptothecin induced lesions, although they robustly decreased the activity of Rad50 in telomere maintenance. However, the sequence based alignments between *T. maritima* and *S. cerevisiae* turned out to be too imprecise and some of the resulting residues were apparently not in direct contact with DNA as observed now in the new eukaryotic Rad50-DNA complex. On the other hand, a mutation of *S. cerevisiae* R1201^{Sc}→E (corresponding to R1204^{Ct}) resulted in severe defects not only in telomere maintenance but also DSB repair, arguing that the observed ATP-dependent interaction of DNA by Rad50 is critical not only for telomere maintenance but also for DSB processing. Although the corresponding mutation did not disrupt the ATP-induced dimer formation of TmRad50, R1201^{Sc}→E might still interfere with a proper ATP-dependent engagement of Rad50^{NBD}s in *S. cerevisiae in vivo*, due to its central location in the dimer interface. Hence, to independently validate the relevance of the observed DNA complex, we mutated K60^{Sc}→E (corresponding to Arg61^{Ct}). Arg61 binds into the minor groove and therefore is intimately involved in DNA interaction, but has no apparent structural role. Intriguingly, K60^{Sc}→E leads to a comparably severe camptothecin sensitivity like the S1205^{Sc}→R and E1235^{Sc}→Q (Walker B) mutations (Fig. 5D, suppl. Fig. S5). We therefore conclude that for the repair of camptothecin induced DSBs DNA binding along the Rad50 groove is as important as ATP binding and hydrolysis by Rad50.

DNA double-strand break tethering

Biochemical studies indicated that MR and to a minor extent Rad50^{NBD} can tether DNA ends in the presence of ATP, a function that is likely important for e.g. MMEJ

(Deshpande *et al.* 2014). While our structure now explains the critical role of ATP in DNA binding by assembling a dsDNA recognition platform that recognizes approximately 18 base pairs of DNA, it also indicates that ATP-Rad50 does not specifically recognize a DNA end. Our observation that a quasi-continuous dsDNA is assembled across Rad50 dimers in the crystal lattice by shorter oligonucleotides raises the question whether Rad50 could directly tether two DNA ends by a mechanism that involves e.g. stacking of two DNA ends across the DNA binding platform. This would explain both, the observation that MR can bind internal sites of DNA, in the vicinity of DNA ends, but also facilitate tethering of DNA ends by ligases *in vitro*.

To address this question, we performed fluorescence anisotropy measurements, which allow the measurements of precise dissociation constants (K_d) (Fig. 6, suppl. Fig. 6, suppl. Table S2). We first tested the effect of the DNA length as well as the presence of ATP on the DNA binding affinity of the Rad50^{NBD}. In the absence of ATP, we do not observe any substantial binding of a 35mer dsDNA (“1” in suppl. Fig. 6 and suppl. Table S2) to CtMre11^{RBD}-Rad50^{NBD}, while in the presence of ATP, the 35mer — short enough to prevent binding of two Rad50 dimers but long enough to reach across a Rad50 dimer — robustly binds to CtRad50^{NBD}-Mre11^{RBD} with a $K_d = 0.45 \pm 0.03 \mu\text{M}$. These data show that ATP is critical for DNA binding to CtMre11^{RBD}-Rad50^{NBD} and validate the structural data. A corresponding dsDNA 17mer (2.1) that is too short to fully reach across the Rad50^{NBD} dimer was bound with a $K_d = 3.1 \pm 0.4 \mu\text{M}$ to ATP-Mre11^{RBD}-CtRad50^{NBD}. This substantially reduced affinity compared to the 35mer DNA (1) is consistent with the structural results that show that Rad50 needs 18 bp to fully reach across its DNA binding platform.

However, instead of binding a single duplex of at least 18 bp, the Rad50 dimer might also bind two DNA ends with either stacked or annealed complementary overhangs. To address this possibility, we also tested DNA substrates with different types of overhangs in the binding studies. A 20mer with a five base 5′ overhang (3.1) has a similar affinity ($K_d = 2.7 \pm 0.3 \mu\text{M}$) to the blunt ended 17mer (2.1). However, a 5 base pair 3′ overhang (4.1) resulted in a notable increase in binding affinity ($K_d = 0.99 \pm 0.10 \mu\text{M}$), indicating a preference for 3′ overhangs. This distinction can be explained by the binding mode of DNA to the Rad50 dimer (see discussion). Extending the 3′ or 5′ overhangs to 20 bases resulted in tight binding with K_d values of $0.34 \pm 0.02 \mu\text{M}$ (5.1) and $0.54 \pm 0.04 \mu\text{M}$ (6.1), respectively. These long DNAs could easily span the Rad50^{NBD} dimer, but at least a

partial DNA duplex is required since a 35bs ssDNA (13) bound with a reduced $K_d = 1.9 \pm 0.3 \mu\text{M}$.

To test the simultaneous binding of two DNA ends to the Rad50 dimer, we mixed two 20mers that contained five nucleotide long complementary 3' (4) or 5' (3) overhangs. The two 20mers in each of the two mixtures can anneal via these overhangs, resembling two tethered partially processed DNA ends with a short homology. In the case of 5' overhangs (3), we calculated a $K_d = 2.2 \pm 0.3 \mu\text{M}$ for the labeled DNA in the presence of a second 20mer with a complementary overhang. Thus, the binding affinity is not notably increased compared to the K_d in the absence of the second 20mer. However, the situation is substantially different in the case of complementary 3' overhangs (4). Here we calculated a $K_d = 0.45 \pm 0.4 \mu\text{M}$ for the labeled DNA in the presence of a second molecule with a complementary overhang. This affinity is the same as observed for the continuous 35bp dsDNA ($K_d = 0.45 \pm 0.03 \mu\text{M}$). In summary, these data provide a quantitative evaluation of ATP-dependent binding of DNA to the Mre11^{RBD}-Rad50^{NBD} module. Consistent with the structural analysis, the equilibrium binding assays suggest that the ATP-bound Rad50 dimer binds either a continuous duplex, a partial duplex of sufficient length, or two DNA ends that are annealed via short 3' overhangs.

Discussion

We provide a first structural framework for the eukaryotic Rad50 nucleotide-binding domain (NBD) and its complexes with either the Rad50-binding domain (RBD) of Mre11 (Mre11^{RBD}) or dsDNA. Our structural and biochemical results clarify the mechanism of ATP-dependent DNA binding by the Rad50 DSB repair enzyme and reveal that ATP-induced Rad50 dimer formation generates a platform to recognize approximately 18bp of a continuous or partial DNA duplex, or shorter DNA with complementary 3' overhangs such as MMEJ substrates.

MRN is a central factor in the metabolism of DNA ends in all kingdoms of life and has functions in the tethering, processing and — in eukaryotes — checkpoint signaling of DSBs (Stracker and Petrini 2011). Hereby, MRN has the ability and key function to clear protein bound or “dirty” DNA ends in order to elicit MMEJ or HR. These DNA ends include meiotic breaks that are blocked by covalently attached Spo11, but also hairpin

structures, other DNA topoisomerase adducts, or DNA ends bound by the NHEJ factor Ku (Liu *et al.* 2002, Lobachev *et al.* 2002, Neale *et al.* 2005, Mimitou and Symington 2010, Langerak *et al.* 2011, Sacho and Maizels 2011). Hereby, MRN cleaves the 5' strand near or at some distance from the DNA end in a reaction that requires ATP hydrolysis, Mre11's nuclease motif and the Sae2/CtIP protein (Garcia *et al.* 2011b, Cannavo and Cejka 2014, Shibata *et al.* 2014).

Current models propose that MRN has distinct structural states that are controlled by ATP binding to Rad50 (Hopfner 2014). In the presence of ATP, prokaryotic MR adopts a closed conformation, in which the ATP-bound Rad50^{NBD} dimer binds into the DNA-binding groove of the Mre11 and blocks its nuclease active sites (Lim *et al.* 2011, Möckel *et al.* 2012). We show here that CtRad50^{NBD}s forms a similar dimer structure, whereby two ATP molecules are sandwiched between opposing Walker A/B and signature motifs. The CtRad50 dimer also has the appropriate dimensions and shape to fit into the DNA binding groove of CtMre11. Together with the SAXS and CXMS studies, our structural analysis suggests that eukaryotic MR can adopt a similar closed complex in the presence of ATP. In the absence of ATP, however, the Rad50 modules would disengage and allow access to the Mre11 dimer active site.

The critical role of ATP binding to Rad50 in most, if not all functions of the MRN complex is well established. A Rad50 signature motif mutant prevents formation of the “closed” Rad50 dimer and phenocopies a rad50 null mutation (Rojowska *et al.* 2014). This suggests that the dimerized Rad50^{NBD}s represent a critical intermediate state in presumably all functional roles of MRN such as telomere maintenance, DSB processing, ATM activation and DNA tethering. Mutations that stabilize the closed conformation by slowing down ATP hydrolysis also render the cells highly sensitive to DNA damaging agents, but appear to be remarkably proficient in DNA tethering, telomere maintenance and ATM activation. Altogether, current models suggest that an engaged Rad50 dimer triggers an MRN conformation that activates ATM and tethers DNA, while both ATP binding and ATP hydrolysis by MRN are required for DNA end processing (Lee *et al.* 2013, Deshpande *et al.* 2014, Rojowska *et al.* 2014).

Our results suggest that the Rad50 DNA binding module has a preference for 3' overhang DNA, whereby two shorter DNA ends with two complementary five base pair 3' overhangs are bound with virtually the same affinity as a longer continuous stretch of

DNA. These data together with our structural results provide a convincing model for the observed ATP-dependent tethering function of MRN and Rad50^{NBD} (Fig. 7A). Thereby, Rad50 could directly link two DNA ends with complementary (5 nt) 3' tails, the substrates expected to undergo MMEJ as an alternative pathway to NHEJ. The preference for 3' tails by the Rad50 module can also be explained by DNA binding data with the full length human MR complex. In the absence of ATP, it was observed that MR has a preference for 5' tails while in the presence of ATP or AMP-PNP, the complex has a strong preference for 3' tails (de Jager *et al.* 2002). Our data would suggest that in the absence of ATP, the Rad50^{NBD}s are disengaged and DNA binding by MRN is dominated by the Mre11 dimer. In the presence of ATP, however, the Rad50^{NBD}s engage, block the Mre11 dimer from binding DNA, and bind DNA either internally or at resected 3' tails. The here reported results also nicely explain how the DNA binding motifs preferentially interact with DNA containing 3' overhangs than with 5' tails (Fig. 7B). Thereby, DNA with a 3' overhang is able to interact with DNA binding motifs I, III of one protomer and the overhang is able to bridge the dimer and to interact with Arg1204 and motif IV of the second protomer. This explains not only the relevance of the Rad50 dimer conformation but also how two complementary 3' overhangs can be stabilized for pairing and subsequently be annealed *in vitro* or during MMEJ (Deshpande *et al.* 2014).

Our structural and functional results clarify the effect of ATP on the interaction of DNA by Rad50 but also by MRN. Consistent with DNA binding along the ATP-bound Rad50 dimer, the critical role of ATP in the DNA binding capacity of both full length Rad50 or the isolated NBD has been seen very early on (Raymond and Kleckner 1993, Hopfner *et al.* 2000b).

Intriguingly, the structure of the eukaryotic Rad50-ATP-DNA complex reported here is quite different to the structure of the bacterial Rad50-ATP-DNA complex. Although the general DNA-binding area, i.e. the NBD surface on lobe I next to the coiled-coils, is the same for both structures, the DNA binding modes are distinct: the DNA in the bacterial complex binds with only one of the two backbone strands to lobe I, only binds to one protomer of the Rad50^{NBD} dimer and does not bind along the Rad50-DNA binding groove to bind the other protomer (suppl. Fig. 7). As a result, this earlier study has failed to explain the requirement of ATP-induced Rad50 dimer formation for DNA recognition by Rad50. What comes as a surprise, however, is the observation that even the binding motifs on lobe I between the two structures are distinct. In particular, the DNAs bind to

non-equivalent, but adjacent β -strands on lobe I. Although the chemistry of the backbone-backbone interaction between DNA and Rad50 appears to be well conserved, the particular residues are not the same. In the bacterial complex, DNA is “rolled” laterally along the β -sheet wall. While the structure of the eukaryotic complex reported here convincingly explains the biochemical and allosteric interplay between ATP and DNA binding to Rad50, the distinct binding mode observed for bacterial Rad50 requires further investigations. We do not want to rule out species dependent differences, but find this rather unlikely. It is possible that the crystal lattice prevented a conformation where DNA reaches across both Rad50 protomers in the bacterial complex. However, structure guided mutagenesis corroborated the DNA complex in solution *in vitro*. It is therefore possible that the bacterial structure resembles a different functional state of MR. It should be noted that the CtRad50^{NBD} displays a robust DNA-binding activity even in the absence of additional domains of the MRN complex. However, results from the work on other species of MRN or MRX revealed that the coiled-coil domains are important for most of the MRN functions and that they increase the binding affinity to DNA (Hohl *et al.* 2011, Lee *et al.* 2013).

Altogether, our results give new insights into the molecular architecture of the eukaryotic MR(N) complex and its function in ATP-dependent DNA tethering. Thereby, dimeric Rad50 can bind dsDNA internally or tether two DNA ends with complementary 3' overhangs, which probably is important for DNA double-strand break repair and MMEJ.

Materials and Methods

Protein preparation

For the expression and purification of the different MR(N) sub-complexes from *Chaetomium thermophilum* (*Chaetomium thermophilum* var. *thermophilum* DSM 1495), the *Mre11* gene was cloned into pET21b vector (Novagen) with NdeI/NotI. Depending on the construct a C-terminal 6xHis affinity tag from the plasmid or a cleavage site for Prescission protease (GE Healthcare) with a 8xHis affinity tag were introduced. Different constructs of N- and C-terminal *Rad50* genes (hypothetical protein CTHT_0073630; XP_006697619) were cloned with or without a fragment of Nbs1 (coding for a start methionine and residues 565–714) into a modified polycistronic pET29b vector

(Novagen) with NdeI/NotI and NotI/Bpu1102I (Fermentas). To stabilize Rad50, the N- and C-termini were fused together with a sequence coding for a GGAGGAGG amino acid linker. See suppl. Figure S1 for list of MRN sub-complexes and constructs.

For co-expression of different MR(N) constructs, pET21b and pET29b plasmids were co-transformed into *E. coli* Rosetta (DE3) cells (Novagen) and cells were grown at 37°C to an OD₆₀₀ of 0.6 in LB. After induction with 0.3 mM IPTG, protein expression was carried out at 18°C overnight. Cells were centrifuged, resuspended in buffer A (25 mM Tris pH 8.0, 300 mM NaCl, 10 mM imidazole) and lysed by sonication. For the purification of the MR head complex (MR^{hc}) complex, which resulted in Rad50^{NBD}-DNA crystals, protease inhibitor (SIGMAFASTTM Protease inhibitor Tablets, Sigma-Aldrich) was added to the lysis buffer. Cell debris was removed by centrifugation and the supernatant was incubated for 1 h with Ni-NTA resin (Qiagen) at 10°C. Subsequently, using gravity flow, three wash steps were performed with buffer A containing 10, 20 and 50 mM imidazole. The protein was eluted with buffer A containing 250 mM imidazole and applied to a size-exclusion chromatography column using a Superdex-200 (GE Healthcare) with gelfiltration buffer (25 mM Tris pH 8.0, 200 mM NaCl). Afterwards the protein was concentrated and flash-frozen in liquid nitrogen for storage at -80°C.

For selenomethionine-derivatized M^{RBD}R^{NBD}, the *E. coli* B834 Rosetta (DE3) strain and selenomethionine media (Molecular Dimensions) were used. Co-expression and co-purification of selenomethionine-labeled M^{RBD}R^{NBD} was performed according to the protocol mentioned above, using buffer A with additional 5 mM beta-mercaptoethanol. For the three wash steps during affinity chromatography purification, buffer A with 10 and 25 mM imidazole as well as 1 M NaCl was used.

In the MR^{hc} complex the linked Rad50 (aa 1-224-GGAGGAGG-1109-1315) contained an E1238→Q mutation in the Walker B motif to inhibit ATP hydrolysis and to increase the dimerization efficiency.

Crystallization, data processing, structure determination and refinement

Crystals of Mre11^{RBD}-Rad50^{NBD} (M^{RBD}R^{NBD}) were grown by hanging drop vapor diffusion method using the purified M^{RBD}R^{NBD} complex (11.8 mg/mL) with 12 mM MgCl₂, 5 mM ATP_γS and 150 μM dsDNA. dsDNA was generated with equimolar

concentrations of 22mer ssDNA (5'-GATTCGTGTAGCTACACGAATC-3') and 23mer ssDNA (5'-GATTCGTGTAGCTACACGAATCA-3') in annealing buffer (500 mM NaCl, 100 mM Tris pH 7.5) and incubating at 95° C for 5 min. and cooling down to 4° C (0.1° C/s). 1 μ L reservoir solution (11% (w/v) PEG 1500; 0.1 M NaCl; 0.1 M MgCl₂; 0.1 M HEPES pH 8) was mixed with 2 μ L protein solution and after three months crystals appeared. These were cryoprotected in reservoir solution containing 15% (v/v) 2, 3-butanediol and flash-cooled in liquid nitrogen. Diffraction data up to a resolution of 3.0 Å were collected at the X06SA beamline (Swiss Light Source (SLS), Villigen, Switzerland) and after indexing with XDS (Kabsch 2010b, Kabsch 2010a), the structure of M^{RBD}R^{NBD} was solved by single-wavelength anomalous dispersion (SAD) using autoSHARP (Vonnrhein *et al.* 2007) and Buccaneer for automated model building (Cowtan 2006, Cowtan 2008). Rounds of manual model building with Coot (Emsley and Cowtan 2004, Emsley *et al.* 2010) and refinement with PHENIX (Adams *et al.* 2010) resulted in a model with good R-factors. The crystals contained one M^{RBD}R^{NBD} dimer per asymmetric unit and the space group was I 222.

To crystallize CtRad50^{NBD}-DNA by the hanging-drop vapor diffusion method, the purified MR^{hc} complex (14.1 mg/mL) was mixed with 12 mM MgCl₂, 5 mM ATP γ S and 95 μ M dsDNA (final concentrations). Therefore, 5 mM ssDNA (5'-GATTCGTGTAGCTACACGAATC-3') was annealed in annealing buffer to final concentration of 2.5 mM dsDNA. For crystallization 2 μ L reservoir solution (42% (v/v) pentaerythritol propoxylate (5/4 PO/OH) and 0.25 M potassium acetate) were mixed with 1 μ L protein-DNA solution. After four months two needle-shaped crystals appeared. Crystals were transferred into 2 μ L reservoir solution for cryoprotection and stored in liquid nitrogen. Data were collected on the X06SA beamline at the SLS in Villigen and one crystal diffracted X-rays up to 2.5 Å. Data were indexed with XDS (Kabsch 2010b, Kabsch 2010a) and the structure was solved by molecular replacement with the CtRad50^{NBD} structure using Phaser (McCoy *et al.* 2007). After rounds of manual model building in Coot (Emsley and Cowtan 2004, Emsley *et al.* 2010) and refinement with PHENIX (Adams *et al.* 2010), difference density for the DNA was suitable for building B-Form dsDNA into the electron map. Further rounds of manual model building and refinement resulted in good R-factors. The space group was P2₁2₁2₁ and Rad50^{NBD}-DNA crystals contained one dimer and 15 bp dsDNA per asymmetric unit.

See suppl. Table S1 for collection and refinement statistics. Figures were prepared using PyMOL (The PyMOL Molecular Graphics System, Version 1.2r3pre. LLC. Schrödinger (Schrodinger 2010)).

Small angle X-ray scattering (SAXS) experiment

C. thermophilum MR^{hc} protein was purified as described above and the flow-through of the concentration step was used as buffer reference for the small-angle X-ray scattering (SAXS) measurements. The MR^{hc} complex without ATP γ S was concentrated up to 4.4 mg/mL and stored at 4° C. For measurement of the MR^{hc} complex in the presence of a non-hydrolysable ATP analog, ATP γ S and MgCl₂ were added (final conc. 2 mM and 8 mM, respectively) before concentrating the protein up to 4.9 mg/mL and storing at 4° C. The two samples were measured at the EMBL P12 beamline of the German Electron Synchrotron (DESY, Hamburg, Germany). The P(r) distribution curve and the maximum inter-particle distance (Dmax) were calculated using the ATSAS 2.5.1 package (Petoukhov *et al.* 2012). The Kratky plot shows a smaller Dmax of the protein in presence of ATP γ S and the mean distance in the protein also decreases.

Chemical cross-linking experiment and mass spectrometry (CXMS) analysis

The MRN^{hc} complex with linked Rad50 N- and C-terminal regions was purified as described above and applied to a S200 GL10/300 (GE Healthcare) size exclusion chromatography column (buffer: 25 mM HEPES pH 8.2, 200 mM NaCl). For analysis in the presence of ATP γ S, the protein was mixed with MgCl₂ and ATP γ S (12 mM and 5 mM final conc., respectively) before the reaction. 57 μ g of the complex (0.45 μ g/ μ L) were cross-linked with an equimolar mixture of isotopically light and heavy labelled disuccinimidyl suberate (DSS-d0/d12, Creative Molecules Inc.; final concentration: 0.11 mM) dissolved at 50 mM in DMF (dimethylformamide, Sigma-Aldrich) immediately prior to cross-linking. The cross-linking reaction was performed at 30°C, 1,000 rpm for 35 min and quenched by the addition of 100 mM final concentration Tris/HCl pH 8.0 and further incubation at 30°C, 1,000 rpm for 15 min. The cross-linking efficiency was visualized by SDS-PAGE in combination with silver staining following standard protocols. The preparation of cross-linked peptides for MS analysis followed a standard

in-solution protocol as described (Herzog *et al.* 2012, Jennebach *et al.* 2012, Leitner *et al.* 2012). In short, proteins were denatured by adding two volumes of 8 M urea. Cross-linked proteins were reduced with 5 mM final concentration tris(2-carboxyethyl)phosphine (TCEP, Thermo Scientific) for 45 min at 35°C and subsequently alkylated in the dark for 30 min at room temperature (10 mM iodoacetamide final concentration) followed by proteolytic digestion for 2h with Lys-C (Wako) and overnight trypsin incubation at 35°C at an enzyme-substrate ratio of 1 to 50 (w/w). Desalted samples were enriched for cross-links by size exclusion chromatography (Superdex Peptide PC 3.2/30 column, GE Healthcare) prior to LC-MS/MS analysis (liquid chromatography coupled to tandem mass spectrometry). Peptide samples were analyzed on an LC-MS/MS system using an UHPLC (EASY-nLC 1000, Thermo Scientific) online coupled to an LTQ Orbitrap Elite system (15 cm x 0.050 mm I.D. reversed phase column packed with 2 µm C18 beads (Acclaim® PepMap RSLC analytical column), Thermo Scientific) equipped with a standard nanoelectrospray source. 5 peptide fractions were separated using each a 60 min gradient of solvent B (98% acetonitrile, 0.1% formic acid) from 2 to 35% at a flow rate of 250 nL/min. Each sample was injected twice to improve identification of cross-linked peptides. The mass spectrometer was operated in data-dependent mode, selecting up to 10 precursors from a MS1 scan (resolution = 120,000) in a mass range of 300-2,000 m/z for rapid collision-induced dissociation (rCID). Singly and doubly charged precursors as well as precursors of unknown charge state were rejected for MS2 selection. rCID was performed for 10 ms using 35% normalized collision energy and an activation q of 0.25. Dynamic exclusion was activated with a repeat count of 1, exclusion duration 30 s at a list size of 500 and a mass window of ±10 ppm. Ion target values were 1,000,000 (or maximum fill time of 10 ms) for the survey scan and 10,000 (or maximum fill time of 100 ms) for the MS2 scan, respectively. Data were identified using the xQUEST/xPROPHET software package assisted by manual validation (Walzthoeni *et al.* 2012). Standard settings were used. Briefly, data were searched against a self-defined protein database containing the sequences of the Mre11, Rad50 and Nbs1 constructs. The maximum number of missed cleavages (excluding the cross-linking site) = 2, peptide length = 4-45, enzyme = trypsin, fixed modifications = carbamidomethyl-Cys (57.02146 Da), variable modification = Met-oxidation (15.99491 Da), mass shift of the light cross-linker (138.0680796 Da), mass shift of the mono-links (156.0786442 Da and 155.0964278 Da), MS1 tolerance = 10 ppm, MS2 tolerance = 0.2 for common ions and 0.3 Da for cross-linked ions. The theoretical candidate spectra were scored according

to their quality of the match and cross-linked candidates were filtered by a MS1 mass tolerance of -5 to 5 ppm and an Id-score of ≥ 22 . All spectra passing the filtering criteria were further manually validated. Identifications were only considered for the final result list in case both peptides had at least four bond cleavages in total or three adjacent ones and a minimum length of five amino acids. Distances for theoretical intra- or inter-molecular cross-links (intra-links or inter-links) were measured using the Xlink Analyzer Chimera plugin (Kosinski *et al.* 2015). Full list of the detected cross-links can be found in supplementary Table S3.

Fluorescence anisotropy measurements

For fluorescence anisotropy measurements labeled and unlabeled ssDNA was dissolved in H₂O, mixed with a 1.1 fold molar excess of unlabeled DNA and annealed by heating up to 95°C with subsequently slow cooling down. For DNA substrates with complementary single-stranded overhangs, the two DNAs were mixed in a 1:1 molar ratio, cooled down and incubated at 4°C for 1–2 h. M^{RBD}R^{NBD} dilutions with protein concentrations of 0, 0.1, 0.16, 0.2, 0.4, 0.6, 0.8, 1.2, 1.6, 1.98, 3.0, 4.0, 6.0, 7.98, 10.0, 12.0, 15.9, 20.1, 25.0 and 30.0 μ M were prepared in assay buffer (100 mM NaCl, 40 mM Tris pH 8, 10 mM MgCl₂, 4 mM ATP). After incubation for 1 h the protein dilutions were mixed with labeled dsDNA (50 nM final conc.) in a 1:1 (v/v) ratio. After 30 min equilibration, the fluorescence anisotropy was measured with the TECAN plate reader (TECAN infinite® M1000). The data were analyzed with GraphPad Prism (Version 6 for Windows, GraphPad Software, La Jolla California USA, www.graphpad.com.) and fit to a single-site binding model accounting for receptor depletion (suppl. Fig. S6 and suppl. Table S3). Following equation was used for K_d calculations:

$$Y = A_f - (A_f - A_b) * (((L_t + x + K_d) - ((L_t + x + K_d)^2 - (4 * L_t * x))^{0.5}) / (2 * L_t))$$

Y = anisotropy; A_f = anisotropy of free ligand; A_b = anisotropy of bound ligand; x = Pt = Receptor concentration (total); L_t = ligand concentration (total) = 50 nM; K_d = dissociation constant

Plate survival assay

The plate survival assay with *S. cerevisiae* carrying wild-type or mutated Rad50 allele was performed as described before (Rojowska *et al.* 2014). Briefly, freshly growing cells from a plate were resuspended in deionized water and diluted to OD₆₀₀ of 1. W303-1a wild-type and W303-1a Δ rad50 strains were kind gifts from Katja Strässer and Steve Jackson, respectively.

Acknowledgements

We thank the staff of the Swiss Light Source (Villigen) and European Synchrotron Radiation Facility (Grenoble) for support with data collection and analysis. This work was supported by the European Research Council Advanced Grant “ATMMACHINE”, the German Research Council (SFBs 684, 664 and GRK1721) and the excellence cluster Center for Integrated Protein Science Munich to K.-P.H.

References

- Adams, P. D., P. V. Afonine, G. Bunkoczi, V. B. Chen, I. W. Davis, N. Echols, J. J. Headd, L. W. Hung, G. J. Kapral, R. W. Grosse-Kunstleve, A. J. McCoy, N. W. Moriarty, R. Oeffner, R. J. Read, D. C. Richardson, J. S. Richardson, T. C. Terwilliger and P. H. Zwart (2010). "PHENIX: a comprehensive Python-based system for macromolecular structure solution." Acta Crystallogr D Biol Crystallogr 66(Pt 2): 213-221.
- Alani, E., R. Padmore and N. Kleckner (1990). "Analysis of wild-type and rad50 mutants of yeast suggests an intimate relationship between meiotic chromosome synapsis and recombination." Cell 61(3): 419-436.
- Berkovich, E., R. J. Monnat, Jr. and M. B. Kastan (2007). "Roles of ATM and NBS1 in chromatin structure modulation and DNA double-strand break repair." Nat Cell Biol 9(6): 683-690.
- Bhattacharyya, M. K., K. M. Matthews and A. J. Lustig (2008). "Mre11 nuclease and C-terminal tail-mediated DDR functions are required for initiating yeast telomere healing." Chromosoma 117(4): 357-366.
- Buchert, F., Y. Schober, A. Rompp, M. L. Richter and C. Forreiter (2012). "Reactive oxygen species affect ATP hydrolysis by targeting a highly conserved amino acid cluster in the thylakoid ATP synthase gamma subunit." Biochim Biophys Acta 1817(11): 2038-2048.
- Cannavo, E. and P. Cejka (2014). "Sae2 promotes dsDNA endonuclease activity within Mre11-Rad50-Xrs2 to resect DNA breaks." Nature 514(7520): 122-125.
- Carney, J. P., R. S. Maser, H. Olivares, E. M. Davis, M. Le Beau, J. R. Yates, 3rd, L. Hays, W. F. Morgan and J. H. Petrini (1998). "The hMre11/hRad50 protein

- complex and Nijmegen breakage syndrome: linkage of double-strand break repair to the cellular DNA damage response." Cell 93(3): 477-486.
- Chen, Y. C., H. Y. Chiang, M. H. Yang, P. M. Chen, S. Y. Chang, S. C. Teng, B. Vanhaesebroeck and K. J. Wu (2008). "Activation of phosphoinositide 3-kinase by the NBS1 DNA repair protein through a novel activation motif." J Mol Med (Berl) 86(4): 401-412.
- Chiruvella, K. K., Z. Liang and T. E. Wilson (2013). "Repair of double-strand breaks by end joining." Cold Spring Harb Perspect Biol 5(5): a012757.
- Connelly, J. C., E. S. de Leau and D. R. Leach (1999). "DNA cleavage and degradation by the SbcCD protein complex from *Escherichia coli*." Nucleic Acids Res 27(4): 1039-1046.
- Costanzo, V., K. Robertson, M. Bibikova, E. Kim, D. Grieco, M. Gottesman, D. Carroll and J. Gautier (2001). "Mre11 protein complex prevents double-strand break accumulation during chromosomal DNA replication." Mol Cell 8(1): 137-147.
- Cowtan, K. (2006). "The Buccaneer software for automated model building. 1. Tracing protein chains." Acta Crystallogr D Biol Crystallogr 62(Pt 9): 1002-1011.
- Cowtan, K. (2008). "Fitting molecular fragments into electron density." Acta Crystallogr D Biol Crystallogr 64(Pt 1): 83-89.
- de Beer, T. A., K. Berka, J. M. Thornton and R. A. Laskowski (2014). "PDBsum additions." Nucleic Acids Res 42(Database issue): D292-296.
- de Jager, M., C. Wyman, D. C. van Gent and R. Kanaar (2002). "DNA end-binding specificity of human Rad50/Mre11 is influenced by ATP." Nucleic Acids Res 30(20): 4425-4431.
- Delia, D., M. Piane, G. Buscemi, C. Savio, S. Palmeri, P. Lulli, L. Carlessi, E. Fontanella and L. Chessa (2004). "MRE11 mutations and impaired ATM-dependent responses in an Italian family with ataxia-telangiectasia-like disorder." Hum Mol Genet 13(18): 2155-2163.
- Desai-Mehta, A., K. M. Cerosaletti and P. Concannon (2001). "Distinct functional domains of nibrin mediate Mre11 binding, focus formation, and nuclear localization." Mol Cell Biol 21(6): 2184-2191.
- Deshpande, R. A., G. J. Williams, O. Limbo, R. S. Williams, J. Kuhnlein, J. H. Lee, S. Classen, G. Guenther, P. Russell, J. A. Tainer and T. T. Paull (2014). "ATP-driven Rad50 conformations regulate DNA tethering, end resection, and ATM checkpoint signaling." EMBO J 33(5): 482-500.
- Emsley, P. and K. Cowtan (2004). "Coot: model-building tools for molecular graphics." Acta Crystallogr D Biol Crystallogr 60(Pt 12 Pt 1): 2126-2132.
- Emsley, P., B. Lohkamp, W. G. Scott and K. Cowtan (2010). "Features and development of Coot." Acta Crystallogr D Biol Crystallogr 66(Pt 4): 486-501.
- Furuse, M., Y. Nagase, H. Tsubouchi, K. Murakami-Murofushi, T. Shibata and K. Ohta (1998). "Distinct roles of two separable in vitro activities of yeast Mre11 in mitotic and meiotic recombination." EMBO J 17(21): 6412-6425.
- Gapud, E. J. and B. P. Sleckman (2011). "Unique and redundant functions of ATM and DNA-PKcs during V(D)J recombination." Cell Cycle 10(12): 1928-1935.
- Garcia, V., S. E. Phelps, S. Gray and M. J. Neale (2011a). "Bidirectional resection of DNA double-strand breaks by Mre11 and Exo1." Nature 479(7372): 241-244.
- Garcia, V., S. E. L. Phelps, S. Gray and M. J. Neale (2011b). "Bidirectional resection of DNA double-strand breaks by Mre11 and Exo1." Nature 479(7372): 241-244.
- Goujon, M., H. McWilliam, W. Li, F. Valentin, S. Squizzato, J. Paern and R. Lopez (2010). "A new bioinformatics analysis tools framework at EMBL-EBI." Nucleic Acids Res 38(Web Server issue): W695-699.

- Guo, Z., S. Kozlov, M. F. Lavin, M. D. Person and T. T. Paull (2010). "ATM activation by oxidative stress." *Science* 330(6003): 517-521.
- Haber, J. E. (2012). "Mating-type genes and MAT switching in *Saccharomyces cerevisiae*." *Genetics* 191(1): 33-64.
- Hanahan, D. and R. A. Weinberg (2011). "Hallmarks of cancer: the next generation." *Cell* 144(5): 646-674.
- Herzog, F., A. Kahraman, D. Boehringer, R. Mak, A. Bracher, T. Walzthoeni, A. Leitner, M. Beck, F. U. Hartl, N. Ban, L. Malmstrom and R. Aebersold (2012). "Structural probing of a protein phosphatase 2A network by chemical cross-linking and mass spectrometry." *Science* 337(6100): 1348-1352.
- Hohl, M., Y. Kwon, S. M. Galvan, X. Xue, C. Tous, A. Aguilera, P. Sung and J. H. Petrini (2011). "The Rad50 coiled-coil domain is indispensable for Mre11 complex functions." *Nat Struct Mol Biol* 18(10): 1124-1131.
- Hopfner, K. P. (2014). "ATP puts the brake on DNA double-strand break repair: a new study shows that ATP switches the Mre11-Rad50-Nbs1 repair factor between signaling and processing of DNA ends." *Bioessays* 36(12): 1170-1178.
- Hopfner, K. P., A. Karcher, D. Shin, C. Fairley, J. A. Tainer and J. P. Carney (2000a). "Mre11 and Rad50 from *Pyrococcus furiosus*: cloning and biochemical characterization reveal an evolutionarily conserved multiprotein machine." *J Bacteriol* 182(21): 6036-6041.
- Hopfner, K. P., A. Karcher, D. S. Shin, L. Craig, L. M. Arthur, J. P. Carney and J. A. Tainer (2000b). "Structural biology of Rad50 ATPase: ATP-driven conformational control in DNA double-strand break repair and the ABC-ATPase superfamily." *Cell* 101(7): 789-800.
- Jennebach, S., F. Herzog, R. Aebersold and P. Cramer (2012). "Crosslinking-MS analysis reveals RNA polymerase I domain architecture and basis of rRNA cleavage." *Nucleic Acids Res* 40(12): 5591-5601.
- Kabsch, W. (2010a). "Integration, scaling, space-group assignment and post-refinement." *Acta Crystallogr D Biol Crystallogr* 66(Pt 2): 133-144.
- Kabsch, W. (2010b). "Xds." *Acta Crystallogr D Biol Crystallogr* 66(Pt 2): 125-132.
- Kosinski, J., A. von Appen, A. Ori, K. Karius, C. W. Muller and M. Beck (2015). "Xlink Analyzer: software for analysis and visualization of cross-linking data in the context of three-dimensional structures." *J Struct Biol* 189(3): 177-183.
- Lam, I. and S. Keeney (2015). "Mechanism and regulation of meiotic recombination initiation." *Cold Spring Harb Perspect Biol* 7(1): a016634.
- Lammens, K., D. J. Bemeleit, C. Möckel, E. Clausing, A. Schele, S. Hartung, C. B. Schiller, M. Lucas, C. Angermüller, J. Söding, K. Strasser and K. P. Hopfner (2011). "The Mre11:Rad50 structure shows an ATP-dependent molecular clamp in DNA double-strand break repair." *Cell* 145(1): 54-66.
- Langerak, P., E. Mejia-Ramirez, O. Limbo and P. Russell (2011). "Release of Ku and MRN from DNA ends by Mre11 nuclease activity and Ctp1 is required for homologous recombination repair of double-strand breaks." *PLoS Genet* 7(9): e1002271.
- Lee, J. H., M. R. Mand, R. A. Deshpande, E. Kinoshita, S. H. Yang, C. Wyman and T. T. Paull (2013). "Ataxia telangiectasia-mutated (ATM) kinase activity is regulated by ATP-driven conformational changes in the Mre11/Rad50/Nbs1 (MRN) complex." *J Biol Chem* 288(18): 12840-12851.
- Leitner, A., L. A. Joachimiak, A. Bracher, L. Monkemeyer, T. Walzthoeni, B. Chen, S. Pechmann, S. Holmes, Y. Cong, B. Ma, S. Ludtke, W. Chiu, F. U. Hartl, R.

- Aebersold and J. Frydman (2012). "The molecular architecture of the eukaryotic chaperonin TRiC/CCT." Structure 20(5): 814-825.
- Leitner, A., T. Walzthoeni and R. Aebersold (2014). "Lysine-specific chemical cross-linking of protein complexes and identification of cross-linking sites using LC-MS/MS and the xQuest/xProphet software pipeline." Nat Protoc 9(1): 120-137.
- Lim, H. S., J. S. Kim, Y. B. Park, G. H. Gwon and Y. Cho (2011). "Crystal structure of the Mre11-Rad50-ATPγS complex: understanding the interplay between Mre11 and Rad50." Genes Dev 25(10): 1091-1104.
- Limbo, O., C. Chahwan, Y. Yamada, R. A. M. de Bruin, C. Wittenberg and P. Russell (2007). "Ctp1 Is a Cell-Cycle-Regulated Protein that Functions with Mre11 Complex to Control Double-Strand Break Repair by Homologous Recombination." Molecular Cell 28(1): 134-146.
- Lisby, M., J. H. Barlow, R. C. Burgess and R. Rothstein (2004). "Choreography of the DNA damage response: spatiotemporal relationships among checkpoint and repair proteins." Cell 118(6): 699-713.
- Liu, C., J. J. Pouliot and H. A. Nash (2002). "Repair of topoisomerase I covalent complexes in the absence of the tyrosyl-DNA phosphodiesterase Tdp1." Proc Natl Acad Sci U S A 99(23): 14970-14975.
- Lobachev, K. S., D. A. Gordenin and M. A. Resnick (2002). "The Mre11 complex is required for repair of hairpin-capped double-strand breaks and prevention of chromosome rearrangements." Cell 108(2): 183-193.
- Mahaney, B. L., K. Meek and S. P. Lees-Miller (2009). "Repair of ionizing radiation-induced DNA double-strand breaks by non-homologous end-joining." Biochem J 417(3): 639-650.
- Matsumoto, Y., T. Miyamoto, H. Sakamoto, H. Izumi, Y. Nakazawa, T. Ogi, H. Tahara, S. Oku, A. Hiramoto, T. Shiiki, Y. Fujisawa, H. Ohashi, Y. Sakemi and S. Matsuura (2011). "Two unrelated patients with *MRE11A* mutations and Nijmegen breakage syndrome-like severe microcephaly." DNA Repair (Amst) 10(3): 314-321.
- McCoy, A. J., R. W. Grosse-Kunstleve, P. D. Adams, M. D. Winn, L. C. Storoni and R. J. Read (2007). "Phaser crystallographic software." J Appl Crystallogr 40(Pt 4): 658-674.
- Mimitou, E. P. and L. S. Symington (2008). "Sae2, Exo1 and Sgs1 collaborate in DNA double-strand break processing." Nature 455(7214): 770-774.
- Mimitou, E. P. and L. S. Symington (2010). "Ku prevents Exo1 and Sgs1-dependent resection of DNA ends in the absence of a functional MRX complex or Sae2." EMBO J 29(19): 3358-3369.
- Miyamoto, R., H. Morino, A. Yoshizawa, Y. Miyazaki, H. Maruyama, N. Murakami, K. Fukada, Y. Izumi, S. Matsuura, R. Kaji and H. Kawakami (2014). "Exome sequencing reveals a novel *MRE11* mutation in a patient with progressive myoclonic ataxia." J Neurol Sci 337(1-2): 219-223.
- Mladenov, E. and G. Iliakis (2011). "Induction and repair of DNA double strand breaks: the increasing spectrum of non-homologous end joining pathways." Mutat Res 711(1-2): 61-72.
- Möckel, C., K. Lammens, A. Schele and K. P. Hopfner (2012). "ATP driven structural changes of the bacterial Mre11:Rad50 catalytic head complex." Nucleic Acids Res 40(2): 914-927.
- Neale, M. J., J. Pan and S. Keeney (2005). "Endonucleolytic processing of covalent protein-linked DNA double-strand breaks." Nature 436(7053): 1053-1057.

- Paull, T. T. and M. Gellert (1998). "The 3' to 5' exonuclease activity of Mre 11 facilitates repair of DNA double-strand breaks." Mol Cell 1(7): 969-979.
- Petoukhov, M. V., D. Franke, A. V. Shkumatov, G. Tria, A. G. Kikhney, M. Gajda, C. Gorba, H. D. Mertens, P. V. Konarev and D. I. Svergun (2012). "New developments in the program package for small-angle scattering data analysis." J Appl Crystallogr 45(Pt 2): 342-350.
- Pommier, Y., C. Redon, V. A. Rao, J. A. Seiler, O. Sordet, H. Takemura, S. Antony, L. Meng, Z. Liao, G. Kohlhausen, H. Zhang and K. W. Kohn (2003). "Repair of and checkpoint response to topoisomerase I-mediated DNA damage." Mutat Res 532(1-2): 173-203.
- Raymond, W. E. and N. Kleckner (1993). "RAD50 protein of *S.cerevisiae* exhibits ATP-dependent DNA binding." Nucleic Acids Res 21(16): 3851-3856.
- Rojowska, A., K. Lammens, F. U. Seifert, C. Drenberger, H. Feldmann and K. P. Hopfner (2014). "Structure of the Rad50 DNA double-strand break repair protein in complex with DNA." EMBO J 33(23): 2847-2859.
- Roset, R., A. Inagaki, M. Hohl, F. Brenet, J. Lafrance-Vanasse, J. Lange, J. M. Scandura, J. A. Tainer, S. Keeney and J. H. Petrini (2014). "The Rad50 hook domain regulates DNA damage signaling and tumorigenesis." Genes Dev 28(5): 451-462.
- Sacho, E. J. and N. Maizels (2011). "DNA repair factor MRE11/RAD50 cleaves 3'-phosphotyrosyl bonds and resects DNA to repair damage caused by topoisomerase 1 poisons." J Biol Chem 286(52): 44945-44951.
- Schiller, C. B., K. Lammens, I. Guerini, B. Coords, H. Feldmann, F. Schlauderer, C. Möckel, A. Schele, K. Strasser, S. P. Jackson and K. P. Hopfner (2012). "Structure of Mre11-Nbs1 complex yields insights into ataxia-telangiectasia-like disease mutations and DNA damage signaling." Nat Struct Mol Biol 19(7): 693-700.
- Schiller, C. B., F. U. Seifert, C. Linke-Winnebeck and K. P. Hopfner (2014). "Structural studies of DNA end detection and resection in homologous recombination." Cold Spring Harb Perspect Biol 6(10): a017962.
- Schrodinger, LLC (2010). The PyMOL Molecular Graphics System, Version 1.3r1.
- Seifert, F. U., K. Lammens and K. P. Hopfner (2015). "Structure of the catalytic domain of Mre11 from *Chaetomium thermophilum*." Acta Crystallogr F Struct Biol Commun 71(Pt 6): 752-757.
- Shibata, A., D. Moiani, A. S. Arvai, J. Perry, S. M. Harding, M. M. Genois, R. Maity, S. van Rossum-Fikkert, A. Kertokallio, F. Romoli, A. Ismail, E. Ismalaj, E. Petricci, M. J. Neale, R. G. Bristow, J. Y. Masson, C. Wyman, P. A. Jeggo and J. A. Tainer (2014). "DNA double-strand break repair pathway choice is directed by distinct MRE11 nuclease activities." Mol Cell 53(1): 7-18.
- Sievers, F., A. Wilm, D. Dineen, T. J. Gibson, K. Karplus, W. Li, R. Lopez, H. McWilliam, M. Remmert, J. Soding, J. D. Thompson and D. G. Higgins (2011). "Fast, scalable generation of high-quality protein multiple sequence alignments using Clustal Omega." Mol Syst Biol 7: 539.
- Stewart, G. S., R. S. Maser, T. Stankovic, D. A. Bressan, M. I. Kaplan, N. G. Jaspers, A. Raams, P. J. Byrd, J. H. Petrini and A. M. Taylor (1999). "The DNA double-strand break repair gene *hMRE11* is mutated in individuals with an ataxia-telangiectasia-like disorder." Cell 99(6): 577-587.
- Stracker, T. H. and J. H. Petrini (2011). "The MRE11 complex: starting from the ends." Nat Rev Mol Cell Biol 12(2): 90-103.

- Sutherland, B. M., P. V. Bennett, O. Sidorkina and J. Laval (2000). "Clustered DNA damages induced in isolated DNA and in human cells by low doses of ionizing radiation." Proc Natl Acad Sci U S A 97(1): 103-108.
- Symington, L. S. (2014). "End resection at double-strand breaks: mechanism and regulation." Cold Spring Harb Perspect Biol 6(8): a016436.
- Tosi, A., C. Haas, F. Herzog, A. Gilmozzi, O. Berninghausen, C. Ungewickell, C. B. Gerhold, K. Lakomek, R. Aebersold, R. Beckmann and K. P. Hopfner (2013). "Structure and subunit topology of the INO80 chromatin remodeler and its nucleosome complex." Cell 154(6): 1207-1219.
- Trujillo, K. M. and P. Sung (2001). "DNA structure-specific nuclease activities in the *Saccharomyces cerevisiae* Rad50-Mre11 complex." J Biol Chem 276(38): 35458-35464.
- Truong, L. N., Y. Li, L. Z. Shi, P. Y. Hwang, J. He, H. Wang, N. Razavian, M. W. Berns and X. Wu (2013). "Microhomology-mediated End Joining and Homologous Recombination share the initial end resection step to repair DNA double-strand breaks in mammalian cells." Proc Natl Acad Sci U S A 110(19): 7720-7725.
- Usui, T., T. Ohta, H. Oshiumi, J. Tomizawa, H. Ogawa and T. Ogawa (1998). "Complex formation and functional versatility of Mre11 of budding yeast in recombination." Cell 95(5): 705-716.
- Varon, R., C. Vissinga, M. Platzer, K. M. Cerosaletti, K. H. Chrzanowska, K. Saar, G. Beckmann, E. Seemanova, P. R. Cooper, N. J. Nowak, M. Stumm, C. M. Weemaes, R. A. Gatti, R. K. Wilson, M. Digweed, A. Rosenthal, K. Sperling, P. Concannon and A. Reis (1998). "Nibrin, a novel DNA double-strand break repair protein, is mutated in Nijmegen breakage syndrome." Cell 93(3): 467-476.
- Vonrhein, C., E. Blanc, P. Roversi and G. Bricogne (2007). "Automated structure solution with autoSHARP." Methods Mol Biol 364: 215-230.
- Waltes, R., R. Kalb, M. Gatei, A. W. Kijas, M. Stumm, A. Sobeck, B. Wieland, R. Varon, Y. Lerenthal, M. F. Lavin, D. Schindler and T. Dork (2009). "Human RAD50 deficiency in a Nijmegen breakage syndrome-like disorder." Am J Hum Genet 84(5): 605-616.
- Walzthoeni, T., M. Claassen, A. Leitner, F. Herzog, S. Bohn, F. Forster, M. Beck and R. Aebersold (2012). "False discovery rate estimation for cross-linked peptides identified by mass spectrometry." Nat Methods 9(9): 901-903.
- Williams, G. J., R. S. Williams, J. S. Williams, G. Moncalian, A. S. Arvai, O. Limbo, G. Guenther, S. SilDas, M. Hammel, P. Russell and J. A. Tainer (2011). "ABC ATPase signature helices in Rad50 link nucleotide state to Mre11 interface for DNA repair." Nat Struct Mol Biol 18(4): 423-431.
- Xu, Z., H. Zan, E. J. Pone, T. Mai and P. Casali (2012). "Immunoglobulin class-switch DNA recombination: induction, targeting and beyond." Nat Rev Immunol 12(7): 517-531.
- You, Z., C. Chahwan, J. Bailis, T. Hunter and P. Russell (2005). "ATM activation and its recruitment to damaged DNA require binding to the C terminus of Nbs1." Mol Cell Biol 25(13): 5363-5379.
- Zaitseva, J., S. Jenewein, T. Jumpertz, I. B. Holland and L. Schmitt (2005). "H662 is the linchpin of ATP hydrolysis in the nucleotide-binding domain of the ABC transporter HlyB." EMBO J 24(11): 1901-1910.

Figures:

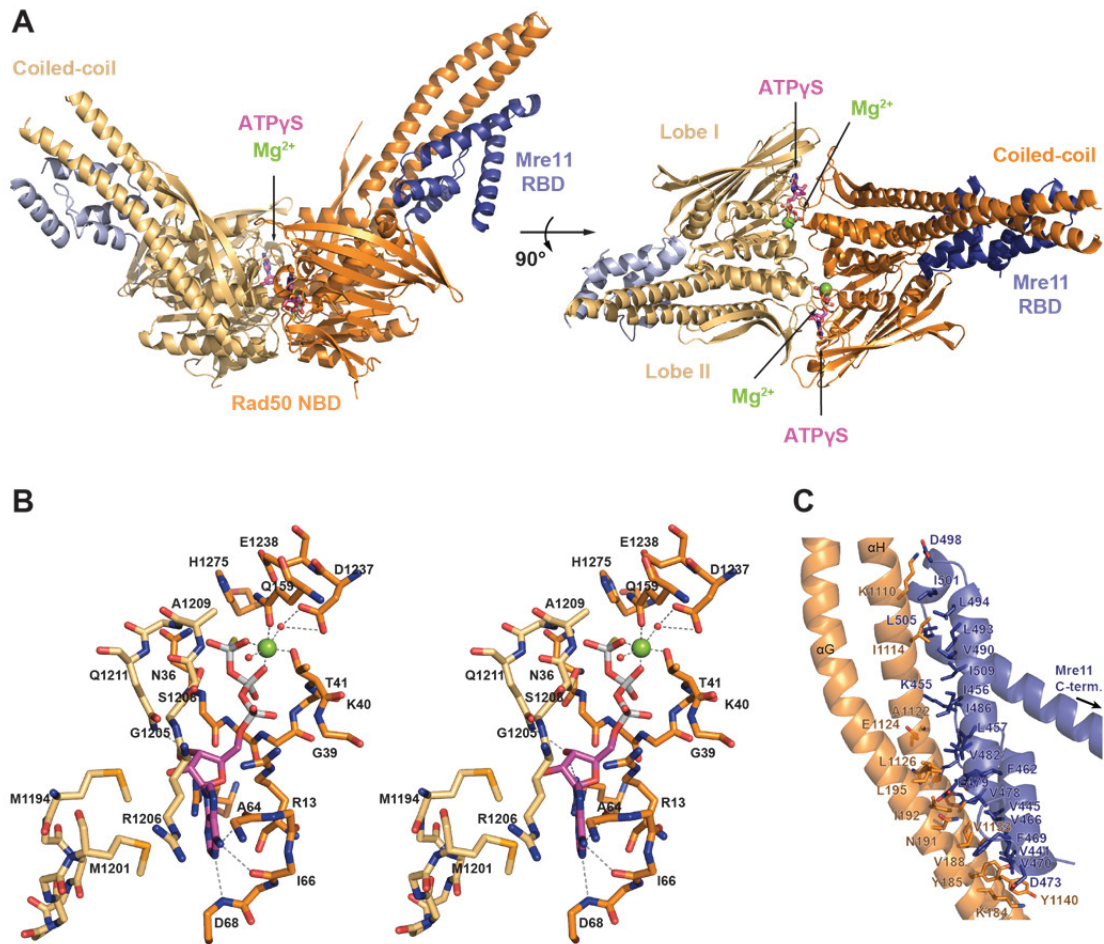


Figure 1: Eukaryotic CtMre11^{RBD}-Rad50^{NBD} crystal structure. (A) Dimeric structure of *C. thermophilum* Mre11 Rad50-binding domain (CtMre11^{RBD}; light and dark blue) bound to the nucleotide-binding domain (NBD) of Rad50 (CtRad50^{NBD}; light and dark orange). Two ATPγS:Mg²⁺ (magenta and green, respectively) molecules are sandwiched in between the CtMre11^{RBD}-Rad50^{NBD} (CtM^{RBD}R^{NBD}) dimer. Rad50 monomers are characterized by lobe I and lobe II, which together form the Rad50^{NBD}. (B) Stereo view of the ATPase active site. The ATP-interacting residues are highlighted and hydrogen bonds are indicated. (C) Detailed view of the CtMre11^{RBD}-Rad50^{NBD} interface. Residues that facilitate the interaction between the CtMre11^{RBD} and the coiled-coil (CC) domain of Rad50 are represented as sticks.

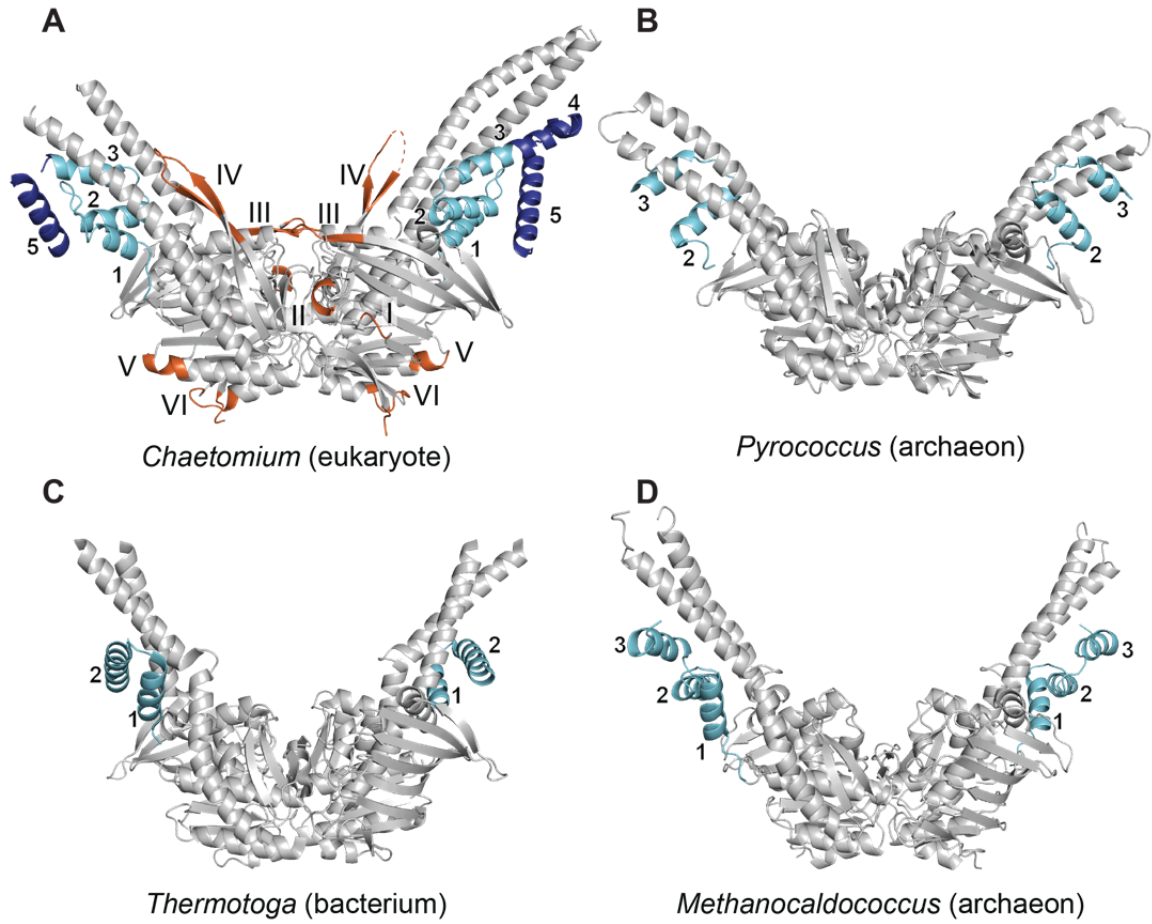


Figure 2: Comparison between dimeric Mre11^{RBD}-Rad50^{NBD} crystal structures. Crystal structures of dimeric *Chaetomium thermophilum* (A), *Pyrococcus furiosus* (B), *Thermotoga maritima* (C) and *Methanocaldococcus jannaschii* (D) Mre11^{RBD}-Rad50^{NBD} (PDB codes: 3QKU, 3QF7 and 3AV0, respectively). The Rad50^{NBD} (gray) and the Mre11^{RBD} (light blue) are depicted. The eukaryotic extended helices in the CtMre11^{RBD} (dark blue) and the eukaryotic insertions (iron) are highlighted.

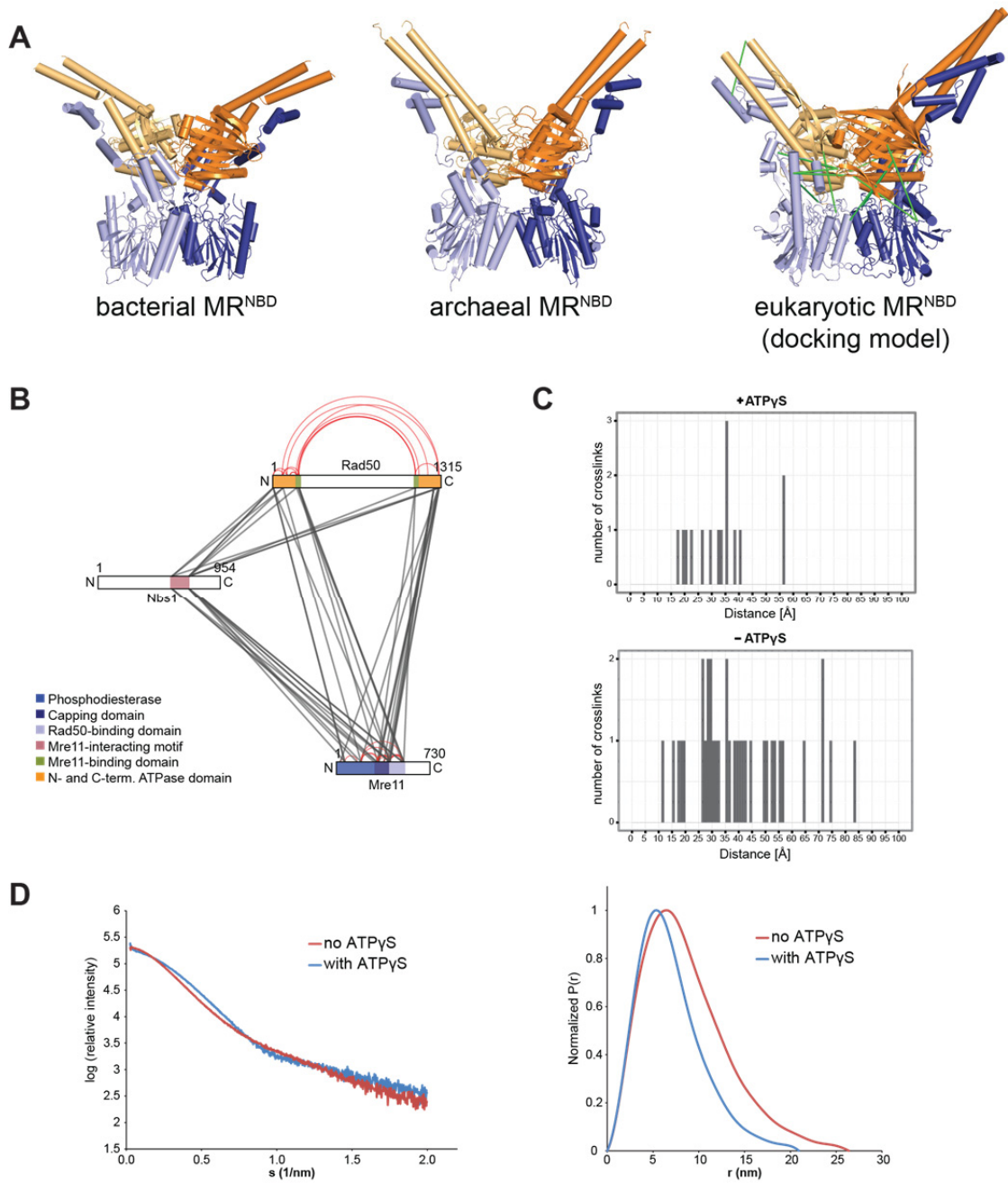


Figure 3: Mre11-Rad50^{NBD} complex in ATP-bound state. (A) Comparison of bacterial, archaeal and eukaryotic MR^{NBD} in ATP-bound state. Eukaryotic MR^{NBD} docking model consists of dimeric CtMre11^{CD} (light and dark blue) and CtMre11^{RBD}-Rad50^{NBD} (Mre11 in light and deep blue; Rad50 in beige and orange) superimposed onto MR^{NBD} (PDB code: 3AV0) from *M. jannaschii*. Identified cross-links between Rad50 and Mre11 subunits are marked as green lines. **(B)** Map of the identified intra- (red) and inter-protein cross-links (blue) between the MRN subunits. **(C)** Distribution of the measured lengths of the cross-links in the ATP-bound CtMR^{NBD} model. Data from protein samples with and without ATPyS are depicted. **(D)** SAXS scattering curve (left) and P(r) distribution curve (right) of MR^{hc} with (blue) and without (red) ATPyS:Mg²⁺.

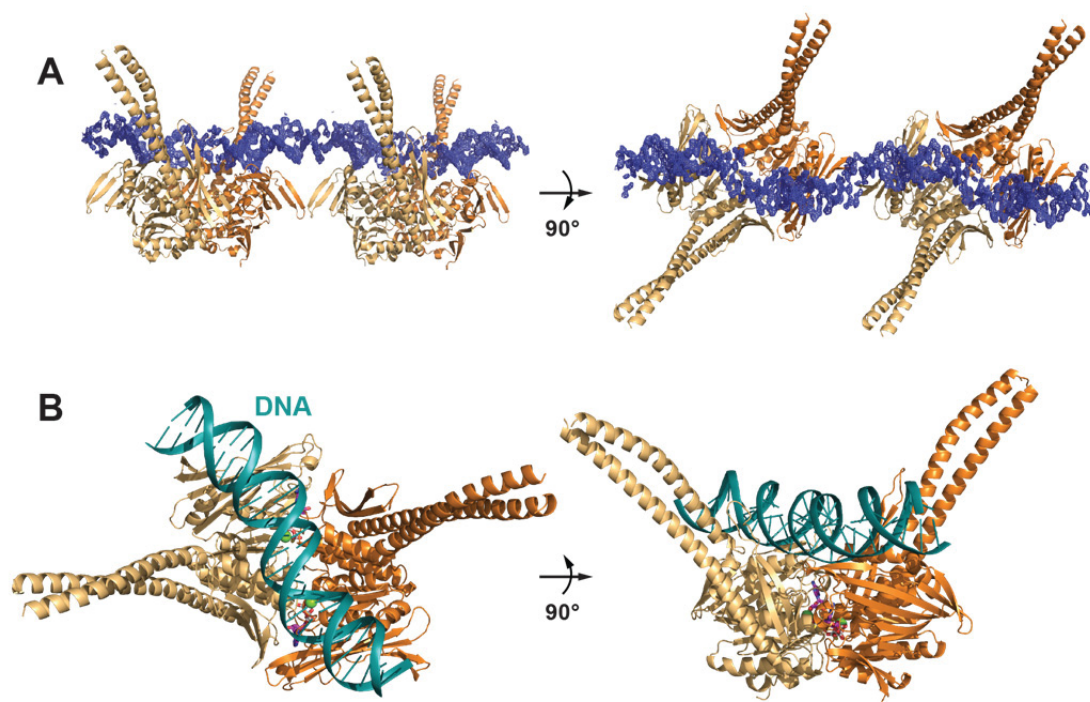


Figure 4: CtRad50^{NBD}-DNA crystal structure. (A) *2mFo-DFc* density (blue) contoured at 1 σ for dsDNA in the Rad50 dimer (light and dark orange) groove is depicted. (B) Modeled dsDNA (teal) in complex with the ATP γ S:Mg²⁺-bound Rad50^{NBD} dimer (light and dark orange).

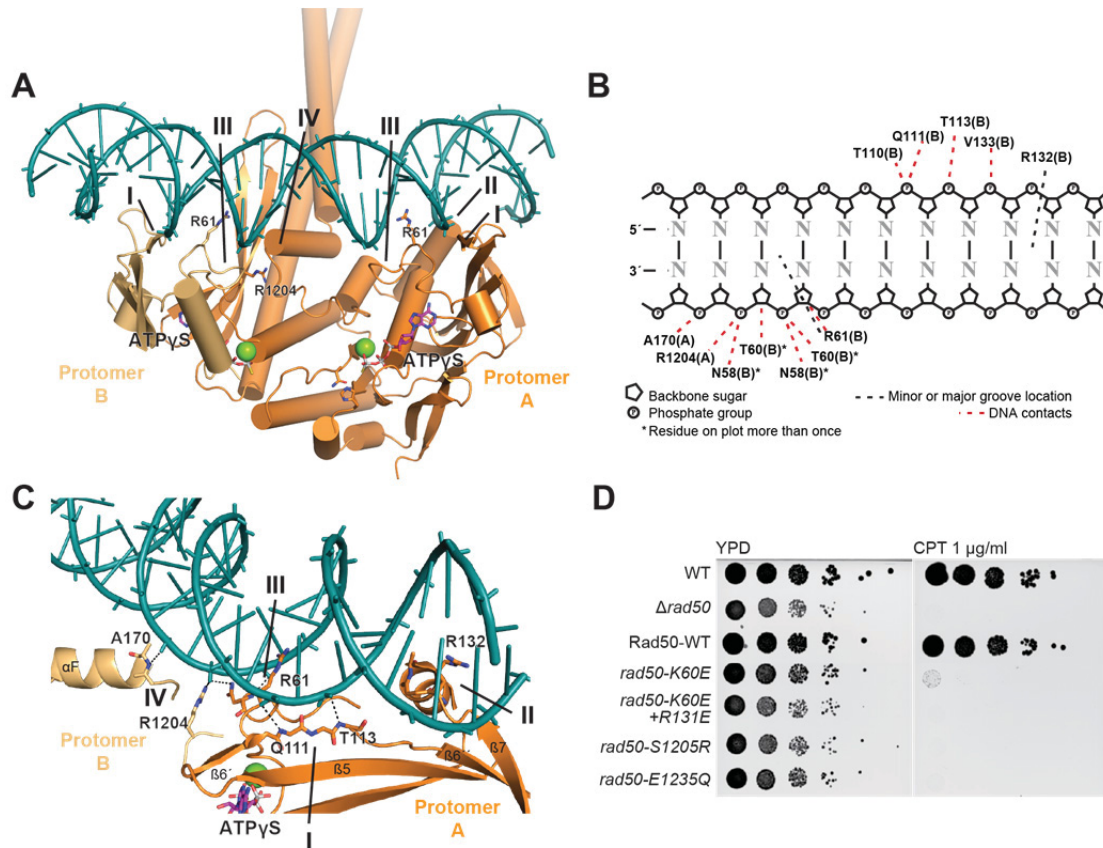


Figure 5: Detailed view on the Rad50-DNA interaction. (A) DNA-binding motifs and important interacting residues are indicated. (B) Scheme of the dsDNA and the interacting residues on one side of the Rad50 dimer. The structure was analyzed with PDBsum (<http://www.ebi.ac.uk/pdbsum>) (de Beer *et al.* 2014) and the scheme was optimized manually. (C) Detailed view onto the Rad50-DNA interaction. (D) Plate survival assay with wild-type, *rad50Δ* and *rad50* mutant strains on YPD and DNA damage inducing camptothecin (CPT).

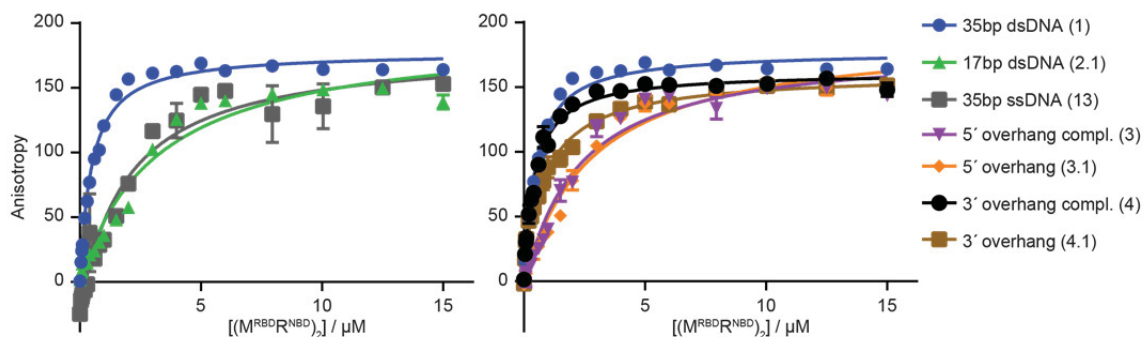


Figure 6: DNA binding analysis by fluorescence anisotropy measurements. Curves of the different DNA substrates are colored according to the color code.

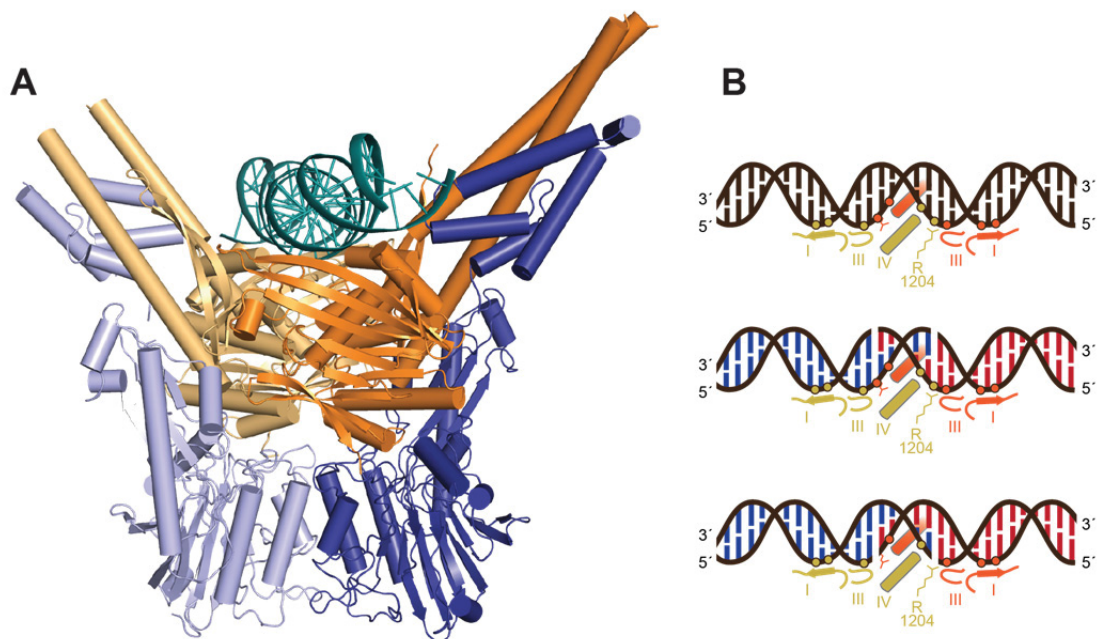
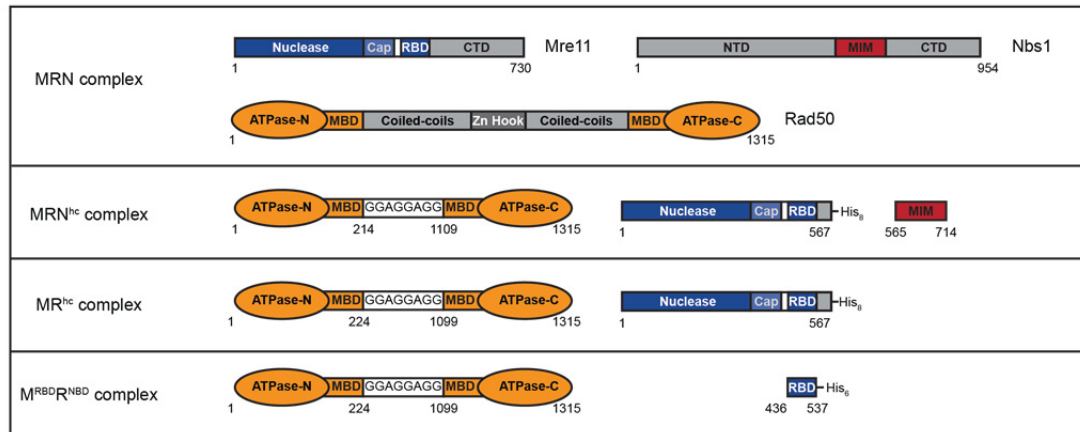


Figure 7: Model of the MR complex in DNA tethering. (A) Model of the ATP-bound MR complex (Rad50 dimer in light and dark orange; Mre11 dimer in light and dark blue) bound to dsDNA (teal). (B) Scheme of the Rad50 DNA binding motifs I-IV explains how additional DNA contacts are formed in the presence of continuous dsDNA or dsDNA with complementary 3' overhangs. DNAs are highlighted in brown, blue or red. DNA binding motifs of each Rad50 protomer are highlighted in light or dark orange.

Supplementary Information

A



B

Complex	Protein	amino acids	aa-linker	Affinity tag	plasmid	mutation
MRN^{hc} (crosslinking analysis)	Mre11	1–567	LEVLFQGP	8xHis	pET21b	D57N
	Rad50	1–214 GGAGGAGG 1109–1315	Fused N- and C-terminus	-	pET29b	E1238Q
	Nbs1	Met565–714	-	-	pET29b	-
MR^{hc} (SAXS analysis, Crystallization)	Mre11	1–567	LEVLFQGP	8xHis	pET21b	-
	Rad50	1–224 GGAGGAGG 1099–1315	Fused N- and C-terminus	-	pET29b	E1238Q
M^{RBD}R^{NBD} (Crystallization, DNA-binding)	Mre11	Met436–537	C-terminal AAAL	6xHis	pET21b	-
	Rad50	1–224 GGAGGAGG 1099–1315	Fused N- and C-terminus	-	pET29b	-

Figure S1: Constructs of the MR(N) (A) Domain models of full-length and truncated MR/N complexes are depicted. Nuclease domain (Nuclease), capping domain (Cap) and the Rad50-binding domain (RBD) of Mre11 are shown (blue). N- and C-terminal ATPase domains and the Mre11-binding domain of Rad50 (orange) as well as the Mre11-interacting module of Nbs1 (MIM, red) were used for purification. For structural analysis predicted flexible regions of the full-length complex (gray) were truncated. Glycine alanine linker (GGAGGAGG) is highlighted in white. CTD: C-terminal domain; NTD: N-terminal domain; Zn Hook: Zinc hook. (B) Table of MRN constructs used in this study.

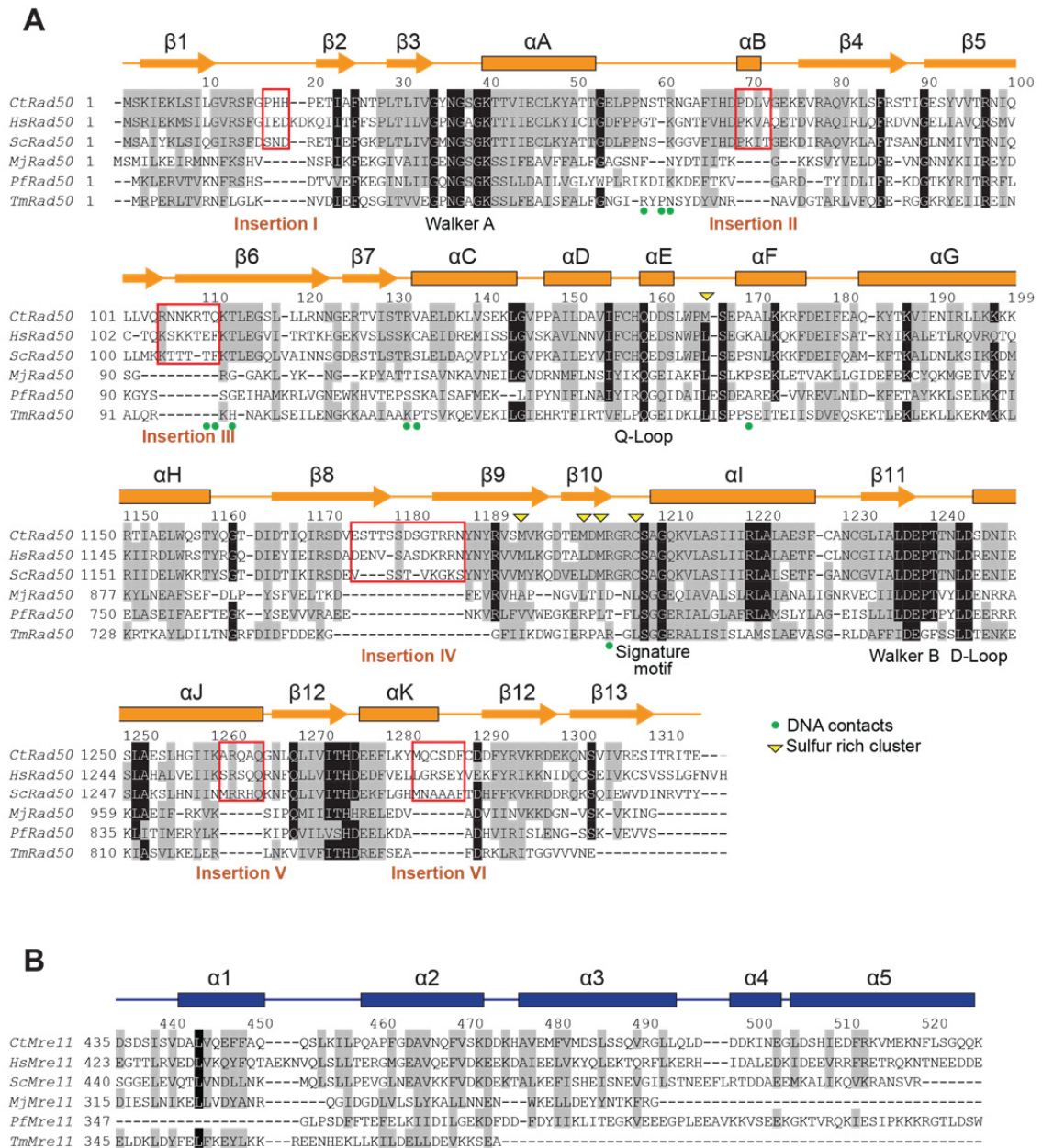


Figure S2: (A) Multiple sequence alignment of the nucleotide-binding domain of *C. thermophilum* Rad50 (CtRad50) with *Homo sapiens* (HsRad50), *S. cerevisiae* (ScRad50), *M. jannaschii* (MjRad50),

P. furiosus (PfRad50) and *T. maritima* (TmRad50). (B) Multiple sequence alignment of the Rad50-binding domain of *C. thermophilum* Mre11 (CtMre11) with *H. sapiens* (HsMre11), *S. cerevisiae* (ScMre11), *M. jannaschii* (MjMre11), *P. furiosus* (PfMre11) and *T. maritima* (TmMre11). In both (A) and (B) the sequences were aligned with Clustal Omega (Goujon *et al.* 2010, Sievers *et al.* 2011) and further optimized manually by comparison of the superimposed structures using PyMOL (Schrodinger 2010). Highly conserved residues are highlighted with black background and residues with conserved properties are depicted in gray. (C) Detailed view onto the sulfur rich cluster in CtRad50. Residues M166, M1194, M1201, M1203, C1207 and ATP γ S are depicted as sticks. Anomalous difference density map of the selenomethionines (gray) is contoured at 8.0 σ and C1207 is highlighted with yellow dots. The magnesium ion is shown as green sphere.

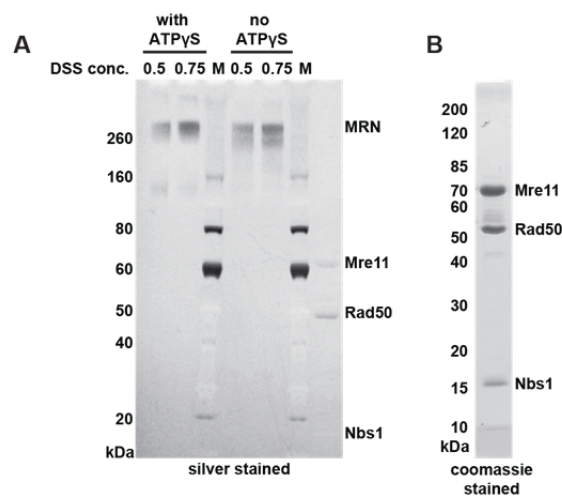


Figure S3: (A) Silver-stained SDS-polyacrylamide gel of cross-linked MRN^{hc} complex in presence and absence of ATP γ S. The samples were cross-linked with 0.5 or 0.75 molar ratio DSS cross-linker compared to the protein amount. (B) Coomassie-stained SDS polyacrylamide gel of the purified MRN^{hc} complex.

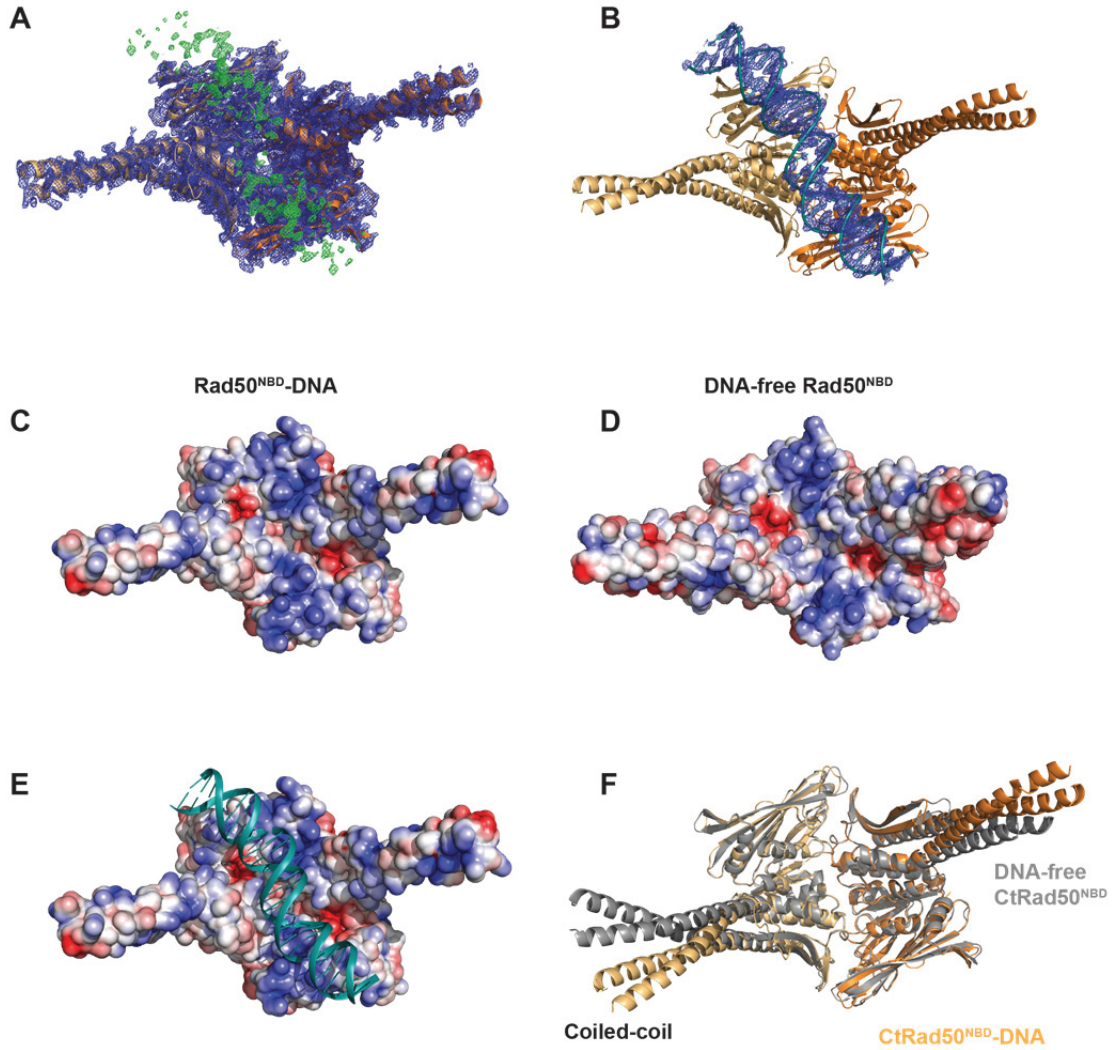


Figure S4: (A) Positive density (green) in the mF_o-DF_c difference electron density map corresponding to dsDNA is contoured at 2.8σ . The $2mF_o-DF_c$ map (blue) for the CtRad50^{NBD} dimer is contoured at 1σ . (B) The final $2mF_o-DF_c$ map (blue) of the dsDNA contoured at 1σ . (C) Electrostatic surface potential of CtRad50^{NBD} from the DNA-bound crystal structure. (D) Electrostatic surface potential of the DNA-free CtRad50^{NBD} structure. (E) CtRad50^{NBD}-DNA structure with electrostatic surface potential of CtRad50^{NBD}. (F) Superimposition of DNA-free and DNA-bound CtRad50^{NBD} crystal structures (gray and orange, respectively) reveal a different orientation of the coiled-coil domain.

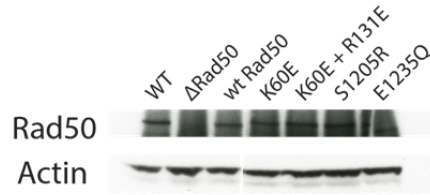


Figure S5: *S. cerevisiae* Rad50 expression levels of wild-type, *rad50Δ* and *rad50* mutant strains by western blot analysis. Comparable levels of Rad50 were detected in wild-type and the mutant strains.

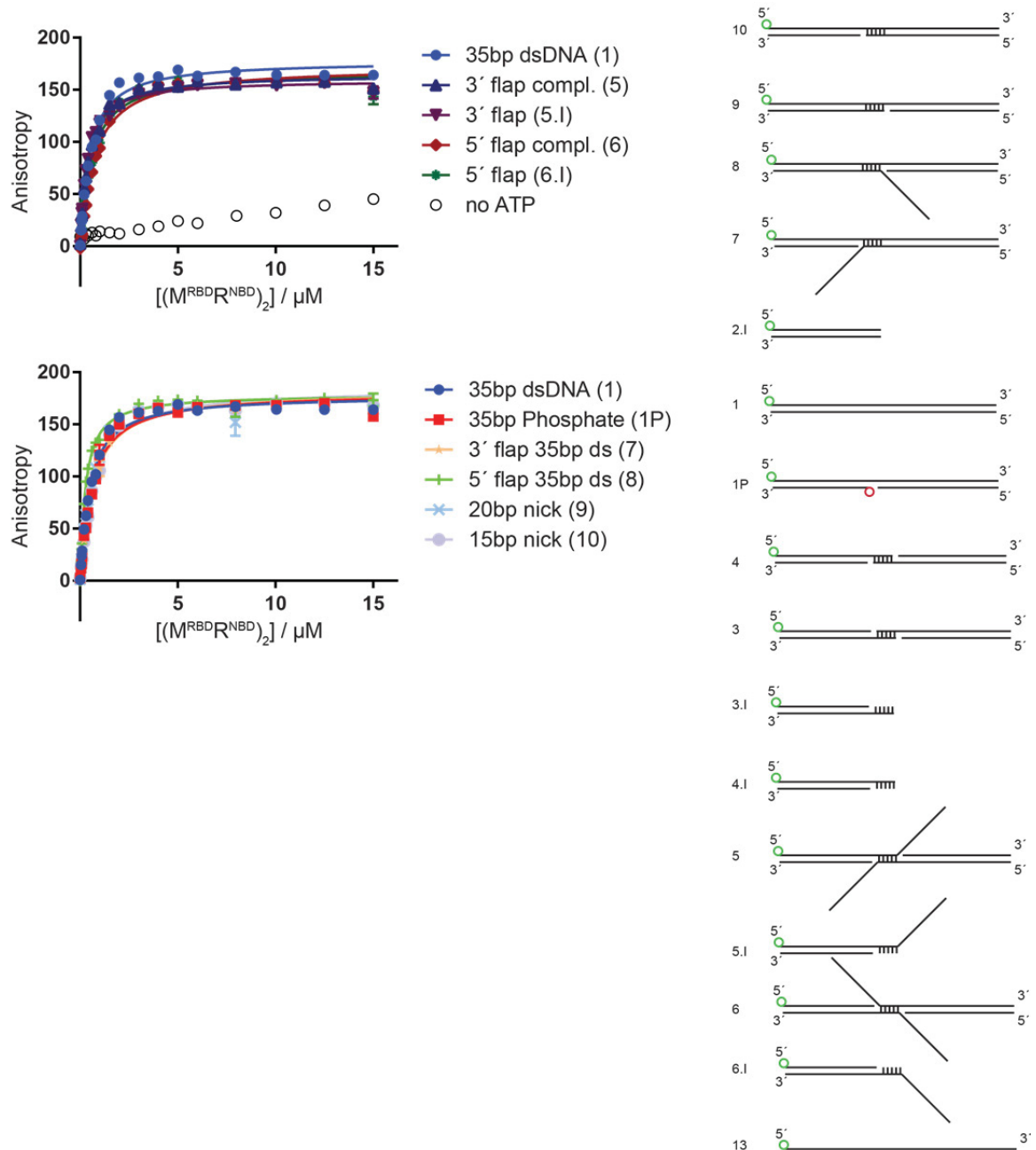


Figure S6: Fluorescence anisotropy measurements for DNA binding analysis of the $M^{RBD}R^{NBD}$ complex. Different DNA substrates are depicted.

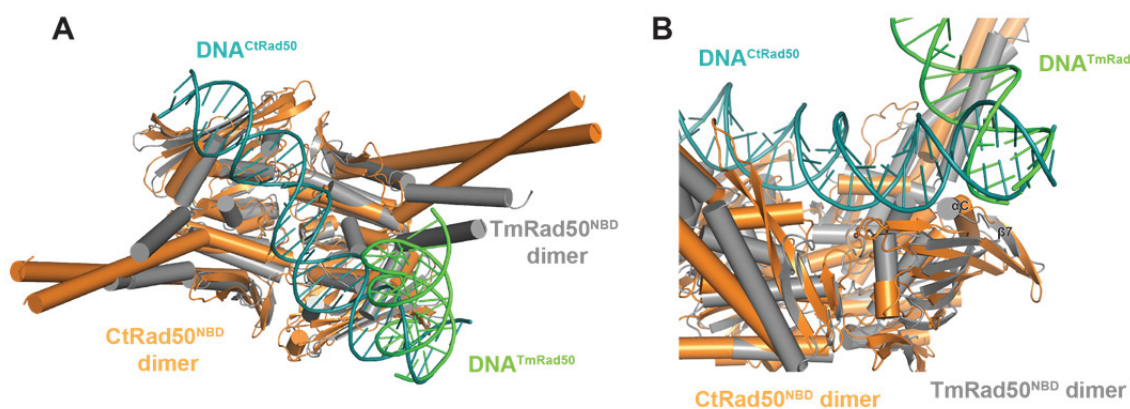


Figure S7: Comparison between CtRad50^{NBD}-DNA and TmRad50^{NBD}-DNA crystal structures. (A) Superimposition of TmRad50^{NBD}-DNA structure onto the Rad50^{NBD}-DNA structure of *C. thermophilum* (CtRad50^{NBD}-DNA). (B) Close-up view of the DNA interaction in lobe I.

Supplementary Table S1: Data collection and refinement statistics of the CtMre11^{RBD}-Rad50^{NBD} and the CtRad50^{NBD}-DNA crystal structures. Values in parentheses are for highest resolution shell.

	CtRad50 ^{NBD} -Mre11 ^{RBD} SeMet	CtRad50 ^{NBD} -DNA
Data collection		
Space group	I222	P2 ₁ 2 ₁ 2 ₁
Cell dimensions		
<i>a</i> , <i>b</i> , <i>c</i> (Å)	116.51, 125.09, 168.30	92.31, 97.08, 115.01
α , β , γ (°)	90.0, 90.0, 90.0	90.0, 90.0, 90.0
Wavelength (Å)	0.97973	0.97155
Resolution (Å)	50.00–3.00 (3.18–3.00)	50.00–2.50 (2.65–2.50)
<i>R</i> _{meas}	0.08 (1.23)	0.21 (1.92)
<i>I</i> / σ <i>I</i>	14.83 (1.58)	11.96 (1.33)
CC _{1/2}	99.9 (70.0)	99.8 (49.6)
Completeness (%)	99.2 (95.2)	99.5 (97.0)
Redundancy	6.9 (6.7)	12.8 (12.6)
Refinement		
Resolution (Å)	47.9–3.0	49.48–2.5
No. reflections	47386	34300
<i>R</i> _{work} / <i>R</i> _{free}	21.5/25.8	21.2/24.6
No. atoms		
Protein	7736	6831
DNA	-	615
Ligand/ion	64	111
Water	14	103
B-factors		
Protein	114.0	62.0
DNA	-	159.0
Ligand/ion	77.0	53.6
Water	90.3	54.4
R.m.s deviations		
Bond lengths (Å)	0.005	0.008
Bond angles (°)	1.0	1.2
Ramachandran plot		
Favoured regions (%)	98.3	98.6
Additionally allowed (%)	1.7	1.3
Outliers (%)	0	0.1

Supplementary Table S2: Dissociation constants (K_d) between dimeric CtM^{RBD}R^{NBD} and different DNA substrates.

	K_d [μ M]	Std. Error	number of experiments
35bp dsDNA (1)	0.45	0.03	3
35bp Phosphate (1P)	0.56	0.04	3
17bp dsDNA (2.I)	3.1	0.4	3
5' overhang compl. (3)	2.2	0.3	3
5' overhang (3.I)	2.7	0.3	3
3' overhang compl. (4)	0.44	0.04	3
3' overhang (4.I)	0.99	0.1	3
3' flap compl. (5)	0.4	0.03	3
3' flap (5.I)	0.34	0.02	3
5' flap compl. (6)	0.67	0.05	3
5' flap (6.I)	0.54	0.04	3
3' flap 35bp dsDNA (7)	0.60	0.04	3
5' flap 35bp dsDNA (8)	0.25	0.02	3
20bp nick (9)	0.47	0.04	3
15bp nick (10)	0.62	0.04	3
35bp ssDNA (13)	1.9	0.3	3
35 bp dsDNA no ATP	~ 320.2	~ 922.4	1

Supplementary Table S3: Detected cross-links

Id	Protei n1	Protei n2	XLTy pe	AbsP os1	AbsP os2	SameP osition	delt aA	Mr	Mz	z	Erro r_ lpp m.	nse en	Matc h Od ds	Xco rrx	Xcorr b	TIC	Tic A	TicB	WTIC	intsu m	delta S	D elta Sc or e2	Id.Scor e	D ec oy	Experit	dist	
VEQDREKILK-LLKKK-a7-b3	decoy	Rad50	decoy	233	196	FALSE	37	2023.237	506.8	17	4	-1.8	1	69	3	0.13	0.47	5	2	0.1	309	0.96	4	36.6	x	MRN_ ATPVs	NA
EVKFGVGGHAPIDLEDNR-TOKLTGSLLR-a3-b3	decoy	Rad50	decoy	365	112	FALSE	253	3390.814	848.7	11	4	-0.1	27	1	0	0.09	0.33	1	2	0.06	379	0.84	16	22.29	x	MRN_ ATPVs	NA
KDDSWR-VKRDEK-a1-b2	Mre11	Rad50	inter	30	1296	FALSE	390	1716.877	430.2	27	4	-1.4	14	02	3	0.21	0.52	2	9	0.08	221	0.71	29	36.58		MRN_ ATPVs	18
DEKQNSVIVR-QEVTKR-a3-b5	Rad50	Mre11	inter	1300	331	FALSE	93	2084.122	695.7	15	3	-0.4	5	9	4	0.19	0.23	5	8	0.04	196	0.49	51	29.22		MRN_ ATPVs	20
SLAESHGIIKAR-KTGTTT-a11-b1	Rad50	Mre11	inter	1260	411	FALSE	27	2194.236	439.8	55	5	-3.4	8	3	2	0.11	0.66	5	2	0.08	114	0.43	57	34.65		MRN_ ATPVs	20
LKVEYSPGTFKFEVENPQR-SLAESHGIIKAR-a2-b11	Mre11	Rad50	inter	371	1260	FALSE	13	3868.04	968.0	18	4	0.9	254	9.8	3	0.08	0.38	4	4	0.06	483	0.61	39	32.56		MRN_ ATPVs	23
SLAESHGIIKAR-LKVEYSPGTFK-a11-b2	Rad50	Mre11	inter	1260	371	FALSE	13	2868.556	574.7	19	5	-1.4	10	1	1	0.1	0.52	9	3	0.08	149	0	0	29.22		MRN_ ATPVs	23
ILKER-KVMEK-a3-b1	Rad50	Mre11	inter	207	514	FALSE	307	1428.83	358.2	15	4	-4.9	4	93	4	0.19	0.5	3	7	0.08	146	0.48	52	38.67		MRN_ ATPVs	26
QDNROEVTKR-VKRDEK-a9-b2	Mre11	Rad50	inter	331	1296	FALSE	89	2184.162	547.0	48	4	0.3	3	5	1	0.02	0.49	6	3	0.1	137	0	0	23.92		MRN_ ATPVs	30
DEKQNSVIVR-KTGTTT-a3-b1	Rad50	Mre11	inter	1300	411	FALSE	13	1987.066	663.3	63	3	-2.2	4	6	0	0.16	0.32	7	6	0.05	370	0	0	30.59		MRN_ ATPVs	32
RDEKQNSVIVR-KTGTTT-a4-b1	Rad50	Mre11	inter	1300	411	FALSE	13	2143.167	536.7	99	4	-2	5	8	2	0.17	0.33	4	9	0.05	462	0	0	29.55		MRN_ ATPVs	32
VKRDEK-DNKVR-a2-b3	Rad50	Mre11	inter	1296	193	FALSE	227	1541.846	514.9	57	3	-4.2	5	9	4	0.11	0.59	1	7	0.09	141	0	0	33.44		MRN_ ATPVs	34
IEKLSILGVR-KAMYQVMR-a3-b1	Rad50	Mre11	inter	6	67	FALSE	61	2290.288	573.5	8	4	-1.1	2	7	1	0.17	0.49	3	6	0.08	623	0	0	33.41		MRN_ ATPVs	35
FAGKVAQNQDVVHPYR-SLAESHGIIKAR-a4-b11	Mre11	Rad50	inter	397	1260	FALSE	13	3395.8	680.1	68	5	-3	2	9	1	0.2	0.34	6	8	0.06	275	0.6	40	29.86		MRN_ ATPVs	36
AQVKLSFR-DNKVR-a4-b3	Rad50	Mre11	inter	82	193	FALSE	111	1715.966	429.9	99	4	-1.6	4	42	2	0.14	0.6	9	1	0.09	310	0.55	45	37.47		MRN_ ATPVs	36
DVDMVLGGNLFHDNKPSPR-IEKLSILGVR-a16-b3	Mre11	Rad50	inter	63	6	FALSE	57	3390.822	848.7	13	4	-3.4	7	7	6	0.05	0.53	0.4	3	0.08	461	0.44	56	27.35		MRN_ ATPVs	39
DVDMVLGGNLFHDNKPSPR-K-IEKLSILGVR-a16-b3	Mre11	Rad50	inter	63	6	FALSE	57	3518.927	880.7	39	4	-0.5	3	5	2	0.09	0.48	9	9	0.07	339	0.25	75	24.93		MRN_ ATPVs	39
KODNRQEVTK-VKRDEK-a1-b2	Mre11	Rad50	inter	322	1296	FALSE	98	2156.149	432.2	38	5	-2.5	9	9	1	0.04	0.5	6	4	0.1	169	0.78	22	31.87		MRN_ ATPVs	41
ETHIKVETTK-KODNRQEVTK-a5-b1	Rad50	Mre11	inter	1115	322	FALSE	83	2567.353	642.8	46	4	-1.2	2	9.2	1	0.07	0.48	6	2	0.08	433	0.81	19	31.65		MRN_ ATPVs	57
ILKER-KODNR-a3-b1	Rad50	Mre11	inter	207	322	FALSE	115	1454.816	364.7	12	4	-3	2	1	6	0.23	0.51	6	5	0.08	168	0.39	61	37.1		MRN_ ATPVs	57
KAMYQVMR-RPKETQ-a1-b3	Mre11	Nbs1	inter	67	711	FALSE	81	1920.988	481.2	55	4	-2	4	84	4	0.19	0.61	0.3	0.3	0.1	441	0	0	39.48		MRN_ ATPVs	NA

AQVKLSFR-RPKETQ-a4-b3	Rad50	Nbs1	inter	82	711	FALSE	66	1843.03	461.7	4	-0.9	4	11.04	0.0	0.19	0.52	1	0.3	0.2	0.08	449	0.38	62	39.1	MRN_ ATPVs	NA
KPKEGKR-RPKETQ-a3-b3	Mre11	Nbs1	inter	419	711	FALSE	271	1736.988	580.0	3	-1.3	41	10.85	0.0	0.23	0.5	4	0.3	0.1	0.08	317	0	10	39.05	MRN_ ATPVs	NA
MSKIEK-RPKETQ-a3-b3	Rad50	Nbs1	inter	3	711	FALSE	145	1629.875	544.2	3	-0.9	2	11.13	0.0	0.16	0.5	2	0.2	0.2	0.08	237	0.29	71	38.84	MRN_ ATPVs	NA
SLAESLHGIIKAR-KPKEGK-a11-b3	Rad50	Mre11	inter	1260	419	FALSE	35	2217.284	555.3	4	-0.3	2	10.45	0.0	0.12	0.74	9	0.6	0.0	0.09	132	0.86	14	38.61	MRN_ ATPVs	NA
RPKETQ-DNKVR-a3-b3	Nbs1	Mre11	inter	711	193	FALSE	45	1525.819	382.4	4	-1.2	60	99	3	0.19	0.43	2	0.3	0.1	0.07	254	0	10	38.18	MRN_ ATPVs	NA
KPKEGK-RPKETQ-a3-b3	Mre11	Nbs1	inter	419	711	FALSE	271	1580.888	396.2	3	-0.6	36	74	2	0.15	0.57	9	0.1	0.3	0.09	260	0	10	38.16	MRN_ ATPVs	NA
TFRDNKVR-RPKETQ-a6-b3	Mre11	Nbs1	inter	193	711	FALSE	45	1930.035	387.0	5	-1.5	56	91	4	0.17	0.47	0.2	0.2	7	0.08	302	0.69	31	37.99	MRN_ ATPVs	NA
KPKEGK-RPKETQ-a1-b3	Mre11	Nbs1	inter	417	711	FALSE	269	1580.888	396.2	3	-0.6	7	22	2	0.21	0.58	9	0.1	0.3	0.09	257	0	10	37.8	MRN_ ATPVs	NA
RPKETQ-VKRDEK-a3-b2	Nbs1	Rad50	inter	711	1296	FALSE	272	1668.911	418.2	4	-2.7	35	03	0	0.22	0.55	6	0.3	0.1	0.09	282	0	10	37.02	MRN_ ATPVs	NA
SLAESLHGIIKAR-KPKEGK-a11-b3	Rad50	Mre11	inter	1260	419	FALSE	35	2373.381	594.3	4	-2	7	76	0	0.06	0.58	2	0.5	0.0	0.08	276	0.62	38	36.94	MRN_ ATPVs	NA
VMEKNFLSGQK-RPKETQ-a4-b3	Mre11	Nbs1	inter	518	711	FALSE	370	2303.192	768.7	3	-0.8	2	93	8	0.11	0.44	6	0.3	0.0	0.06	805	0	10	36.89	MRN_ ATPVs	NA
ETHIKVETTK-RPKETQ-a5-b3	Rad50	Nbs1	inter	1115	711	FALSE	91	2080.114	521.0	4	-1.3	4	23	4	0.08	0.38	8	0.1	0.1	0.07	316	0.7	30	36.56	MRN_ ATPVs	NA
KPKEGK-MSKIEK-a3-b3	Mre11	Rad50	inter	419	3	FALSE	416	1557.877	390.4	10	-2.1	2	52	4	0.12	0.47	1	0.1	0.3	0.08	199	0	10	36.12	MRN_ ATPVs	NA
IEKLSILGVR-RPKETQ-a3-b3	Rad50	Nbs1	inter	6	711	FALSE	142	2022.178	506.5	4	-2.7	3	8	4	0.13	0.52	7	0.3	0.1	0.08	528	0	10	35.21	MRN_ ATPVs	NA
VPEADNIHVKPILLQK-RPKETQ-a10-b3	Mre11	Nbs1	inter	161	711	FALSE	13	2708.519	542.7	5	-1.3	17	05	2	0.14	0.48	9	0.1	0.2	0.11	262	0	10	35.04	MRN_ ATPVs	NA
KPKEGKR-ILKER-a3-b3	Mre11	Rad50	inter	419	207	FALSE	212	1636.993	410.2	4	-3.9	5	5	6	0.15	0.48	9	0.1	0.2	0.08	179	0	10	34.79	MRN_ ATPVs	NA
NFLSGQKQAKR-KKGDELK-a8-b2	Mre11	Rad50	inter	526	199	FALSE	327	2358.267	590.5	4	0.4	3	8	4	0.15	0.43	9	0.2	0.1	0.07	276	0.53	47	34.1	MRN_ ATPVs	NA
RPKETQ-KVMEK-a3-b1	Nbs1	Mre11	inter	711	514	FALSE	366	1528.826	383.2	4	-1.8	4	4	4	0.18	0.35	4	0.2	0.1	0.06	234	0	10	33.07	MRN_ ATPVs	NA
NFLSGQKQAKR-YTKVIENIR-a8-b3	Mre11	Rad50	inter	526	187	FALSE	339	2676.426	670.1	4	-3.4	3	4	1	0.19	0.48	7	0.3	0.1	0.07	379	0	10	32.95	MRN_ ATPVs	NA
IKQDEENVLELAR-AQVKLSFR-a2-b4	Nbs1	Rad50	inter	577	82	FALSE	68	2770.479	693.6	4	-2.8	2	7	5	0.11	0.46	6	0.3	0.1	0.07	418	0	10	32.21	MRN_ ATPVs	NA
KIKQDEENVLELAR-VKRDEK-a3-b2	Nbs1	Rad50	inter	577	1296	FALSE	406	2724.459	682.1	4	-2.6	6	9.1	2	0.12	0.47	7	0.2	0.2	0.09	259	0.51	49	31.97	MRN_ ATPVs	NA
IKQDEENVLELAR-EITLATDKR-a2-b8	Nbs1	Mre11	inter	577	314	FALSE	300	2868.5	718.1	3	-2.9	2	8	1	0.13	0.44	6	0.2	0.1	0.07	480	0.16	84	31.81	MRN_ ATPVs	NA
RDEKONSIVVR-RPKETQ-a4-b3	Rad50	Nbs1	inter	1300	711	FALSE	276	2238.203	560.5	4	-2.3	3	5	1	0.07	0.35	0.2	0.1	0.1	0.06	418	0.77	23	30.16	MRN_ ATPVs	NA
RFKGLEK-RPKETQ-a3-b3	Mre11	Nbs1	inter	317	711	FALSE	169	1771.988	591.6	3	-3.5	2	7	7	0.1	0.25	4	0.1	0.1	0.04	274	0.74	26	29.68	MRN_ ATPVs	NA
KIKQDEENVLELAR-KPKEGKR-a3-b3	Nbs1	Mre11	inter	577	419	FALSE	405	2792.534	559.5	5	-2.2	2	8	2	0.06	0.59	9	0.4	0.1	0.08	402	0	10	29.54	MRN_ ATPVs	NA
YTKVIENIR-RPKETQ-a3-b3	Rad50	Nbs1	inter	187	711	FALSE	39	2030.111	677.7	3	-2.5	3	1	6	0.13	0.4	7	0.3	0.0	0.06	447	0	10	29.46	MRN_ ATPVs	NA
NFLSGQKQAKR-ETHIKVETTK-a8-b5	Mre11	Rad50	inter	526	1115	FALSE	287	2726.433	909.8	3	-0.6	6	8	1	0.08	0.3	0.1	0.1	0.1	0.05	319	0.28	72	29.2	MRN_ ATPVs	NA

RDEKQNSVVR-KPKEGK-a4-b3	Rad50	Mre11	inter	1300	419	FALSE	5	2166.209	542.5	4	-1.2	5	8.2	0.0	0.11	0.36	0.1	0.2	0.07	426	0.68	32	28.45	MRN_ATPVs	NA	
IKQEDENVLEIAR-IEKLSILGVR-a2-b3	Nbs1	Rad50	inter	577	6	FALSE	8	2949.635	738.4	4	-1.4	2	7.6	0	0.09	0.42	5	6	0.07	549	0	0	27	MRN_ATPVs	NA	
KIKQEDENVLEIAR-SFEVEKPILR-a3-b6	Nbs1	Mre11	inter	577	294	FALSE	280	3167.708	792.9	35	4	0.1	1	9	0	0.12	0.39	5	4	0.08	496	0.81	19	23.93	MRN_ATPVs	NA
KGDELK-LLKKK-a1-b3	Rad50	Rad50	intra	199	196	FALSE	3	1454.903	364.7	34	4	-2.5	16	64	0	0.18	0.58	2	6	0.1	174	0	0	38.37	MRN_ATPVs	5
KGDELK-LLKKK-a1-b4	Rad50	Rad50	intra	199	197	FALSE	2	1454.902	364.7	33	4	-3.2	5	5	6	0.11	0.58	2	6	0.1	188	0.65	35	34.88	MRN_ATPVs	5
IEKLSILGVR-AQVKLSFR-a3-b4	Rad50	Rad50	intra	6	82	FALSE	76	2212.329	554.0	9	4	-0.6	847	71	3	0.31	0.64	5	9	0.1	553	0	0	41.4	MRN_ATPVs	8
MSKIEKLSILGVR-AQVKLSFR-a6-b4	Rad50	Rad50	intra	6	82	FALSE	76	2558.498	640.6	32	4	-0.1	1	5	1	0.1	0.43	0.2	3	0.08	315	0.66	34	28.1	MRN_ATPVs	8
KQDNRRQVTK-FKGLEK-a1-b2	Mre11	Mre11	intra	322	317	FALSE	5	2103.131	526.7	91	4	-0.6	63	24	5	0.08	0.57	8	8	0.1	495	0.67	33	38.39	MRN_ATPVs	8
KQDNRRQVTK-RFKGLEK-a1-b3	Mre11	Mre11	intra	322	317	FALSE	5	2259.228	377.5	46	6	-2.3	93	4	3	0.23	0.45	4	1	0.08	217	0.84	16	37.3	MRN_ATPVs	8
RFKGLEK-KQDNR-a3-b1	Mre11	Mre11	intra	317	322	FALSE	5	1673.916	335.7	91	5	-3.3	41	2	5	0.18	0.56	2	3	0.08	226	0.49	51	35.17	MRN_ATPVs	8
FKGLEK-KQDNR-a2-b1	Mre11	Mre11	intra	317	322	FALSE	5	1517.815	380.4	62	4	-3.2	27	08	8	0.18	0.34	2	2	0.06	225	0	0	34.74	MRN_ATPVs	8
ETHIKVETTK-ILKER-a5-b3	Rad50	Rad50	intra	1115	207	FALSE	32	1980.121	496.0	38	4	-2.3	9	17	0	0.11	0.29	7	2	0.06	109	0.64	36	33.06	MRN_ATPVs	9
ETHIKVETTK-KGDELK-a5-b2	Rad50	Rad50	intra	1115	199	FALSE	40	2139.176	535.8	02	4	-1.3	114	85	3	0.17	0.39	2	7	0.06	633	0.84	16	37.05	MRN_ATPVs	11
ETHIKVETTK-KGDELK-a5-b1	Rad50	Rad50	intra	1115	199	FALSE	40	2011.084	671.3	69	3	0.1	108	23	2	0.25	0.39	1	8	0.06	408	0.73	27	36.56	MRN_ATPVs	11
GDELKILK-LLKKK-a5-b4	Rad50	Rad50	intra	204	197	FALSE	7	1681.073	421.2	76	4	-1.6	2	2	6	0.21	0.51	1	4	0.1	219	0.79	21	34.85	MRN_ATPVs	11
KGDELKILK-LLKKK-a6-b4	Rad50	Rad50	intra	204	197	FALSE	7	1809.162	453.2	98	4	-4.8	4	8	0.1	0.06	0.27	5	2	0.05	327	0.93	7	29.31	MRN_ATPVs	11
KAMYQVMR-KDDSWR-a1-b1	Mre11	Mre11	intra	67	30	FALSE	37	1968.949	493.2	45	4	-3	8	9	7	0.19	0.62	8	4	0.09	303	0	0	35.38	MRN_ATPVs	11
DVDMVLLGGNLFHDNKPSPR-KAMYQVMR-a16-b1	Mre11	Mre11	intra	63	67	FALSE	4	3289.634	658.9	35	5	-2.1	5	4	1	0.1	0.57	2	5	0.07	218	0.99	1	35.03	MRN_ATPVs	11
DVDMVLLGGNLFHDNKPSPR-K-KAMYQVMR-a16-b1	Mre11	Mre11	intra	63	67	FALSE	4	3417.731	570.6	3	6	-1.5	9	7	0	0.13	0.4	6	3	0.07	229	0	0	29.11	MRN_ATPVs	11
KGDELK-ILKER-a1-b3	Rad50	Rad50	intra	199	207	FALSE	8	1483.856	371.9	72	4	-3.2	3	39	3	0.35	0.83	9	4	0.15	164	0	0	45.75	MRN_ATPVs	12
KKGDELK-ILKER-a2-b3	Rad50	Rad50	intra	199	207	FALSE	8	1611.953	403.9	96	4	-2.2	14	27	8	0.17	0.7	0.1	0.6	0.13	187	0	0	38.47	MRN_ATPVs	12
ILKEREVQDK-KGDELKILK-a3-b1	Rad50	Rad50	intra	207	199	FALSE	8	2437.422	407.2	45	6	2.8	2	5	2	0.01	0.22	1	1	0.04	259	0.9	10	22.98	MRN_ATPVs	12
KGDELKILK-LLKKK-a6-b3	Rad50	Rad50	intra	204	196	FALSE	8	1809.168	604.0	64	3	-1.4	9	1	2	0.1	0.45	2	3	0.07	331	0.76	24	34.42	MRN_ATPVs	13
ETHIKVETTK-KGDELK-a5-b1	Rad50	Rad50	intra	1115	198	FALSE	41	2139.173	714.0	66	3	-2.5	46	32	0.1	0.04	0.36	7	9	0.06	552	0.82	18	33.38	MRN_ATPVs	14
KKGDELK-ILKER-a1-b3	Rad50	Rad50	intra	198	207	FALSE	9	1611.949	403.9	95	4	-4.4	5	57	2	0.15	0.59	7	2	0.11	182	0	0	37.79	MRN_ATPVs	14
NGAFHPDLVGKEVR-TQKTLGSLLR-a14-b3	Rad50	Rad50	intra	75	112	FALSE	37	3390.809	679.1	7	5	-1.8	471	3	2	0.11	0.48	7	1	0.07	416	0.76	24	32.07	MRN_ATPVs	14
NGAFHPDLVGKEVR-TQKTLGSLLR-a14-b4	Rad50	Rad50	intra	75	112	FALSE	37	3546.913	710.3	9	5	-0.8	17	6	1	0.06	0.55	9	6	0.08	220	0.54	46	27.7	MRN_ATPVs	14

EITLATDKR-KQDNR-a8-b1	Mre11	Mre11	intra	314	322	FALSE	8	1842.974	615.3	3	-3	10	8.2	0.0	0.08	0.64	0.6	0.0	0.08	301	0	10	30.84	MRN_ ATPVs	15
KODNRQEVTK-EITLATDKR-a1-b8	Mre11	Mre11	intra	322	314	FALSE	8	2428.291	810.4	38	-0.6	11	8.3	0.0	0.03	0.41	0.1	0.2	0.07	488	0.64	36	28.02	MRN_ ATPVs	15
RFKLEK-QEVTKR-a3-b5	Mre11	Mre11	intra	317	331	FALSE	14	1774.005	355.8	09	-3	4	9.5	0	0.2	0.38	8	0.1	0.06	367	0.6	40	33.89	MRN_ ATPVs	15
RFDEIFEAKQYTK-VAELDKLVEK-a10-b6	Rad50	Rad50	intra	184	138	FALSE	46	3041.584	761.4	04	-3.8	3	10	0.0	0.17	0.63	2	1	0.11	294	0.64	36	37.18	MRN_ ATPVs	15
LVKEYSSPEGTK-KKTGTTR-a2-b2	Mre11	Mre11	intra	371	411	FALSE	40	2265.219	756.0	81	-1.3	6	10	0.0	0.2	0.44	8	0.0	0.06	642	0	10	35.91	MRN_ ATPVs	16
LVKEYSSPEGTKFEVENPQR-KTGTRPK-a2-b1	Mre11	Mre11	intra	371	411	FALSE	40	3489.85	873.4	7	0.8	4	9	0.0	0.07	0.31	4	0.0	0.05	503	0.42	58	23.02	MRN_ ATPVs	16
FAGKVAONQDVVHFYRK-QDNRQEVTKR-a4-b9	Mre11	Mre11	intra	397	331	FALSE	66	3402.751	851.6	96	-1.1	30	6.9	0.0	0.06	0.29	0.2	0.0	0.04	455	0.22	78	23.33	MRN_ ATPVs	17
QEVTKR-KQDNR-a5-b1	Mre11	Mre11	intra	331	322	FALSE	9	1556.824	390.2	14	-1.7	117	9.2	0.0	0.07	0.52	6	0.2	0.08	401	0.98	2	32.24	MRN_ ATPVs	18
NGAFIHPDLVGEKEVR-DEKQNSVVR-a14-b3	Rad50	Rad50	intra	75	1300	FALSE	349	3219.648	805.9	2	-1.4	3	10	0.0	0.16	0.43	7	0.1	0.08	702	0.74	26	34.95	MRN_ ATPVs	19
GMAAVDHAIMQYHSHKMM-EQJNR-RFDEIFEAKQYTK-a15-b10	Rad50	Rad50	intra	1143	184	FALSE	83	4372.103	875.4	28	3	1	7.9	0.0	0.08	0.28	2	0.0	0.04	484	0.69	31	26.25	MRN_ ATPVs	19
VAELDKLVSEK-YTKVIENIR-a6-b3	Rad50	Rad50	intra	138	187	FALSE	49	2502.393	835.1	39	-0.8	7	18	0.0	0.21	0.5	4	0.2	0.08	738	0	10	36.77	MRN_ ATPVs	20
FKGLEK-KTGTR-a2-b1	Mre11	Mre11	intra	317	411	FALSE	94	1520.853	507.9	59	-1.9	4	1	8	0.1	0.41	3	0.1	0.07	251	0	10	30.77	MRN_ ATPVs	21
GLQLDDDKINEGLDISHIED-FRK-VMEKNFLSGQOK-a9-b4	Mre11	Mre11	intra	500	518	FALSE	18	4215.111	1054.	79	-1.1	2	4	0.0	0.07	0.23	2	0.1	0.04	600	0.75	25	23.63	MRN_ ATPVs	23
NGAFIHPDLVGEKEVR-AQVKLSFR-a14-b4	Rad50	Rad50	intra	75	82	FALSE	7	2980.571	597.1	22	-2	2	6	0.0	0.06	0.44	8	0.2	0.1	452	0.48	52	28.15	MRN_ ATPVs	24
TQKTLEGSLLLR-IEKLSILGVR-a3-b3	Rad50	Rad50	intra	112	6	FALSE	106	2622.565	656.6	49	-1.2	2	3	0.0	0.15	0.3	0.2	0.1	0.05	213	0.56	44	27.69	MRN_ ATPVs	25
YTKVIENIR-ILKER-a3-b3	Rad50	Rad50	intra	187	207	FALSE	20	1930.121	483.5	38	-2.1	2	8	0.0	0.19	0.42	1	0.1	0.06	472	0	10	32.94	MRN_ ATPVs	30
VPEADNIHVKPILLQK-KAMYQVMR-a10-b1	Mre11	Mre11	intra	161	67	FALSE	94	2976.626	596.3	33	-1.1	6	7.3	0.0	0.12	0.53	8	0.0	0.4	332	0	10	27.61	MRN_ ATPVs	35
YTKVIENIR-AQVKLSFR-a3-b4	Rad50	Rad50	intra	187	82	FALSE	105	2220.259	556.0	73	-1.8	2	1	0.0	0.18	0.55	0.2	0.3	0.09	407	0.56	44	35.82	MRN_ ATPVs	36
CSAGQKVLASIIIR-TQKTLEGSLLLR-a6-b3	Rad50	Rad50	intra	1212	112	FALSE	224	3010.715	753.6	87	-2.2	3	4	0.0	0.08	0.39	9	0.1	0.06	502	0.57	43	24.64	MRN_ ATPVs	37
TFRDNKVR-KVMEK-a6-b1	Mre11	Mre11	intra	193	514	FALSE	321	1805.977	452.5	02	-2.7	1	6	0.0	0.1	0.3	7	0.1	0.05	270	0	10	28.65	MRN_ ATPVs	59
TFRDNKVR-QEVTKR-a6-b5	Mre11	Mre11	intra	193	331	FALSE	138	1932.049	484.0	2	-2.7	3	7.7	0.0	0.08	0.46	1	0.3	0.08	311	0.87	13	27.46	MRN_ ATPVs	59
AQVKLSFR-ILKER-a4-b3	Rad50	Rad50	intra	82	207	FALSE	125	1743.037	436.7	67	-2.2	4	10	0.0	0.21	0.68	0.6	0.0	0.1	314	0	10	40.26	MRN_ ATPVs	62
KQDNRQEVTK-DNKVR-a1-b3	Mre11	Mre11	intra	322	193	FALSE	129	2013.058	504.2	72	-1.1	3	9.5	0.0	0.11	0.46	7	0.2	0.09	268	0.67	33	32.87	MRN_ ATPVs	63
KQDNRQEVTK-TFRDNKVR-a1-b6	Mre11	Mre11	intra	322	193	FALSE	129	2417.275	605.3	27	-1.1	5	7.8	0.0	0.03	0.33	0.2	0.1	0.05	346	0.72	28	25.95	MRN_ ATPVs	63
KKGDELK-VKREK-a2-b2	Rad50	Rad50	intra	199	1296	FALSE	221	1727.976	346.6	03	-1.4	2	8.7	0.0	0.12	0.27	5	0.1	0.04	403	0.79	21	29.11	MRN_ ATPVs	66
ETHIKVETTK-VKREK-a5-b2	Rad50	Rad50	intra	1115	1296	FALSE	181	2096.146	525.0	44	-0.9	4	8.4	0	0.12	0.36	0.2	0.1	0.06	174	0	10	29.16	MRN_ ATPVs	73

KODNRQEVTK-KODNIR-a1-b1	Mre11	Mre11	intra	322	322	TRUE	0	2042.051	511.5	4	0.1	2	8.6	4	0	0.08	0.38	0.2	0.1	0.07	331	0	10	29.18	MRN_ ATPVs	96
KPKEGKR-FKGLEK-a3-b2	Mre11	Mre11	intra	419	317	FALSE	102	1699.995	341.0	5	-1.9	22	11.	0.0	4	0.23	0.53	0.0	0.4	0.09	223	0.84	16	40.6	MRN_ ATPVs	NA
RFKGLEK-KPKEGK-a3-b3	Mre11	Mre11	intra	317	419	FALSE	102	1699.993	426.0	4	-3.2	13	27	5	5	0.14	0.54	0.1	0.3	0.09	253	0.89	11	39.22	MRN_ ATPVs	NA
NFLSGQKQAKR-KPKEGKR-a8-b3	Mre11	Mre11	intra	526	419	FALSE	107	2383.303	795.4	3	-2.2	8	62	1	0.1	0.2	0.56	0.4	0.0	0.08	290	0	10	38.82	MRN_ ATPVs	NA
KPKEGKR-RFKGLEK-a3-b3	Mre11	Mre11	intra	419	317	FALSE	102	1856.098	465.0	4	-1	17	25	1	0.0	0.1	0.56	0.4	0.1	0.09	309	0.85	15	38.61	MRN_ ATPVs	NA
VMEKNFLSGQK-KPKEGKR-a4-b3	Mre11	Mre11	intra	518	419	FALSE	99	2387.298	796.7	3	-0.8	4	89	5	0.0	0.16	0.45	0.2	0.1	0.07	819	0.7	30	37.69	MRN_ ATPVs	NA
EITLATDKR-KPKEGKR-a8-b3	Mre11	Mre11	intra	314	419	FALSE	105	2025.155	676.0	3	-1.8	46	77	8	0.0	0.12	0.54	0.4	0.1	0.08	430	0.37	63	37.63	MRN_ ATPVs	NA
KPKEGKR-KVMEK-a3-b1	Mre11	Mre11	intra	419	514	FALSE	95	1612.934	404.2	4	0.2	11	3	2	0.0	0.16	0.28	0.1	0.1	0.05	343	0	10	37.01	MRN_ ATPVs	NA
NFLSGQKQAKR-KTGTTT-a8-b1	Mre11	Mre11	intra	526	411	FALSE	115	2204.163	552.0	4	-1.5	3	9.9	8	0.0	0.15	0.64	0.6	0.0	0.08	309	0	10	36.72	MRN_ ATPVs	NA
LKVEYSSPEGTK-KPKEGKR-a2-b3	Mre11	Mre11	intra	371	419	FALSE	48	2316.265	773.0	3	-1.6	25	3	6	0.0	0.23	0.5	0.4	0.0	0.07	537	0	10	35.78	MRN_ ATPVs	NA
TFRDNKVR-KPKEGKR-a6-b3	Mre11	Mre11	intra	193	419	FALSE	226	2014.137	403.8	5	-3.3	9	78	1	0.0	0.13	0.32	0.2	0.1	0.05	269	0	10	35.51	MRN_ ATPVs	NA
LKVEYSSPEGTKFEVENPQR-KPKEGKR-a2-b3	Mre11	Mre11	intra	371	419	FALSE	48	3315.739	829.9	4	-2.1	16	9	2	0.0	0.15	0.39	0.3	0.0	0.06	705	0.46	54	33.8	MRN_ ATPVs	NA
NFLSGQKQAKR-KVMEK-a8-b1	Mre11	Mre11	intra	526	514	FALSE	12	2175.142	726.0	3	-2.3	4	2	2	0.0	0.08	0.57	0.5	0.0	0.07	189	0.12	88	33.28	MRN_ ATPVs	NA
FKGLEK-KPKEGK-a2-b3	Mre11	Mre11	intra	317	419	FALSE	102	1543.893	386.9	4	-2.5	2	8	2	0.0	0.11	0.27	0.1	0.1	0.04	236	0.65	35	29.65	MRN_ ATPVs	NA
KODNRQEVTK-KPKEGK-a1-b3	Mre11	Mre11	intra	322	419	FALSE	97	2068.123	414.6	5	-2.1	1	7	0	0.1	0.1	0.24	0.1	0.1	0.04	157	0.69	31	29.19	MRN_ ATPVs	NA
NFLSGQKQAKR-KLLREIVNK-a8-b1	Mre11	decoy_ revers e_Mre11	decoy y inter	526	#### ##	#VALU E!	282	2766.587	692.6	4	0	4	4	4	0.0	0.13	0.55	0.4	0.1	0.09	267	0	10	31.05	noATP yS	NA
KEGLKFR-KPKEGK-a5-b3	Mre11	decoy_ revers e_Mre11	decoy y intra	267	419	FALSE	152	1699.996	426.0	4	-1.5	3	2	0	0	0.1	0.44	0.1	0.2	0.07	273	0.89	11	33.2	noATP yS	NA
DDKHAVEMFVMDLSQV-R-YTKVIENIR-a3-b3	Mre11	Rad50	inter	475	187	FALSE	288	3465.727	867.4	4	-0.1	15	3	1	0.0	0.13	0.53	0.4	0.1	0.08	728	0	10	34.67	noATP yS	12
FAGKAVANONDVVHFYR-DEKQNSVIVR-a4-b3	Mre11	Rad50	inter	397	1300	FALSE	27	3188.63	798.1	4	-2.2	2	7	2	0.0	0.1	0.3	0.0	0.2	0.06	440	0.78	22	29.42	noATP yS	16
FAGKAVANONDVVHFYR-RDEKQNSVIVR-a4-b4	Mre11	Rad50	inter	397	1300	FALSE	27	3344.73	669.9	5	-2.5	2	3	1	0.0	0.14	0.17	0.1	0.0	0.03	142	0.57	43	24.53	noATP yS	16
KDDSWR-VKRDEK-a1-b2	Mre11	Rad50	inter	30	1296	FALSE	390	1716.884	573.3	3	2.8	8	5	2	0.0	0.08	0.53	0.1	0.4	0.09	160	0.69	31	31.64	noATP yS	18
LKVEYSSPEGTKFEVENPQR-VSMVKGDTEMDMR-a2-b5	Mre11	Rad50	inter	371	1196	FALSE	51	3971.889	993.9	4	-1.6	3	7	3	0.0	0.12	0.37	0.1	0.2	0.07	395	0.65	35	25.92	noATP yS	19
RDEKQNSVIVR-ODNRQEVTKR-a4-b9	Rad50	Mre11	inter	1300	331	FALSE	93	2753.449	551.6	5	-1.4	3	4	1	0.0	0.16	0.39	0.2	0.1	0.06	395	0	10	30.4	noATP yS	20
CSAGQKVLASIIR-KTGTTT-a6-b1	Rad50	Mre11	inter	1212	411	FALSE	75	2315.293	772.7	3	-2.7	6	4	3	0.0	0.15	0.51	0.4	0.0	0.07	661	0.46	54	34.9	noATP yS	26

ILKER-KVMEK-a3-b1	Rad50	Mre11	inter	207	514	FALSE	307	1428.835	358.2	4	-1.8	4	11.22	0.0	0.19	0.6	0.54	0.0	0.0	0.1	181	0	10	40.41	noATP yS	26
ILPQAPFGDAVNQFVSKDD K-TOKTLEGSLLLR-a17-b3	Mre11	Rad50	inter	472	112	FALSE	360	3683.974	922.0	4	-1	2	5.53	0.0	0.05	0.61	0.55	0.0	0.0	0.08	176	0.46	54	22.43	noATP yS	28
YTKVNIENR-KVMEK-a3-b1	Rad50	Mre11	inter	187	514	FALSE	327	1906.056	636.3	6	-1.9	3	9.15	0.0	0.17	0.45	0.4	0.0	2	0.06	485	0	10	32.87	noATP yS	29
KTGTTR-MSKIEK-a1-b3	Mre11	Rad50	inter	411	3	FALSE	408	1534.838	512.6	2	-0.7	2	9.31	0.0	0.18	0.31	0.1	0.1	8	0.05	374	0.68	32	32.04	noATP yS	29
DVDMVLGGNLFHDKNPKSR K-CSAGQKVLAJIIR-a16-b6	Mre11	Rad50	inter	63	1212	FALSE	273	3907.073	977.7	7	-2.2	7	7.07	0.0	0.07	0.47	0.2	0.2	3	0.08	401	0.58	42	25.61	noATP yS	30
DVDMVLGGNLFHDKNPKSR -CSAGQKVLAJIIR-a16-b6	Mre11	Rad50	inter	63	1212	FALSE	273	3778.975	756.8	03	-2.9	1	6.73	0.0	0.1	0.39	0.2	0.1	7	0.06	275	0.81	19	24.33	noATP yS	30
QEVTKR-VKRDEK-a5-b2	Mre11	Rad50	inter	331	1296	FALSE	89	1670.925	418.7	39	-4.1	6	9.90	0.0	0.14	0.37	0.2	0.1	2	0.06	112	0	10	33.97	noATP yS	30
DEKQNSVIVR- KAMYQVMR-a3-b1	Rad50	Mre11	inter	1300	67	FALSE	357	2350.207	588.5	6	-2.8	2	03.11	0.0	0.19	0.39	0.4	0.6	4	0.06	509	0	10	37.92	noATP yS	31
RDEKQNSVIVR- KQDNRQEVTK-a4-b1	Rad50	Mre11	inter	1300	322	FALSE	102	2725.439	682.3	68	-2.8	2	8.12	0.0	0.12	0.36	0.0	0.3	5	0.06	344	0.75	25	28.21	noATP yS	31
DEKQNSVIVR-KTGTTR-a3- b1	Rad50	Mre11	inter	1300	411	FALSE	13	1987.067	663.3	63	-1.6	4	8.80	0.0	0.22	0.47	0.4	0.0	3	0.07	348	0	10	33.3	noATP yS	32
RDEKQNSVIVR-KTGTTR- a4-b1	Rad50	Mre11	inter	1300	411	FALSE	13	2143.165	536.7	99	-2.5	8	8.15	0.0	0.22	0.31	0.2	0.0	3	0.05	429	0	10	29.39	noATP yS	32
IEKLSILGVR-KAMYQVMR- a3-b1	Rad50	Mre11	inter	6	67	FALSE	61	2290.282	573.5	78	-3.9	2	71.10	0.0	0.13	0.58	0.4	0.1	2	0.09	871	0.25	75	37.94	noATP yS	35
AQVKLSFR-DNKVR-a4-b3	Rad50	Mre11	inter	82	193	FALSE	111	1715.965	429.9	4	-2.1	4	39.10	0.0	0.18	0.62	0.5	0.1	2	0.09	302	0.54	46	38.19	noATP yS	36
SLAESLHGIKAR- EITLATDKR-a11-b8	Rad50	Mre11	inter	1260	314	FALSE	70	2577.452	860.1	59	1.2	3	7.7	0.0	0.03	0.58	0.5	0.0	1	0.09	413	0.46	54	25.12	noATP yS	37
DVDMVLGGNLFHDKNPKSR K-IEKLSILGVR-a16-b3	Mre11	Rad50	inter	63	6	FALSE	57	3518.93	880.7	4	0.4	6	7.88	0.0	0.12	0.64	0.4	0.3	4	0.11	422	0.49	51	33.08	noATP yS	39
DVDMVLGGNLFHDKNPKSR -IEKLSILGVR-a16-b3	Mre11	Rad50	inter	63	6	FALSE	57	3390.833	679.1	74	-0.2	7	7.90	0.0	0.16	0.45	0.2	0.0	5	0.07	282	0.33	67	29.32	noATP yS	39
ILPQAPFGDAVNQFVSKDD K-CSAGQKVLAJIIR-a17-b6	Mre11	Rad50	inter	472	1212	FALSE	136	3841.041	769.2	16	-1	3	1.1	0.0	0.07	0.34	0.6	0.0	8	0.05	338	0.75	25	23.62	noATP yS	39
AQVKLSFR-KTGTTR-a4-b1	Rad50	Mre11	inter	82	411	FALSE	329	1747.99	438.0	05	-2.4	4	6.4	0.0	0.18	0.65	0.3	0.0	3	0.09	280	0.52	48	36.03	noATP yS	41
SLAESLHGIKAR- KQDNRQEVTK-a11-b1	Rad50	Mre11	inter	1260	322	FALSE	62	2776.513	695.1	36	-2.3	3	7.80	0.0	0.06	0.46	0.3	0.0	7	0.07	439	0.79	21	28.17	noATP yS	41
RDEKQNSVIVR- TFRDNKVR-a4-b6	Rad50	Mre11	inter	1300	193	FALSE	231	2515.359	504.0	8	-1	3	8.22	0.0	0.08	0.42	0.3	0.0	1	0.06	568	0.86	14	28.49	noATP yS	42
TQKTLEGSLLLR-KTGTTR- a3-b1	Rad50	Mre11	inter	112	411	FALSE	299	2158.231	720.4	18	-0.5	4	5.9	0.0	0.15	0.53	0.4	0.0	9	0.07	621	0.44	56	33.87	noATP yS	44
DVDMVLGGNLFHDKNPKSR -TQKTLEGSLLLR-a16-b3	Mre11	Rad50	inter	63	112	FALSE	49	3621.904	725.3	89	-4.2	4	3.1	0.0	0.19	0.4	0.2	0.1	8	0.06	350	0.78	22	32.9	noATP yS	50
DVDMVLGGNLFHDKNPKSR K-TOKTLEGSLLLR-a16-b3	Mre11	Rad50	inter	63	112	FALSE	49	3750.011	751.0	1	-0.9	3	2.2	0.0	0.1	0.33	0.1	0.1	4	0.06	243	0.52	48	29.33	noATP yS	50
TQKTLEGSLLLR- KAMYQVMR-a3-b1	Rad50	Mre11	inter	112	67	FALSE	45	2521.37	631.3	5	-2.3	2	7.0	0.0	0.09	0.35	0.3	0.0	5	0.05	328	0.57	43	24.64	noATP yS	51
CSAGQKVLAJIIR- VMEKNFLSGQOK-a6-b4	Rad50	Mre11	inter	1212	518	FALSE	182	3060.637	766.1	67	-3	2	8.20	0.0	0.16	0.42	0.2	0.1	5	0.07	496	0.68	32	29.68	noATP yS	53
KRFDEIFAQK-DNKVR-a1- b3	Rad50	Mre11	inter	174	193	FALSE	19	2178.143	545.5	44	0	1	7.9	0	0.14	0.41	0.2	0.2	1	0.08	242	0.57	43	32.45	noATP yS	53
EITLATDKR-AQVKLSFR-a8- b4	Mre11	Rad50	inter	314	82	FALSE	232	2131.197	711.4	07	-1.5	4	7.8	0.0	0.07	0.41	0.3	0.0	6	0.06	398	0	10	29.15	noATP yS	56

KODNRQEVTK-ILKER-a1-b3	Mre11	Rad50	inter	322	207	FALSE	115	2040.129	409.0	5	-1.7	4	9.5	0.0	0.15	0.63	0.0	9	4	0.5	0.14	175	0.75	25	35.21		noATP	57	
ILKER-KODNR-a3-b1	Rad50	Mre11	inter	207	322	FALSE	115	1454.817	485.9	3	-2.6	2	9.6	0	0.15	0.52	5	6	0.08	235	0	10	235	0	10	34.41		noATP	57
YTKVIENIR-KAMYQVMR-a3-b1	Rad50	Mre11	inter	187	67	FALSE	120	2298.217	767.0	8	-2.4	4	9	6	0.09	0.47	4	3	0.07	682	0.25	75	682	0.25	75	31.42		noATP	64
ETHIKVETTK-QEVTKR-a5-b5	Rad50	Mre11	inter	1115	331	FALSE	92	2082.13	521.5	4	-1.2	10	39	6	0.13	0.22	2	9	0.04	249	0.9	10	249	0.9	10	33.48		noATP	71
TFRDNKVR-KKGDELK-a6-b2	Mre11	Rad50	inter	193	199	FALSE	6	1989.097	398.8	27	-2.1	1	19	1	0.16	0.56	5	2	0.09	224	0.68	32	224	0.68	32	36.76		noATP	71
KGDELK-DNKVR-a1-b3	Rad50	Mre11	inter	199	193	FALSE	6	1456.783	486.6	02	-3.5	5	7	5	0.21	0.31	3	7	0.05	264	0.7	30	264	0.7	30	33.88		noATP	71
ETHIKVETTK-DNKVR-a5-b3	Rad50	Mre11	inter	1115	193	FALSE	46	1953.049	489.2	7	-2.2	11	29	3	0.17	0.38	1	6	0.07	346	0.8	20	346	0.8	20	38.15		noATP	75
DNKVR-ILKER-a3-b3	Mre11	Rad50	inter	193	207	FALSE	14	1425.827	476.2	83	-2.6	3	62	1	0.12	0.67	7	9	0.11	163	0.83	17	163	0.83	17	38.46		noATP	83
KKTGTTR-RPKETQ-a2-b3	Mre11	Nbs1	inter	411	711	FALSE	263	1685.941	422.4	93	-0.9	9	32	5	0.17	0.6	1	9	0.1	263	0.86	14	263	0.86	14	40.32		noATP	NA
RPKETQ-DNKVR-a3-b3	Nbs1	Mre11	inter	711	193	FALSE	45	1525.819	509.6	14	-1.4	70	76	5	0.23	0.59	9	0.1	0.09	252	0	10	252	0	10	39.82		noATP	NA
RPKETQ-VVRDEK-a3-b2	Nbs1	Rad50	inter	711	1296	FALSE	272	1668.915	418.2	37	-0.5	16	8	2	0.22	0.6	8	1	0.1	284	0	10	284	0	10	39.69		noATP	NA
AQVKLSFR-RPKETQ-a4-b3	Rad50	Nbs1	inter	82	711	FALSE	66	1843.028	461.7	65	-1.7	4	79	0	0.25	0.52	1	1	0.08	480	0.66	34	480	0.66	34	39.46		noATP	NA
ETHIKVETTK-RPKETQ-a5-b3	Rad50	Nbs1	inter	1115	711	FALSE	91	2080.115	521.0	36	-1	12	39	3	0.2	0.37	8	9	0.06	279	0.76	24	279	0.76	24	38.83		noATP	NA
KPKEGK-RPKETQ-a3-b3	Mre11	Nbs1	inter	419	711	FALSE	271	1580.888	396.2	3	-0.5	25	96	4	0.18	0.5	7	3	0.08	256	0.84	16	256	0.84	16	38.55		noATP	NA
KAMYQVMR-RPKETQ-a1-b3	Mre11	Nbs1	inter	67	711	FALSE	81	1920.989	481.2	55	-1.1	4	52	5	0.18	0.6	1	9	0.1	468	0	10	468	0	10	38.31		noATP	NA
IEKLSILGVR-RPKETQ-a3-b3	Rad50	Nbs1	inter	6	711	FALSE	142	2022.18	506.5	53	-2	5	52	3	0.19	0.55	5	2	0.09	663	0	10	663	0	10	38.04		noATP	NA
KTGTTR-RPKETQ-a1-b3	Mre11	Nbs1	inter	411	711	FALSE	263	1557.844	390.4	69	-2	14	49	2	0.2	0.51	9	2	0.08	249	0.56	44	249	0.56	44	37.69		noATP	NA
NFLSGQQQAQR-YTKVIENIR-a8-b3	Mre11	Rad50	inter	526	187	FALSE	339	2676.429	670.1	15	-2.1	3	47	3	0.17	0.54	3	0.1	0.08	296	0	10	296	0	10	37.4		noATP	NA
RPKETQ-ILKER-a3-b3	Nbs1	Rad50	inter	711	207	FALSE	59	1552.89	518.6	38	-2.2	1	84	5	0.1	0.53	8	5	0.09	317	0.82	18	317	0.82	18	37.28		noATP	NA
TFRDNKVR-RPKETQ-a6-b3	Mre11	Nbs1	inter	193	711	FALSE	45	1930.035	387.0	15	-1.5	36	74	5	0.23	0.33	3	0.2	0.06	309	0.65	35	309	0.65	35	37.19		noATP	NA
SLAESLHGIKAR-KPKEGK-a11-b3	Rad50	Mre11	inter	1260	419	FALSE	35	2217.281	555.3	28	-1.4	3	01	4	0.11	0.71	6	5	0.09	140	0.51	49	140	0.51	49	37		noATP	NA
RDEKONSIVR-KPKEGK-a4-b3	Rad50	Mre11	inter	1300	419	FALSE	5	2166.21	542.5	6	-0.9	4	02	4	0.11	0.4	0.2	1	0.07	373	0.7	30	373	0.7	30	36.71		noATP	NA
NFLSGQQQAQR-RPKETQ-a8-b3	Mre11	Nbs1	inter	526	711	FALSE	378	2299.199	575.8	07	-2	3	51	3	0.18	0.42	1	1	0.06	364	0.72	28	364	0.72	28	36.6		noATP	NA
NFLSGQQQAQR-ETHIKVETTK-a8-b5	Mre11	Rad50	inter	526	1115	FALSE	287	2726.434	546.2	95	-0.5	5	05	5	0.23	0.4	3	7	0.06	405	0	10	405	0	10	36		noATP	NA
KPKEGKR-ILKER-a3-b3	Mre11	Rad50	inter	419	207	FALSE	212	1636.998	328.4	07	-0.6	2	3	1	0.17	0.63	7	7	0.11	152	0	10	152	0	10	35.73		noATP	NA
AQVKLSFR-KPKEGKR-a4-b3	Rad50	Mre11	inter	82	419	FALSE	337	1927.134	643.3	86	-1.2	4	9.7	6	0.14	0.45	9	5	0.07	505	0.73	27	505	0.73	27	33.97		noATP	NA
MSKIEK-RPKETQ-a3-b3	Rad50	Nbs1	inter	3	711	FALSE	145	1629.875	544.3	3	-0.4	2	9	2	0.16	0.44	9	6	0.07	240	0.58	42	240	0.58	42	33.88		noATP	NA

RPKETQ-KVMEK-a3-b1	Nbs1	Mre11	inter	711	514	FALSE	366	1528.825	510.6	3	-2.2	3	9.4	0.0	0.08	0.53	0.3	0.2	0.09	220	0.54	46	33.2	noATP yS	NA
ETHIKVETTK-KPKEGKR-a5-b3	Rad50	Mre11	inter	1115	419	FALSE	180	2164.217	542.0	4	-2.1	4	9.5	0.0	0.15	0.4	0.3	0.0	0.06	451	0.85	15	33.17	noATP yS	NA
YTKVNIENR-RPKETQ-a3-b3	Rad50	Nbs1	inter	187	711	FALSE	39	2030.109	508.5	4	-3.5	4	8.9	0.0	0.18	0.47	0.2	0.2	0.08	478	0.72	28	32.72	noATP yS	NA
KKGDELK-RPKETQ-a1-b3	Rad50	Nbs1	inter	198	711	FALSE	50	1711.946	571.6	3	-0.3	2	9.5	0.0	0.11	0.35	0.2	0.1	0.06	379	0.83	17	32.04	noATP yS	NA
RDEKQNSVIVR-RPKETQ-a4-b3	Rad50	Nbs1	inter	1300	711	FALSE	276	2238.2	560.5	4	-3.4	4	9.8	0	0.05	0.33	0.1	0.1	0.06	390	0.34	66	31.75	noATP yS	NA
TQKTLEGSLLLR-RPKETQ-a3-b3	Rad50	Nbs1	inter	112	711	FALSE	36	2253.266	752.0	3	-1.4	11	8.9	0.0	0.12	0.46	0.4	0.0	0.06	611	0.43	57	31.54	noATP yS	NA
FAGKVAONQDVVHFYR-RPKETQ-a4-b3	Mre11	Nbs1	inter	397	711	FALSE	249	2759.408	552.8	5	-2.2	4	8.9	0	0.11	0.39	0.1	0.2	0.1	310	0.78	22	30.48	noATP yS	NA
DEKQNSVIVR-KPKEGKR-a3-b6	Rad50	Mre11	inter	1300	422	FALSE	2	2166.207	434.2	49	-2.3	3	8.5	0	0.16	0.33	0.2	0.0	0.05	457	0.82	18	29.85	noATP yS	NA
NGAFIHPDPLVGEKEVR-KPKEGKR-a14-b3	Rad50	Mre11	inter	75	419	FALSE	344	2874.53	719.6	4	-1.6	5	2	0	0.08	0.4	0.3	0.0	0.06	426	0.68	32	29.69	noATP yS	NA
VSMVKGDTMDMR-RPKETQ-a5-b3	Rad50	Nbs1	inter	1196	711	FALSE	172	2393.133	798.7	3	-2.3	1	5	0.1	0.08	0.5	0.4	0.0	0.06	344	0.37	63	29.63	noATP yS	NA
CSAGQKVLAIIIR-NFLSGQKQAKR-a6-b8	Rad50	Mre11	inter	1212	526	FALSE	190	3056.655	765.1	4	-0.1	5	2	2	0.13	0.39	0.1	0.2	0.06	290	0.25	75	28.38	noATP yS	NA
CSAGQKVLAIIIR-IKQDEENVLELAR-a6-b2	Rad50	Nbs1	inter	1212	577	FALSE	322	3337.787	835.4	55	-1.3	2	7	1	0.17	0.31	0.1	0.1	0.05	566	0.61	39	27.57	noATP yS	NA
KDDSWR-RPKETQ-a1-b3	Mre11	Nbs1	inter	30	711	FALSE	118	1700.844	567.9	3	-2.7	1	7.5	0.0	0.09	0.47	0.0	0.4	0.08	244	0.88	12	27.17	noATP yS	NA
IKQDEENVLELAR-EITLATDKR-a2-b8	Nbs1	Mre11	inter	577	314	FALSE	300	2868.502	718.1	33	-2.1	2	7.6	0.0	0.08	0.37	0.2	0.1	0.06	346	0	0	26.52	noATP yS	NA
VPEADNIHVKPILLQK-KIKQDEENVLELAR-a10-b3	Mre11	Nbs1	inter	161	577	FALSE	147	3764.068	753.8	21	-1.1	6	5	2	0.08	0.4	0.1	0.2	0.07	483	0.51	49	26.09	noATP yS	NA
VPEADNIHVKPILLQK-KIKQDEENVLELAR-a10-b1	Mre11	Nbs1	inter	161	575	FALSE	149	3764.067	942.0	24	-1.5	2	4	1	0.08	0.28	0.1	0.1	0.04	719	0.68	32	26.04	noATP yS	NA
KQDNRQEVTK-GKGKK-a1-b2	Mre11	Nbs1	inter	322	572	FALSE	313	1899.054	475.7	71	0.1	1	7	5	0.04	0.42	0.3	0.0	0.06	233	0.84	16	25.54	noATP yS	NA
QEVTKR-RPKETQ-a5-b3	Mre11	Nbs1	inter	331	711	FALSE	183	1654.895	552.6	4	-3	4	2	4	0.04	0.2	0.1	0.0	0.03	211	0.73	27	24.02	noATP yS	NA
TKEYGDDYWLEDEGRV-PR-VPEADNIHVKPILLQK-a2-b10	Nbs1	Mre11	inter	689	161	FALSE	35	4477.272	1120.	33	-1.8	8	5	0	0.09	0.29		0.1			10			noATP yS	NA
KGDELK-LLKKK-a1-b3	Rad50	Rad50	intra	199	196	FALSE	3	1454.904	364.7	34	-2.4	17	19	4	0.28	0.38	0.2	0.1	0.06	240	0.62	38	39.8	noATP yS	5
KGDELK-LLKKK-a1-b4	Rad50	Rad50	intra	199	197	FALSE	2	1454.902	364.7	33	-3.3	15	5	2	0.17	0.6	0.1	0.4	0.1	188	0.75	25	33.75	noATP yS	5
IEKLSILGVR-AQVLSLFR-a3-b4	Rad50	Rad50	intra	6	82	FALSE	76	2212.328	554.0	9	-1.1	697	2	1	0.27	0.5	0.2	0.2	0.08	546	0	0	40.61	noATP yS	8
MSKIEKLSILGVR-AQVLSLFR-a6-b4	Rad50	Rad50	intra	6	82	FALSE	76	2558.497	512.7	07	-0.5	1	2	2	0.16	0.52	0.2	0.2	0.09	530	0	0	35.5	noATP yS	8
RFKGLEK-KQDNR-a3-b1	Mre11	Mre11	intra	317	322	FALSE	5	1673.917	335.7	91	-2.5	45	1	0	0.29	0.57	0.5	0.0	0.08	234	0.54	46	37.39	noATP yS	8
KQDNRQEVTK-FKGLEK-a1-b2	Mre11	Mre11	intra	322	317	FALSE	5	2103.128	526.7	9	-2.3	44	77	1	0.12	0.47	0.2	0.2	0.08	443	0.74	26	36.78	noATP yS	8

FKGLEK-KODNR-a2-b1	Mre11	Mre11	intra	317	322	FALSE	5	1517.817	380.4	4	-1.9	50	10.04	0.0	0.25	0.32	0.2	0.1	0.05	228	0	10	35.45		noATP yS	8
KODNRQEVTK-RFKGLEK-a1-b3	Mre11	Mre11	intra	322	317	FALSE	5	2259.229	377.5	6	-1.8	79	9.8	0	0.08	0.56	5	1	0.1	229	0.75	25	34.4		noATP yS	8
ETHIKVETTK-ILKEREVQDK-a5-b3	Rad50	Rad50	intra	1115	207	FALSE	32	2579.415	516.8	5	-0.6	5	10	0.0	0.12	0.25	2	2	0.04	164	0.64	36	34.38		noATP yS	9
ETHIKVETTK-KKGDELK-a5-b2	Rad50	Rad50	intra	1115	199	FALSE	40	2139.176	714.0	3	-1.4	119	34	6	0.2	0.38	7	2	0.06	556	0.7	30	38.89		noATP yS	11
ETHIKVETTK-KGDELK-a5-b1	Rad50	Rad50	intra	1115	199	FALSE	40	2011.082	503.7	4	-0.7	92	49	0	0.17	0.38	5	4	0.06	395	0.83	17	35.96		noATP yS	11
GDELKILK-LLKKK-a5-b4	Rad50	Rad50	intra	204	197	FALSE	7	1681.071	421.2	4	-2.4	2	9	4	0.09	0.5	0.1	1	0.1	192	0.91	9	33.86		noATP yS	11
KGDELKILK-LLKKK-a6-b4	Rad50	Rad50	intra	204	197	FALSE	7	1809.164	604.0	3	-3.5	6	3	2	0.1	0.27	6	2	0.05	308	0.84	16	30.44		noATP yS	11
KAMYQVMR-KDDSWR-a1-b1	Mre11	Mre11	intra	67	30	FALSE	37	1968.953	493.2	4	-1	16	8	5	0.23	0.6	6	5	0.09	382	0.76	24	37.44		noATP yS	11
RDEKQNSVIVR-VKRDEK-a4-b2	Rad50	Rad50	intra	1300	1296	FALSE	4	2254.237	564.5	4	-1.1	4	19	1	0.09	0.63	1	2	0.11	129	0	10	36.1		noATP yS	11
DVDMVLLGGNLFHDNKP SR-KAMYQVMR-a16-b1	Mre11	Mre11	intra	63	67	FALSE	4	3289.633	658.9	5	-2.4	5	8	2	0.16	0.69	9	0.1	0.1	238	0.78	22	36.88		noATP yS	11
DVDMVLLGGNLFHDNKP SR-K-KAMYQVMR-a16-b1	Mre11	Mre11	intra	63	67	FALSE	4	3417.73	684.5	5	-1.6	9	8	2	0.09	0.34	4	1	0.06	178	0	10	28.41		noATP yS	11
KGDELK-ILKER-a1-b3	Rad50	Rad50	intra	199	207	FALSE	8	1483.857	371.9	4	-2.8	4	4	4	0.4	0.8	7	3	0.14	162	0.67	33	46.35		noATP yS	12
KKGDELK-ILKER-a2-b3	Rad50	Rad50	intra	199	207	FALSE	8	1611.952	403.9	4	-2.2	16	67	0	0.22	0.72	0.1	2	0.13	186	0.8	20	40.44		noATP yS	12
ILKEREVQDK-KGDELK-a3-b1	Rad50	Rad50	intra	207	199	FALSE	8	2083.145	417.6	5	-3.4	6	06	3	0.11	0.52	3	9	0.08	186	0.9	10	35.19		noATP yS	12
TKOVDVLLGGNLFHDNKP SRK-SFEVEKIPLR-a2-b6	Mre11	Mre11	intra	47	294	FALSE	247	3838.039	549.2	7	-1.6	2	2	2	0.07	0.55	4	1	0.08	264	0	10	30.05		noATP yS	12
LKVEYSPGEGTKFEVENPQR-KKTGTTR-a2-b1	Mre11	Mre11	intra	371	410	FALSE	39	3264.696	817.1	4	-0.8	6	4	2	0.1	0.3	6	3	0.04	328	0.37	63	25.5		noATP yS	12
GDELKILK-LLKKK-a5-b3	Rad50	Rad50	intra	204	196	FALSE	8	1681.074	421.2	4	-1.1	1	1	2	0.09	0.51	1	0.4	0.1	203	0.86	14	32.74		noATP yS	13
KGDELKILK-LLKKK-a6-b3	Rad50	Rad50	intra	204	196	FALSE	8	1809.168	604.0	3	-1.2	6	9.8	4	0.1	0.25	7	8	0.04	155	0.77	23	31.6		noATP yS	13
ETHIKVETTK-KKGDELK-a5-b1	Rad50	Rad50	intra	1115	198	FALSE	41	2139.175	535.8	4	-1.5	18	6	1	0.18	0.4	8	2	0.06	591	0.9	10	33.12		noATP yS	14
KKGDELK-ILKER-a1-b3	Rad50	Rad50	intra	198	207	FALSE	9	1611.952	403.9	4	-2.7	3	2	0	0.18	0.7	6	4	0.13	176	0	10	35.25		noATP yS	14
KODNRQEVTK-EITLATDKR-a1-b8	Mre11	Mre11	intra	322	314	FALSE	8	2428.287	810.4	3	-2	8	8	3	0.11	0.43	3	9	0.07	313	0.92	8	32.27		noATP yS	15
EITLATDKR-KODNR-a8-b1	Mre11	Mre11	intra	314	322	FALSE	8	1842.978	615.3	3	-1.2	6	3	2	0.11	0.53	8	4	0.07	313	0	10	28.91		noATP yS	15
RFKGLEK-QEVTKR-a3-b5	Mre11	Mre11	intra	317	331	FALSE	14	1774.008	355.8	5	-1.3	6	6	4	0.08	0.4	9	1	0.06	351	0.86	14	33.02		noATP yS	15
LKVEYSPGEGTK-KKTGTTR-a2-b2	Mre11	Mre11	intra	371	411	FALSE	40	2265.218	756.0	3	-1.6	5	8	2	0.14	0.43	5	7	0.06	635	0	10	31.38		noATP yS	16
LKVEYSPGEGTKFEVENPQR-KKTGTTR-a2-b2	Mre11	Mre11	intra	371	411	FALSE	40	3264.696	817.1	4	-1	15	5	6	0.1	0.39	3	6	0.05	385	0.34	66	28.55		noATP yS	16
LKVEYSPGEGTKFEVENPQR-KTGTTR-a2-b1	Mre11	Mre11	intra	371	411	FALSE	40	3136.6	785.1	4	-1.4	57	6	4	0.12	0.21	6	5	0.04	102	0.55	45	28.31		noATP yS	16
CSAGQKVLSIIIR-	Rad50	Rad50	intra	1212	1196	FALSE	16	3150.585	1051.	3	-1.8	53	7	3	0.14	0.38	3	5	0.06	532	0.72	28	33.62		noATP yS	16
VSMVKGDTEMDMR-a6-b5	Rad50	Rad50	intra	1212	1196	FALSE	16	3150.585	1051.	3	-1.8	53	7	3	0.14	0.38	3	5	0.06	532	0.72	28	33.62		noATP yS	16

QDNROEVTKR-GLEKK-a9-b4	Mre11	Mre11	intra	331	321	FALSE	10	1984.066	662.3	3	-2.1	1	7.5	0	0.02	0.37	0.1	0.1	0.07	295	0.8	20	25.15		noATP yS	16
FAGKAVQNDVVHFYRK-QDNROEVTKR-a4-b9	Mre11	Mre11	intra	397	331	FALSE	66	3402.752	851.6	4	-0.7	47	6	0.0	0.09	0.29	0.1	0.0	0.05	448	0.26	74	23.02		noATP yS	17
KRFDEIFEAQK-YTKVIENIR-a1-b3	Rad50	Rad50	intra	174	187	FALSE	13	2682.438	537.4	5	-0.2	115	39	1	0.16	0.77	0.6	0.0	0.12	260	0.5	50	39.37		noATP yS	17
TQKTLEGSLLR-AQVKLSFR-a3-b4	Rad50	Rad50	intra	112	82	FALSE	30	2443.413	815.4	79	-1.2	4	1	3	0.11	0.43	0.3	0.1	0.06	638	0.46	54	31.35		noATP yS	18
NGAFHDPDLVGEKEVR-DEKQNSVIVR-a14-b3	Rad50	Rad50	intra	75	1300	FALSE	349	3219.657	805.9	22	1.5	9	13	5	0.19	0.45	0.2	0.2	0.08	723	0.6	40	38.78		noATP yS	19
YTKVIENIR-KKGDELK-a3-b2	Rad50	Rad50	intra	187	199	FALSE	12	2089.173	697.3	99	-2.7	5	2	4	0.11	0.46	0.3	0.1	0.07	608	0.83	17	31.71		noATP yS	19
YTKVIENIR-KGDELK-a3-b1	Rad50	Rad50	intra	187	199	FALSE	12	1961.082	835.1	02	-0.7	3	1	4	0.09	0.41	0.3	0.0	0.06	538	0.81	19	31.41		noATP yS	19
VAELDKLVSEK-YTKVIENIR-a6-b3	Rad50	Rad50	intra	138	187	FALSE	49	2502.391	38	3	-1.5	3	11	9	0.16	0.51	0.2	0.2	0.08	727	0.21	79	38.92		noATP yS	20
TTVIECLKYATTGELPPNSTR-KRFEIFEAQK-a8-b1	Rad50	Rad50	intra	48	174	FALSE	126	3897.98	780.6	04	-0.5	5	7	0	0.07	0.51	0.4	0.0	0.07	457	0.17	83	25.78		noATP yS	20
TQKTLEGSLLR-VAELDKLVSEK-a3-b6	Rad50	Rad50	intra	112	138	FALSE	26	2725.548	909.5	24	0.2	2	2	5	0.12	0.36	0.2	0.1	0.06	624	0.63	37	27.26		noATP yS	21
AQVKLSFR-VKRDEK-a4-b2	Rad50	Rad50	intra	82	1296	FALSE	338	1859.061	465.7	73	-1.1	7	9	3	0.15	0.45	0.3	0.0	0.07	191	0.54	46	31.05		noATP yS	21
FKGLEK-KTGTR-a2-b1	Mre11	Mre11	intra	317	411	FALSE	94	1520.854	507.9	59	-1.8	4	3	7	0.2	0.34	0.1	0.2	0.06	245	0	0	32.52		noATP yS	21
RFDEIFEAQKYTK-KKGDELK-a10-b1	Rad50	Rad50	intra	184	198	FALSE	14	2628.378	658.1	02	-0.8	1	14	1	0.12	0.31	0.1	0.1	0.06	427	0.73	27	33.39		noATP yS	22
GMAAAMDHAIMQYHKSMMEQINR-YTKVIENIR-a15-b3	Rad50	Rad50	intra	1143	187	FALSE	80	3832.876	959.2	27	-3.3	6	9	4	0.08	0.3	0.2	0.0	0.05	458	0.06	94	27.17		noATP yS	22
GLQLDDDKINEGLDISHIEDFRK-VMKEKNFLSGQK-a9-b4	Mre11	Mre11	intra	500	518	FALSE	18	4215.113	1054.	79	-0.7	4	6	2	0.07	0.28	0.1	0.1	0.05	474	0.67	33	24.85		noATP yS	23
NGAFHDPDLVGEKEVR-AQVKLSFR-a14-b4	Rad50	Rad50	intra	75	82	FALSE	7	2980.57	746.1	5	-2.4	9	48	1	0.11	0.43	0.1	0.2	0.08	378	0.65	35	35.24		noATP yS	24
DEKQNSVIVR-IEKLSILGVR-a3-b3	Rad50	Rad50	intra	1300	6	FALSE	418	2451.405	613.8	59	-0.4	1	1	0	0.14	0.38	0.1	0.2	0.06	910	0.19	81	34.27		noATP yS	25
TQKTLEGSLLR-IEKLSILGVR-a3-b3	Rad50	Rad50	intra	112	6	FALSE	106	2622.566	656.6	49	-1	4	3	5	0.14	0.33	0.2	0.3	0.05	263	0.54	46	34.38		noATP yS	25
VSMVKGDTMDMR-TQKTLEGSLLR-a5-b3	Rad50	Rad50	intra	1196	112	FALSE	208	2993.521	998.8	48	-0.9	2	3	3	0.04	0.33	0.2	0.1	0.05	283	0.7	30	26.5		noATP yS	27
ETHIKVETTK-YTKVIENIR-a5-b3	Rad50	Rad50	intra	1115	187	FALSE	52	2457.339	615.3	43	-3.7	3	3	4	0.1	0.34	0.0	0.2	0.06	422	0.26	74	26.98		noATP yS	28
NGAFHDPDLVGEKEVR-CSAGQKVASIIR-a14-b6	Rad50	Rad50	intra	75	1212	FALSE	261	3547.895	710.5	87	3.5	9	5	4	0.06	0.5	0.4	0.0	0.08	219	0.83	17	25.48		noATP yS	28
CSAGQKVASIIR-VKRDEK-a6-b2	Rad50	Rad50	intra	1212	1296	FALSE	84	2426.363	607.5	99	-1.9	2	5	4	0.1	0.4	0.3	0.0	0.06	535	0.57	43	29.8		noATP yS	30
YTKVIENIR-ILKER-a3-b3	Rad50	Rad50	intra	187	207	FALSE	20	1930.122	483.5	38	-1.7	4	9.2	1	0.21	0.44	0.3	0.1	0.07	434	0.28	72	33.65		noATP yS	30
SLAESLHGIIKAR-AQVKLSFR-a11-b4	Rad50	Rad50	intra	1260	82	FALSE	302	2479.421	620.8	63	-2.8	2	6	4	0.1	0.63	0.2	0.3	0.11	184	0	0	34.64		noATP yS	31
CSAGQKVASIIR-IEKLSILGVR-a6-b3	Rad50	Rad50	intra	1212	6	FALSE	330	2779.633	695.9	16	-1	4	4	1	0.22	0.44	0.2	0.1	0.07	665	0	0	29.61		noATP yS	32
TQKTLEGSLLR-YTKVIENIR-a3-b3	Rad50	Rad50	intra	112	187	FALSE	75	2630.499	877.8	41	-0.8	2	1	9	0.12	0.35	0.2	0.1	0.06	636	0.55	45	25.24		noATP yS	33

VPEADNIHVKPIILQK-KAMYQVMR-a10-b1	Mre11	intra	161	67	FALSE	94	2976.628	745.1	4	-0.3	10	9.6	0.0	0.06	0.42	0.2	0.1	0.07	676	0	10	32.09	noATP yS	35
CSAGQKVIASIIIR-YTKVNIENR-a6-b3	Rad50	intra	1212	187	FALSE	149	2787.575	930.1	3	2.5	1	8.3	0.0	0.08	0.34	0.2	0.0	0.05	632	0	10	28.03	noATP yS	35
YTKVNIENR-AQVKLSFR-a3-b4	Rad50	intra	187	82	FALSE	105	2220.257	556.0	4	-2.7	2	8.3	0.0	0.21	0.47	0.2	0.2	0.08	386	0.72	28	31.52	noATP yS	36
SLAESLHGIIKAR-DEKQNSVIVR-a11-b3	Rad50	intra	1260	1300	FALSE	40	2718.496	907.1	3	-2.3	1	7.0	0.0	0.01	0.6	0.5	0.0	0.09	356	0.12	88	26.05	noATP yS	37
YTKVNIENR-VKRDEK-a3-b2	Rad50	intra	187	1296	FALSE	233	2046.145	512.5	4	-1.2	6	8.1	0.0	0.17	0.4	0.3	0.0	0.06	566	0	10	29.67	noATP yS	49
LKVEYSSPGTKFEVENPQR-VMEKNFLSGGQK-a2-b4	Mre11	intra	371	518	FALSE	147	3881.94	971.4	4	-2.9	3	6.7	0.0	0.13	0.34	0.2	0.1	0.06	709	0.51	49	24.46	noATP yS	51
VMEKNFLSGGQK-EITLATDKR-a4-b8	Mre11	intra	518	314	FALSE	204	2591.363	648.8	4	-0.2	4	6.6	0.0	0.09	0.52	0.0	0.4	0.09	307	0	10	24.94	noATP yS	52
DNKVR-KVMEK-a3-b1	Mre11	intra	193	514	FALSE	321	1401.76	351.4	4	-3.8	5	10	0.0	0.09	0.41	0.3	0.0	0.07	168	0	10	33.55	noATP yS	59
TFRDNKVR-KVMEK-a6-b1	Mre11	intra	193	514	FALSE	321	1805.98	362.2	5	-1.2	8	8.3	0	0.19	0.26	0.1	0.1	0.04	199	0.63	37	28.75	noATP yS	59
QEVTKR-KVMEK-a5-b1	Mre11	intra	331	514	FALSE	183	1530.842	89	3	-1	3	8.5	7	0.06	0.36	0.3	0.0	0.06	320	0	10	28.55	noATP yS	61
AQVKLSFR-ILKER-a4-b3	Rad50	intra	82	207	FALSE	125	1743.039	436.7	4	-0.9	4	10	0.0	0.27	0.69	0.6	0.0	0.1	329	0.49	51	39.72	noATP yS	62
KODNRQEVTK-DNKVR-a1-b3	Mre11	intra	322	193	FALSE	129	2013.056	672.0	3	-1.9	3	8.8	0.0	0.08	0.4	0.2	0.1	0.06	530	0.79	21	30.31	noATP yS	63
KODNRQEVTK-TFRDNKVR-a1-b6	Mre11	intra	322	193	FALSE	129	2417.274	605.3	4	-1.6	5	7.4	0.0	0.07	0.47	0.4	0.0	0.07	484	0.92	8	26.82	noATP yS	63
KKGDCLK-VKRDEK-a2-b2	Rad50	intra	199	1296	FALSE	221	1727.975	433.0	4	-2	8	9.2	0.0	0.16	0.48	0.1	0.1	0.08	191	0.72	28	33.42	noATP yS	66
VPEADNIHVKPIILQK-KODNRQEVTK-a10-b1	Mre11	intra	161	322	FALSE	161	3195.752	799.9	4	-3.1	4	9.2	0.0	0.13	0.35	0.2	0.1	0.05	805	0.85	15	31.5	noATP yS	68
VPEADNIHVKPIILQK-KODNR-a10-b1	Mre11	intra	161	322	FALSE	161	2610.446	653.6	4	-1.2	4	7.8	0.0	0.09	0.63	0.5	0.0	0.08	253	0	10	29.63	noATP yS	68
ETHIKVETTK-VKRDEK-a5-b2	Rad50	intra	1115	1296	FALSE	181	2096.145	525.0	4	-1.4	6	9.9	0.0	0.12	0.39	0.2	0.1	0.06	191	0.78	22	33.62	noATP yS	73
KODNRQEVTK-KODNR-a1-b1	Mre11	intra	322	322	TRUE	0	2042.052	511.5	4	0.8	1	7.6	0.0	0.04	0.42	0.1	0.2	0.08	361	0.89	11	26.09	noATP yS	96
KPKEGKR-RFKGLEK-a3-b3	Mre11	intra	419	317	FALSE	102	1856.097	465.0	4	-1.5	13	11	0.0	0.19	0.52	0.3	0.2	0.09	341	0.89	11	39.43	noATP yS	NA
TFRDNKVR-KPKEGKR-a6-b3	Mre11	intra	193	419	FALSE	226	2014.14	403.8	5	-2	2	99	4	0.19	0.37	0.2	0.1	0.06	279	0.79	21	37.46	noATP yS	NA
NFLSGGQKQAGR-KQDNR-a8-b1	Mre11	intra	526	322	FALSE	204	2201.123	734.7	3	-3.1	4	9.7	0.0	0.17	0.66	0.6	0.0	0.09	265	0	10	37	noATP yS	NA
NFLSGGQKQAGR-DNKVR-a8-b3	Mre11	intra	526	193	FALSE	333	2172.136	544.0	4	-1.7	3	65	0	0.14	0.44	0.3	0.0	0.06	113	0	10	36.5	noATP yS	NA
EITLATDKR-KPKEGKR-a8-b3	Mre11	intra	314	419	FALSE	105	2025.157	676.0	3	-0.8	14	9.8	0.0	0.15	0.54	0.4	0.1	0.08	389	0.89	11	35.68	noATP yS	NA
TKEYGIDDYWIIEEGRVPR-RPKETO-a2-b3	Nbs1	intra	690	712	FALSE	22	3421.64	685.3	5	-0.7	9	9.9	0.0	0.15	0.51	0.4	0.0	0.07	330	0.32	68	35.27	noATP yS	NA
KPKEGKR-GLEKK-a3-b4	Mre11	intra	419	321	FALSE	98	1552.927	389.2	4	-2.1	3	32	2	0.19	0.33	0.0	0.2	0.06	87	0.7	30	35.16	noATP yS	NA
NFLSGGQKQAGR-KPKEGKR-a8-b3	Mre11	intra	526	419	FALSE	107	2383.304	596.8	4	-2	6	9.3	0.0	0.14	0.68	0.6	0.0	0.09	257	0.87	13	35.15	noATP yS	NA
NFLSGGQKQAGR-KTGTTTR-a8-b1	Mre11	intra	526	411	FALSE	115	2204.162	552.0	4	-2.1	7	9.5	0.0	0.1	0.65	0.6	0.0	0.08	286	0	10	34.93	noATP yS	NA

FKLEK-KPKEGK-a2-b3	Mre11	Mre11	intra	317	419	FALSE	102	1543.894	386.9	4	-2.2	2	10.44	0.0	0.15	0.29	0.1	0.1	0.05	241	0.9	10	34.63		noATP	NA
NFLSGQKQQAQR-KPKEGK-a8-b3	Mre11	Mre11	intra	526	419	FALSE	107	2227.203	743.4	3	-1.9	4	8.8	0.1	0.13	0.57	0.5	0.0	0.07	314	0.4	60	32.88		noATP	NA
KPKEGKR-KVMEK-a3-b1	Mre11	Mre11	intra	419	514	FALSE	95	1612.928	404.2	4	-3.6	8	9.8	0	0.19	0.21	0.1	0.1	0.03	187	0.76	24	32.6		noATP	NA
ILPQAPFGDAVNQFVSKDD									1244.																	
K-NFLSGQKQQAQR-a17-b8	Mre11	Mre11	intra	472	526	FALSE	54	3729.911	31	3	-0.2	6	4	2	0.07	0.68	0.6	0.0	0.09	169	0	10	31.91		noATP	NA
NFLSGQKQQAQR-EITLATDKR-a8-b8	Mre11	Mre11	intra	526	314	FALSE	212	2587.368	863.4	3	-1.5	4	6	7	0.07	0.51	0.3	0.1	0.08	394	0	10	31.68		noATP	NA
VMEKNFLSGQK-KPKEGKR-a4-b3	Mre11	Mre11	intra	518	419	FALSE	99	2387.294	796.7	3	-2.4	4	5	3	0.1	0.34	0.2	0.1	0.05	778	0.78	22	31.56		noATP	NA
LKVEYSSPEGTK-KPKEGKR-a2-b3	Mre11	Mre11	intra	371	419	FALSE	48	2316.267	773.0	3	-0.9	18	8	1	0.09	0.48	0.3	0.1	0.07	658	0	10	31.45		noATP	NA
FAGKVANQNDVVHFPYR-NFLSGQKQQAQR-a4-b8	Mre11	Mre11	intra	397	526	FALSE	129	3405.73	54	5	-0.7	1	1	1	0.11	0.46	0.0	0.3	0.08	324	0.78	22	30.63		noATP	NA
LKVEYSSPEGTKFEVENPQRPKEGKR-a2-b3	Mre11	Mre11	intra	371	419	FALSE	48	3315.744	829.9	4	-0.7	41	8	4	0.12	0.42	0.3	0.1	0.07	534	0.88	12	30.53		noATP	NA
KPKEGK-KTGTR-a3-b1	Mre11	Mre11	intra	419	411	FALSE	8	1485.851	496.2	3	-0.4	5	2	5	0.12	0.42	0.3	0.1	0.07	227	0.8	20	29.17		noATP	NA
DVDMVLLGNLFHDKPSRK-NFLSGQKQQAQR-a16-b8	Mre11	Mre11	intra	63	526	FALSE	463	3795.935	949.9	4	-3.5	2	1	0	0.09	0.48	0.3	0.1	0.07	440	0.72	28	28.34		noATP	NA
KODNRQEVTK-KPKEGKR-a1-b3	Mre11	Mre11	intra	322	419	FALSE	97	2224.228	557.0	65	-0.6	1	2	1	0.09	0.38	0.2	0.1	0.06	287	0.67	33	27.93		noATP	NA
Headers																										
Definition																										
seq1-seq2-pos1-pos2																										
Name of Protein 1																										
Name of Protein 2																										
intra-protein xl, inter-protein xl or decay inter-protein xl																										
Position of the linked Lys within the Protein Sequence 1																										
Position of the linked Lys within the Protein Sequence 2																										
TRUE for a same Lys protein position number, otherwise FALSE																										
Difference between the Lys protein position numbers from Protein 1 and Protein 2																										
relative mass of the detected cross-link species																										
m/z value of the detected cross-link species																										
charge of the detected cross-link species																										
relative error of the mass [ppm]																										
how often results the xQUEST search in exactly this cross-link species																										
Score for the reliability of this cross-link species																										

Seifert *et al.*

Xcorr	Score for the reliability of this cross-link species
Xcorrb	Score for the reliability of this cross-link species
TIC	Score for the reliability of this cross-link species
TicA	Score for the reliability of this cross-link species
TicB	Score for the reliability of this cross-link species
WTIC	Score for the reliability of this cross-link species
intsum	Score for the reliability of this cross-link species
deltaS	Score for the reliability of this cross-link species
DeltaScore2	Definition: (1-deltaS)*100
Id.Score	Main Score for ranking cross-linked Species
Decoy	"x" for a decoy hit
Experit	Experiment Name
dist	Distance derived with the Xlink Analyzer software
Experiments	
MRN_ATPyS	Inter- and Intra-Links derived from the ATPyS experiment
noATPyS	Inter- and Intra-Links derived from the experiment without ATPyS

Supplementary Table S4: List of DNA oligonucleotides used for fluorescence anisotropy measurements

Used for DNA	Sequence (5'-3')	Length	5' label
		[nt]	
1; 1P; 7; 8; 9;10; 13	CATTGCTTAGGTAGTGGGGGCGACAAACGCCGACG	35	Fluorescein
1	CGTCGGCGTTTGTGCGCCCCACTACCTAAGCAATG	35	
2.1	CATTGCTTAGGTAGTGG	17	Fluorescein
2.1	CCACTACCTAAGCAATG	17	
2	GGGCGACAAACGCCGACG	18	
2	CGTCGGCGTTTGTGCGCCC	18	
1P	ACTACCTAAGCAATG	15	Phosphate
1P	CGTCGGCGTTTGTGCGCCCC	20	
3.I; 3; 6.1; 6	CATTGCTTAGGTAGT	15	Fluorescein
3.1; 3; 9	CCCCCACTACCTAAGCAATG	20	
3	GGGGGCGACAAACGCCGACG	20	
3; 6; 9	CGTCGGCGTTTGTGCG	15	
4.1; 4;	CATTGCTTAGGTAGTGGGGG	20	Fluorescein
4.1; 4; 5.1; 5; 7	ACTACCTAAGCAATG	15	
4; 5	CGACAAACGCCGACG	15	
4; 10	CGTCGGCGTTTGTGCGCCCC	20	
5.1; 5	CATTGCTTAGGTAGTGGGGGTTTTTTTTTTTTTT	35	Fluorescein
5; 7	CGTCGGCGTTTGTGCGCCCCCTTTTTTTTTTTTTT	35	
6.1; 6; 8	TTTTTTTTTTTTTTCCCCCACTACCTAAGCAATG	35	
6	TTTTTTTTTTTTTTTGGGGGCGACAAACGCCGACG	35	

2.3 Structure of the Rad50 DNA double-strand break repair protein in complex with DNA

Structure of the Rad50 DNA double-strand break repair protein in complex with DNA

Anna Rojowska¹, Katja Lammens¹, Florian U Seifert¹, Carolin Direnberger^{1,†}, Heidi Feldmann¹ & Karl-Peter Hopfner^{1,2,*}

Abstract

The Mre11–Rad50 nuclease–ATPase is an evolutionarily conserved multifunctional DNA double-strand break (DSB) repair factor. Mre11–Rad50's mechanism in the processing, tethering, and signaling of DSBs is unclear, in part because we lack a structural framework for its interaction with DNA in different functional states. We determined the crystal structure of *Thermotoga maritima* Rad50^{NBD} (nucleotide-binding domain) in complex with Mre11^{HLH} (helix-loop-helix domain), AMPPNP, and double-stranded DNA. DNA binds between both coiled-coil domains of the Rad50 dimer with main interactions to a strand-loop-helix motif on the NBD. Our analysis suggests that this motif on Rad50 does not directly recognize DNA ends and binds internal sites on DNA. Functional studies reveal that DNA binding to Rad50 is not critical for DNA double-strand break repair but is important for telomere maintenance. In summary, we provide a structural framework for DNA binding to Rad50 in the ATP-bound state.

Keywords crystal structure; DNA double-strand break repair; homologous recombination; Mre11–Rad50; protein:DNA complex

Subject Categories DNA Replication, Repair & Recombination; Structural Biology

DOI 10.15252/embj.201488889 | Received 5 May 2014 | Revised 3 September 2014 | Accepted 25 September 2014 | Published online 27 October 2014

The EMBO Journal (2014) 33: 2847–2859

Introduction

DNA double-strand breaks (DSBs) are highly genotoxic DNA lesions and result in cell death, genome instability, and gross chromosomal aberrations (Chen & Kolodner, 1999; Rothkamm & Lobrich, 2002). DSBs can be formed by ionizing radiation, genotoxic agents, or replicative stress, but are also introduced into the genome in a programmed manner during V(D)J recombination, meiosis, or yeast mating type switching (Costanzo *et al.*, 2001; Longhese *et al.*, 2009; Haber, 2012; Alt *et al.*, 2013). Due to their highly genotoxic nature, DSBs require sensitive detection and repair. Eukaryotic cells react to

DSBs through a very complex DNA damage response (DDR) that includes activation of DNA damage checkpoint kinases, chromatin modifications, cell cycle delay, and repair by non-homologous end joining (NHEJ) or homology-directed repair (HDR) (Harper & Elledge, 2007; Lee *et al.*, 2008; Jackson & Bartek, 2009; Stracker *et al.*, 2013).

The evolutionarily conserved Mre11–Rad50 (MR) complex consists of the endo/exonuclease Mre11 and the ATP-binding cassette (ABC)-type ATPase Rad50. In eukaryotes, the complex is a critical factor in the early stages of DNA double-strand break repair and involved in the initial recognition and nucleolytic processing of DSBs (Williams *et al.*, 2007; Stracker & Petrini, 2011). It contains the third component Xrs2 and is referred to as Mre11–Rad50–Xrs2 (MRX) in *Saccharomyces cerevisiae* and Mre11–Rad50–NBS1 (MRN) in mammals (Dolganov *et al.*, 1996; Carney *et al.*, 1998; Varon *et al.*, 1998). MRN plays a decisive role in HDR (Bressan *et al.*, 1999; Yamaguchi-Iwai *et al.*, 1999) and NHEJ (Moore & Haber, 1996; Xie *et al.*, 2009), meiosis (Moreau *et al.*, 1999), in addition to telomere maintenance (Wilson *et al.*, 1999; Tsukamoto *et al.*, 2001; Reis *et al.*, 2012), and the recruitment of DDR factors such as ATM/Tel1 (D'Amours & Jackson, 2001; Usui *et al.*, 2001; Lee & Paull, 2005). MRN subunits are essential for embryonic viability, while hypomorphic mutations are implicated in severe human genetic disorders that are characterized by genome instability, cancer, and neurological aberration (Petrini, 2000). The bacterial Mre11 and Rad50 homologs are named SbcD and SbcC, respectively. The SbcCD complex helps to prevent gross chromosomal aberrations through degradation of hairpins at inverted repeats facilitating replication restart by recombination (Darmon *et al.*, 2010).

The nuclease activities of MRN are required for DNA end processing and involve endonucleolytic cleavage as well as 3'–5' exonucleolytic processing in the vicinity of DNA ends (Hopkins & Paull, 2008; Mimitou & Symington, 2008; Zhu *et al.*, 2008; Cejka *et al.*, 2010; Garcia *et al.*, 2011; Shibata *et al.*, 2013). The endonucleolytic cut made by MRN near DSBs, possibly in conjunction with 3'–5' exonucleolytic degradation towards the DNA end (Garcia *et al.*, 2011; Shibata *et al.*, 2013), liberates covalently attached proteins, such as Spo11, at meiotic breaks and enables subsequent repair by HDR (Neale *et al.*, 2005). A similar ability to remove proteins from DNA ends by introducing endonucleolytic cuts has been demonstrated for the bacterial MR (SbcCD) *in vitro* (Connelly *et al.*, 2003).

¹ Department of Biochemistry and Gene Center, Ludwig-Maximilians-University, Munich, Germany

² Center for Integrated Protein Sciences, Munich, Germany

*Corresponding author. Tel: +49 89 2180 76953; Fax: +49 89 2180 76999; E-mail: hopfner@genzentrum.lmu.de

[†]Present address: SuppreMol GmbH, Munich, Germany

The MR complex consists of a central Mre11 dimer and two Rad50 subunits. These assemble into a large elongated tetrameric complex with an ATP-regulated catalytic head, which binds and processes DNA, and long protruding Rad50 coiled-coil tails, which are able to tether DNA (Hopfner *et al*, 2000, 2001, 2002; de Jager *et al*, 2001). The Mre11 helix-loop-helix (HLH) motif C-terminal to the nuclease domain interacts with the base of Rad50's coiled-coil near its nucleotide-binding domain (NBD) and flexibly connects Rad50 to the nuclease dimer (Williams *et al*, 2011). In the absence of ATP, the two Rad50 NBDs in the MR complex are positioned on the outside of the Mre11 nuclease dimer and both the dsDNA- and metal-binding sites of Mre11 are accessible for DNA (Lammens *et al*, 2011). In the presence of ATP, however, the two Rad50 NBDs engage through sandwiching two ATP molecules (Hopfner *et al*, 2000). The engaged Rad50 NBD dimer binds into the Mre11 nuclease and DNA-binding cleft, thereby temporarily blocking the active site of Mre11 (Lim *et al*, 2011; Mockel *et al*, 2012).

While the ATP-free open conformation exhibits exonuclease activity, the ATP-bound closed conformation lacks, or has reduced, processive exonuclease activity (Herdendorf *et al*, 2011; Lim *et al*, 2011; Majka *et al*, 2012). The ATP-bound closed conformation still possesses endonuclease activity against ssDNA (archaeal system) (Majka *et al*, 2012), can clip off the terminal nucleotide on dsDNA *in vitro* (bacteriophage T4 system) (Herdendorf *et al*, 2011), or introduce an endonucleolytic cut near the DNA end (Connelly *et al*, 2003). Finally, eukaryotic MRN requires ATP binding to activate ATM and tether DNA (Lee *et al*, 2013; Deshpande *et al*, 2014).

Taken together, the available information suggests that ATP binding and hydrolysis switches MR/MRN between functional states: an open state in which Mre11 DNA binding at the nuclease active sites are accessible, and a closed state in which they are occluded. These different states provide the structural scaffold for the various functions of MR and are correlated to DSB processing on one hand and tethering as well as signaling on the other hand (Deshpande *et al*, 2014). To correlate the diverse functions with a structural mechanism, it is essential to understand how MR interacts with DNA in each functional state. While structural insights into dsDNA binding by the Mre11 dimer (Williams *et al*, 2008) may explain the interaction of DNA with the ATP-free open complex, no information is available about DNA binding to Rad50 in the ATP-bound closed conformation. This information is necessary to explain the structural basis for DNA tethering and—in the case of eukaryotic MRN—DSB signaling functions.

We report here the crystal structure of the *Thermotoga maritima* Rad50 nucleotide-binding domain (tmRad50^{NBD}) in complex with the Rad50-interacting helix-loop-helix motif of Mre11 (tmMre11^{HLH}), Mg²⁺, AMPPNP, and a dsDNA 15mer. The structural analysis reveals that DNA binds mainly to the N-terminal part of the Rad50 NBD (denoted 'lobe I') but forms additional contacts with the coiled-coil region (Fig 1). An *in vitro* DNA-binding analysis validates the observed contacts, but also indicates that positively charged flanking residues contribute to DNA binding. In summary, our results provide a framework for the interaction of MR with DNA in different functional states and establish at the structural level that MR has at least two distinct DNA-binding sites, one on Rad50 in the ATP-bound form and one on Mre11 that is accessible after Rad50 ATP hydrolysis (Fig 5C).

Results

Structure of the Rad50^{NBD}–Mre11^{HLH}–DNA complex

We crystallized tmRad50^{NBD} (residues 1–190 and 686–852 connected by GGAGGAGG linker) in complex with the C-terminal helix-loop-helix motif of tmMre11 (Mre11^{HLH} residues 347–383), AMPPNP, Mg²⁺, and a 15mer dsDNA oligonucleotide in space group P1. The crystals diffracted to a limiting resolution of 2.7 Å and contained two (Rad50^{NBD})₂–(Mre11^{HLH})₂–(Mg²⁺–AMPPNP)₂–DNA complexes in the asymmetric unit. Model building and refinement resulted in a final model with good *R*-factors and stereochemistry (Supplementary Table S1). Both complexes in the asymmetric unit are structurally very similar (Supplementary Fig S1C) (r.m.s.d. values for C α atoms: 0.25 Å; r.m.s.d. values for DNA backbone phosphates: 0.35 Å) and the following description will be limited to one of these complexes.

Rad50^{NBD} displays the dimer characteristic of ABC ATPases: the two Mg²⁺ ions and AMPPNP reside in the dimer interface and are sandwiched between the opposing Walker A/B and signature motifs (Hopfner & Tainer, 2003) (Fig 1; Supplementary Fig S1). The coordination of Mg²⁺ and AMPPNP in the Rad50^{NBD} dimer interface is similar to that in several Rad50/SMC dimer structures in complex with ATP or non-hydrolysable analogs, indicating that the complex represents the typical ATP-bound form of Rad50/SMC proteins (Hopfner *et al*, 2000; Lammens *et al*, 2004; Williams *et al*, 2009, 2011; Lim *et al*, 2011; Mockel *et al*, 2012) (Supplementary Fig S1A). Proper ATP coordination is important in the context of the DNA complex reported here, because biochemical studies have shown that the ATP- or analogue-bound form of Rad50 is necessary for interaction with dsDNA (Raymond & Kleckner, 1993; Hopfner *et al*, 2000; Mockel *et al*, 2012).

The 15mer dsDNA binds in an orientation in which it is positioned between both coiled-coil arms of the Rad50 NBD dimer (Fig 1) and interacts with both the NBD and the coiled-coil domain. On the basis of the number and distance of protein–DNA contacts, the main interaction site is located at the tip of the N-terminal part of Rad50 near the dimer interface (lobe I of the NBD fold). DNA binding is sequence independent and mediated by interactions between the protein main chain and side chain atoms and the sugar–phosphate backbone of the DNA. The DNA does not display significant deviations from the B-form. It protrudes at an approximately 45° angle relative to the Rad50 dimer axis and does not follow the twofold symmetry of the protein.

In lobe I, residues K115 and S118 bind to two consecutive phosphate moieties and additional interactions are made by the β 7-strand main chain atoms of A111 and A114 (Fig 2A). Amino acids K99, K108, and K109 are located on the top and outer face of the lobe I β -sheets 6 and 7, respectively, and are positioned so that they may form additional interactions. These latter side chains are in close vicinity to a symmetry-related DNA molecule (DNA 2) that forms a quasi-continuous DNA helix with the directly bound DNA molecule (Fig 2A; Supplementary Fig S1B).

We also observe a second, minor contact site for DNA in helix α 7 of the Rad50 coiled-coil domain (Fig 2B). This second interaction site is mediated by three lysine–phosphate interactions that are approximately 3 Å distant between residues K175, K178, and K182

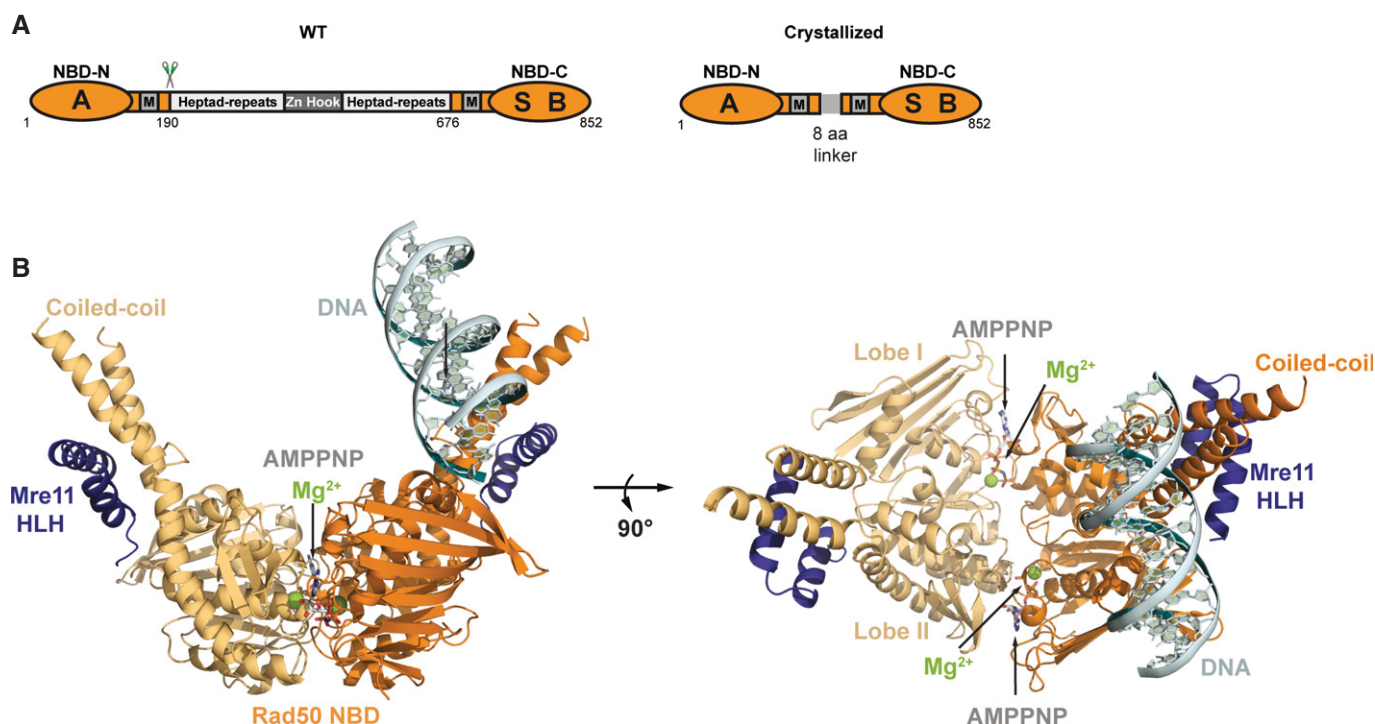


Figure 1. Structure of the tmRad50^{NBD}–Mre11^{HLH}–DNA complex.

A Domain structure of wild-type Rad50 (WT, left) and the crystallized Rad50^{NBD} construct (right). RAD50 contains a bipartite ATP-binding cassette-type nucleotide-binding domain (NBD, orange) consisting of N-terminal (NBD-N) and C-terminal (NBD-C) segments. The N-terminal segment harbors the Walker A motif (A); the C-terminal segment harbors the Walker B (B) and signature motifs (S). M: Mre11 binding sites. NBD-N and NBD-C are at the ends of a heptad-repeat segment that forms an antiparallel coiled-coil. The center of the heptad-repeat segment contains the Zn-hook dimerization motif.

B Ribbon representation with highlighted secondary structure of the nucleotide-binding domain (NBD) dimer of Rad50 (yellow and orange) in complex with the Mre11 C-terminal helix-loop-helix (HLH) motif, Mg²⁺-AMPPNP (Mg²⁺: green sphere, AMPPNP: gray-color-coded sticks), and double-strand DNA (cyan ribbon and sticks) shown in two orientations. Rad50 dimerizes in the typical head-to-tail arrangement, sandwiching two Mg²⁺-AMPPNP moieties in the dimer interface. The DNA binds to a strand-loop-helix motif on one NBD of Rad50 and additional contacts are observed to the adjacent coiled-coil.

and the DNA. While residues K109 and K115 of the strand-loop-helix (SLH) motif are conserved across species (Fig 2C), residues K175 and K182 of the coiled-coil domain are less conserved. Despite these two sites of interaction, the DNA molecule has considerably higher B-factor values compared with the neighboring protein regions, suggesting that the DNA is quite flexibly bound in the crystal lattice (Supplementary Table S1).

Comparison of tmRad50^{NBD}–Mre11^{HLH} structures with and without DNA reveals that the globular NBDs and their complexes are largely identical. Nevertheless, the coiled-coil domains and the Mre11 HLH motifs are repositioned by 2–3 Å relative to the *apo* structure (Supplementary Fig S2).

In summary, we identify here a SLH motif as the main DNA interaction site of Rad50 NBDs, with additional DNA contacts contributed by the coiled-coil region. Remarkably, the interactions are limited to internal sites within dsDNA and are apparently not directed toward the ends of DNA.

Biochemical analysis validates the positively charged DNA-binding groove

In order to validate the structurally identified DNA-binding sites on Rad50, we performed electrophoretic mobility shift assays (EMSAs) of several site-specific mutants of tmRad50^{NBD}–Mre11^{HLH} (Fig 3). In

parallel, we analyzed the ATP- or AMPPNP-dependent dimer formation properties of wild-type and all examined mutant tmRad50^{NBD}–Mre11^{HLH} constructs through size-exclusion chromatography (Supplementary Fig S3).

Consistent with previous observations, we find that tmRad50^{NBD}–Mre11^{HLH} is a ‘monomeric’ complex in the absence of ATP/AMPPNP but forms a ‘dimeric’ complex (i.e. two tmRad50^{NBD}–Mre11^{HLH} protomers) in the presence of ATP/AMPPNP. The wild-type construct failed to form a stable dimer in the presence of ATP, likely because of ATP hydrolysis. Residue E798 in the Walker B motif positions and polarizes the attacking water molecule in the ATP hydrolysis site and the E-to-Q mutant can be used to ‘trap’ the ATP-bound state (see e.g. Lammens *et al*, 2004). In agreement with this, mutation of E798 to Q resulted in efficient dimer formation in the presence of ATP. Another notable mutation in this context is the signature motif mutation S768R that was previously shown to prevent ATP-induced engagement of the NBDs of Rad50 (Hopfner *et al*, 2000; Moncalian *et al*, 2004). Consistent with this observation, we observed no tmRad50^{NBD}–Mre11^{HLH} dimers even in the presence of AMPPNP. With the exception of S768R, all other mutants examined displayed wild-type-like dimer formation in size-exclusion chromatography, suggesting that the effects of these mutations on DNA binding are not due to aberrant AMPPNP-induced tmRad50^{NBD}–Mre11^{HLH} dimerization.

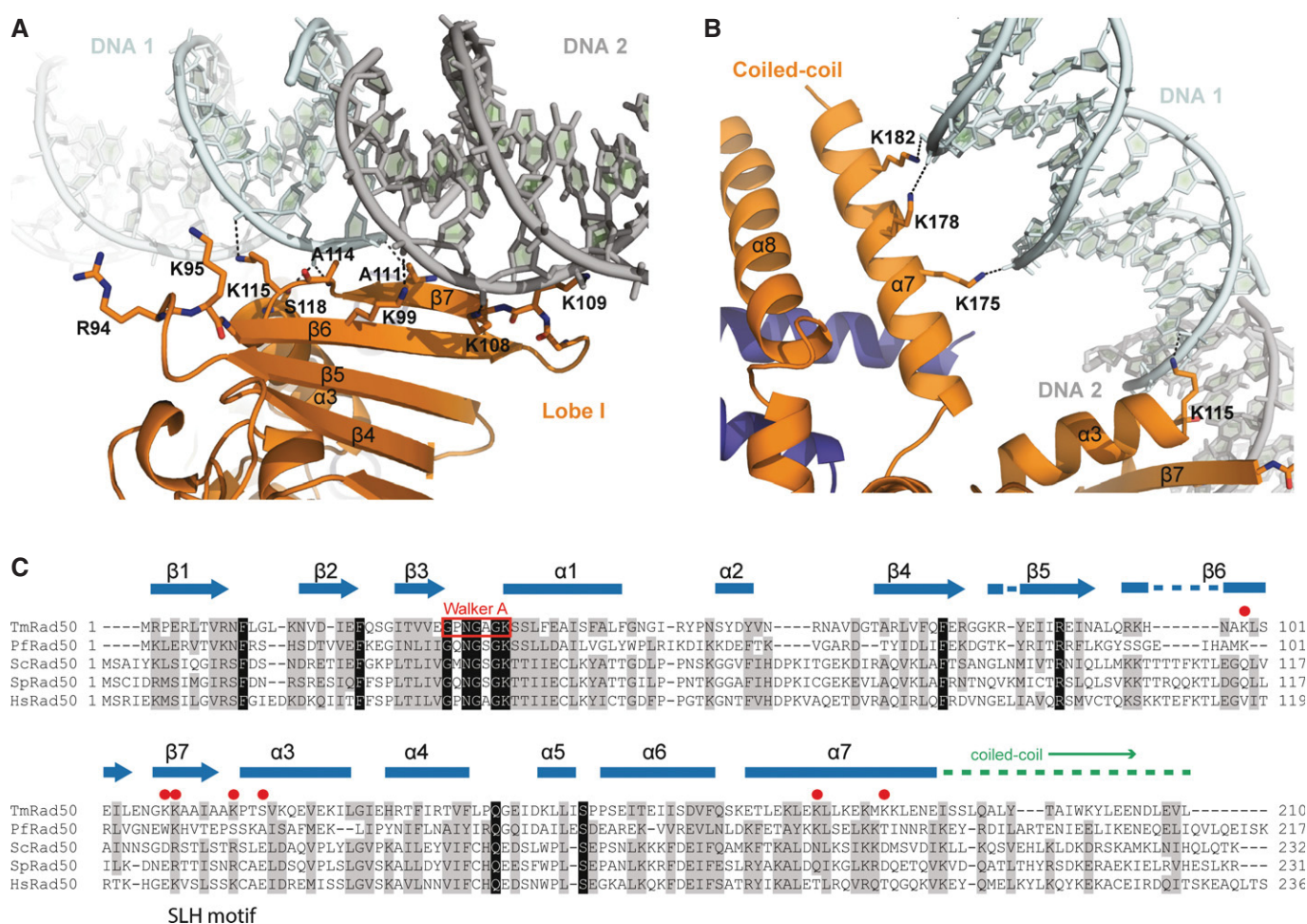


Figure 2. Details of the Rad50^{NBD}–Mre11^{HLH}:DNA interface.

- A** Detailed view of the DNA interactions with the Rad50 NBD (orange) shown in ribbon representation with the contacting residues highlighted as sticks. DNA contacts involve interactions of the strand-loop-helix motif of the Rad50 dimer (residues K99, K108, K109, A111, A114, K115, and S118) with the sugar–phosphate backbone of the two DNA molecules (cyan and gray). The second DNA molecule, depicted in gray, belongs to the symmetry-related molecule and forms a quasi-continuous DNA strand in the crystal structure. Residues R94 and K95 are in close proximity of the DNA-binding region and evidently involved in DNA binding.
- B** Details of the DNA–protein contacts at the Rad50 coiled-coil region mediated by interactions of lysine residues K175, K178, and K182 with the DNA–phosphate backbone.
- C** Sequence alignment showing the conservation of residues involved in DNA binding.

EMSA performed with the ΦX174 RF II closed double-stranded DNA plasmid revealed that tmRad50^{NBD}–Mre11^{HLH} possesses robust DNA-binding activity only in the presence of AMPPNP (Fig 3; Supplementary Fig S4). Mutation of any of the three lysine residues (K115E, K175E, and K182E) involved in direct protein–DNA contacts affected DNA binding *in vitro*. Mutation of the coiled-coil residues K175E and K182E substantially reduced DNA binding, whereas the mutation K115E almost abolished DNA interactions *in vitro*. In agreement with our structural results, these data indicate that K115 on the tip of lobe I is the principal interaction site for DNA. Since its high B-factor indicates that the DNA is flexibly bound, we also mutated a number of conserved residues that flank these lysine residues. R94E and K95E are evidently also important for DNA binding, suggesting that the DNA-binding surface likely involves a more extended positively charged surface area than the direct contacts observed in the

crystal structure. We also mutated the residue R765 in the center of the Rad50 dimer cavity to check whether the DNA may reach the symmetry-related binding site within the Rad50 dimer by traversing the positively charged Rad50 groove. The R765E mutation significantly diminished DNA binding without affecting dimer formation *in vitro*, lending support to the aforementioned hypothesis.

Finally, the Walker B motif ‘ATP trapping’ mutation E798Q showed robust DNA-binding ability in the presence of ATP. The slight reduction in affinity for DNA, compared to the wild-type protein in the presence of AMPPNP, could result from residual ATP hydrolysis of the E-to-Q mutant. The signature motif mutation S768R, however, substantially reduced DNA-binding activity in the presence of AMPPNP, suggesting that formation of an ATP/AMPPNP-bound NBD dimer of Rad50 is essential for robust DNA interaction (Fig 3).

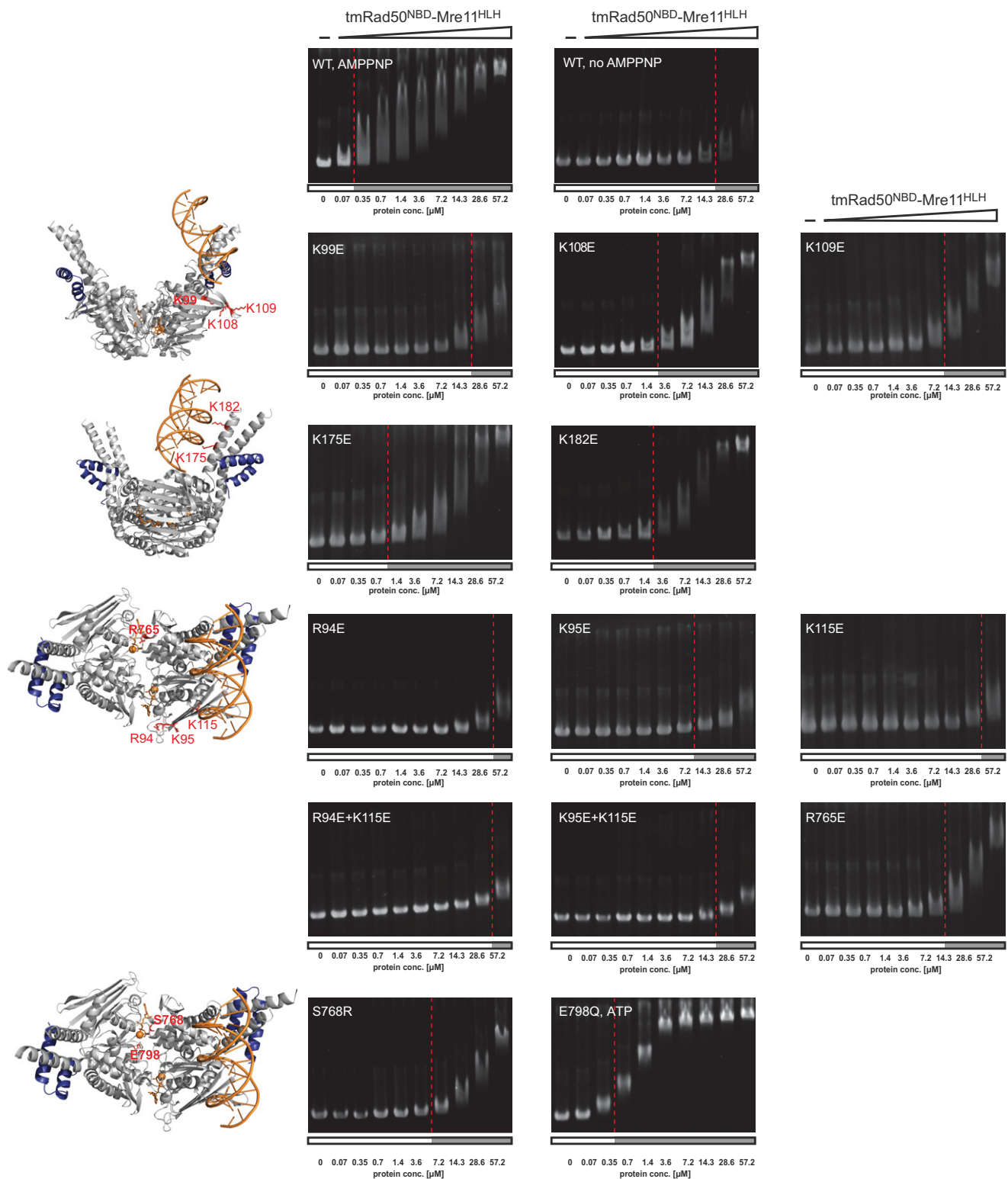


Figure 3. DNA-binding activity of the wild-type and mutant $tmRad50^{NBD}$ - $Mre11^{HLH}$.

Shown are electrophoretic mobility shift assays of the Φ X174 RF II plasmid in the absence or presence of AMPPNP (or ATP if indicated) with increasing protein concentrations as indicated. For clarity, the positions of the mutations are marked in the structural cartoons left of the agarose gel images. The red lines mark the protein concentrations at which approximately half of the free DNA is shifted (see Supplementary Fig S4). K99E, K108E, K109E, K175E, K182E, and R765E mutants exhibit impaired DNA binding, whereas R94E, K95E, and K115E fail to bind DNA in these assays. ATP-induced structural changes and NBD dimer formation are important for the interaction with DNA as shown by the lack of DNA-binding activity in the absence of AMPPNP and of the non-dimerizing signature motif mutant S768R. In contrast, the Walker B mutation (E798Q) is proficient in DNA binding.

While these studies were performed with Φ X174 RF II plasmid DNA, binding of the wild-type protein was also analyzed with short dsDNA oligonucleotides. We observe that increasing the length of dsDNA from 30mer to 60mer substantially enhanced the affinity of tmRad50^{NBD}–Mre11^{HLH} for the DNA (Supplementary Fig S5A). This length-dependent increase in affinity is consistent with the structural finding that tmRad50^{NBD}–Mre11^{HLH} does not directly bind DNA ends but rather at internal sites of DNA. Taken together, the biochemical DNA-binding analysis confirms the importance of the structurally identified contact residues of Rad50 to the tip of NBD lobe I and suggests that the groove between the two coiled-coil domains, formed following ATP-dependent NBD engagement, provides a positively charged surface for DNA interaction (Fig 5; Supplementary Fig S6).

Analysis of the Rad50 DNA-binding site for DSB repair in *Saccharomyces cerevisiae*

To further investigate the significance of the structurally observed DNA-binding site in the context of the eukaryotic MRN complex, we performed a mutational analysis of the equivalent residues in the *S. cerevisiae* Rad50 and determined the functional consequences with *in vivo* assays (Fig 4A and B). Western blot analysis of the mutants confirmed that all mutant proteins were expressed to wild-type levels (Supplementary Fig S6A). We first analyzed the viability and growth of *S. cerevisiae* transformants on topoisomerase I inhibitor camptothecin (CPT), ribonucleotide reductase inhibitor hydroxyurea (HU), and bleomycin-supplemented medium (Fig 4A), as the Δ rad50 strain grows poorly on media containing these DNA-damaging agents (D'Amours & Jackson, 2001). While plasmid-expressed wild-type Rad50 rescues the impaired DNA damage response of the Δ rad50 strain, Rad50 carrying mutations in the signature motif (S1205^{Sc}R) and the Walker B motif E1235^{Sc}Q failed to rescue Δ rad50, consistent with previous studies (Moncalian *et al*, 2004; Bhaskara *et al*, 2007). These mutations show the functional importance of ATP-binding-induced NBD engagement and ATP hydrolysis-induced NBD disengagement in the DSB repair activity of the MRN complex.

We also mutated the residues corresponding to R94, K95, and K115 in tmRad50^{NBD}–Mre11^{HLH} since these residues strongly affected DNA binding *in vitro* (Fig 3). The equivalent mutations K103^{Sc}E, K104^{Sc}E, and R131^{Sc}E had little influence on the DSB repair function of *S. cerevisiae* Rad50 (Fig 4; Supplementary Fig S5B).

In the crystal structure, amino acids K99, K108, and K109 interact with a second DNA molecule forming a quasi-continuous DNA helix in the crystal lattice (Supplementary Fig S1B). This raised the question whether these residues are involved in the end-joining function of the MR complex. Indeed, two of these residues, K99 and K109, seem to be conserved in *S. cerevisiae* (Fig 2C) and the equivalent residues K110^{Sc} and R125^{Sc} have been mutated to glutamic acid to test the influence of these amino acids in a plasmid transformation assay *in vivo* (Supplementary Fig S6B). Whereas the Δ rad50 strain showed substantially reduced transformant yields for NcoI-linearized pRS315-Kan plasmids relative to supercoiled plasmid transformation, the Rad50 point mutants K110E^{Sc} and R125E^{Sc} led to only insignificant reduction in plasmid recovery (Supplementary Fig S6B). This result argues

against an involvement of these residues in end-joining processes in *S. cerevisiae*.

Rad50–DNA interactions are important for telomere length maintenance in *Saccharomyces cerevisiae*

MRN plays an important function in telomere maintenance, for example through activation or recruitment of the Tel1 kinase. We performed telomere maintenance assays to analyze the importance of the DNA-binding site on the Rad50 NBDs in this context. Interestingly, we observed a moderate reduction in telomere length in the case of K103^{Sc}E, K104^{Sc}E, and R131^{Sc}E, while the double mutant K103^{Sc}E+R131^{Sc}E at the SLH motif and the R1201^{Sc}E mutant at the center of the positive cleft substantially reduced the length of telomeres, almost equal to Δ rad50 levels. This suggests that DNA binding by Rad50 at the SLH motif and possibly in the groove is critical for telomere length maintenance (Fig 4B). Notably, while the signature motif mutant S1205^{Sc}R also substantially reduced telomere lengths, the Walker B mutant E1235^{Sc}Q is fully proficient in telomere maintenance. Together, this analysis suggests that MRN functions in telomere length maintenance in engaged conformation with DNA and ATP-bound NBDs.

Discussion

We report the first structural analysis of DNA binding to an SMC/Rad50/RecN family member of chromosome-associated ABC enzymes. Rad50 is the ATP-binding subunit of the Mre11–Rad50 (prokaryotes and phages) and Mre11–Rad50–Nbs1/Xrs2 (eukaryotes) complexes that are key genome maintenance factors in all kingdoms of life. Although considerable knowledge regarding the architecture of MR and MRN complexes has been acquired (reviewed in e.g. Schiller *et al*, 2014), the molecular mechanisms of MR/MRN complexes in replication-associated hairpin degradation, telomere maintenance, or DSB repair are still unclear.

Within MR/MRN, Rad50 is suggested to undergo a large structural change that is controlled by ATP binding and hydrolysis (Lammens *et al*, 2011). In the presence of ATP, the engaged Rad50 dimer sterically blocks the nuclease active site of Mre11 (Lim *et al*, 2011; Mockel *et al*, 2012), while following ATP hydrolysis and Rad50 disengagement, the Mre11 nuclease active sites become exposed (Lammens *et al*, 2011). Whereas Rad50 in its ATP-bound form apparently blocks the Mre11 DNA-binding and nuclease active sites, it becomes proficient for DNA binding in the presence of ATP. Therefore, ATP appears to switch MR/MRN between Mre11 and Rad50 DNA-binding modes.

Our structural analysis reveals how DNA interacts with MR in the Rad50 DNA-binding mode and, together with earlier studies on DNA binding by Mre11 (Williams *et al*, 2008), provides now a framework to understand DNA interaction of MR in different functional states. DNA predominantly binds to the strand-loop-helix (SLH) motif on the Rad50 NBD. This motif is located on the N-terminal lobe I of the conserved NBD fold. Lobe I harbors also the ATP-binding P-loop, while lobe II carries the signature motif and the coiled-coil protrusion. Besides the SLH motif, additional interactions are found between DNA and two lysine residues of the coiled-coil domain. These contacts of the coiled-coil domains to

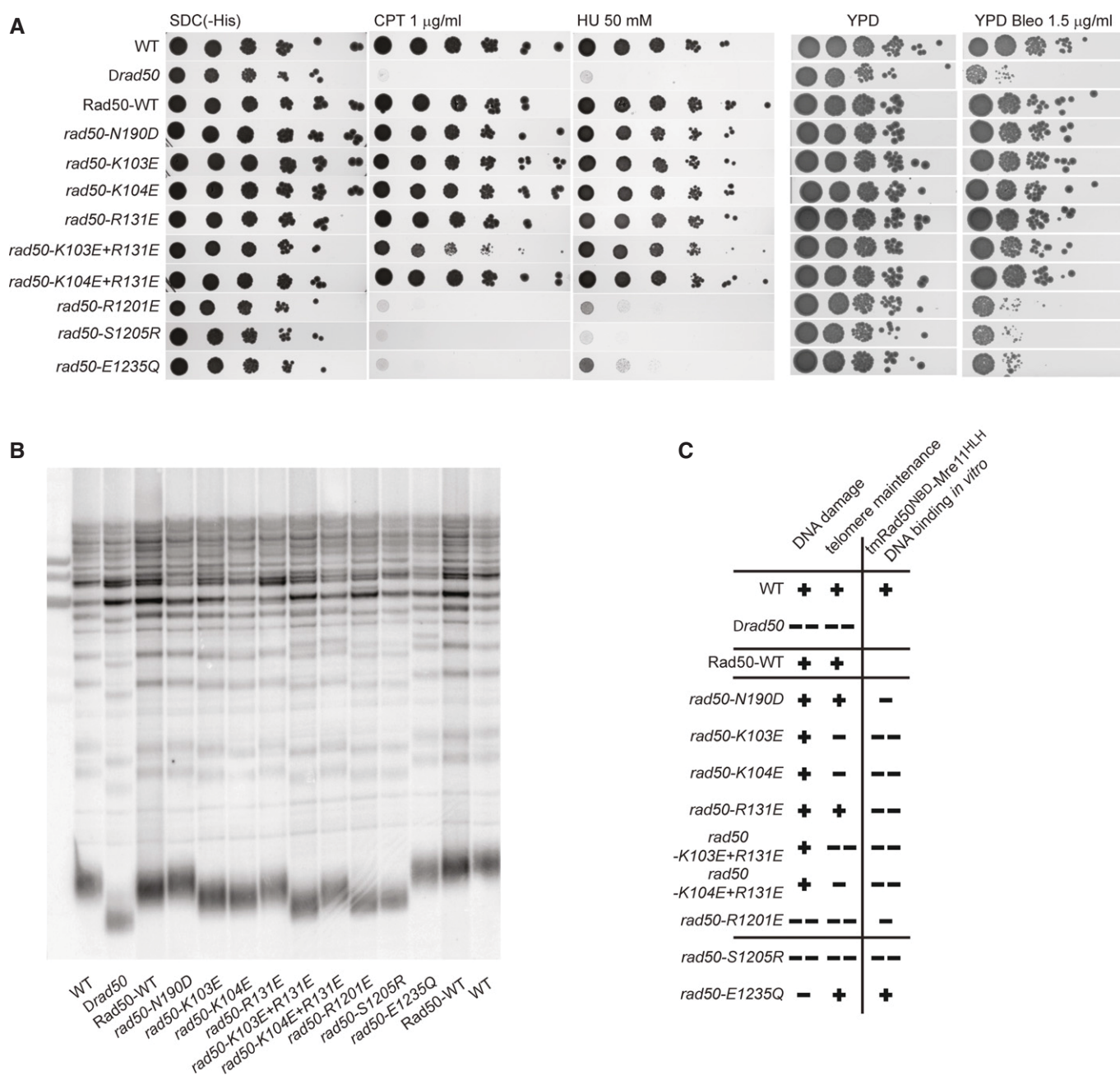


Figure 4. *In vivo* analysis of Rad50 mutations in *Saccharomyces cerevisiae*.

A Effects of *rad50* mutants on *S. cerevisiae* survival in the presence of DNA-damaging agents. Plate survival assays show that R1201^{ScE}, S1205^{ScR}, and E1235^{ScQ} mutants are deficient in the DNA damage response, comparable to the *Δrad50* strain. K103^{ScE} + R131^{ScE} double mutant shows partially inhibited DNA damage response.

B Telomere maintenance assays show altered telomere metabolism for mutations or double mutations at the proposed Rad50 DNA-binding groove (K103^{ScE}, K104^{ScE}, K104^{ScE} + R131^{ScE}, R1201^{ScE}) and the signature motif mutant S1205^{ScR}. A notable exception is the Walker B mutant E1235^{ScQ}, which is not proficient in ATP hydrolysis, suggesting that the ATP-bound, engaged Rad50 dimer is essential for the role of MRN at telomeres.

C Summary of *S. cerevisiae* phenotypic behavior in DNA repair and telomere maintenance compared with the effect of the corresponding tmRad50 mutations on DNA binding *in vitro*.

DNA are interesting in the context of DNA-induced mesoscale conformational changes between the two coiled-coil domains of MRN (Moreno-Herrero *et al*, 2005). Such a repositioning could be a direct consequence of DNA binding because of, for example, binding of K175 and K182 in the coiled-coil domain to DNA. On the other hand, the coiled-coil domains are notoriously flexible and the

amount of their repositioning between apo- and DNA-bound Rad50^{NBD}-Mre11^{HLH} structures is also in the range of crystal lattice-induced differences, so further analysis is necessary to directly link DNA binding and coiled-coil movements. Nevertheless, binding of DNA to the coiled-coil domains is not unexpected and may proceed even further than the observed site in our truncated construct,

because the coiled-coil domains are important for high-affinity DNA binding by human MRN (Lee *et al*, 2013).

The *in vitro* DNA-binding data indicate that although both interaction sites contribute to DNA binding, the residues within the SLH motif have a considerably larger impact *in vitro* (Fig 3), suggesting this as the main DNA-binding motif in Rad50. Furthermore, we found that positively charged residues flanking the SLH motif R94 and R95 are also required for robust DNA binding, even though they do not directly contact the DNA in our crystal form. These observations suggest that DNA is recognized by lobe I on both sides of the Rad50 dimer, presumably through the extensive positive electrostatic surface potential across both NBDs (Fig 5). Importantly, a comparison of the DNA-bound structure with the DNA-free structure of the bacterial MR complex (containing the nuclease domain of Mre11) confirms that there is no steric hindrance between Mre11 and DNA binding on Rad50 and shows that DNA binds to Rad50 on the opposite side of the Mre11 nuclease domain (Fig 5B).

It was unexpected that DNA is bound only to one of the two NBDs, considering the internal symmetry of the Rad50 dimer and the biochemical data that clearly show that ATP-induced NBD dimer formation is important for DNA binding (Fig 3) (Hopfner *et al*, 2000; Mockel *et al*, 2012). How is ATP binding to Rad50 linked to DNA binding? One possibility is that we visualize an intermediate where DNA is bound to only one of the two SLH motifs of the NBD dimer. A shift of the DNA, taking the lobe I interaction with the SLH motif on one NBD as anchor point, would bring the DNA backbone into a suitable position to also bind the second SLH motif on the other NBD. Such a dual recognition on both SLH motifs requires at least 22-base-pair-long DNA consistent with the length dependence of the DNA binding (Supplementary Fig S5). Such a binding mode would also explain the strong effect of the R1201E mutant, which resides right at the surface of the NBD:NBD interface cleft. *In vitro*, this mutation still forms NBD dimers in the presence of ATP (tmRad50^{NBD R765E}), so the effect of the mutation might proceed via

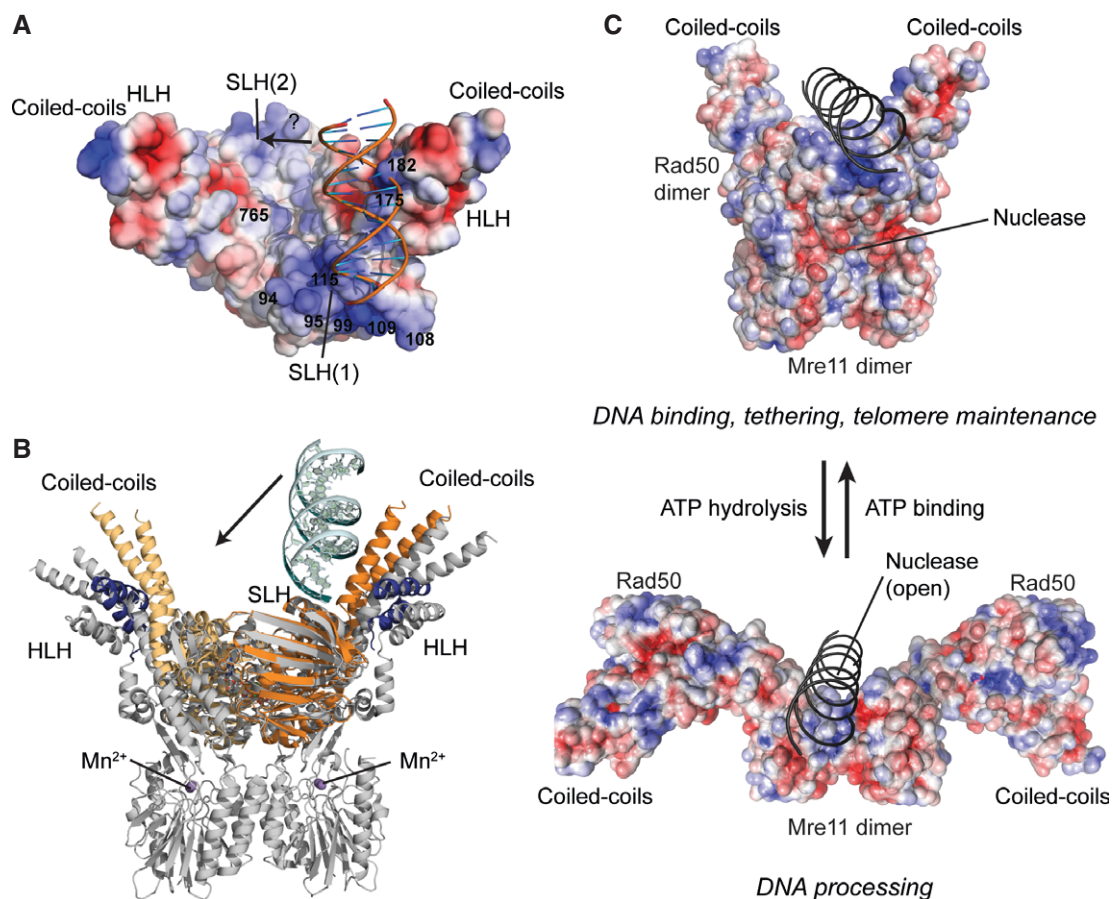


Figure 5. Framework for the interaction of DNA with Mre11–Rad50 functional states.

- A** Surface representation of tmRad50^{NBD}–Mre11^{HLH} with mapped electrostatic potential (blue: positive; red: negative). DNA is shown as cartoon. The SLH motifs and the surface in the groove between the coiled-coil domains carry a strong positively charged surface potential. A moderate shift of the bound DNA would enable additional contacts to the second SLH motif (see text).
- B** Superposition of the tmRad50^{NBD}–Mre11^{HLH}–DNA (color code of Fig 1) and tmRad50^{NBD}–Mre11^{FL} (gray; PDB code 3THO) models. DNA binds to Rad50 on the opposite side of the Mre11 nuclease dimer and does not sterically compete with Mre11 binding.
- C** Model of DNA binding and its implication for the functions of the MRN complex. Top: the ATP-bound ‘closed’ conformation with DNA bound to Rad50 is implicated for DNA binding, tethering, and telomere maintenance functions. Upon ATP hydrolysis, Rad50 NBDs move away from each other, exposing the Mre11 active sites to allow for DNA processing.

perturbation of the electrostatics in the groove, but it could also affect the dimer structure in a way that DNA binding is compromised. ATP-dependent NBD dimer formation also leads to a strong positive electrostatic surface potential along the groove between the coiled-coils as previously noted (Hopfner *et al*, 2000; Lim *et al*, 2011; Mockel *et al*, 2012) (Fig 5; Supplementary Fig S7). Thus, NBD dimerization can contribute to robust DNA binding directly by forming a positively charged surface potential. Such a mechanism is consistent with our observation that robust *in vitro* binding of DNA to the NBDs is affected not only by mutations in directly interacting residues but also by mutations of basic side chains in the vicinity of the DNA in the structure. Finally, ATP binding induces structural changes between both lobes of a single NBD and repositions the SLH domain and the coiled-coil with respect to each other. Since both elements interact with DNA, ATP-triggered positioning of coiled-coil and SLH within a single NBD could be an important step for DNA recognition.

The SLH motif and its flanking residues turned out to play significant but divergent roles in the DNA damage response and telomere maintenance in *S. cerevisiae*. Single point mutations in the SLH motif had only minor effects on DNA repair functions in response to damaging agents as demonstrated by yeast survival assays. This suggests that the DNA repair pathway can still operate near wild-type physiological level, even if Rad50–DNA interactions are substantially weakened. It is also unlikely, given these minor consequences, that the nuclease activity of MRN is influenced by mutations in the Rad50 DNA-binding site. On the other hand, the strong negative effect of the signature motif mutant S2105^{Sc}R clearly argues against a role in which Rad50 merely blocks Mre11 nuclease prior to DNA processing, otherwise this mutation would not have such a strong effect. Likewise, imposing an ATP-bound dimer state through the Walker B motif E1235^{Sc}Q mutant abolishes DNA repair activities. We conclude that while DNA interactions to Rad50 appear to be less critical for the DNA repair activities of MRN, the ability to engage and disengage the NBDs in response to ATP binding and hydrolysis remains critical. We do not want to rule out, however, that mutating more than two residues in the identified DNA-binding surface, or combining these mutations with mutations in the coiled-coil domain will more substantially affect DNA repair activities. The coiled-coil domain is necessary for high-affinity DNA interactions—either directly or by promoting higher-order conglomerates—and might be sufficient to promote repair activities even when the DNA-binding site of the NBD is compromised (Lee *et al*, 2013).

This situation changes in a remarkable way in the context of telomere maintenance. The function of MRN in telomere maintenance includes the recruitment and activation of Tel1^{ATM} (Hector *et al*, 2007), but also involves DNA-tethering activities (Reis *et al*, 2012). Here, the SLH mutations had much more severe effects, with the double mutant at the Rad50 DNA-binding site affecting telomere length nearly as much as a Rad50 deletion. Most notably, our analyses revealed that the SLH (K103E and K104E) and Walker B (E1235Q) motif mutations lead to a separation of function phenotype: while mutation of the SLH motif strongly impaired telomere maintenance but had little effect on repair activities, mutation of the Walker B motif resulted in the opposite behavior. Prohibiting, or at least severely delaying, ATP hydrolysis in Rad50 and consequently

promoting formation of the closed complex do not influence telomere maintenance, while preventing ATP-induced NBD dimer formation through mutation of the signature motif has detrimental effects on telomere maintenance. Together, our analysis suggests that the Rad50 dimer with bound ATP and DNA is the functional state of MRN in the context of telomere maintenance. These data are consistent with findings that ATP binding but not hydrolysis is important for ATM activation by MRN (Lee *et al*, 2013; Deshpande *et al*, 2014).

We do not observe a direct molecular preference for a DNA end by Rad50 in our structural analysis. In general, it has been difficult to demonstrate a strong preference of MR/MRN for DNA ends, except in the case of scanning force microscopy studies, where the clustering of MRN complexes occurred preferentially at DNA ends (Chen *et al*, 2001; de Jager *et al*, 2001, 2002). Even in this case, one complex could bind to the end, while others may bind internal sites of DNA. In this regard, we analyzed the Rad50–Rad50 crystal lattice contacts on the quasi-continuous DNA as they might show how MR/MRN clusters on DNA. However, the lattice interactions would clash with the interfaces between Rad50 and Mre11 nuclease dimer in the Mre11–Rad50 complexes (Lim *et al*, 2011; Mockel *et al*, 2012), so it is unlikely that they represent interaction sites of MRN clusters on DNA.

With respect to DSB recognition, our results suggest that the affinity for DNA ends might reside in the Mre11 dimer, which can interact with one or two DNA ends or hairpins (Williams *et al*, 2008), or possibly in an yet to be characterized interplay between Mre11 and Rad50. It is also possible that binding of two DNA molecules via both SLH motifs in the Rad50 dimer and additional DNA: DNA contacts via DNA end stacking or overhangs with microhomologies can lead to DNA end recognition and tethering. These models will be addressed now in future studies. Nevertheless, DNA binding by Rad50 at internal sites could function in initial loading of the complex at or near DNA ends that are blocked by proteins such as Spo11 or Ku (Wasko *et al*, 2009; Bonetti *et al*, 2010; Mimitou & Symington, 2010; Garcia *et al*, 2011; Langerak *et al*, 2011; Sun *et al*, 2012), or at sites remote from breaks (Neale *et al*, 2005; Shibata *et al*, 2013).

Our data lead to a mechanistic model for MRN activity in which the ATP-bound ‘closed’ conformation of the complex recognizes internal sites of DNA via Rad50, yet also allows for the scaffolding and presumably ATM/Tel1 activation functions of the complex (Fig 5C). Hereby, DNA binds between the coiled-coil domains and is suitably positioned to access the Mre11 dimer after ATP hydrolysis, which is suggested to switch MRN from the tethering and signaling mode to the ‘open’ DNA processing mode (Deshpande *et al*, 2014). In the open mode, MRN might also preferentially interact with DNA ends. It yet needs to be explained how these ATP-driven conformations communicate with the Rad50 coiled-coil structures and zinc hook, since heterozygous mutation of the zinc hook dimerization domains lead to increased ATM activation (Roset *et al*, 2014).

In general, the structure of the Rad50–DNA complex allows for a better understanding of the mechanism of Rad50/SMC/RecN/RecF-type chromosome-associated ABC ATPases as all these proteins contain an SLH-like secondary structure motif. SMC ATPases form dimers in the context of the cohesin, condensin, and SMC5/6 complexes (Hirano, 2006). For instance, a loop near the SLH motif

is critical for DNA-stimulated ATPase activity in archaeal SMC NBDs (Lammens *et al*, 2004). Likewise, a lysine in the equivalent region is acetylated in eukaryotic SMC3 (part of the condensin complex) and results in the stable establishment of chromosome cohesion (Lee *et al*, 2008; Rolef Ben-Shahar *et al*, 2008; Unal *et al*, 2008), although the mechanistic role of this lysine acetylation still needs to be determined. On the basis of surface electrostatics, it was suggested that also the bacterial RecF and archaeal SMC proteins bind DNA at the NBD surface that contains the SLH motif (Lammens *et al*, 2004; Koroleva *et al*, 2007). Although the DNA binding mechanisms of these related chromosome-associated ABC ATPases each need to be determined experimentally, it is conceivable that DNA interacts with the ATP-bound NBD dimers in these complexes in a similar way as with the Rad50 NBDs.

Materials and Methods

Protein expression and purification

Rad50^{NBD}–Mre11^{HLH} from *T. maritima* was engineered and purified as described before (Lammens *et al*, 2011).

Crystallization and data collection

Crystals of tmRad50^{NBD}–Mre11^{HLH}–DNA were grown by hanging drop vapor diffusion method. 1 μ l of protein–AMPPNP–DNA solution (12 mg/ml protein, 5 mM AMPPNP, 1.275 mM DNA) was mixed with 1 μ l reservoir solution (150 mM D-maleic acid pH 6.5, 21% (v/v) PEG3350) and incubated over 400 μ l reservoir solution at 20°C. DNA used for crystallization was prepared by annealing oligonucleotides 5'-GGTCGGTGACCGACC-3' and 5'-GGTCGGTCACCGACC-3'. To this end, oligonucleotides were mixed at 1:1 molar ratio in annealing buffer (40 mM Tris pH 7.5, 100 mM NaCl, 10 mM MgCl₂), preheated to 94°C, and cooled down to 4°C at the rate of 0.1°C/s. Prior to flash-freezing, crystals were transferred to cryoprotective condition containing 20% (v/v) glycerol. Native dataset collected at –170°C at wavelength 1.000020 Å at PXI beamline at Swiss Light Source (SLS, Villigen, Switzerland) was indexed and integrated with XDS (Kabsch, 1993). Crystals grew in the P1 space group with cell dimensions: a = 50.2 Å, b = 97.1 Å, c = 107.6 Å, α = 90.6°, β = 89.4°, γ = 98.3° and contained two dimer molecules per asymmetric unit.

Structure determination and refinement

The structure of tmRad50^{NBD}–Mre11^{HLH}–DNA was determined by molecular replacement phasing with PHASER (McCoy *et al*, 2007), using the AMPPNP–tmRad50^{NBD}–Mre11^{HLH} structure, determined in the absence of DNA, as a search model (PDB entry: 3QF7). The initial model was rebuilt manually in COOT (Emsley & Cowtan, 2004) and refined in PHENIX (Adams *et al*, 2002). At an early stage of manual building and refinement, a 15-bp DNA molecule was manually build into the F_o–F_c difference density. Further refinements included interactive cycles of bulk solvent corrections, overall B-value refinement, positional and individual B-value refinement, TLS refinement, and manual building. Prior to refinement, 5% of the reflections were randomly omitted to monitor the

R_{free} value. The Ramachandran statistics, calculated using Procheck (Lovell *et al*, 2003), of the final model are outliers (%): 0.5, allowed (%): 5.0, and favored (%): 94.5. The outliers are N713, which interacts with the Mre11 HLH motif and the DNA interacting residue K115. Statistics of data collection and model refinement are summarized in Supplementary Table S1. All figures of structural models were prepared with PyMOL (DeLano Scientific).

Electrophoretic mobility shift analyses

DNA-binding activity of tmRad50^{NBD}–Mre11^{HLH} (wild-type and mutants) was analyzed in electrophoretic mobility shift assay. Increasing amounts of dimerised protein (0, 71.5 nM, 357.5 nM, 715 nM, 1.43 μ M, 3.57 μ M, 7.15 μ M, 14.3 μ M, 28.6 μ M and 57.2 μ M) were incubated with 7.15 nM Φ X174 RF II plasmid DNA and 1 mM AMPPNP (ATP in case of E798Q mutant) in 5 mM Tris pH 7.8, 100 mM NaCl, 5 mM MgCl₂ in a total volume of 20 μ l for 15 min on ice. Reaction samples were then mixed with a loading buffer and separated in 0.5% agarose gel in TA buffer (40 mM Tris, 20 mM acetic acid) for 3.5 h at 80 V and 8°C. Protein–DNA complexes were stained with DNA-intercalating agent GelRed and visualized by UV Imaging System (Intas).

DNA-binding activity of wild-type tmRad50^{NBD}–Mre11^{HLH} was compared with 30mer and 60mer dsDNA. To this end, increasing amounts of dimerised tmRad50^{NBD}–Mre11^{HLH} (0, 125 nM, 250 nM, 375 nM, 625 nM, 1.25 μ M, 2.5 μ M, 5 μ M and 12.5 μ M) were incubated with 1 mM AMPPNP and 25 nM 30mer or 60mer fluorescently labeled dsDNA in 5 mM Tris pH 7.8, 100 mM NaCl, 5 mM MgCl₂ in a total volume of 10 μ l for 15 min on ice. Reaction samples were then mixed with a loading buffer and separated on 8% polyacrylamide native gels in TA buffer for 1–1.5 h at 100 V and 8°C. Protein–DNA complexes were visualized with a Typhoon System (Amersham Biosciences) using the green-excited (488 nm) fluorescence mode.

30mer and 60mer dsDNA were prepared by annealing oligonucleotides 6-FAM-5'-CCGGAAGCATCTAGCATCTGTCTCAGCTGC-3' with 5'-GCAGCTGACAGGATGCTAGATGCTTTCCGG-3' and 6-FAM-5'-GCTAATGCCGCGTGCCTGTCTCACCTTCGATTTAGCATGGTATCAGCAGAGCAAGCCTC-3' with 5'-GAGGCTTGCTCTGCTGATACCATGCTAAATCGAAGGTGAGACAAGGCACGCGGCATTAC-3', respectively. To this end, oligonucleotides were mixed with 1.2 molar excess of fluorescently labeled oligonucleotide in annealing buffer (40 mM Tris pH 7.5, 100 mM NaCl, 10 mM MgCl₂), preheated to 94°C, and cooled down to 4°C at the rate of 0.1°C/s.

Yeast complementation assay

Overnight cultures of *S. cerevisiae* transformed with empty pRS313 plasmid (W303-1a wild-type and W303-1a Δ rad50 strains, kind gifts of Katja Strässer and Steve Jackson, respectively) or pRS313 carrying wild-type or mutated alleles of Rad50 (W303-1a Δ rad50 strain) were diluted in deionised water to OD₆₀₀ of 1. Serial tenfold dilutions were prepared, and 4 μ l of each dilution was plated on SDC(-His)-agar or YPD medium supplemented with DNA-damaging agents: 1 μ g/ml camptothecin (CPT), 50 mM hydroxyurea (HU), or 1.5 μ g/ml bleomycin (Bleo). Cells were incubated for 72 h at 30°C. All experiments were performed in triplicates.

Western blot analysis

Trichloroacetate (TCA)-precipitated *S. cerevisiae* lysates were prepared as described before (Yaffe & Schatz, 1984) with modifications: Cells from 20 OD units of overnight culture were pelleted and lysed with 1.5 ml 0.2 M NaOH, 1% β -ME. Total protein was precipitated by addition of 150 μ l 0.1% TCA. Protein pellet was resuspended in 25 μ l twofold SDS–PAGE sample buffer. For analysis, protein extract corresponding to 5 OD units was resolved in 8% SDS–polyacrylamide gel, transferred onto nitrocellulose membrane, and immunodetected using standard Western blotting technique. Antibodies against *S. cerevisiae* Rad50 were a kind gift of John Petrini.

Analysis of telomere lengths

Telomere length in *S. cerevisiae* carrying wild-type and mutated Rad50 allele was analyzed as described before (Schiller et al, 2012).

Dimerization analysis by gel filtration chromatography

Dimerization of the monomeric tmRad50^{NBD}–Mre11^{HLH} complex was initiated by addition of AMPPNP (ATP in case of E798Q mutant). Protein was mixed to a final concentration of 20 mg/ml protein and 5 mM AMPPNP (or ATP) in dimerization buffer (5 mM Tris pH 7.8, 100 mM NaCl, 5 mM MgCl₂) and incubated at 8°C. Dimerization was monitored by analytical gel filtration after 1, 5, 24, and 72 h after reaction start. Maximal dimerization was usually achieved after 1–5 h and not longer than 24 h. For practical reasons, protein was always dimerized for 24 h prior to *in vitro* activity assays.

Saccharomyces cerevisiae plasmid repair assay

The yeast strain used in this experiment was W303-1A Δ rad50 transformed with empty pRS313 or pRS313 containing wild-type or mutated Rad50. Competent cells for yeast strains of the respective genotype were transformed with 5 μ g of either supercoiled pRS315-Kan or NcoI-linearized pRS315-Kan plasmids by the method of Gietz and Schiestl (2007). Transformation reactions were then plated as serial dilutions onto selective media, and colonies were counted after plates had been incubated for 3–4 days. The relative transformation recovery after plasmid cleavage has been calculated by dividing the number of obtained transformants with the linearized plasmid by the number of transformants with intact plasmids.

Accession codes

Coordinates and structure factors have been deposited in the Protein Data Bank under accession code 4W9M.

Supplementary information for this article is available online: <http://emboj.embopress.org>

Acknowledgements

We thank Robert Byrne for discussions and comments on the manuscript. We thank the staff of the Swiss Light Source (Villigen) and European Synchrotron Radiation Facility (Grenoble) for support with data collection and analysis. We

thank John Petrini for providing antibodies against *S. cerevisiae* Rad50, Steve Jackson and Katja Strässer for kind gifts of *S. cerevisiae* W303-1a Δ rad50 and strain W303-1a wild-type strains, respectively. We are grateful to Brigitte Keßler for technical support. This work was supported by the European Research Council Advanced Grant 'ATMMACHINE', the German Research Council (SFBs 684, 646 and GRK1721) and the excellence cluster Center for Integrated Protein Science Munich to K-PH. AR acknowledges support by the International Max-Planck-Research School Molecular and Cellular Life Sciences and an Boehringer Ingelheim PhD Fellowship.

Author contributions

AR purified and crystallized the protein–DNA complex, built the atomic model, performed biochemical and yeast *in vivo* experiments, and participated in paper writing. KL performed and supervised the structure determination, model building, yeast *in vivo* experiment and participated in writing the paper. FUS performed yeast *in vivo* experiments and participated in writing the paper. CD obtained initial crystals. HF performed the yeast telomere maintenance and plasmid repair assays. K-PH designed and supervised the research and wrote the paper.

Conflict of interest

The authors declare that they have no conflict of interest.

References

- Adams PD, Grosse-Kunstleve RW, Hung LW, Ioerger TR, McCoy AJ, Moriarty NW, Read RJ, Sacchettini JC, Sauter NK, Terwilliger TC (2002) PHENIX: building new software for automated crystallographic structure determination. *Acta Crystallogr D Biol Crystallogr* 58: 1948–1954
- Alt FW, Zhang Y, Meng FL, Guo C, Schwer B (2013) Mechanisms of programmed DNA lesions and genomic instability in the immune system. *Cell* 152: 417–429
- Bhaskara V, Dupre A, Lengsfeld B, Hopkins BB, Chan A, Lee JH, Zhang X, Gautier J, Zakian V, Paull TT (2007) Rad50 adenylate kinase activity regulates DNA tethering by Mre11/Rad50 complexes. *Mol Cell* 25: 647–661
- Bonetti D, Clerici M, Manfrini N, Lucchini G, Longhese MP (2010) The MRX complex plays multiple functions in resection of Yku- and Rif2-protected DNA ends. *PLoS One* 5: e14142
- Bressan DA, Baxter BK, Petrini JH (1999) The Mre11–Rad50–Xrs2 protein complex facilitates homologous recombination-based double-strand break repair in *Saccharomyces cerevisiae*. *Mol Cell Biol* 19: 7681–7687
- Carney JP, Maser RS, Olivares H, Davis EM, Le Beau M, Yates JR 3rd, Hays L, Morgan WF, Petrini JH (1998) The hMre11/hRad50 protein complex and Nijmegen breakage syndrome: linkage of double-strand break repair to the cellular DNA damage response. *Cell* 93: 477–486
- Cejka P, Cannavo E, Polaczek P, Masuda-Sasa T, Pokharel S, Campbell JL, Kowalczykowski SC (2010) DNA end resection by Dna2–Sgs1–RPA and its stimulation by Top3–Rmi1 and Mre11–Rad50–Xrs2. *Nature* 467: 112–116
- Chen C, Kolodner RD (1999) Gross chromosomal rearrangements in *Saccharomyces cerevisiae* replication and recombination defective mutants. *Nat Genet* 23: 81–85
- Chen L, Trujillo K, Ramos W, Sung P, Tomkinson AE (2001) Promotion of Dnl4-catalyzed DNA end-joining by the Rad50/Mre11/Xrs2 and Hdf1/Hdf2 complexes. *Mol Cell* 8: 1105–1115
- Connelly JC, de Leau ES, Leach DR (2003) Nucleolytic processing of a protein-bound DNA end by the *E. coli* SbcCD (MR) complex. *DNA Repair (Amst)* 2: 795–807

- Costanzo V, Robertson K, Bibikova M, Kim E, Grieco D, Gottesman M, Carroll D, Gautier J (2001) Mre11 protein complex prevents double-strand break accumulation during chromosomal DNA replication. *Mol Cell* 8: 137–147
- D'Amours D, Jackson SP (2001) The yeast Xrs2 complex functions in S phase checkpoint regulation. *Genes Dev* 15: 2238–2249
- Darmon E, Eykelboom JK, Lincker F, Jones LH, White M, Okely E, Blackwood JK, Leach DR (2010) *E. coli* SbcCD and RecA control chromosomal rearrangement induced by an interrupted palindrome. *Mol Cell* 39: 59–70
- Deshpande RA, Williams GJ, Limbo O, Williams RS, Kuhnlein J, Lee JH, Classen S, Guenther G, Russell P, Tainer JA, Paull TT (2014) ATP-driven Rad50 conformations regulate DNA tethering, end resection, and ATM checkpoint signaling. *EMBO J* 33: 482–500
- Dolganov GM, Maser RS, Novikov A, Tosto L, Chong S, Bressan DA, Petrini JH (1996) Human Rad50 is physically associated with human Mre11: identification of a conserved multiprotein complex implicated in recombinational DNA repair. *Mol Cell Biol* 16: 4832–4841
- Emsley P, Cowtan K (2004) Coot: model-building tools for molecular graphics. *Acta Crystallogr D Biol Crystallogr* 60: 2126–2132
- Garcia V, Phelps SEL, Gray S, Neale MJ (2011) Bidirectional resection of DNA double-strand breaks by Mre11 and Exo1. *Nature* 479: 241–244
- Gietz RD, Schiestl RH (2007) High-efficiency yeast transformation using the LiAc/SS carrier DNA/PEG method. *Nature protocols* 2: 31–34
- Haber JE (2012) Mating-type genes and MAT switching in *Saccharomyces cerevisiae*. *Genetics* 191: 33–64
- Harper JW, Elledge SJ (2007) The DNA damage response: ten years after. *Mol Cell* 28: 739–745
- Hector RE, Shtofman RL, Ray A, Chen BR, Nyun T, Berkner KL, Runge KW (2007) Tel1p preferentially associates with short telomeres to stimulate their elongation. *Mol Cell* 27: 851–858
- Herdendorf TJ, Albrecht DW, Benkovic SJ, Nelson SW (2011) Biochemical characterization of bacteriophage T4 Mre11–Rad50 complex. *J Biol Chem* 286: 2382–2392
- Hirano T (2006) At the heart of the chromosome: SMC proteins in action. *Nat Rev Mol Cell Biol* 7: 311–322
- Hopfner KP, Craig L, Moncalian G, Zinkel RA, Usui T, Owen BA, Karcher A, Henderson B, Bodmer JL, McMurray CT, Carney JP, Petrini JH, Tainer JA (2002) The Rad50 zinc-hook is a structure joining Mre11 complexes in DNA recombination and repair. *Nature* 418: 562–566
- Hopfner KP, Karcher A, Craig L, Woo TT, Carney JP, Tainer JA (2001) Structural biochemistry and interaction architecture of the DNA double-strand break repair Mre11 nuclease and Rad50-ATPase. *Cell* 105: 473–485
- Hopfner KP, Karcher A, Shin DS, Craig L, Arthur LM, Carney JP, Tainer JA (2000) Structural biology of Rad50 ATPase: ATP-driven conformational control in DNA double-strand break repair and the ABC-ATPase superfamily. *Cell* 101: 789–800
- Hopfner KP, Tainer JA (2003) Rad50/SMC proteins and ABC transporters: unifying concepts from high-resolution structures. *Curr Opin Struct Biol* 13: 249–255
- Hopkins BB, Paull TT (2008) The *P. furiosus* mre11/rad50 complex promotes 5' strand resection at a DNA double-strand break. *Cell* 135: 250–260
- Jackson SP, Bartek J (2009) The DNA-damage response in human biology and disease. *Nature* 461: 1071–1078
- de Jager M, van Noort J, van Gent DC, Dekker C, Kanaar R, Wyman C (2001) Human Rad50/Mre11 is a flexible complex that can tether DNA ends. *Mol Cell* 8: 1129–1135
- de Jager M, Wyman C, van Gent DC, Kanaar R (2002) DNA end-binding specificity of human Rad50/Mre11 is influenced by ATP. *Nucleic Acids Res* 30: 4425–4431
- Kabsch W (1993) Automatic processing of rotation diffraction data from crystals of initially unknown symmetry and cell constants. *J Appl Crystallogr* 26: 795–800
- Koroleva O, Makharashvili N, Courcelle CT, Courcelle J, Korolev S (2007) Structural conservation of RecF and Rad50: implications for DNA recognition and RecF function. *EMBO J* 26: 867–877
- Lammens A, Schele A, Hopfner KP (2004) Structural biochemistry of ATP-driven dimerization and DNA-stimulated activation of SMC ATPases. *Curr Biol* 14: 1778–1782
- Lammens K, Bemeleit DJ, Mockel C, Clausen E, Schele A, Hartung S, Schiller CB, Lucas M, Angermuller C, Soding J, Strasser K, Hopfner KP (2011) The Mre11:Rad50 structure shows an ATP-dependent molecular clamp in DNA double-strand break repair. *Cell* 145: 54–66
- Langerak P, Mejia-Ramirez E, Limbo O, Russell P (2011) Release of Ku and MRN from DNA ends by Mre11 nuclease activity and Ctp1 is required for homologous recombination repair of double-strand breaks. *PLoS Genet* 7: e1002271
- Lee JH, Mand MR, Deshpande RA, Kinoshita E, Yang SH, Wyman C, Paull TT (2013) Ataxia telangiectasia-mutated (ATM) kinase activity is regulated by ATP-driven conformational changes in the Mre11/Rad50/Nbs1 (MRN) complex. *J Biol Chem* 288: 12840–12851
- Lee JH, Paull TT (2005) ATM activation by DNA double-strand breaks through the Mre11–Rad50–Nbs1 complex. *Science* 308: 551–554
- Lee K, Zhang Y, Lee SE (2008) *Saccharomyces cerevisiae* ATM orthologue suppresses break-induced chromosome translocations. *Nature* 454: 543–546
- Lim HS, Kim JS, Park YB, Gwon GH, Cho Y (2011) Crystal structure of the Mre11–Rad50–ATPγS complex: understanding the interplay between Mre11 and Rad50. *Genes Dev* 25: 1091–1104
- Longhese MP, Bonetti D, Guerini I, Manfrini N, Clerici M (2009) DNA double-strand breaks in meiosis: checking their formation, processing and repair. *DNA Repair (Amst)* 8: 1127–1138
- Lovell SC, Davis IW, Arendall WB 3rd, de Bakker PI, Word JM, Prisant MG, Richardson JS, Richardson DC (2003) Structure validation by Calpha geometry: phi, psi and Cbeta deviation. *Proteins* 50: 437–450
- Majka J, Alford B, Ausio J, Finn RM, McMurray CT (2012) ATP hydrolysis by RAD50 protein switches MRE11 enzyme from endonuclease to exonuclease. *J Biol Chem* 287: 2328–2341
- McCoy AJ, Grosse-Kunstleve RW, Adams PD, Winn MD, Storoni LC, Read RJ (2007) Phaser crystallographic software. *J Appl Crystallogr* 40: 658–674
- Mimitou EP, Symington LS (2008) Sae2, Exo1 and Sgs1 collaborate in DNA double-strand break processing. *Nature* 455: 770–774
- Mimitou EP, Symington LS (2010) Ku prevents Exo1 and Sgs1-dependent resection of DNA ends in the absence of a functional MRX complex or Sae2. *EMBO J* 29: 3358–3369
- Mockel C, Lammens K, Schele A, Hopfner KP (2012) ATP driven structural changes of the bacterial Mre11:Rad50 catalytic head complex. *Nucleic Acids Res* 40: 914–927
- Moncalian G, Lengsfeld B, Bhaskara V, Hopfner KP, Karcher A, Alden E, Tainer JA, Paull TT (2004) The rad50 signature motif: essential to ATP binding and biological function. *J Mol Biol* 335: 937–951
- Moore JK, Haber JE (1996) Cell cycle and genetic requirements of two pathways of nonhomologous end-joining repair of double-strand breaks in *Saccharomyces cerevisiae*. *Mol Cell Biol* 16: 2164–2173
- Moreau S, Ferguson JR, Symington LS (1999) The nuclease activity of Mre11 is required for meiosis but not for mating type switching, end joining, or telomere maintenance. *Mol Cell Biol* 19: 556–566

- Moreno-Herrero F, de Jager M, Dekker NH, Kanaar R, Wyman C, Dekker C (2005) Mesoscale conformational changes in the DNA-repair complex Rad50/Mre11/Nbs1 upon binding DNA. *Nature* 437: 440–443
- Neale MJ, Pan J, Keeney S (2005) Endonucleolytic processing of covalent protein-linked DNA double-strand breaks. *Nature* 436: 1053–1057
- Petrini JH (2000) The Mre11 complex and ATM: collaborating to navigate S phase. *Curr Opin Cell Biol* 12: 293–296
- Raymond WE, Kleckner N (1993) RAD50 protein of *S. cerevisiae* exhibits ATP-dependent DNA binding. *Nucleic Acids Res* 21: 3851–3856
- Reis CC, Batista S, Ferreira MG (2012) The fission yeast MRN complex tethers dysfunctional telomeres for NHEJ repair. *EMBO J* 31: 4576–4586
- Rolef Ben-Shahar T, Heeger S, Lehane C, East P, Flynn H, Skehel M, Uhlmann F (2008) Eco1-dependent cohesin acetylation during establishment of sister chromatid cohesion. *Science* 321: 563–566
- Roset R, Inagaki A, Hohl M, Brenet F, Lafrance-Vanasse J, Lange J, Scandura JM, Tainer JA, Keeney S, Petrini JH (2014) The Rad50 hook domain regulates DNA damage signaling and tumorigenesis. *Genes Dev* 28: 451–462
- Rothkamm K, Lobrich M (2002) Misrepair of radiation-induced DNA double-strand breaks and its relevance for tumorigenesis and cancer treatment (review). *Int J Oncol* 21: 433–440
- Schiller CB, Lammens K, Guerini I, Cordes B, Feldmann H, Schlauderer F, Mockel C, Schele A, Strasser K, Jackson SP, Hopfner KP (2012) Structure of Mre11–Nbs1 complex yields insights into ataxia-telangiectasia-like disease mutations and DNA damage signaling. *Nat Struct Mol Biol* 19: 693–700
- Schiller CB, Seifert FU, Linke-Winnebeck C, Hopfner KP (2014) Structural studies of DNA end detection and resection in homologous recombination. *Cold Spring Harb Perspect Biol* 6: a017962
- Shibata A, Moiani D, Arvai AS, Perry J, Harding SM, Genois MM, Maity R, Van Rossum-Fikkert S, Kertokallio A, Romoli F, Ismail A, Ismalaj E, Petricci E, Neale MJ, Bristow RG, Masson JY, Wyman C, Jeggo PA, Tainer JA (2013) DNA double-strand break repair pathway choice is directed by distinct MRE11 nuclease activities. *Mol Cell* 53: 7–18
- Stracker TH, Petrini JH (2011) The MRE11 complex: starting from the ends. *Nat Rev Mol Cell Biol* 12: 90–103
- Stracker TH, Roig I, Knobel PA, Marjanovic M (2013) The ATM signaling network in development and disease. *Front Genet* 4: 37
- Sun J, Lee KJ, Davis AJ, Chen DJ (2012) Human Ku70/80 protein blocks exonuclease 1-mediated DNA resection in the presence of human Mre11 or Mre11/Rad50 protein complex. *J Biol Chem* 287: 4936–4945
- Tsukamoto Y, Taggart AK, Zakian VA (2001) The role of the Mre11–Rad50–Xrs2 complex in telomerase-mediated lengthening of *Saccharomyces cerevisiae* telomeres. *Curr Biol* 11: 1328–1335
- Unal E, Heidinger-Pauli JM, Kim W, Guacci V, Onn I, Gygi SP, Koshland DE (2008) A molecular determinant for the establishment of sister chromatid cohesion. *Science* 321: 566–569
- Usui T, Ogawa H, Petrini JH (2001) A DNA damage response pathway controlled by Tel1 and the Mre11 complex. *Mol Cell* 7: 1255–1266
- Varon R, Vissinga C, Platzer M, Cerosaletti KM, Chrzanowska KH, Saar K, Beckmann G, Seemanova E, Cooper PR, Nowak NJ, Stumm M, Weemaes CM, Gatti RA, Wilson RK, Digweed M, Rosenthal A, Sperling K, Concannon P, Reis A (1998) Nibrin, a novel DNA double-strand break repair protein, is mutated in Nijmegen breakage syndrome. *Cell* 93: 467–476
- Wasko BM, Holland CL, Resnick MA, Lewis LK (2009) Inhibition of DNA double-strand break repair by the Ku heterodimer in mrx mutants of *Saccharomyces cerevisiae*. *DNA Repair (Amst)* 8: 162–169
- Williams GJ, Williams RS, Williams JS, Moncalian G, Arvai AS, Limbo O, Guenther G, SilDas S, Hammel M, Russell P, Tainer JA (2011) ABC ATPase signature helices in Rad50 link nucleotide state to Mre11 interface for DNA repair. *Nat Struct Mol Biol* 18: 423–431
- Williams RS, Dodson GE, Limbo O, Yamada Y, Williams JS, Guenther G, Classen S, Glover JN, Iwasaki H, Russell P, Tainer JA (2009) Nbs1 flexibly tethers Ctp1 and Mre11–Rad50 to coordinate DNA double-strand break processing and repair. *Cell* 139: 87–99
- Williams RS, Moncalian G, Williams JS, Yamada Y, Limbo O, Shin DS, Grocock LM, Cahill D, Hitomi C, Guenther G, Moiani D, Carney JP, Russell P, Tainer JA (2008) Mre11 dimers coordinate DNA end bridging and nuclease processing in double-strand-break repair. *Cell* 135: 97–109
- Williams RS, Williams JS, Tainer JA (2007) Mre11–Rad50–Nbs1 is a keystone complex connecting DNA repair machinery, double-strand break signaling, and the chromatin template. *Biochem Cell Biol* 85: 509–520
- Wilson S, Warr N, Taylor DL, Watts FZ (1999) The role of *Schizosaccharomyces pombe* Rad32, the Mre11 homologue, and other DNA damage response proteins in non-homologous end joining and telomere length maintenance. *Nucleic Acids Res* 27: 2655–2661
- Xie A, Kwok A, Scully R (2009) Role of mammalian Mre11 in classical and alternative nonhomologous end joining. *Nat Struct Mol Biol* 16: 814–818
- Yaffe MP, Schatz G (1984) Two nuclear mutations that block mitochondrial protein import in yeast. *Proc Natl Acad Sci USA* 81: 4819–4823
- Yamaguchi-Iwai Y, Sonoda E, Sasaki MS, Morrison C, Haraguchi T, Hiraoka Y, Yamashita YM, Yagi T, Takata M, Price C, Kakazu N, Takeda S (1999) Mre11 is essential for the maintenance of chromosomal DNA in vertebrate cells. *EMBO J* 18: 6619–6629
- Zhu Z, Chung WH, Shim EY, Lee SE, Ira G (2008) Sgs1 helicase and two nucleases Dna2 and Exo1 resect DNA double-strand break ends. *Cell* 134: 981–994

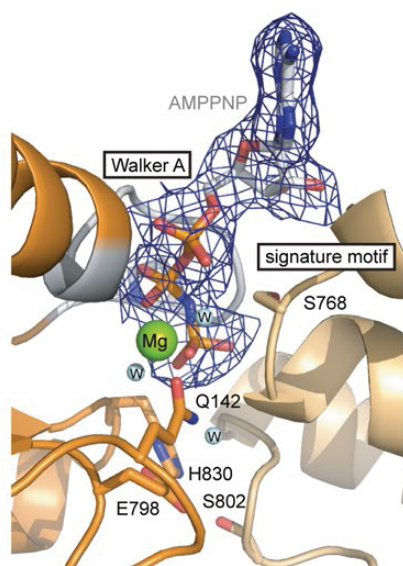
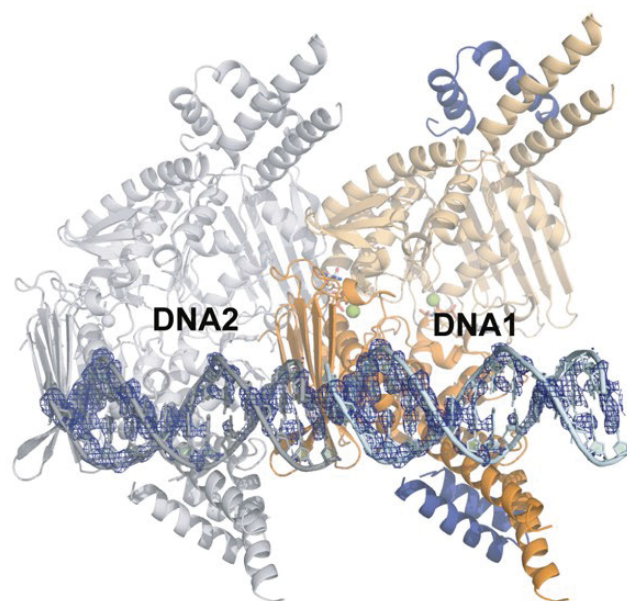
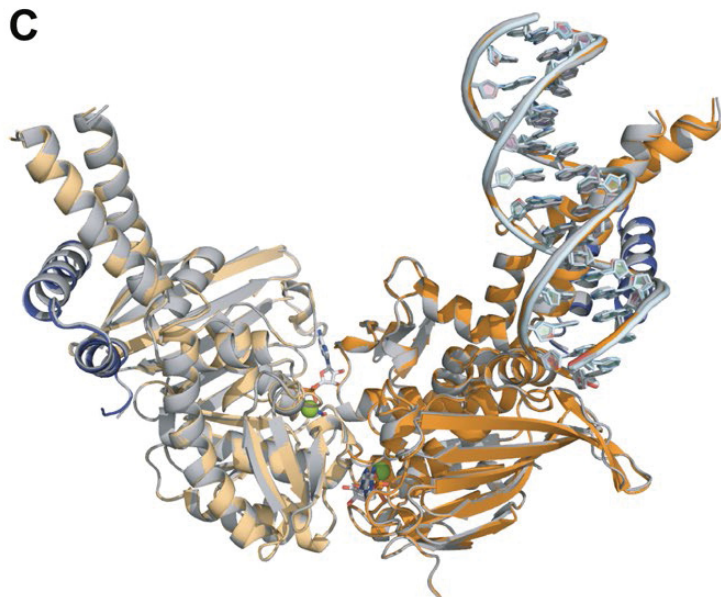
Supplementary Table S1 Data collection and refinement statistics (**Molecular replacement**)

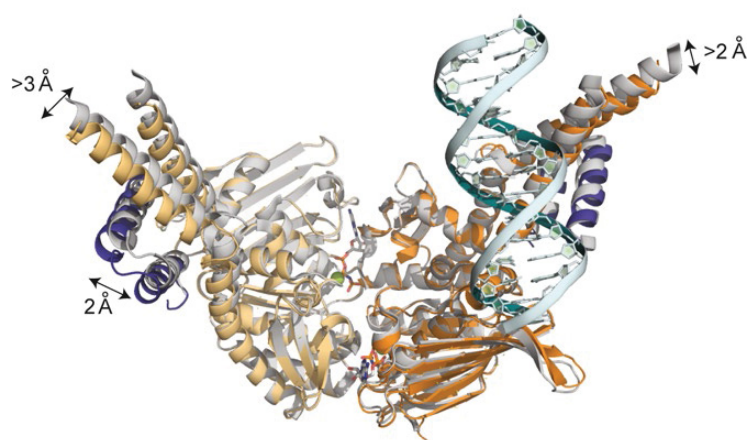
tmRad50 ^{NBD} -Mre11 ^{HLH}	
Data collection	
Space group	P1
Cell dimensions	
<i>a</i> , <i>b</i> , <i>c</i> (Å)	50.2, 107.6, 97.1
α , β , γ (°)	90.6, 98.3, 89.4
Resolution (Å)	50.2-2.7
<i>R</i> _{sym} or <i>R</i> _{merge}	13.5 (68.6)*
<i>I</i> / σ <i>I</i>	9.3(1.9)
Completeness (%)	93.8(80.5)
Redundancy	3.4(3.1)
Refinement	
Resolution (Å)	47.7-2.7
No. reflections	51439
<i>R</i> _{work} / <i>R</i> _{free}	21.5/27.0
No. atoms	14169
Protein	12556
DNA/AMPPNP/Mg ²⁺	1218/124/4
Water	267
B-factors	43.4 (overall)
Protein	35.1
DNA/AMPPNP/Mg ²⁺	146.1/19.3/14.9
Water	30.8
R.m.s deviations	
Bond lengths (Å)	0.010
Bond angles (°)	1.3

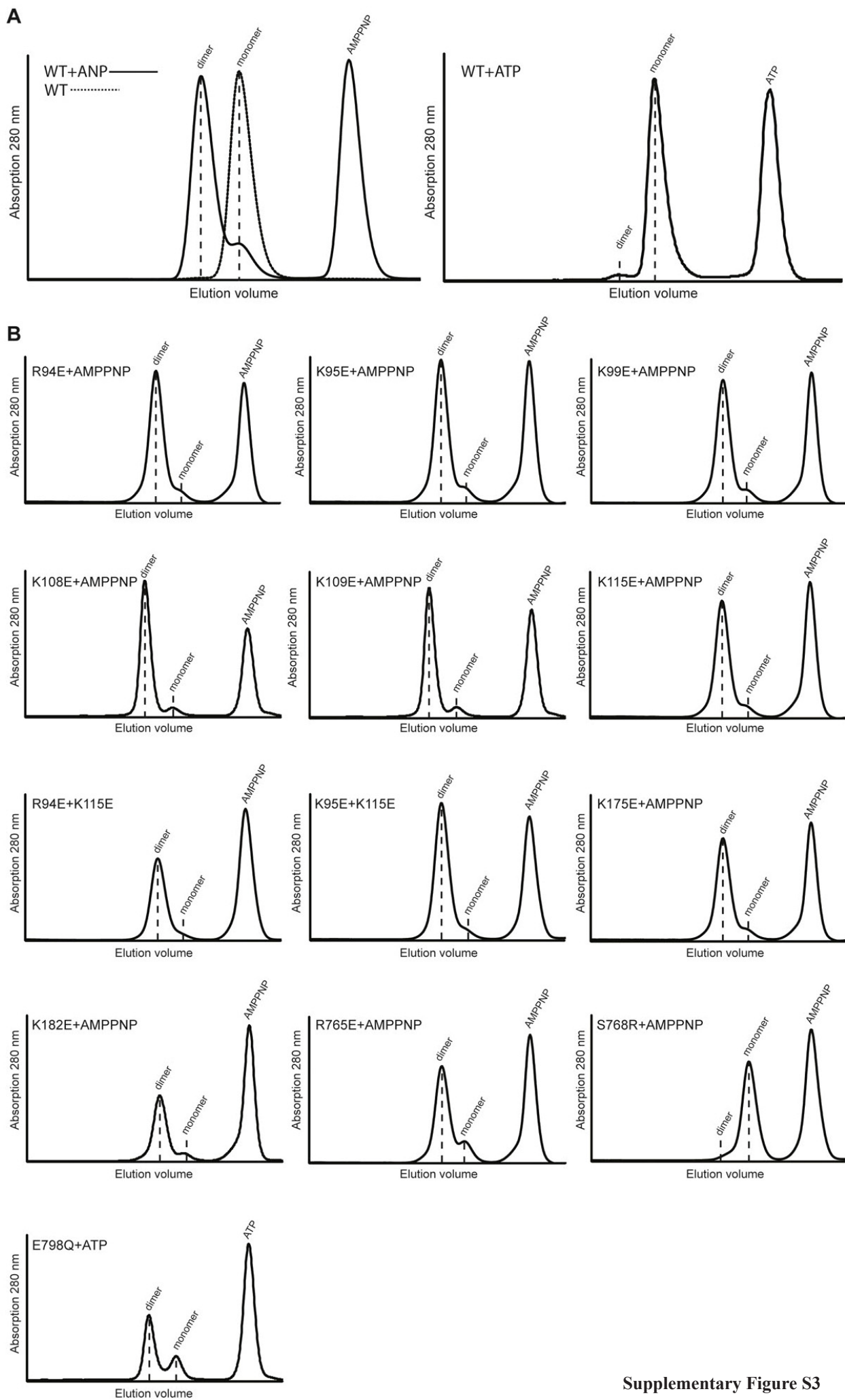
*Highest resolution shells (2.8- 2.7 Å) are shown in parenthesis.

Ramachandran statistics

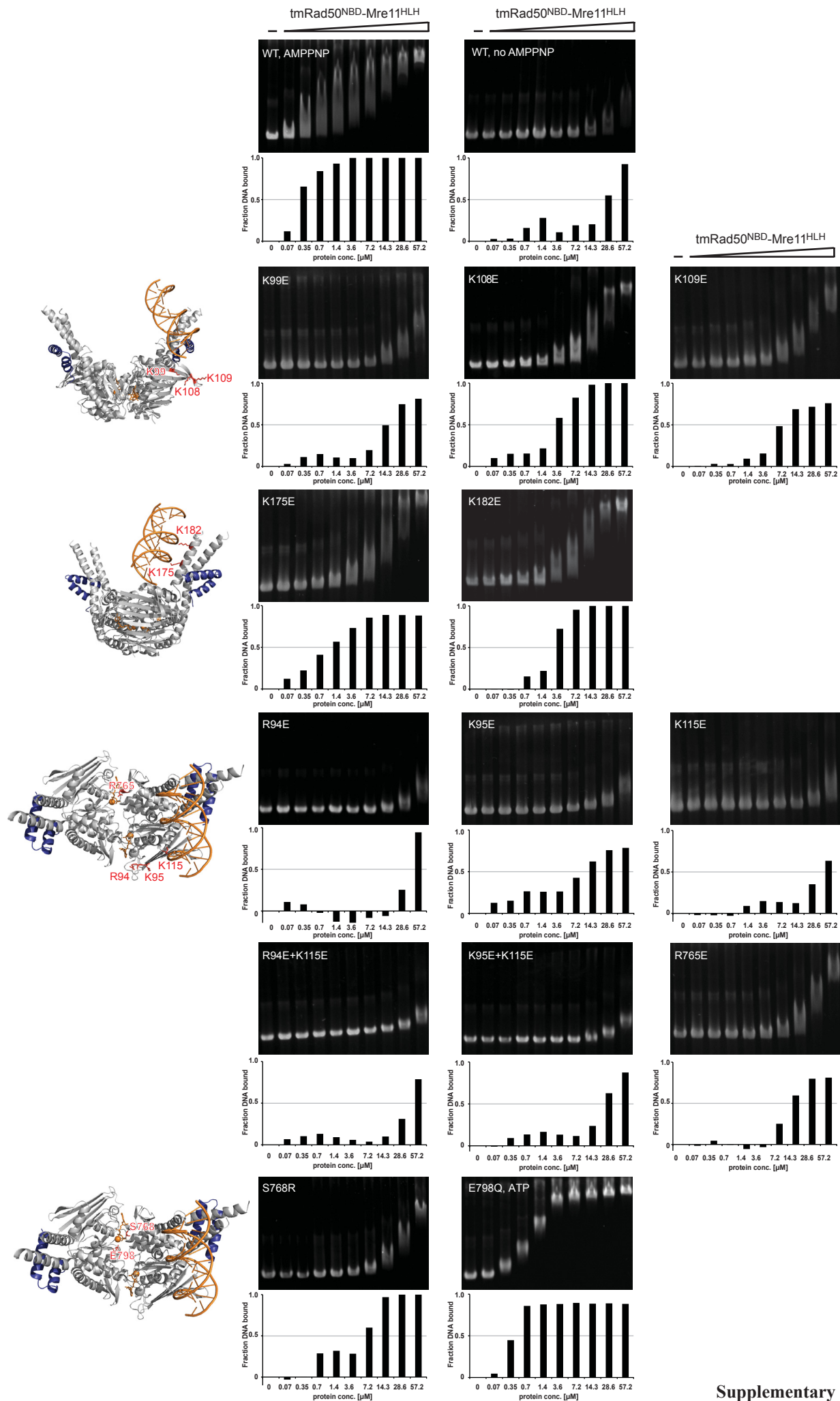
outliers (%): 0.5
allowed (%): 5.0
favoured (%): 94.5

A**B****C**

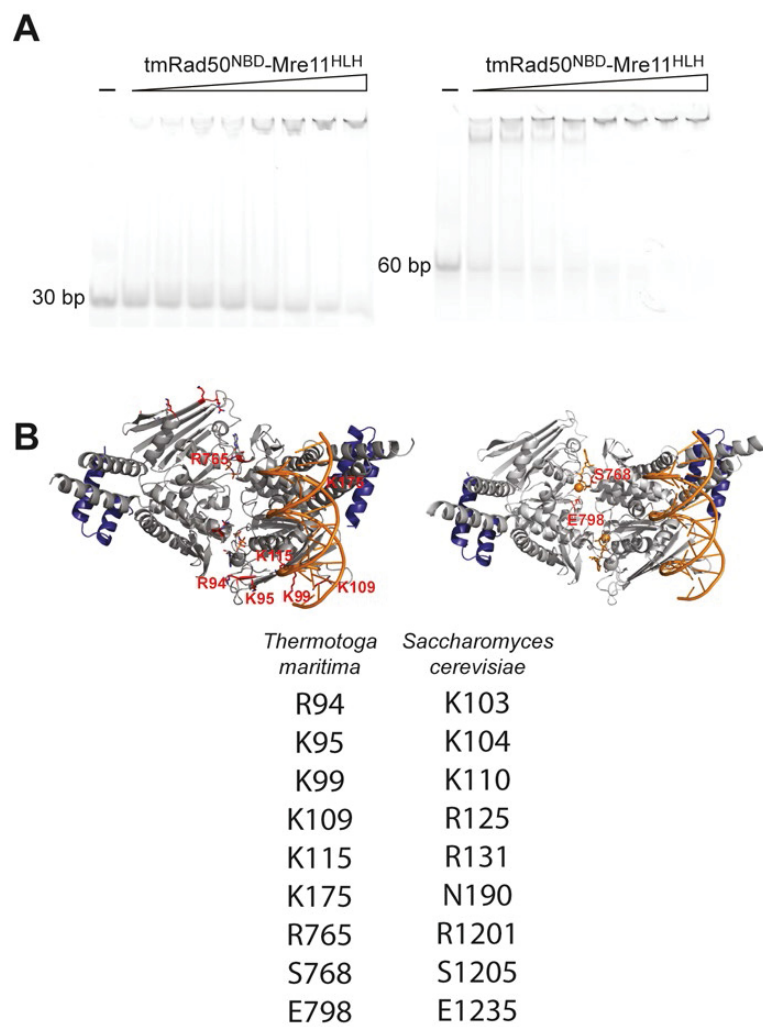


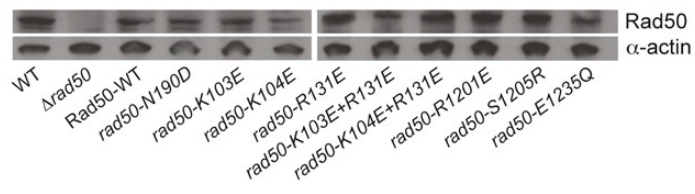
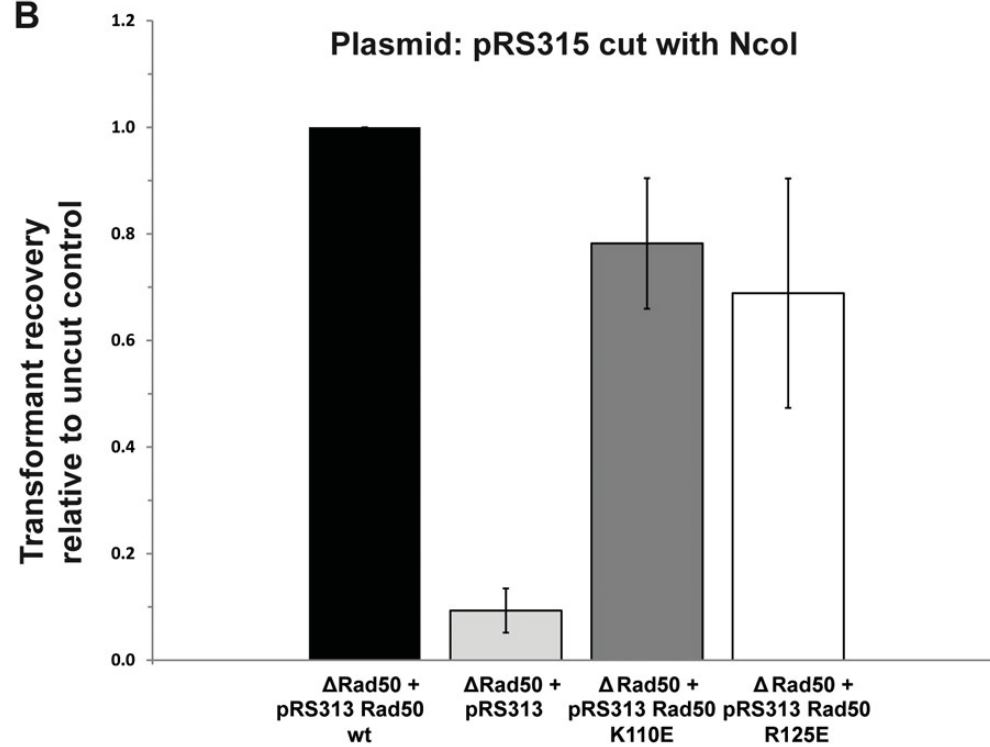


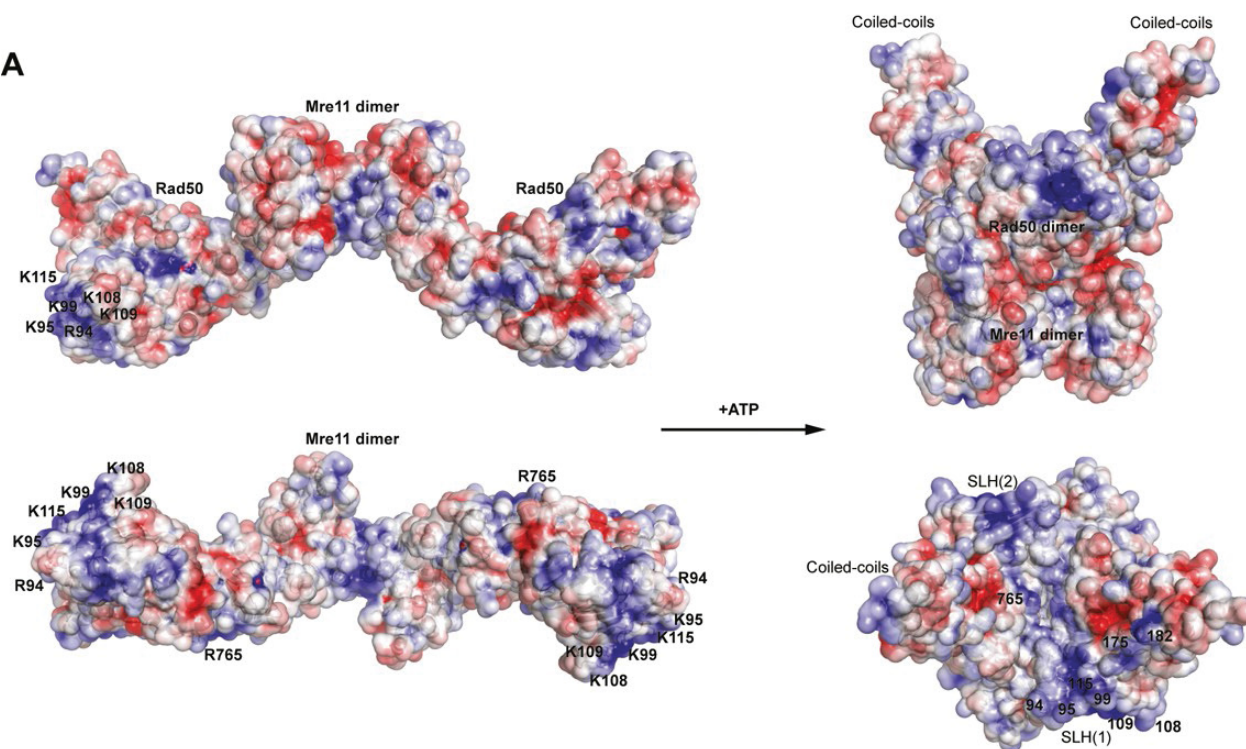
Supplementary Figure S3



Supplementary Figure S4



A**B**

A

Supplementary Legends:

Figure S1. A: Close up view of AMPPNP and Mg^{2+} coordination within the Rad50 ATPase active site. AMPPNP is marked as color coded sticks; the final $2F_o-F_c$ density around AMPPNP is contoured at 1.0σ and colored in dark blue. Walker A and signature motifs coordinate the phosphate moieties in the AMPPNP molecule. Mg^{2+} is coordinated by two water molecules, oxygen of phosphate moieties in AMPPNP and side chains of the Walker A motif and Q-loop (Q142).

B: Depicted are two adjacent symmetry related molecules indicating the quasi-continuous DNA double strand in the crystal lattice. The final $2F_o-F_c$ density around DNA is contoured at 0.8σ and marked in dark blue.

Figure S2. Structural comparison of the tmRad50^{NBD}-Mre11^{HLH} apo (PDB code: 3QF7) and DNA-bound structures. Both models show almost identical architecture. The most pronounced repositioning is visible at the coil-coil domains and the HLH motifs.

Figure S3. AMPPNP-induced tmRad50^{NBD}-Mre11^{HLH} dimerization.

A Left panel: wild-type tmRad50^{NBD}-Mre11^{HLH} complex remains in a monomeric form in the absence of AMPPNP and Mg^{2+} (dotted line) and forms a stable dimer upon AMPPNP addition (solid line); A right panel: ATP fails to form a stable tmRad50^{NBD}-Mre11^{HLH} dimer.

B: Point mutations do not impair tmRad50^{NBD}-Mre11^{HLH} dimerization and dimer stability except from the signature motif mutant S768R.

Figure S4: Quantitation (bar graphs) of the residual unbound DNA for different tmRad50^{NBD}-Mre11^{HLH} mutants (see Fig. 3). The estimated half-maximal value is depicted in Fig. 3 to assess the approximate binding strength of different mutant proteins.

Figure S5. A: DNA binding activity of the wild-type tmRad50^{NBD}-Mre11^{HLH} complex with 30mer or 60mer dsDNA. Binding efficiency is significantly increased with the longer DNA species.

B: Table of mutations analysed in yeast *in vivo* assays and the corresponding residue in *Thermotoga maritima* shown together with the position of the relevant residues in the tmRad50 DNA structure.

Figure S6. A Rad50 expression levels in *S. cerevisiae* Rad50 mutants. Western blot analysis performed on yeast lysate show comparable levels of Rad50 in wild-type and mutated *S. cerevisiae*.

B: In vivo plasmid repair assay of the yeast mutant strains Rad50 K110E, R125E and Δ Rad50. Whereas the Δ Rad50 strain lead to dramatically reduced transformant yields for NcoI-linearized pRS315-Kan plasmids, the Rad50 point mutants showed only minor changes in plasmid rescue efficiency which are negligible considering the standard error of the experiment. For this experiment competent cells for yeast strains of the indicated genotype were transformed with either supercoiled pRS315-Kan or NcoI linearized pRS315-Kan plasmids. For each strain the value plotted is the number of transformants obtained with NcoI linearized vector relative to the number obtained with supercoiled vector. Thereby the number of transformants obtained with the Δ Rad50 strain rescued with the pRS313 Rad50 wild type plasmid has been normalized to 1.

2.4 Structural Studies of DNA End Detection and Resection in Homologous Recombination



Cold Spring Harbor Perspectives in Biology

Structural Studies of DNA End Detection and Resection in Homologous Recombination

Christian Bernd Schiller, Florian Ulrich Seifert, Christian Linke-Winnebeck and Karl-Peter Hopfner

Cold Spring Harb Perspect Biol published online July 31, 2014

Subject Collection [DNA Recombination](#)

The Role of Double-Strand Break Repair Pathways at Functional and Dysfunctional Telomeres

Ylli Doksanli and Titia de Lange

Regulation of DNA Pairing in Homologous Recombination

James M. Daley, William A. Gaines, YoungHo Kwon, et al.

Mechanism and Regulation of Meiotic Recombination Initiation

Isabel Lam and Scott Keeney

The Meiotic Checkpoint Network: Step-by-Step through Meiotic Prophase

Vijayalakshmi V. Subramanian and Andreas Hochwagen

Holliday Junction Resolvases

Haley D.M. Wyatt and Stephen C. West

End Resection at Double-Strand Breaks: Mechanism and Regulation

Lorraine S. Symington

Mediators of Homologous DNA Pairing

Alex Zelensky, Roland Kanaar and Claire Wyman

Recombination and Replication

Aisha H. Syeda, Michelle Hawkins and Peter McGlynn

Structural Studies of DNA End Detection and Resection in Homologous Recombination

Christian Bernd Schiller, Florian Ulrich Seifert, Christian Linke-Winnebeck, et al.

Sources of DNA Double-Strand Breaks and Models of Recombinational DNA Repair

Anuja Mehta and James E. Haber

Transcription and Recombination: When RNA Meets DNA

Andrés Aguilera and Hélène Gaillard

The Dissolution of Double Holliday Junctions

Anna H. Bizard and Ian D. Hickson

For additional articles in this collection, see <http://cshperspectives.cshlp.org/cgi/collection/>

Structural Studies of DNA End Detection and Resection in Homologous Recombination

Christian Bernd Schiller^{1,3}, Florian Ulrich Seifert^{1,3}, Christian Linke-Winnebeck^{1,3}, and Karl-Peter Hopfner^{1,2}

¹Department of Biochemistry and Gene Center, Ludwig-Maximilians-University, 81377 Munich, Germany

²Center for Integrated Protein Sciences, 81377 Munich, Germany

Correspondence: hopfner@genzentrum.lmu.de

DNA double-strand breaks are repaired by two major pathways, homologous recombination or nonhomologous end joining. The commitment to one or the other pathway proceeds via different steps of resection of the DNA ends, which is controlled and executed by a set of DNA double-strand break sensors, endo- and exonucleases, helicases, and DNA damage response factors. The molecular choreography of the underlying protein machinery is beginning to emerge. In this review, we discuss the early steps of genetic recombination and double-strand break sensing with an emphasis on structural and molecular studies.

All domains of life maintain genomes and ensure genetic diversity through homologous recombination (HR) or homology directed repair. HR is initiated by single unprotected DNA ends, which arise at collapsed replication forks and unprotected telomeres, or by DNA double-strand breaks (DSBs), which are products of ionizing radiation, reactive oxygen species, genotoxic chemicals, or abortive topoisomerase reactions (Sutherland et al. 2000; Aguilera and Gomez-Gonzalez 2008; Cadet et al. 2012; Mehta and Haber 2014). In special cellular states, programmed DSBs are introduced by endonucleases to initiate the generation of genetic variability by processes such as meiotic recombination of homologous chromosomes (Lam and Keeney 2014; Zickler and Kleckner 2014), V(D)J and class switch recombination

to generate antibody diversity and yeast-mating-type switching (Gapud and Sleckman 2011; Haber 2012; Xu et al. 2012b). Failure to repair DSBs can lead to cell death or gross chromosomal aberrations, which in humans are a hallmark of cancer (Myung et al. 2001a,b; Hanahan and Weinberg 2011).

Beside HR, DSBs can also be repaired by nonhomologous end joining (NHEJ). Although HR requires a template such as a sister chromatid or a homologous chromosome and is limited to S and G₂ phases of the cell cycle, NHEJ is template-independent and can occur in all cell cycle states. Indeed, the choice of pathways is to a significant extent not stochastic but a function of the cell cycle (Ferretti et al. 2013), with NHEJ being the predominant pathway in mammals outside of S phase. NHEJ is basically a

³These authors contributed equally to this work.

Editors: Stephen Kowalczykowski, Neil Hunter, and Wolf-Dietrich Heyer

Additional Perspectives on DNA Recombination available at www.cshperspectives.org

Copyright © 2014 Cold Spring Harbor Laboratory Press; all rights reserved

Advanced Online Article. Cite this article as *Cold Spring Harb Perspect Biol* doi: 10.1101/cshperspect.a017962

C.B. Schiller et al.

ligation reaction of two DNA ends that are only minimally processed. Derivatives of NHEJ such as microhomology-mediated end joining (MMEJ) or alternative NHEJ (alt-NHEJ) require more substantial processing and may lead to the loss of genetic information. For recent reviews of NHEJ, which is not covered in detail here, please refer to, for example, Thompson (2012) and Chiruvella et al. (2013).

HR has multiple steps and requires extensive processing of DNA ends (Symington 2014). First, the free DNA ends are recognized by DSB sensors, followed by 5'-3' resection of the DNA ends. In eukaryotes and archaea, this step may be divided into initial short-range resection, after which MMEJ/alt-NHEJ can still occur, followed by processive long-range resection that commits the pathway to HR. The 3' single-stranded DNA (ssDNA) filament, bound by the DNA strand exchange protein RecA/Rad51, pairs with the homologous sequence on the template and thus forms a D-loop. The 3' tail serves as a primer for a repair polymerase and is extended by using the homologous strand as template, a process that "restores" the disrupted genetic information. Various pathways involve the displacement of the free strand, the capture of the second strand to form Holliday junctions, or the cleavage of the D-loop (Mehta and Haber 2014).

In this review, we focus on structural aspects of the early steps in homologous recombination. Of particular interest is the Mre11-Rad50-Nbs1 (MRN) complex, which recognizes DSBs, performs initial resection, and sets off a DNA damage response (DDR) signaling network. We further discuss the nucleases and helicases that are involved in long-range resection. Recent reviews of later steps in HR, which are not covered here, have been published elsewhere (Amunugama and Fishel 2012; Chiruvella et al. 2013; Jasin and Rothstein 2013).

DSB END RECOGNITION

The Mre11-Rad50-Nbs1 Complex

Among the early and central players in DNA end metabolism are Ku and the Mre11-Rad50-Nbs1 (MRN) complex, which are considered

"sensors" for DSBs. Ku binds to DNA ends as a ring-shaped heterodimer (Fig. 1) consisting of Ku70/Ku80 and initiates NHEJ (Walker et al. 2001; Chiruvella et al. 2013). The *Saccharomyces cerevisiae* MRN homolog, Mre11-Rad50-Xrs2 (MRX), has been shown to be one of the first complexes that are recruited to DSBs (Lisby et al. 2004). MRN is involved in the selection of DSB repair pathways that require end resection (HR, MMEJ, alt-NHEJ) as opposed to NHEJ (Truong et al. 2013). Homologs of Mre11 and Rad50 (MR) are present in all domains of life and may be fused into a single peptide chain (Yoshida et al. 2011).

MRN is a multifunctional ATP-regulated nuclease with endo- and exonuclease activity and long structural tails. In vitro, the MR(N) complex is able to partially melt and unwind DNA and displays both 3' to 5' exonuclease and ssDNA endonuclease activity to process DSBs (Connelly et al. 1997, 1999; Furuse et al. 1998; Paull and Gellert 1998; Trujillo et al. 1998; Hopfner et al. 2000a, 2001; Trujillo and Sung 2001; Lobachev et al. 2002; Hopkins and Paull 2008; Cannon et al. 2013). Bacteriophage T4 also possesses homologs of Mre11 and Rad50 (gp46/gp47), which play an essential role in initiation of recombination-dependent replication at later stages of infection (Kreuzer and Brister 2010; Almond et al. 2013). In bacteria, MR (denoted SbcCD) degrades hairpin structures in the wake of replication forks and protects the cell against inverted chromosome duplication together with RecA (Zahra et al. 2007; Eykelenboom et al. 2008; Darmon et al. 2010). In archaea, like in eukaryotes, MR(N) is recruited to and repairs DSBs that are induced using ionizing radiation or genotoxic agents and that arise at stalled replication forks (Costanzo et al. 2001; Neale et al. 2005; Trenz et al. 2006; Frols et al. 2007; Quaiser et al. 2008; Delmas et al. 2009, 2013). In eukaryotes, MRN also processes newly replicated telomeres and DSBs that are blocked by DNA hairpin structures or by proteins, such as Ku and the meiotic recombination factor Spo11 (Lobachev et al. 2002; Connelly et al. 2003; Neale et al. 2005; Bonetti et al. 2010; Mimitou and Symington 2010; Langerak et al. 2011).

Structural Mechanisms of Recombination

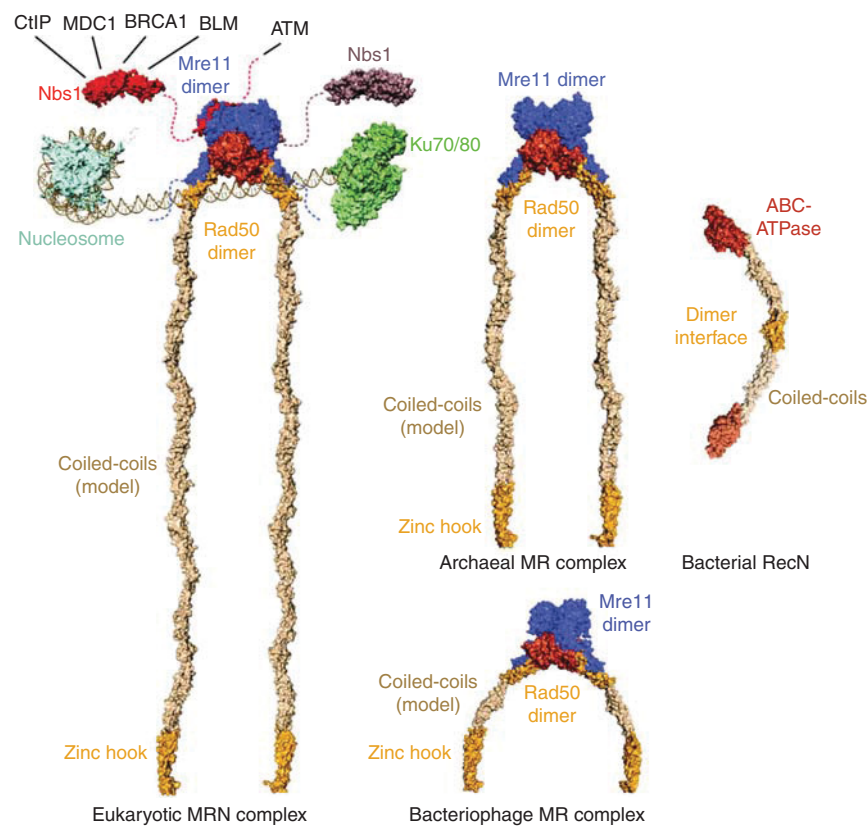


Figure 1. The Mre11-Rad50-Nbs1 complex and phylogenetic orthologs. Structural model of MR(N) complexes together with a nucleosome, the Ku-DNA complex and RecN. Nbs1 interaction partners are indicated. The eukaryotic MRN model was built from *Schizosaccharomyces pombe* MN and Nbs1 (PDB code 4FBW, Schiller et al. 2012), *Methanocaldococcus jannaschii* MR, *Pyrococcus furiosus* Zn-hook and a coiled-coil model. The archaeal model is based on the *M. jannaschii* MR structure and the *P. furiosus* Zn-hook. Bacteriophage MR is modeled on the *Thermotoga maritima* MR complex together with the *P. furiosus* Zn-hook and a coiled-coil model. PDB codes are 1AOI (nucleosome, Luger et al. 1997), 1JEY (Ku-DNA complex, Walker et al. 2001), 4AD8 and 4ABX (RecN, Pellegrino et al. 2012), 4FBW (MN complex, Schiller et al. 2012), 3HUE (Nbs1, Williams et al. 2009), 3AVO (MR complex, Lim et al. 2011), and 1L8D (Zn-hook, Hopfner et al. 2002).

How MR(N) functions as a DNA end sensor and processing factor is still poorly understood. Although Ku forms a ring structure with DSB-binding affinity in the nanomolar range (Fig. 1) (Blier et al. 1993; Walker et al. 2001), readily explaining how it acts as a DSB sensor, we have not yet arrived at a model that explains the mechanism of DSB detection by MR(N). Many bulk biochemistry experiments on MRN or MR homologs show a relatively moderate DNA-binding affinity in the high nanomolar to micromolar range and, in general, no clear binding specificity for DNA ends (e.g., Lee et al.

2003; Möckel et al. 2012). However, recent single-molecule fluorescence resonance energy transfer (FRET) analysis of human MRN determined an extraordinarily high DNA-binding affinity in the picomolar range (Cannon et al. 2013). This discrepancy may be caused by differing experimental conditions. MR(N) is intrinsically able to form large macromolecular assemblies in vitro (de Jager et al. 2001), and the ratio of higher-order to lower-order multimers of MR(N) might influence its affinity to DNA. This relationship may partly explain the apparent involvement of the Rad50 coiled-

C.B. Schiller et al.

coil domain in high affinity DNA binding, as this domain mediates MR(N) multimerization (Lee et al. 2013).

During the last decade, a substantial number of high- and low-resolution structural studies of MR and MRN components have led to plausible models for MR and MRN complexes from different domains of life (Fig. 1). MR or MRN form large bipolar complexes with globular heads that harbor the nucleotide-binding domains (NBDs) of Rad50 and the nuclease domain of Mre11 (Connelly et al. 1998; Anderson et al. 2001; de Jager et al. 2001; Hopfner et al. 2001). The Mre11 nuclease dimerizes and forms the center of the head module (Hopfner et al. 2001; Williams et al. 2008; Das et al. 2010; Park et al. 2011). Each Mre11 protomer binds one Rad50 coiled-coil domain near the Rad50 NBD, generating a conserved M₂R₂ architecture (Hopfner et al. 2001; Lammens et al. 2011; Lim et al. 2011; Limbo et al. 2012). Prokaryotic Mre11 binds to Rad50 through a carboxy-terminal helix-loop-helix motif (Fig. 2A) (Lammens et al. 2011; Lim et al. 2011; Möckel et al. 2012). The interaction of eukaryotic Mre11 and Rad50 has not been described on a structural level yet. However, structural information is available for the interaction of *S. pombe* Mre11 with Nbs1, which binds to the Mre11 nuclease dimer through a conserved motif near the carboxyl terminus of Nbs1 (Schiller et al. 2012).

The Mre11 Nuclease

Mre11 interacts with both Rad50 and Nbs1 and can be envisioned as the core of the MRN complex. Crystal structures of Mre11 homologs from all three domains of life emphasize the high structural conservation of the amino-terminal Mre11 domain and a universally conserved dimer architecture (Fig. 2B,C) (Hopfner et al. 2001; Arthur et al. 2004; Williams et al. 2008; Das et al. 2010; Lammens et al. 2011; Lim et al. 2011; Limbo et al. 2012; Möckel et al. 2012; Schiller et al. 2012; Liu et al. 2014). The functional importance of Mre11 dimerization is highlighted by findings that mutations of the yeast Mre11 dimer interface phenocopy an *mre11* knockout (Williams et al. 2008; Schiller

et al. 2012). The conserved amino-terminal domain of Mre11 consists of a phosphoesterase domain and an adjacent capping domain (Fig. 2B). The phosphoesterase active site coordinates two manganese ions, which are essential for exonuclease and ssDNA endonuclease activities (Trujillo et al. 1998; Hopfner et al. 2001).

The Mre11 dimer can directly bind and bridge two DNA ends in vitro (Fig. 2B) (Chen et al. 2001; Williams et al. 2008; Ghodke and Muniyappa 2013), a function that could be important in the context of HR and end-joining reactions (Reis et al. 2012). It is also known that the carboxyl terminus of eukaryotic Mre11 contains additional DNA-binding sites. One site maps to a region adjacent to the capping domain and is crucial for DSB-repair functions. A second DNA-binding motif at the carboxyl terminus of Mre11 was shown to be essential for DSB formation and spore viability in meiosis in *S. cerevisiae* (Furuse et al. 1998; Usui et al. 1998). Metazoan Mre11 homologs contain, in addition, a glycine/arginine-rich (GAR) motif, which is important for DNA binding and nuclease activity in vitro and localization to DSBs in vivo (Dery et al. 2008).

Comparison of all published structures reveals that the Mre11 dimer angle is not fixed, but it shows a large pivot angle range of one protomer with respect to the other (Fig. 2C). The observed variation of the dimer angle is not necessarily species specific, as *S. pombe* Mre11, for instance, was crystallized in very different dimer angles in the presence and absence of Nbs1 (Schiller et al. 2012). There might be a correlation between the Mre11 dimer angle and different binding states of Rad50, DNA, and Nbs1. Thus, the observed conformational flexibility might be an important functional aspect that should be addressed in future studies. An exceptional and somewhat surprising case is that of human Mre11, which was crystallized as a dimer cross-linked by an unexpected disulfide bond that leads to an unusual dimer interface and abolishes flexibility (Park et al. 2011).

At present, we have some basic understanding of the interaction of Mre11 with DNA, but important questions remain open. The metal-binding site with its conserved dimetal coordi-

Structural Mechanisms of Recombination

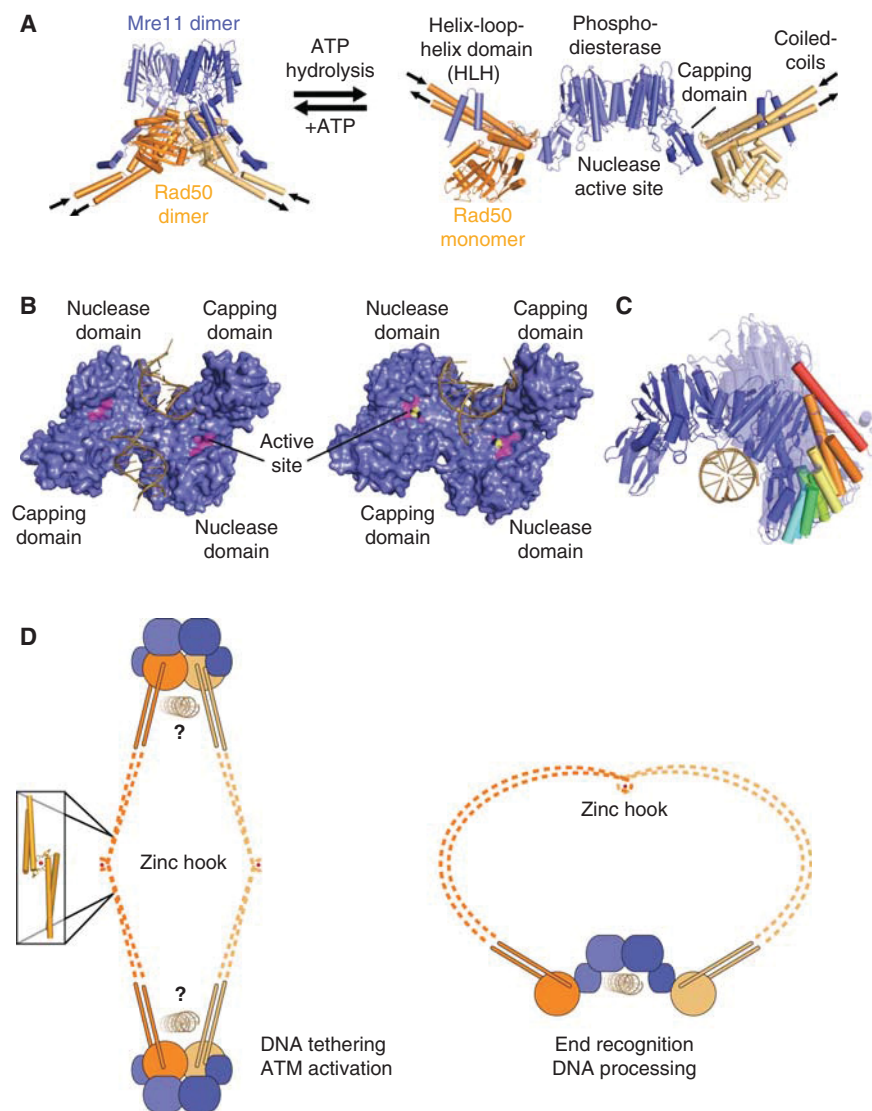


Figure 2. The Mre11 nuclease and its regulation by Rad50. (A) Structure of the ATP-bound and ATP-free *T. maritima* MR complex. The PDB codes are 3QG5 and 3THO (Lammens et al. 2011; Möckel et al. 2012). (B) Comparison of Mre11-DNA structures: the surface of the Mre11 dimer (blue) bound to synaptic DNA (left) and branched DNA (right). In the right structure, the active site (magenta) coordinates two manganese ions (yellow). The PDB codes are 3DSC (synaptic DNA) and 3DSD (branched DNA, Williams et al. 2008). (C) Mre11 structure comparison: dimeric crystal structures are aligned onto the left monomer of *P. furiosus* Mre11 (blue) (PDB code is 1S8E, Arthur et al. 2004). For clarity, the overlaid monomers are not depicted, the right monomers are transparent, and the first α -helix from the capping domain is marked from blue to red to highlight the differences. DNA (sand) indicates the accessible nuclease active site. The PDB codes are 1II7 (Hopfner et al. 2001), 3DSD, 3DSC (Williams et al. 2008), 4HD0 (Limbo et al. 2012), 3AUZ, 3AV0 (Lim et al. 2011), 3THO, 3THN (Möckel et al. 2012), 3QG5 (Lammens et al. 2011), 2Q8U (Das et al. 2010), 4FBQ, 4FBW, 4FBK, and 4FCX (Schiller et al. 2012). (D) MR model for DNA tethering and processing: Mre11 (blue) in complex with Rad50 (orange) forms intercomplex (left) and intracomplex (right) interactions through the zinc hook (zinc ion, red).

C.B. Schiller et al.

nating histidines readily explains the preference for manganese over magnesium for the 3' exonuclease. However, *P. furiosus* Mre11 was also shown to possess magnesium-dependent endonuclease activity that promotes 5' strand resection, the structural features of which remain elusive so far (Hopkins and Paull 2008). Moreover, our understanding of the molecular mechanism of DNA processing by Mre11 is still limited by the lack of a structure of Mre11 bound to a transition state DNA substrate.

The Rad50 Coiled-Coils

Arguably, the most distinguished yet most poorly understood structural feature of the MRN complex is the long coiled-coil extensions of Rad50. They emerge from the NBDs of Rad50 and carry the universally conserved “zinc-hook” dimerization motif at their apices (Fig. 1) (Hopfner et al. 2002). Two zinc hooks can dimerize by jointly coordinating a zinc ion via four invariant cysteines, two from each zinc hook (Fig. 2D) (Hopfner et al. 2002). In vitro, this dimerization can tether different MRN complexes or help to form supramolecular assemblies to cross-link DNA (de Jager et al. 2001; Hopfner et al. 2002), a feature that may explain the ability of MRN to aggregate DNA in *Xenopus* cell extracts (Costanzo et al. 2004).

Although the lengths of the coiled-coils are rather conserved between more closely related phylogenetic taxa, they can considerably vary between the different domains of life (Fig. 1). Studies in yeast have shown that the zinc hooks are critical for the function of the complex, but can be partly substituted by dimerization domains of a different type (Wiltzius et al. 2005) or can be compensated for by higher concentrations of MRN in the context of ATM activation (Lee et al. 2013). However, reduction of the length of the coiled-coil dramatically impairs functionality of the MRN complex (Hohl et al. 2011; Deshpande et al. 2014). It is interesting to note that yeast MRN is impaired when the length of the Rad50 coiled-coils is reduced to that of the bacteriophage protein. These results suggest that the dimensions of the Rad50 coiled-coil regions seem to be functionally relevant, but

the mechanistic requirements differ strongly between phylogenetic kingdoms and phages. However, care should be taken in the interpretation of these results and the design of such studies, as it is difficult to alter the length of coiled-coil domains without affecting their proper assembly or the orientation of the zinc hooks because of the helical nature of coiled-coils.

Scanning force microscopy (SFM) shows that the coiled-coil domains of Rad50 are organized into segments with flexible hinges that seem to coincide with regions of lower coiled-coil propensity (van Noort et al. 2003; de Jager et al. 2004). Because of this flexibility, two coiled-coil domains can form both inter- and intracomplex interactions, mediated by the dimerization of two zinc-hook motifs (Fig. 2D) (de Jager et al. 2001; Hopfner et al. 2001, 2002; Moreno-Herrero et al. 2005). Importantly, the recent structure of a small, Rad50-like prokaryotic DSB repair factor, RecN, described, for the first time, an atomic model for a full Rad50/SMC/RecN-type structure, assembled from overlapping, crystallographically resolved fragments (Fig. 1) (Pellegrino et al. 2012). This RecN dimer model illustrates the segmental nature of the coiled-coils, but at the same time, it suggests that the coiled-coil domain is overall rather stiff (Fig. 1).

Integrative Model for MR Mechanism

The ATP-binding and hydrolysis motifs of Rad50 are functionally critical elements of MRN. The NBDs of Rad50 dimerize in response to ATP binding, and studies with isolated NBDs show that Rad50 binds DNA in this ATP-engaged conformation (Hopfner et al. 2000b). ATP binding to the NBDs is also important for other functions of the complex such as activation of DNA damage checkpoint regulator ATM (Lee et al. 2013; Deshpande et al. 2014). Recent structural analysis on Mre11-Rad50^{NBD} head complexes revealed that the NBDs of Rad50 are far apart in the absence of ATP, allowing DNA to access the Mre11 nuclease active sites (Fig. 2A) (Lammens et al. 2011). In the presence of ATP, however, the two NBDs dimerize and bind into the DNA-binding/nuclease

cleft of the Mre11 dimer (Lim et al. 2011; Möckel et al. 2012; Deshpande et al. 2014). In this conformation, the two active sites of the Mre11 dimer are blocked, at least for binding of double-stranded DNA (dsDNA). These structural studies are consistent with reports that ATP binding to Rad50 negatively regulates the processive 3' dsDNA exonuclease and dsDNA endonuclease activity (but not the ssDNA endonuclease activity) of Mre11 (Herdendorf et al. 2011; Lim et al. 2011; Majka et al. 2012; Deshpande et al. 2014). The closed, ATP-bound conformation is also the conformation that activates ATM (Lee et al. 2013; Deshpande et al. 2014). Thus, a model may be formulated that was confirmed in a very recent study (Deshpande et al. 2014): The closed MR(N) complex is involved in ATM activation and DSB recognition or tethering, whereas the open complex after ATP hydrolysis is involved in DNA processing (Fig. 2D). It is yet unclear, however, how MRN binds DNA in the closed conformation, in which the Mre11 dsDNA-binding sites are blocked. We also do not know how Rad50 interacts with DNA.

The nature of supramolecular structures of MR and MRN that involve additional interactions mediated by the coiled-coils still needs to be resolved. Several different architectures are conceivable and may play roles in recombination and end joining. Using scanning force microscopic analysis of human MRN, DNA binding was shown to cause a shift from intra-MRN to inter-MRN hook–hook interactions through a mesoscale conformational change (Fig. 2D) (Moreno-Herrero et al. 2005). Therefore, the formation of higher-order structures could be directly coupled to DNA binding. The situation may be different for the rather short coiled-coil structures of the bacteriophage Rad50 orthologs, which leave little room for intramolecular coiled-coil interactions; thus, more work is needed to functionally dissect and validate different superstructures.

Nbs1

The eukaryote-specific subunit of the MRN complex, Nbs1 (or Xrs2 in *S. cerevisiae*), has multiple functions. It was found to stimulate

DNA binding and unwinding of MRN (Paull and Gellert 1999; Trujillo et al. 2003) and is necessary for the nuclear localization of Mre11 and Rad50 (Carney et al. 1998; Desai-Mehta et al. 2001; Tsukamoto et al. 2005). Nbs1 recruits and helps to activate the DNA damage checkpoint regulator ATM/Tel1p (Nakada et al. 2003; Falck et al. 2005; You et al. 2005; Berkovich et al. 2007). Although MR alone seems to be able to interact with ATM in vitro (Costanzo et al. 2004; Lee and Paull 2004; Lee and Paull 2005), the Nbs1 carboxyl terminus was shown to interact with and activate ATM through an acidic patch and a FFX/Y motif (Falck et al. 2005; You et al. 2005). A carboxy-terminal 147-amino-acid fragment of Nbs1 carrying these two motifs was sufficient to restore ATM activation in an Nbs1-depleted *Xenopus* egg extract (You et al. 2005). In addition, the carboxyl terminus of Nbs1 was found to be necessary for control of cell cycle arrest and apoptosis signals in a mouse model (Stracker et al. 2007).

Nbs1 comprises a folded amino-terminal region and a carboxy-terminal part predicted to be of low structural order (Williams et al. 2009). Crystal structures of the amino-terminal folded region revealed a rigid structure that consists of a fork-head-associated (FHA) domain and tandem BRCA1 carboxy-terminal (BRCT) domains (Lloyd et al. 2009; Williams et al. 2009). FHA and BRCT domains have been shown to recognize phosphoproteins (Durocher and Jackson 2002; Yu et al. 2003). In Nbs1, these domains serve as a recruitment platform for various DSB repair factors such as mediator of DNA damage checkpoint protein 1 (MDC1), Bloom syndrome mutated (BLM), breast cancer 1 (BRCA1), CtBP-interacting protein (CtIP), and phosphorylated histone H2AX (via MDC1) (Fig. 1) (Wang et al. 2000; Burma et al. 2001; Kobayashi et al. 2002; Chapman and Jackson 2008; Chen et al. 2008; Melander et al. 2008; Spycher et al. 2008; Wu et al. 2008). At least in the case of MDC1, both FHA and BRCT domains participate in an interdependent fashion (Lloyd et al. 2009; Hari et al. 2010).

Because of its flexible nature, only limited structural information is available for the carboxy-terminal region of Nbs1. Nbs1 binds to

C.B. Schiller et al.

Mre11 through a conserved NFKxFxK motif in this carboxy-terminal region (Desai-Mehta et al. 2001; Tauchi et al. 2001; You et al. 2005; Schiller et al. 2012). Significantly, the crystal structure of *S. pombe* Mre11 in complex with a carboxy-terminal fragment of Nbs1 showed that this peptide binds across the Mre11 dimer and breaks its symmetry (Schiller et al. 2012). Whether this binding has only the function to tether Mre11 to Nbs1 or—as the peculiar interaction at the Mre11 dimer axis may indicate—is functionally linked to Mre11-Rad50 conformations should be subject of future studies. It also remains to be clarified how this apparently asymmetric binding translates into the stoichiometry of the MRN complex (2:2:2 or 2:2:1).

Mutations in Mre11-Rad50-Nbs1 in Human Disease

Although knockouts of *MRE11*, *RAD50*, and *NBS1* are lethal in mice (Luo et al. 1999; Zhu et al. 2001; Buis et al. 2008), there are hypomorphic mutations of these genes that are associated with a set of related but phenotypically distinct syndromes such as ataxia-telangiectasia-like disease (ATLD), Nijmegen breakage syndrome (NBS), and NBS-like disorder (NBSLD). These diseases are related to ataxia telangiectasia (A-T), which is caused by mutations in *ATM* (Savitsky et al. 1995). All three MRN-associated syndromes and A-T share phenotypes on a cellular level, but patients differ with respect to the extent of neurological, immunological, and cancer predisposition disorders. Whereas NBS and NBSLD lead to microcephaly, A-T and ATLD are associated with neurodegeneration (Carney et al. 1998; Varon et al. 1998; Stewart et al. 1999; Maser et al. 2001; Waltes et al. 2009; Matsumoto et al. 2011).

Presently, the literature describes 18 cases of ATLD and one case of NBSLD that were all linked to mutations in the *MRE11* gene and one NBSLD patient with two *RAD50* mutations (Hernandez et al. 1993; Stewart et al. 1999; Pitts et al. 2001; Delia et al. 2004; Fernet et al. 2005; Uchisaka et al. 2009; Matsumoto et al. 2011; Palmeri et al. 2013). The availability of atomic structures of eukaryotic Mre11 and Nbs1 and

prokaryotic Rad50 and the high degree of conservation of MRN allow us to map the underlying mutations onto a structural model of the MRN complex (Fig. 3). Most mutations described so far, apart from truncation mutants, map to the interface between Nbs1 and Mre11. As this interface is quite extended, point mutations reduce, but do not abolish, the interaction between Nbs1 and Mre11, explaining their hypomorphic nature. Functional analysis of some mutations by mutating corresponding conserved residues in *S. cerevisiae* MRX showed that an ATLD-mimicking mutation did impair mitotic repair functions solely by lowering the nuclear concentration of MRX (Schiller et al. 2012). In addition, telomere maintenance was affected, suggesting a defect in Tel1/ATM activation. For another ATLD-mimicking mutation, a study in *S. pombe* showed that DSB repair was affected, but not Tel1/ATM activation (Limbo et al. 2012). This situation is somewhat surprising because ATLD is similar to A-T, which is caused by inactivation of ATM. Very recently, progressive myoclonic ataxia (PMA) was also linked to an *MRE11* mutation that maps to the surroundings of the Nbs1–Mre11 interface (Miyamoto et al. 2013).

Further work is thus necessary to correlate the molecular defects in MRN with the observed disease phenotypes. However, the structural studies on the conformational and functional states of MRN will now allow a more detailed structure–function correlation. The mutations may affect these distinct states of MRN and may lead to partial separation of function, which may explain how different disease phenotypes such as NBS and ATLD can result from mutations in a single complex.

RESECTION

Once a DNA DSB has been recognized, 5′-3′ resection of the DNA ends may proceed, which requires a 5′-3′ nuclease and, in most pathways, a helicase. Although this principle holds true for all three domains of life, resection and the initiation thereof are governed by different machineries with conservation limited to single domains. In bacteria, the multisubunit com-

Structural Mechanisms of Recombination

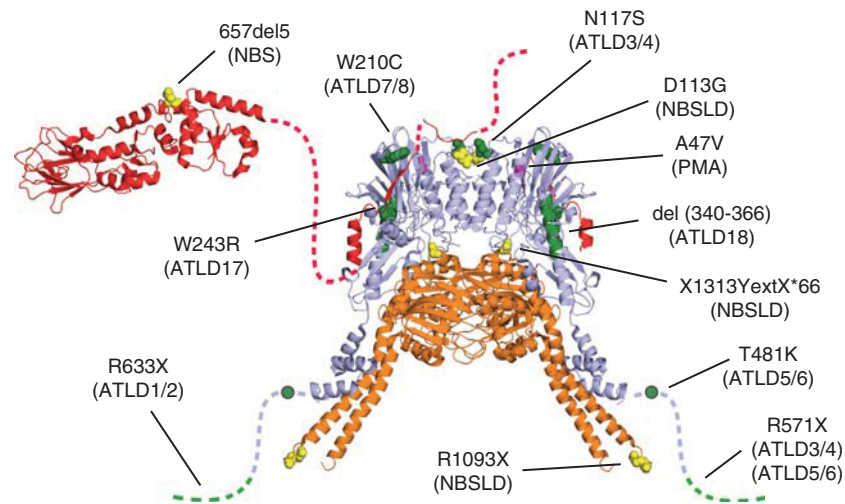


Figure 3. MRN and human disease. Mapping of MRN mutations found in human disorders onto a model of MRN (model and color code from Fig. 1). ATLD, NBS/-LD, and PMA mutations are indicated in green, yellow, and lilac, respectively.

plexes RecBCD and AddAB are stand-alone machineries that recognize DSBs, initiate resection, and perform long-range resection in a highly processive way (for an excellent recent review, see Wigley 2013). Under certain circumstances, an alternative resection pathway may take over that involves the nuclease RecJ and the helicase RecQ (Handa et al. 2009). In archaea, the MRN complex identifies DSBs and initiates resection, but a complex comprising the nuclease NuraA and the helicase HerA executes long-range resection (Hopkins and Paull 2008; Blackwood et al. 2012). There is evidence, however, that NuraA-HerA may form a larger resection complex together with MR (Quaiser et al. 2008). In eukaryotes, the MRN complex initiates resection together with the protein CtIP (Limbo et al. 2007; Mimitou and Symington 2008). Eukaryotic long-range resection has been found to follow partly redundant pathways that involve either the processive nuclease Exo1 or the complex of the nuclease/helicase DNA2 and the RecQ-like helicase Bloom syndrome mutated (BLM, Sgs1 in yeast) (Gravel et al. 2008; Mimitou and Symington 2008; Nimonkar et al. 2008; Zhu et al. 2008). In the following section, we will describe the initiation of resection in eukaryotes, followed by a discussion of the re-

cent advances of our structural understanding of the Exo1, DNA2/BLM, and NuraA/HerA pathways.

Initiation of Resection in Eukaryotes

In eukaryotes, initial resection of DSBs requires the MRN complex and CtIP. The precise biochemical function of CtIP is still controversial. CtIP was first characterized as an interaction factor of the transcriptional repressor CtBP, RB1, and the DNA repair and checkpoint protein BRCA1 (Fusco et al. 1998; Schaeper et al. 1998; Wong et al. 1998; Yu et al. 1998). Putative orthologs of CtIP are found in most eukaryotic species, although sequence identity is limited to small regions at the amino and carboxyl termini. CtIP orthologs (Sae2 in *S. cerevisiae* and Ctp1 in *S. pombe*) also vary considerably in length and may have diverged in their exact function, for example, with regard to the interaction with other proteins. Nonetheless, both Sae2 and Ctp1 were reported to play roles in initial DNA end resection similar to vertebrate CtIP (McKee and Kleckner 1997; Prinz et al. 1997; Lengsfeld et al. 2007; Limbo et al. 2007; Akamatsu et al. 2008; Nicolette et al. 2010).

C.B. Schiller et al.

Two sequence motifs are conserved between CtIP orthologs from most species. One motif is a predicted coiled-coil region at the amino terminus, which appears to mediate dimerization of CtIP and Sae2, a prerequisite to its functionality (Dubin et al. 2004; Kim et al. 2008; Wang et al. 2012). The second conserved region maps to the carboxyl terminus. It harbors a phosphorylation site (T847 in human and S267 in *S. cerevisiae*, but absent in *S. pombe* Ctp1 and some other fungi) that is phosphorylated by CDK to initiate resection (Huertas et al. 2008; Huertas and Jackson 2009). The carboxyl terminus also contains a functionally important CxxC motif (absent in *S. cerevisiae* Sae2) (Limbo et al. 2007; Akamatsu et al. 2008), mutations of which lead to defects in fission yeast DSB repair almost as severe as a *ctp1* knockout. However, the biochemical function of this motif remains to be characterized.

Mammalian CtIP was shown in several studies to physically interact with MRN (Sartori et al. 2007; Chen et al. 2008; Yuan and Chen 2009). In the case of *S. pombe* Ctp1, two crystal structures illustrate how the amino-terminal FHA domain of Nbs1 binds to a phosphorylated Thr-Asp motif in Ctp1 (Fig. 4A) (Lloyd et al. 2009; Williams et al. 2009). This motif in Ctp1 is phosphorylated in a cell cycle-dependent manner by kinase CK2 (Dodson et al. 2010). Recently, a direct interaction was also reported for recombinant *S. cerevisiae* MRX and Sae2 (Ghodke and Muniyappa 2013).

On the basis of studies in budding yeast, Sae2/Ctp1/CtIP has been suggested to initiate resection at DSB ends together with MRN by removing a short stretch of 50 to 100 bp from the 5' strand. Then, processive nucleases and nuclease-helicase complexes like Exo1 and Sgs1-Dna2 take over to resect the 5' strand up to the level of several kilobases (Mimitou and Symington 2008; Zhu et al. 2008). It is unclear, however, what defines the number of nucleotides to be removed by MRN and CtIP.

Priming endonucleolytic cleavage by MRN and CtIP may help to process DNA ends blocked by chemical modifications or by proteins and also offers a way to prevent uncontrolled resection and hyperrecombination. Blocked DNA

ends occur in meiosis or during abortive topoisomerase reactions (Hartsuiker et al. 2009; Longhese et al. 2009). The MRN(X) complex and Sae2/CtIP may indeed be dispensable for the resection of "clean" DNA ends, as shown for HO-endonuclease and I-SceI-induced DSBs in yeast (Llorente and Symington 2004; Westmoreland and Resnick 2013). In contrast to a model, in which MRN(X) and Sae2/CtIP start resection directly at a DNA end, newer studies provide an alternative model, in which MRN(X) incises DNA away from the DNA end (Fig. 4B). For yeast meiotic DNA breaks that are covalently bound by Spo11 (Keeney et al. 1997), it was shown that the MRX complex and Sae2 incise this blocked DNA up to 300 bases downstream from the DSB and resect the DNA strand in a 3'-5' direction toward the break (Fig. 4B) (Garcia et al. 2011). This model reconciles the discrepancy between the 3'-5' exonuclease activity of Mre11 observed in vitro and the 5'-3' resection observed in vivo. DNA incision away from the DSB was found for HR also in mitotic mammalian cells (Shibata et al. 2014), suggesting that this mode of action is not limited to meiosis. However, some issues remain unclear. What defines the distance between the meiotic or mitotic break and the endonucleolytic incision? The observed distance could be particular to the experiment, but may also reflect the influence of nucleosomes or the tethering function of the Rad50 coiled-coils. Another open question is how MRN distinguishes the two DNA strands during the endonucleolytic cut so that it processes toward and not away from the break.

The biochemical mechanisms by which Sae2/Ctp1/CtIP promote DSB resection are not understood and may differ between species. Although *S. cerevisiae* Sae2 shows in vitro endonuclease activity on ssDNA and degrades hairpin DNA structures cooperatively with MRN (Lengsfeld et al. 2007), human CtIP seems to lack nuclease activity, but stimulates the ssDNA endonuclease activity of Mre11 (Sartori et al. 2007). Structural data for Sae2/Ctp1/CtIP or its interaction with MRN(X) so far remain elusive. Thus, many questions are still unanswered: (1) Where is the active site in *S. cerevisiae* Sae2 located? (2) Does it represent

Structural Mechanisms of Recombination

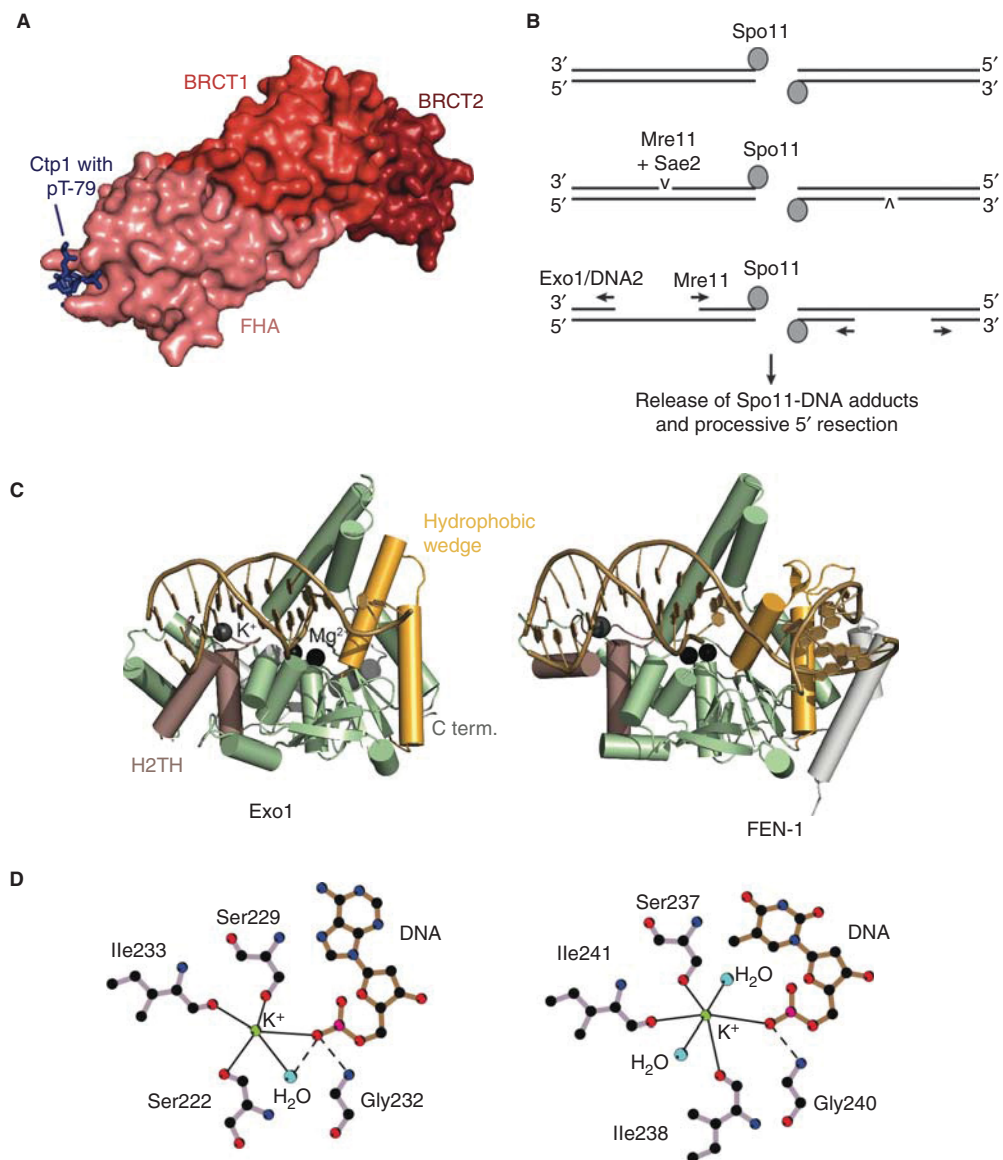


Figure 4. Resection initiation and the Exo1 resection pathway. (A) Structure of an Nbs1-Ctp1 complex from *S. pombe* (PDB code is 3HUF, Williams et al. 2009). Nbs1 surface with highlighted FHA (salmon), BRCT1 (red), and BRCT2 (dark red) domains. Peptide from Ctp1 (blue) with phosphorylated T99 bound to the FHA domain. (B) Model for bidirectional resection at meiotic DSBs by Mre11 and Exo1/Sgs1-Dna2. A study of meiotic resection in *S. cerevisiae* suggests an endonucleotic cleavage of the 5' strand by Mre11/Sae2 at a distance of up to 300 bp away from the Spo11-blocked DNA end. The nicked DNA can then be processed bidirectionally by Mre11 in the 3'-5' direction and by Exo1 or Sgs1-Dna2 in the 5'-3' direction (Garcia et al. 2011). (C) Comparison of human Exo1 and FEN-1. Features discussed in the text are highlighted and labeled for Exo1. The PDB codes are 3QEA (Exo1, Orans et al. 2011) and 3Q8K (FEN-1, Tsutakawa et al. 2011). (D) The helix-two-turn-helix (H2TH)-K⁺ motif in Exo1 (left) and FEN-1 (right). Straight lines indicate metal coordination, and dashed lines indicate hydrogen bonds. Only residues involved in K⁺-coordination and binding of the K⁺-coordinating DNA base are shown. The scheme was drawn using LIGPLOT (Laskowski and Swindells 2011). C term., carboxy terminal.

C.B. Schiller et al.

a new class of nuclease domains that is absent in vertebrate CtIP? (3) How can this protein stimulate and regulate the nuclease activities of Mre11 in pathways such as mitotic and meiotic HR, telomere maintenance, and MMEJ?

Exonuclease 1 Resection Pathway

The long-range resection nuclease exonuclease 1 (Exo1, in humans, also Hex1) was first described as a 5'-3' exonuclease from *S. pombe* (Szankasi and Smith 1992) and then found in *S. cerevisiae* (Fiorentini et al. 1997; Tishkoff et al. 1997) and humans (Schmutte et al. 1998; Tishkoff et al. 1998; Wilson et al. 1998). Besides its involvement in resection (Tsubouchi and Ogawa 2000; Mimitou and Symington 2008; Zhu et al. 2008; Nicolette et al. 2010), Exo1 has major roles in mismatch repair (Szankasi and Smith 1995; Genschel et al. 2002) and telomere maintenance (Wu et al. 2012). During resection, human Exo1 is stimulated by BLM, MRN, and the replication protein A (RPA), as shown by experiments using purified proteins (Nimonkar et al. 2008, 2011). However, this situation may be different in yeast (Cannavo et al. 2013).

Exo1 belongs to the XPG/Rad2 and FEN-1 family of structure-specific nucleases, a class of metalloenzymes (Shen et al. 1997; Lee and Wilson 1999; Orans et al. 2011). All members of this family share a conserved amino-terminal nuclease domain (amino acids 1–350 in human Exo1), whereas the carboxyl terminus (the remaining 500 amino acids) is divergent. Human Exo1 is dependent on Mg^{2+} , and significantly less active in the presence of Mn^{2+} (Lee and Wilson 1999). For many years, structural information was limited to crystal structures of the paralog flap endonuclease 1 (FEN-1) (Hosfield et al. 1998; Hwang et al. 1998; Matsui et al. 2002; Chapados et al. 2004; Feng et al. 2004; Sakurai et al. 2005; Doré et al. 2006; Devos et al. 2007), which, among other roles, removes Okazaki fragments during replication (reviewed in Balakrishnan and Bambara 2013). However, these structures were incomplete with regard to the metal center or DNA complexation. Only recently, the crystal structures of human Exo1

and FEN-1, each in complex with a DNA substrate, were reported (Fig. 4C) (Orans et al. 2011; Tsutakawa et al. 2011).

The Exo1 fold comprises a central, twisted β -sheet surrounded by α -helices and is structurally very similar to FEN-1 and related endonucleases (Orans et al. 2011). In the crystal structure, a bound DNA substrate is simulated using a short DNA duplex with a 3' single-strand extension. The double-stranded part of the DNA interacts with Exo1 only at two points that are set one turn apart. A helix-two-turn-helix (H2TH) motif binding a K^+ makes non-specific bonds with the nonsubstrate strand (Fig. 4C,D). At the active site, two structurally conserved helices form a hydrophobic wedge that drives the nonsubstrate strand into a sharp bend away from the nuclease. The 5' end of the substrate strand is led to the active site, which consists of two divalent cations that are coordinated by five conserved acidic residues and a conserved lysine and arginine. A remarkable feature is the fraying of the duplex DNA. As a consequence, the substrate strand becomes a single strand that exposes its scissile bond to the metal center. It was proposed that one of the metals activates a water molecule that can attack the scissile bond, whereas the other metal stabilizes the leaving group (Beese and Steitz 1991; Steitz and Steitz 1993; Orans et al. 2011).

Many of these structural features are conserved between the paralogs Exo1 and FEN-1 despite different substrate specificities (Fig. 4C) (Orans et al. 2011; Tsutakawa et al. 2011). Exo1 is primarily an exonuclease at DNA nicks, FEN-1 removes DNA flaps, and other family members such as XPG or GEN cut at DNA bubbles or Holliday junctions, respectively (Tsutakawa and Tainer 2012). Common to all these DNA structures is a nick or gap, and the insights gained from the Exo1 and FEN-1 structures allow the formulation of a single, common mechanism for their processing by FEN-1 family members (for an in-depth discussion of the two crystal structures and their implications, see Grasby et al. 2012; Tsutakawa and Tainer 2012). The presence of a DNA nick or gap is required by the hydrophobic wedge that induces a sharp bend into the template DNA strand and

thus prevents the processing of dsDNA. Together with the wedge, the H2TH/K⁺ motif (Fig. 4D) orientates the substrate strands toward the active site metal center. This potassium ion is absent in FEN-1 crystal structures that lack DNA (e.g., Chapados et al. 2004). A similar configuration was observed in the DNA polymerase β , where a K⁺ is involved in binding of a helix-hairpin-helix motif to DNA and was suggested to support processivity (Pelletier et al. 1996). Access to the active site is restricted to ssDNA, again excluding a continuous dsDNA. The ssDNA is generated by melting of two residues of the substrate strand.

Still under discussion is the interaction between FEN-1 paralogs and the substrate ssDNA upstream of the incision. A threading mechanism has been postulated that requires the threading of the ssDNA through a helical arch that is disordered in the absence of bound DNA (Ceska et al. 1996; Tsutakawa et al. 2011; Tsutakawa and Tainer 2012; Balakrishnan and Bambara 2013). Threading has to be ruled out for a DNA bubble in the case of XPG. Some argue that XPG probably does not have a helical arch (Tsutakawa et al. 2011; Tsutakawa and Tainer 2012), whereas others posit that the ssDNA may circumvent the helical arch and bind on surface grooves, which may extend to all FEN-1-related nucleases, including XPG and GEN (Orans et al. 2011).

The Sgs1/BLM-DNA2 Resection Pathway

The second main pathway for processive 5'-resection in HR, beside Exo1-mediated resection, depends on the cooperative action of the nuclease DNA2 and the helicase activity of Sgs1 in *S. cerevisiae* or its functional homolog BLM in vertebrates (Gravel et al. 2008; Mimitou and Symington 2008; Nimonkar et al. 2008; Zhu et al. 2008). Sgs1 or BLM unwind duplex DNA by their 3'-5' helicase activity. The ssDNA-binding protein, replication protein-A (RPA), then coats ssDNA unwound by Sgs1 and promotes 5'-3' degradation by Dna2 while inhibiting 3' to 5' degradation (Cejka et al. 2010a; Niu et al. 2010; Nimonkar et al. 2011). Recombinant Dna2 and Sgs1 physically interact even in the absence of a

DNA substrate, and a similar interaction was also reported for human DNA2 and BLM (Cejka et al. 2010a; Nimonkar et al. 2011). In addition, Sgs1 is part of the Sgs1-Top3-Rmi1 (STR) complex, together with the topoisomerase class I enzyme Topoisomerase III and the regulatory protein Rmi1 (Gangloff et al. 1994; Chang et al. 2005; Mullen et al. 2005). This complex is responsible for dissolution of double Holliday junctions in the late stage of homologous recombination (Cejka et al. 2010b). Top3 and Rmi1 are also important for the resection function of Sgs1. Deletion mutants of all three proteins share similar resection defects in vivo (Zhu et al. 2008), and Top3-Rmi1 also stimulates the 5'-resection capacity of Sgs1-Dna2 in vitro (Cejka et al. 2010a; Niu et al. 2010). A very recent crystal structure of the conserved core of the human TopIII α -RMI1 complex illustrates how RMI1 might regulate TopIII α through a long insertion loop that invades the central gate of the toroidal topoisomerase (Bocquet et al. 2014).

Sgs1 and BLM both belong to the RecQ family of helicases. Most prokaryotes and yeasts possess only one or two RecQ homologs (like Sgs1 in *S. cerevisiae*), whereas in vertebrates multiple homologs are found. For *Homo sapiens*, five RecQ-like helicases have been described: BLM, WRN, RECQ1, RECQ4, and RECQ5 β . All of these helicases play important roles in different pathways of genome maintenance (Chu and Hickson 2009).

The RecQ-like helicases belong to the SF-2 helicase family and share a conserved core, which consists of two RecA-like domains and a carboxy-terminally adjacent RQC (RecQ carboxy-terminal) region (lacking in RecQ4) (Vindigni et al. 2010; Manthei and Keck 2013). The RQC region is needed for strand separation of DNA substrates (Hu et al. 2005; Pike et al. 2009; Kitano et al. 2010). Many RecQ-like helicases, including bacterial RecQ, yeast Sgs1, and vertebrate BLM also possess a helicase and RNaseD carboxy-terminal (HDRC) domain that is important for DNA substrate recognition and translocation (Liu et al. 1999; Bernstein and Keck 2005; Kocsis et al. 2014).

Several atomic resolution structures are now available and yield insights into the functional

C.B. Schiller et al.

architecture of these helicases. The crystal structure of *Escherichia coli* RecQ revealed the principal architecture of the catalytic core (Fig. 5A) (Bernstein et al. 2003). The RecA-like domains and the RQC region, consisting of a zinc-binding motif and a winged helix domain, compose a compact modular arrangement, which is also

found in the structure of human RecQ1 (Pike et al. 2009). The HRDC domains from *E. coli* RecQ, SGS1, and BLM possess a very similar fold. However, they exhibit different DNA substrate specificities. This is reflected in their differing composition of DNA-interacting residues and distinct surface charge distributions

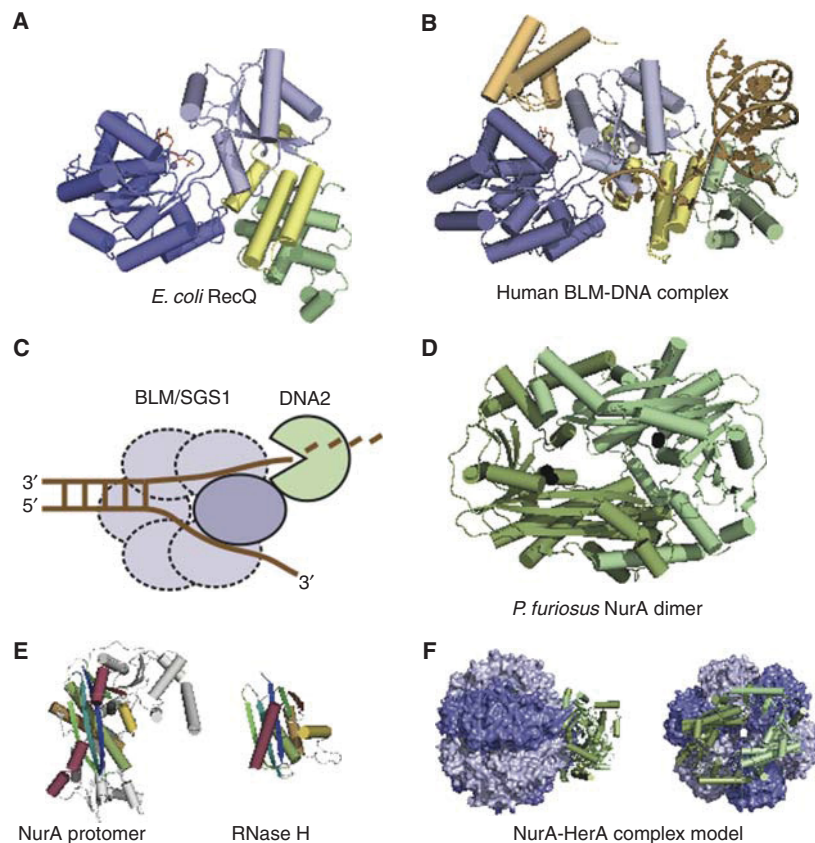


Figure 5. Structures of nuclease-helicase complexes involved in resection. (A) Structure of the helicase catalytic core of *E. coli* RecQ bound to ATPγS. The structure consists of the RecA-like helicase domains (dark and light blue) bound to ATPγS (orange) and the RecQ carboxy-terminal region, consisting of the zinc-binding domain (yellow) and a winged-helix domain (green). The PDB code is 10YY (Bernstein et al. 2003). (B) Structure of human BLM helicase in complex with DNA. The color coding is similar to that in A. The HRDC domain and ADP are drawn in orange, and the DNA in brown. The PDB code is 4CGZ. (C) The RecQ-like helicases BLM in vertebrates or Sgs1 in yeast are both cooperating with DNA2 in DSB resection. Sgs1 or BLM unwind dsDNA by their 3'-5' helicase activity. The ssDNA-binding protein RPA then coats ssDNA unwound by Sgs1 and promotes 5'-3' degradation by Dna2 (Cejka et al. 2010a; Niu et al. 2010; Nimmonkar et al. 2011). The potential of BLM and Sgs1 to form multimers is indicated using dashed lines. (D) Structure of the *P. furiosus* NurA dimer. The PDB code is 3TAL (Chae et al. 2012). (E) RNase H fold of NurA. A comparison of a *P. furiosus* NurA protomer with *E. coli* RNase H (PDB code 1RNH, Yang et al. 1990). Homologous elements are highlighted using the same color. (F) Model of the NurA-HerA complex. The crystal structure of *Sulfolobus solfataricus* NurA (PDB code 2YGG, Blackwood et al. 2012) is fitted to a HerA homolog, the conjugation protein TrwB (PDB code 1E9R, Gomis-Ruth et al. 2001).

(Liu et al. 1999; Bernstein and Keck 2005; Kim and Choi 2010; Sato et al. 2010).

Very recently, structures of human BLM in complex with partially unwound DNA were determined (PDB code 4CGZ, Fig. 5B) (Swan et al. 2014; O Gileadi, pers. comm.). This structure reveals extensive interactions of the winged helix domain with the upstream dsDNA “substrate” and shows that the β -hairpin wing acts as a DNA-splitting element. The zinc-binding insertion domain functions as single-stranded DNA ratchet, whereas the RecA-like domains binds to the ssDNA “product.” The HRDC domain does not make any DNA contacts but is positioned on top of the nucleotide-binding cleft of the RecA-like domains. It will be interesting to see whether the observed position of the HRDC domain is important for the regulation of BLM helicase activity. Bacterial RecQ and BLM structures share high fold conservation, although the winged-helix domain is positioned differently in both structures, indicating flexibility for this element (Fig 5A,B).

Many RecQ-like helicases including BLM are known to form oligomers, at least in vitro (Fig. 5C) (Karow et al. 1999; Xue et al. 2002; Perry et al. 2006; Vindigni and Hickson 2009). However, a more recent study describes that BLM oligomers dissociate into monomers upon ATP hydrolysis and that only monomeric but not oligomeric BLM displays DNA unwinding activity (Xu et al. 2012a). Thus, it remains an open question which functional role oligomerization of Sgs1 or BLM plays in the context of 5'-strand resection in HR.

Homologs of the nuclease-helicase protein Dna2 are found both in archaea and eukarya but are absent in bacteria, although the bacterial AddAB system bears some structural similarity. Although archaeal Dna2 is only poorly characterized (Higashibata et al. 2003), the eukaryotic protein was found to play crucial roles in several genome maintenance processes beside homologous recombination, including Okazaki fragment processing (Kang et al. 2010) and telomere stabilization (Lin et al. 2013). Initial genetic studies in *S. cerevisiae* revealed that the nuclease activity of Dna2 is essential in vivo, whereas a helicase-dead mutant strain is via-

ble at lower growth temperatures (Budd et al. 2000). A later study then clarified that the nuclease of Dna2 is responsible for processive 5' strand resection in DSB repair by HR where it is the second important processive nuclease beside Exo1 (Zhu et al. 2008). Both Exo1 and Dna2 function independently of each other and seem to play redundant roles (Zhu et al. 2008; Cannavo et al. 2013). The nuclease module of Dna2 belongs to the RecB family and maps to the amino terminus of the protein. Remarkably, it was shown to contain an iron-sulfur cluster, which is crucial for both nuclease and ATPase activity (Yeeles et al. 2009; Pokharel and Campbell 2012). This situation is reminiscent of the bacterial DSB resection protein AddB, which possesses a nuclease domain with a 4Fe-4S cluster (Yeeles et al. 2009).

In contrast to its nuclease activity, the helicase activity of Dna2 is dispensable for 5'-strand resection, which was a rather surprising finding. Instead, the unwinding activity of RecQ-like helicases such as Sgs1 or BLM provides the 5'-ssDNA for resection by Dna2 (Cejka et al. 2010a; Niu et al. 2010). The Dna2 helicase exhibits only a weak 5'-3' unwinding activity on dsDNA and depends on the binding to free DNA ends before acting as a helicase (Bae et al. 2002). However, recently, it was shown that Dna2 is a vigorous 5'-3' helicase in an *S. cerevisiae* nuclease dead mutant (Levikova et al. 2013). Apparently, Dna2 depends on the binding to 5'-ssDNA flaps for processive helicase activity, and these flaps are degraded by the Dna2 nuclease domain of the wild-type protein (Levikova et al. 2013). There may be a structural switch in Dna2 that regulates the balance between its nuclease and helicase activities. Atomic resolution structures of Dna2, Sgs1, and their DNA substrates, which are still lacking at the moment, could provide important information to better understand how these key enzymes cooperate to specifically resect 5'-DNA at DSBs.

Resection in Archaea

Archaea, like eukaryotes, use homologs of Mre11-Rad50 for resection. However, for long-range resection, Mre11-Rad50 are joined by two

C.B. Schiller et al.

proteins unique to archaea, the helicase HerA and the nuclease NurA (Manzan et al. 2004; Hopkins and Paull 2008; Blackwood et al. 2012; Chae et al. 2012). Archaeal resection is thus similar to the eukaryotic process with regard to common players such as Mre11-Rad50 and the overall principle. In contrast, the archaeal resection machinery is completely distinct from bacterial proteins such as RecBCD, AddAB, or AdnAB, although some archaeal species may have taken up AddAB-like proteins by horizontal gene transfer (Cromie 2009).

The genes *nurA* and *herA* are encoded in one operon together with *mre11* and *rad50* in almost all archaea (Constantinesco et al. 2002, 2004; Manzan et al. 2004). NurA is a dimer and has been described as both a 5' and 3' exonuclease for dsDNA and ssDNA and an endonuclease for ssDNA (Constantinesco et al. 2002; Hopkins and Paull 2008; Wei et al. 2008, 2011; Blackwood et al. 2012; Chae et al. 2012). HerA is a hexameric, ATP-dependent DNA helicase that is activated by and unwinds dsDNA in both the 5' and 3' direction (Constantinesco et al. 2004; Manzan et al. 2004; Zhang et al. 2008).

For full activity, NurA and HerA have to form a complex, which is stable in vitro, at least for species such as *P. furiosus* and *S. solfataricus* (Hopkins and Paull 2008; Blackwood et al. 2012; Chae et al. 2012). However, this physical interaction may be less stable or absent in *Sulfolobus acidocaldarius* (Quaiser et al. 2008). The stoichiometry of the complex (if formed) seems to be 2:6, that is, a NurA dimer and a HerA hexamer (Hopkins and Paull 2008; Blackwood et al. 2012; Chae et al. 2012).

The HerA monomers assemble into a hexameric ring, as visualized by electron microscopy analysis (Manzan et al. 2004). Thus, HerA is a typical member of the FtsK class of P-loop ATPases and is likely to have a similar fold (Constantinesco et al. 2004; Iyer et al. 2004). The HerA amino terminus is predicted to comprise a distinct domain that folds into a β -barrel and was called the HAS (HerA-ATP synthase) domain (Iyer et al. 2004).

The crystal structures of two NurA orthologs from *P. furiosus* and *S. solfataricus* were recently reported (Fig. 5D) (Blackwood et al.

2012; Chae et al. 2012). The conserved, active domain is of the RNaseH-like fold (Fig. 5E) with nonconserved extensions that make extensive dimer interactions. The overall shape of the NurA dimer is ring-like, with the active sites of each monomer facing each other within the ring pore (Fig. 5D). Conserved acidic residues bind one or two Mn^{2+} cations in the active site of *P. furiosus* NurA, depending on the crystallization conditions (Chae et al. 2012). Mutation of these manganese-binding residues completely inactivates NurA (Hopkins and Paull 2008; Wei et al. 2011; Blackwood et al. 2012; Chae et al. 2012). Also, Mg^{2+} is known to be essential for NurA activity (Constantinesco et al. 2002; Hopkins and Paull 2008; Chae et al. 2012). Thus, the catalytic mechanism of NurA could be similar to that postulated for the RNaseH-like nuclease Argonaute (Wang et al. 2009) or RNase H itself (Nowotny et al. 2005). Structures of these proteins bound to divalent cations and DNA have led to a model in which one cation activates a water for nucleophilic attack on the DNA backbone and the second cation stabilizes the leaving group (Beese and Steitz 1991; Steitz and Steitz 1993; Nowotny et al. 2005; Wang et al. 2009).

The structures of NurA also yielded insight into the cooperative DNA processing of NurA and HerA. The cavity of the NurA ring is positively charged, as expected for a DNA-processing enzyme. However, it holds space only for one or two ssDNA strands, but not for B-form dsDNA (Blackwood et al. 2012; Chae et al. 2012). The interaction interface of NurA and HerA could be mapped to residues on the flat surface of the NurA ring close to the active site, which are bound by the HerA HAS domain (Fig. 5F) (Blackwood et al. 2012). These data imply that the helicase HerA unwinds dsDNA and passes one or both single strands directly on to the NurA dimer.

The NurA structure does not answer the question of whether, in vivo, the NurA/HerA complex digests one or both strands of dsDNA. However, it has been observed that the rate of ATP hydrolysis by NurA/HerA varies with the nature of the DNA substrate. This rate is higher for dsDNA with blunt ends or short overhangs

and lower in the presence of longer overhangs (Blackwood et al. 2012). In consequence, the nature of the DNA end may trigger complete digestion of the DNA double strand or the 5'-3' resection necessary to produce a DNA tail. Blackwood et al. (2012) suggest that the former could be an archaeal defense mechanism against foreign DNA, whereas the latter might rely on the preparation of the DNA by the MR complex. Experimental evidence indeed supports a model in which the MR complex and the NurA/HerA complex cooperate to produce a 3' overhang that is then bound by RadA (archaeal RecA) for homologous recombination (Hopkins and Paull 2008).

OPEN QUESTIONS AND CONCLUDING REMARKS

The past decade has brought a plethora of new insights into the composition, biochemistry, and regulation of the DSB detection and resection machineries. We now have an inventory of enzymatic activities at DSBs in all three domains of life. Nonetheless, from a mechanistic and also an evolutionary point of view, we are far from understanding the molecular choreography of DSB detection, repair, and resection. Although the bacterial resection machineries, RecBCD and AddAB, are well characterized, the structural nature of the resection machineries in eukaryotes and archaea requires further attention. New developments in electron microscopy and hybrid methods in structural biology may help to better understand the interaction architectures of these complexes and the interplay of different nuclease, helicase, and topoisomerase activities. Likewise, despite progress over the last years, the mechanism of the MR(N) complex in DNA end processing is still unclear. Several fundamental issues remain unsolved, in particular, the mechanism of DSB detection by MRN, the nature of its cryptic endonuclease activity, and the role and mechanism of the cofactor CtIP/Ctp1/Sae2. Other issues such as identifying the site of the initial endonucleolytic cleavage of DNA ends will require the reconstitution of more complete biochemical systems. It will also be important to

mechanistically address the resection in chromatin templates and integrate the activities of chromatin modifying enzymes with resection enzymes. Recent studies have begun to look at exactly that and showed in vitro that Sgs1-Dna2 resection requires some nucleosome-free DNA but can then proceed through nucleosomes. In contrast, nucleosomes provide an obstacle for Exo1-based resection that may be lifted by chromatin-remodeling activities (Adkins et al. 2013).

ACKNOWLEDGMENTS

We apologize to all authors whose work we could not cite owing to space limitations. Work in the K.-P.H. laboratory on DNA double-strand breaks is supported by the European Research Council (ERC) advanced grant "ATMMACHINE," the German Excellence Initiative Research Cluster CIPSM, and German Research Council Program projects SFB646 and GRK1721.

REFERENCES

*Reference is also in this collection.

- Adkins NL, Niu H, Sung P, Peterson CL. 2013. Nucleosome dynamics regulates DNA processing. *Nat Struct Mol Biol* **20**: 836–842.
- Aguilera A, Gomez-Gonzalez B. 2008. Genome instability: A mechanistic view of its causes and consequences. *Nat Rev Genet* **9**: 204–217.
- Akamatsu Y, Murayama Y, Yamada T, Nakazaki T, Tsutsui Y, Ohta K, Iwasaki H. 2008. Molecular characterization of the role of the *Schizosaccharomyces pombe* *nip1⁺/ctp1⁺* gene in DNA double-strand break repair in association with the Mre11-Rad50-Nbs1 complex. *Mol Cell Biol* **28**: 3639–3651.
- Almond JR, Stohr BA, Panigrahi AK, Albrecht DW, Nelson SW, Kreuzer KN. 2013. Coordination and processing of DNA ends during double-strand break repair: The role of the bacteriophage T4 Mre11/Rad50 (MR) complex. *Genetics* **195**: 739–755.
- Amunugama R, Fishel R. 2012. Homologous recombination in eukaryotes. *Prog Mol Biol Transl Sci* **110**: 155–206.
- Anderson DE, Trujillo KM, Sung P, Erickson HP. 2001. Structure of the Rad50-Mre11 DNA repair complex from *Saccharomyces cerevisiae* by electron microscopy. *J Biol Chem* **276**: 37027–37033.
- Arthur LM, Gustavsson K, Hopfner KP, Carson CT, Stracker TH, Karcher A, Felton D, Weitzman MD, Tainer J, Carney JP. 2004. Structural and functional analysis of Mre11-3. *Nucleic Acids Res* **32**: 1886–1893.

C.B. Schiller et al.

- Bae SH, Kim DW, Kim J, Kim JH, Kim DH, Kim HD, Kang HY, Seo YS. 2002. Coupling of DNA helicase and endonuclease activities of yeast Dna2 facilitates Okazaki fragment processing. *J Biol Chem* **277**: 26632–26641.
- Balakrishnan L, Bambara RA. 2013. Flap endonuclease 1: A central component of DNA metabolism. *Annu Rev Biochem* **82**: 119–138.
- Beese LS, Steitz TA. 1991. Structural basis for the 3'-5' exonuclease activity of *Escherichia coli* DNA polymerase: A two metal ion mechanism. *EMBO J* **10**: 25–33.
- Berkovich E, Monnat RJ Jr, Kastan MB. 2007. Roles of ATM and NBS1 in chromatin structure modulation and DNA double-strand break repair. *Nat Cell Biol* **9**: 683–690.
- Bernstein DA, Keck JL. 2005. Conferring substrate specificity to DNA helicases: Role of the RecQ HRDC domain. *Structure* **13**: 1173–1182.
- Bernstein DA, Zittel MC, Keck JL. 2003. High-resolution structure of the *E. coli* RecQ helicase catalytic core. *EMBO J* **22**: 4910–4921.
- Blackwood JK, Rzechorzek NJ, Abrams AS, Maman JD, Pellegrini L, Robinson NP. 2012. Structural and functional insights into DNA-end processing by the archaeal HerA helicase–NurA nuclease complex. *Nucleic Acids Res* **40**: 3183–3196.
- Blier PR, Griffith AJ, Craft J, Hardin JA. 1993. Binding of Ku protein to DNA. Measurement of affinity for ends and demonstration of binding to nicks. *J Biol Chem* **268**: 7594–7601.
- Bocquet N, Bizard AH, Abdulrahman W, Larsen NB, Faty M, Cavadini S, Bunker RD, Kowalczykowski SC, Cejka P, Hickson ID, et al. 2014. Structural and mechanistic insight into Holliday-junction dissolution by Topoisomerase III α and RMI1. *Nat Struct Mol Biol* **21**: 261–268.
- Bonetti D, Clerici M, Manfrini N, Lucchini G, Longhese MP. 2010. The MRX complex plays multiple functions in resection of Yku- and Rif2-protected DNA ends. *PLoS ONE* **5**: e14142.
- Budd ME, Choe W, Campbell JL. 2000. The nuclease activity of the yeast DNA2 protein, which is related to the RecB-like nucleases, is essential in vivo. *J Biol Chem* **275**: 16518–16529.
- Buis J, Wu Y, Deng Y, Leddon J, Westfield G, Eckersdorff M, Sekiguchi JM, Chang S, Ferguson DO. 2008. Mre11 nuclease activity has essential roles in DNA repair and genomic stability distinct from ATM activation. *Cell* **135**: 85–96.
- Burma S, Chen BP, Murphy M, Kurimasa A, Chen DJ. 2001. ATM phosphorylates histone H2AX in response to DNA double-strand breaks. *J Biol Chem* **276**: 42462–42467.
- Cadet J, Ravanat JL, TavernaPorro M, Menoni H, Angelov D. 2012. Oxidatively generated complex DNA damage: Tandem and clustered lesions. *Cancer Lett* **327**: 5–15.
- Cannavo E, Cejka P, Kowalczykowski SC. 2013. Relationship of DNA degradation by *Saccharomyces cerevisiae* exonuclease 1 and its stimulation by RPA and Mre11-Rad50-Xrs2 to DNA end resection. *Proc Natl Acad Sci* **110**: E1661–E1668.
- Cannon B, Kuhnlein J, Yang SH, Cheng A, Schindler D, Stark JM, Russell R, Paull TT. 2013. Visualization of local DNA unwinding by Mre11/Rad50/Nbs1 using single-molecule FRET. *Proc Natl Acad Sci* **110**: 18868–18873.
- Carney JB, Maser RS, Olivares H, Davis EM, Le Beau M, Yates JR III, Hays L, Morgan WF, Petrini JH. 1998. The hMre11/hRad50 protein complex and Nijmegen breakage syndrome: Linkage of double-strand break repair to the cellular DNA damage response. *Cell* **93**: 477–486.
- Cejka P, Cannavo E, Polaczek P, Masuda-Sasa T, Pokharel S, Campbell JL, Kowalczykowski SC. 2010a. DNA end resection by Dna2-Sgs1-RPA and its stimulation by Top3-Rmi1 and Mre11-Rad50-Xrs2. *Nature* **467**: 112–116.
- Cejka P, Plank JL, Bachrati CZ, Hickson ID, Kowalczykowski SC. 2010b. Rmi1 stimulates decatenation of double Holliday junctions during dissolution by Sgs1-Top3. *Nat Struct Mol Biol* **17**: 1377–1382.
- Ceska TA, Sayers JR, Stier G, Suck D. 1996. A helical arch allowing single-stranded DNA to thread through T5 5'-exonuclease. *Nature* **382**: 90–93.
- Chae J, Kim YC, Cho Y. 2012. Crystal structure of the NurA-dAMP-Mn²⁺ complex. *Nucleic Acids Res* **40**: 2258–2270.
- Chang M, Bellaoui M, Zhang C, Desai R, Morozov P, Delgado-Cruzata L, Rothstein R, Freyer GA, Boone C, Brown GW. 2005. RMI1/NCE4, a suppressor of genome instability, encodes a member of the RecQ helicase/Topo III complex. *EMBO J* **24**: 2024–2033.
- Chapados BR, Hosfield DJ, Han S, Qiu J, Yelent B, Shen B, Tainer JA. 2004. Structural basis for FEN-1 substrate specificity and PCNA-mediated activation in DNA replication and repair. *Cell* **116**: 39–50.
- Chapman JR, Jackson SP. 2008. Phospho-dependent interactions between NBS1 and MDC1 mediate chromatin retention of the MRN complex at sites of DNA damage. *EMBO Rep* **9**: 795–801.
- Chen L, Trujillo K, Ramos W, Sung P, Tomkinson AE. 2001. Promotion of Dnl4-catalyzed DNA end-joining by the Rad50/Mre11/Xrs2 and Hdf1/Hdf2 complexes. *Mol Cell* **8**: 1105–1115.
- Chen L, Nievera CJ, Lee AY, Wu X. 2008. Cell cycle-dependent complex formation of BRCA1-CtIP-MRN is important for DNA double-strand break repair. *J Biol Chem* **283**: 7713–7720.
- Chiruvella KK, Liang Z, Wilson TE. 2013. Repair of double-strand breaks by end joining. *Cold Spring Harb Perspect Biol* **5**: a012757.
- Chu WK, Hickson ID. 2009. RecQ helicases: Multifunctional genome caretakers. *Nat Rev Cancer* **9**: 644–654.
- Connelly JC, de Leau ES, Okely EA, Leach DR. 1997. Overexpression, purification, and characterization of the SbcCD protein from *Escherichia coli*. *J Biol Chem* **272**: 19819–19826.
- Connelly JC, Kirkham LA, Leach DR. 1998. The SbcCD nuclease of *Escherichia coli* is a structural maintenance of chromosomes (SMC) family protein that cleaves hairpin DNA. *Proc Natl Acad Sci* **95**: 7969–7974.
- Connelly JC, de Leau ES, Leach DR. 1999. DNA cleavage and degradation by the SbcCD protein complex from *Escherichia coli*. *Nucleic Acids Res* **27**: 1039–1046.
- Connelly JC, de Leau ES, Leach DR. 2003. Nucleolytic processing of a protein-bound DNA end by the *E. coli* SbcCD (MR) complex. *DNA Repair (Amst)* **2**: 795–807.
- Constantinesco F, Forterre P, Elie C. 2002. NurA, a novel 5'-3' nuclease gene linked to rad50 and mre11 homologs of thermophilic *Archaea*. *EMBO Rep* **3**: 537–542.

Structural Mechanisms of Recombination

- Constantinesco F, Forterre P, Koonin EV, Aravind L, Elie C. 2004. A bipolar DNA helicase gene, *herA*, clusters with *rad50*, *mre11* and *nurA* genes in thermophilic archaea. *Nucleic Acids Res* **32**: 1439–1447.
- Costanzo V, Robertson K, Bibikova M, Kim E, Grieco D, Gottesman M, Carroll D, Gautier J. 2001. Mre11 protein complex prevents double-strand break accumulation during chromosomal DNA replication. *Mol Cell* **8**: 137–147.
- Costanzo V, Paull T, Gottesman M, Gautier J. 2004. Mre11 assembles linear DNA fragments into DNA damage signaling complexes. *PLoS Biol* **2**: E110.
- Cromie GA. 2009. Phylogenetic ubiquity and shuffling of the bacterial RecBCD and AddAB recombination complexes. *J Bacteriol* **191**: 5076–5084.
- Darmon E, Eykelenboom JK, Lincker F, Jones LH, White M, Okely E, Blackwood JK, Leach DR. 2010. *E coli* SbcCD and RecA control chromosomal rearrangement induced by an interrupted palindrome. *Mol Cell* **39**: 59–70.
- Das D, Moiani D, Axelrod HL, Miller MD, McMullan D, Jin KK, Abdubek P, Astakhova T, Burra P, Carlton D, et al. 2010. Crystal structure of the first eubacterial Mre11 nuclease reveals novel features that may discriminate substrates during DNA repair. *J Mol Biol* **397**: 647–663.
- de Jager M, van Noort J, van Gent DC, Dekker C, Kanaar R, Wyman C. 2001. Human Rad50/Mre11 is a flexible complex that can tether DNA ends. *Mol Cell* **8**: 1129–1135.
- de Jager M, Trujillo KM, Sung P, Hopfner KP, Carney JP, Tainer JA, Connelly JC, Leach DR, Kanaar R, Wyman C. 2004. Differential arrangements of conserved building blocks among homologs of the Rad50/Mre11 DNA repair protein complex. *J Mol Biol* **339**: 937–949.
- Delia D, Piane M, Buscemi G, Savio C, Palmeri S, Lulli P, Carlessi L, Fontanella E, Chessa L. 2004. *MRE11* mutations and impaired ATM-dependent responses in an Italian family with ataxia-telangiectasia-like disorder. *Hum Mol Genet* **13**: 2155–2163.
- Delmas S, Shunburne L, Ngo HP, Allers T. 2009. Mre11-Rad50 promotes rapid repair of DNA damage in the polyploid archaeon *Haloferax volcanii* by restraining homologous recombination. *PLoS Genet* **5**: e1000552.
- Delmas S, Duggin IG, Allers T. 2013. DNA damage induces nucleoid compaction via the Mre11-Rad50 complex in the archaeon *Haloferax volcanii*. *Mol Microbiol* **87**: 168–179.
- Dery U, Coulombe Y, Rodrigue A, Stasiak A, Richard S, Masson JY. 2008. A glycine-arginine domain in control of the human MRE11 DNA repair protein. *Mol Cell Biol* **28**: 3058–3069.
- Desai-Mehta A, Cerosaletti KM, Concannon P. 2001. Distinct functional domains of nibrin mediate Mre11 binding, focus formation, and nuclear localization. *Mol Cell Biol* **21**: 2184–2191.
- Deshpande RA, Williams GJ, Limbo O, Williams RS, Kuhnlein J, Lee JH, Classen S, Guenther G, Russell P, Tainer JA, et al. 2014. ATP-driven Rad50 conformations regulate DNA tethering, end resection, and ATM checkpoint signaling. *EMBO J* **33**: 482–500.
- Devos JM, Tomanicek SJ, Jones CE, Nossal NG, Mueser TC. 2007. Crystal structure of bacteriophage T4 5' nuclease in complex with a branched DNA reveals how flap endonuclease-1 family nucleases bind their substrates. *J Biol Chem* **282**: 31713–31724.
- Dodson GE, Limbo O, Nieto D, Russell P. 2010. Phosphorylation-regulated binding of Ctp1 to Nbs1 is critical for repair of DNA double-strand breaks. *Cell Cycle* **9**: 1516–1522.
- Doré AS, Kilkenny ML, Jones SA, Oliver AW, Roe SM, Bell SD, Pearl LH. 2006. Structure of an archaeal PCNA1-PCNA2-FEN1 complex: Elucidating PCNA subunit and client enzyme specificity. *Nucleic Acids Res* **34**: 4515–4526.
- Dubin MJ, Stokes PH, Sum EY, Williams RS, Valova VA, Robinson PJ, Lindeman GJ, Glover JN, Visvader JE, Matthews JM. 2004. Dimerization of CtIP, a BRCA1- and CtBP-interacting protein, is mediated by an N-terminal coiled-coil motif. *J Biol Chem* **279**: 26932–26938.
- Durocher D, Jackson SP. 2002. The FHA domain. *FEBS Lett* **513**: 58–66.
- Eykelenboom JK, Blackwood JK, Okely E, Leach DR. 2008. SbcCD causes a double-strand break at a DNA palindrome in the *Escherichia coli* chromosome. *Mol Cell* **29**: 644–651.
- Falck J, Coates J, Jackson SP. 2005. Conserved modes of recruitment of ATM, ATR and DNA-PKcs to sites of DNA damage. *Nature* **434**: 605–611.
- Feng M, Patel D, Dervan JJ, Ceska T, Suck D, Haq I, Sayers JR. 2004. Roles of divalent metal ions in flap endonuclease-substrate interactions. *Nat Struct Mol Biol* **11**: 450–456.
- Fernet M, Gribaa M, Salih MA, Seidahmed MZ, Hall J, Koenig M. 2005. Identification and functional consequences of a novel *MRE11* mutation affecting 10 Saudi Arabian patients with the ataxia telangiectasia-like disorder. *Hum Mol Genet* **14**: 307–318.
- Ferretti LP, Lafranchi L, Sartori AA. 2013. Controlling DNA-end resection: A new task for CDKs. *Front Genet* **4**: 99.
- Fiorentini P, Huang KN, Tishkoff DX, Kolodner RD, Symington LS. 1997. Exonuclease I of *Saccharomyces cerevisiae* functions in mitotic recombination in vivo and in vitro. *Mol Cell Biol* **17**: 2764–2773.
- Frols S, Gordon PM, Panlilio MA, Duggin IG, Bell SD, Sensen CW, Schleper C. 2007. Response of the hyperthermophilic archaeon *Sulfolobus solfataricus* to UV damage. *J Bacteriol* **189**: 8708–8718.
- Furuse M, Nagase Y, Tsubouchi H, Murakami-Murofushi K, Shibata T, Ohta K. 1998. Distinct roles of two separable *in vitro* activities of yeast Mre11 in mitotic and meiotic recombination. *EMBO J* **17**: 6412–6425.
- Fusco C, Reymond A, Zervos AS. 1998. Molecular cloning and characterization of a novel retinoblastoma-binding protein. *Genomics* **51**: 351–358.
- Gangloff S, McDonald JB, Bendixen C, Arthur L, Rothstein R. 1994. The yeast type I topoisomerase Top3 interacts with Sgs1, a DNA helicase homolog: A potential eukaryotic reverse gyrase. *Mol Cell Biol* **14**: 8391–8398.
- Gapud EJ, Sleckman BP. 2011. Unique and redundant functions of ATM and DNA-PKcs during V(D)J recombination. *Cell Cycle* **10**: 1928–1935.
- Garcia V, Phelps SEL, Gray S, Neale MJ. 2011. Bidirectional resection of DNA double-strand breaks by Mre11 and Exo1. *Nature* **479**: 241–244.

C.B. Schiller et al.

- Genschel J, Bazemore LR, Modrich P. 2002. Human exonuclease I is required for 5' and 3' mismatch repair. *J Biol Chem* **277**: 13302–13311.
- Ghodke I, Muniyappa K. 2013. Processing of DNA double-stranded breaks and intermediates of recombination and repair by *Saccharomyces cerevisiae* Mre11 and its stimulation by Rad50, Xrs2, and Sae2 proteins. *J Biol Chem* **288**: 11273–11286.
- Gomis-Ruth FX, Moncalian G, Perez-Luque R, Gonzalez A, Cabezon E, de la Cruz F, Coll M. 2001. The bacterial conjugation protein TrwB resembles ring helicases and F1-ATPase. *Nature* **409**: 637–641.
- Grasby JA, Finger LD, Tsutakawa SE, Attack JM, Tainer JA. 2012. Unpairing and gating: Sequence-independent substrate recognition by FEN superfamily nucleases. *Trends Biochem Sci* **37**: 74–84.
- Gravel S, Chapman JR, Magill C, Jackson SP. 2008. DNA helicases Sgs1 and BLM promote DNA double-strand break resection. *Genes Dev* **22**: 2767–2772.
- Haber JE. 2012. Mating-type genes and MAT switching in *Saccharomyces cerevisiae*. *Genetics* **191**: 33–64.
- Hanahan D, Weinberg RA. 2011. Hallmarks of cancer: The next generation. *Cell* **144**: 646–674.
- Handa N, Morimatsu K, Lovett ST, Kowalczykowski SC. 2009. Reconstitution of initial steps of dsDNA break repair by the RecF pathway of *E. coli*. *Genes Dev* **23**: 1234–1245.
- Hari FJ, Spycher C, Jungmichel S, Pavic L, Stucki M. 2010. A divalent FHA/BRCT-binding mechanism couples the MRE11-RAD50-NBS1 complex to damaged chromatin. *EMBO Rep* **11**: 387–392.
- Hartsuiker E, Neale MJ, Carr AM. 2009. Distinct requirements for the Rad32^{Mre11} nuclease and Ctp1^{CIP} in the removal of covalently bound topoisomerase I and II from DNA. *Mol Cell* **33**: 117–123.
- Herdendorf TJ, Albrecht DW, Benkovic SJ, Nelson SW. 2011. Biochemical characterization of bacteriophage T4 Mre11-Rad50 complex. *J Biol Chem* **286**: 2382–2392.
- Hernandez D, McConville CM, Stacey M, Woods CG, Brown MM, Shutt P, Rysiecki G, Taylor AM. 1993. A family showing no evidence of linkage between the ataxia telangiectasia gene and chromosome 11q22-23. *J Med Genet* **30**: 135–140.
- Higashibata H, Kikuchi H, Kawarabayashi Y, Matsui I. 2003. Helicase and nuclease activities of hyperthermophile *Pyrococcus horikoshii* Dna2 inhibited by substrates with RNA segments at 5'-end. *J Biol Chem* **278**: 15983–15990.
- Hohl M, Kwon Y, Galvan SM, Xue X, Tous C, Aguilera A, Sung P, Petrini JH. 2011. The Rad50 coiled-coil domain is indispensable for Mre11 complex functions. *Nat Struct Mol Biol* **18**: 1124–1131.
- Hopfner KP, Karcher A, Shin D, Fairley C, Tainer JA, Carney JP. 2000a. Mre11 and Rad50 from *Pyrococcus furiosus*: Cloning and biochemical characterization reveal an evolutionarily conserved multiprotein machine. *J Bacteriol* **182**: 6036–6041.
- Hopfner KP, Karcher A, Shin DS, Craig L, Arthur LM, Carney JP, Tainer JA. 2000b. Structural biology of Rad50 ATPase: ATP-driven conformational control in DNA double-strand break repair and the ABC-ATPase superfamily. *Cell* **101**: 789–800.
- Hopfner KP, Karcher A, Craig L, Woo TT, Carney JB, Tainer JA. 2001. Structural biochemistry and interaction architecture of the DNA double-strand break repair Mre11 nuclease and Rad50-ATPase. *Cell* **105**: 473–485.
- Hopfner KP, Craig L, Moncalian G, Zinkel RA, Usui T, Owen BA, Karcher A, Henderson B, Bodmer JL, McMurray CT, et al. 2002. The Rad50 zinc-hook is a structure joining Mre11 complexes in DNA recombination and repair. *Nature* **418**: 562–566.
- Hopkins BB, Paull TT. 2008. The *P. furiosus* mre11/rad50 complex promotes 5' strand resection at a DNA double-strand break. *Cell* **135**: 250–260.
- Hosfield DJ, Mol CD, Shen B, Tainer JA. 1998. Structure of the DNA repair and replication endonuclease and exonuclease FEN-1: Coupling DNA and PCNA binding to FEN-1 activity. *Cell* **95**: 135–146.
- Hu JS, Feng H, Zeng W, Lin GX, Xi XG. 2005. Solution structure of a multifunctional DNA- and protein-binding motif of human Werner syndrome protein. *Proc Natl Acad Sci* **102**: 18379–18384.
- Huertas P, Jackson SP. 2009. Human CtIP mediates cell cycle control of DNA end resection and double strand break repair. *J Biol Chem* **284**: 9558–9565.
- Huertas P, Cortes-Ledesma F, Sartori AA, Aguilera A, Jackson SP. 2008. CDK targets Sae2 to control DNA-end resection and homologous recombination. *Nature* **455**: 689–692.
- Hwang KY, Baek K, Kim HY, Cho Y. 1998. The crystal structure of flap endonuclease-1 from *Methanococcus jannaschii*. *Nat Struct Biol* **5**: 707–713.
- Iyer LM, Makarova KS, Koonin EV, Aravind L. 2004. Comparative genomics of the FtsK-HerA superfamily of pumping ATPases: Implications for the origins of chromosome segregation, cell division and viral capsid packaging. *Nucleic Acids Res* **32**: 5260–5279.
- Jasin M, Rothstein R. 2013. Repair of strand breaks by homologous recombination. *Cold Spring Harb Perspect Biol* **5**: a012740.
- Kang YH, Lee CH, Seo YS. 2010. Dna2 on the road to Okazaki fragment processing and genome stability in eukaryotes. *Crit Rev Biochem Mol Biol* **45**: 71–96.
- Karow JK, Newman RH, Freemont PS, Hickson ID. 1999. Oligomeric ring structure of the Bloom's syndrome helicase. *Curr Biol* **9**: 597–600.
- Keeney S, Giroux CN, Kleckner N. 1997. Meiosis-specific DNA double-strand breaks are catalyzed by Spo11, a member of a widely conserved protein family. *Cell* **88**: 375–384.
- Kim YM, Choi BS. 2010. Structure and function of the regulatory HRDC domain from human Bloom syndrome protein. *Nucleic Acids Res* **38**: 7764–7777.
- Kim HS, Vijayakumar S, Reger M, Harrison JC, Haber JE, Weil C, Petrini JH. 2008. Functional interactions between Sae2 and the Mre11 complex. *Genetics* **178**: 711–723.
- Kitano K, Kim SY, Hakoshima T. 2010. Structural basis for DNA strand separation by the unconventional winged-helix domain of RecQ helicase WRN. *Structure* **18**: 177–187.
- Kobayashi J, Tauchi H, Sakamoto S, Nakamura A, Morishima K, Matsuura S, Kobayashi T, Tamai K, Tanimoto K, Komatsu K. 2002. NBS1 localizes to γ -H2AX foci

Structural Mechanisms of Recombination

- through interaction with the FHA/BRCT domain. *Curr Biol* **12**: 1846–1851.
- Kocsis ZS, Sarlos K, Harami GM, Martina M, Kovacs M. 2014. A nucleotide- and HRDC-domain-dependent structural transition in DNA-bound RecQ helicase. *J Biol Chem* **289**: 5938–5949.
- Kreuzer KN, Brister JR. 2010. Initiation of bacteriophage T4 DNA replication and replication fork dynamics: A review in the *Virology Journal* series on bacteriophage T4 and its relatives. *Virology* **7**: 358.
- * Lam I, Keeney S. 2014. Mechanism and regulation of meiotic recombination initiation. *Cold Spring Harb Perspect Biol* doi: 10.1101/cshperspect.a016634.
- Lammens K, Bemeleit DJ, Möckel C, Clausing E, Schele A, Hartung S, Schiller CB, Lucas M, Angermüller C, Söding J, et al. 2011. The Mre11:Rad50 structure shows an ATP-dependent molecular clamp in DNA double-strand break repair. *Cell* **145**: 54–66.
- Langerak P, Mejia-Ramirez E, Limbo O, Russell P. 2011. Release of Ku and MRN from DNA ends by Mre11 nuclease activity and Ctp1 is required for homologous recombination repair of double-strand breaks. *PLoS Genet* **7**: e1002271.
- Laskowski RA, Swindells MB. 2011. LigPlot⁺: Multiple ligand–protein interaction diagrams for drug discovery. *J Chem Inf Model* **51**: 2778–2786.
- Lee JH, Paull TT. 2004. Direct activation of the ATM protein kinase by the Mre11/Rad50/Nbs1 complex. *Science* **304**: 93–96.
- Lee JH, Paull TT. 2005. ATM activation by DNA double-strand breaks through the Mre11-Rad50-Nbs1 complex. *Science* **308**: 551–554.
- Lee BI, Wilson DM III. 1999. The RAD2 domain of human exonuclease 1 exhibits 5′ to 3′ exonuclease and flap structure-specific endonuclease activities. *J Biol Chem* **274**: 37763–37769.
- Lee JH, Ghirlando R, Bhaskara V, Hoffmeyer MR, Gu J, Paull TT. 2003. Regulation of Mre11/Rad50 by Nbs1: Effects on nucleotide-dependent DNA binding and association with ataxia-telangiectasia-like disorder mutant complexes. *J Biol Chem* **278**: 45171–45181.
- Lee JH, Mand MR, Deshpande RA, Kinoshita E, Yang SH, Wyman C, Paull TT. 2013. Ataxia telangiectasia-mutated (ATM) kinase activity is regulated by ATP-driven conformational changes in the Mre11/Rad50/Nbs1 (MRN) complex. *J Biol Chem* **288**: 12840–12851.
- Lengsfeld BM, Rattray AJ, Bhaskara V, Ghirlando R, Paull TT. 2007. Sae2 is an endonuclease that processes hairpin DNA cooperatively with the Mre11/Rad50/Xrs2 complex. *Mol Cell* **28**: 638–651.
- Levikova M, Klaue D, Seidel R, Cejka P. 2013. Nuclease activity of *Saccharomyces cerevisiae* Dna2 inhibits its potent DNA helicase activity. *Proc Natl Acad Sci* **110**: E1992–E2001.
- Lim HS, Kim JS, Park YB, Gwon GH, Cho Y. 2011. Crystal structure of the Mre11-Rad50-ATPγS complex: Understanding the interplay between Mre11 and Rad50. *Genes Dev* **25**: 1091–1104.
- Limbo O, Chahwan C, Yamada Y, de Bruin RAM, Wittenberg C, Russell P. 2007. Ctp1 is a cell-cycle-regulated protein that functions with Mre11 complex to control double-strand break repair by homologous recombination. *Mol Cell* **28**: 134–146.
- Limbo O, Moiani D, Kertokallio A, Wyman C, Tainer JA, Russell P. 2012. Mre11 ATLD17/18 mutation retains Tel1/ATM activity but blocks DNA double-strand break repair. *Nucleic Acids Res* **40**: 11435–11449.
- Lin W, Sampathi S, Dai H, Liu C, Zhou M, Hu J, Huang Q, Campbell J, Shin-Ya K, Zheng L, et al. 2013. Mammalian DNA2 helicase/nuclease cleaves G-quadruplex DNA and is required for telomere integrity. *EMBO J* **32**: 1425–1439.
- Lisby M, Barlow JH, Burgess RC, Rothstein R. 2004. Choreography of the DNA damage response: Spatiotemporal relationships among checkpoint and repair proteins. *Cell* **118**: 699–713.
- Liu Z, Macias MJ, Bottomley MJ, Stier G, Linge JP, Nilges M, Bork P, Sattler M. 1999. The three-dimensional structure of the HRDC domain and implications for the Werner and Bloom syndrome proteins. *Structure* **7**: 1557–1566.
- Liu S, Tian LE, Liu YP, An XM, Tang Q, Yan XX, Liang DC. 2014. Structural basis for DNA recognition and nuclease processing by the Mre11 homologue SbcD in double-strand breaks repair. *Acta Crystallogr D Biol Crystallogr* **70**: 299–309.
- Llorente B, Symington LS. 2004. The Mre11 nuclease is not required for 5′ to 3′ resection at multiple HO-induced double-strand breaks. *Mol Cell Biol* **24**: 9682–9694.
- Lloyd J, Chapman JR, Clapperton JA, Haire LE, Hartsuiker E, Li J, Carr AM, Jackson SP, Smerdon SJ. 2009. A supra-modular FHA/BRCT-repeat architecture mediates Nbs1 adaptor function in response to DNA damage. *Cell* **139**: 100–111.
- Lobachev KS, Gordenin DA, Resnick MA. 2002. The Mre11 complex is required for repair of hairpin-capped double-strand breaks and prevention of chromosome rearrangements. *Cell* **108**: 183–193.
- Longhese MP, Bonetti D, Guerini I, Manfrini N, Clerici M. 2009. DNA double-strand breaks in meiosis: Checking their formation, processing and repair. *DNA Repair (Amst)* **8**: 1127–1138.
- Luger K, Mader AW, Richmond RK, Sargent DE, Richmond TJ. 1997. Crystal structure of the nucleosome core particle at 2.8 Å resolution. *Nature* **389**: 251–260.
- Luo G, Yao MS, Bender CE, Mills M, Bladl AR, Bradley A, Petrini JH. 1999. Disruption of *mRad50* causes embryonic stem cell lethality, abnormal embryonic development, and sensitivity to ionizing radiation. *Proc Natl Acad Sci* **96**: 7376–7381.
- Majka J, Alford B, Ausio J, Finn RM, McMurray CT. 2012. ATP hydrolysis by RAD50 protein switches MRE11 enzyme from endonuclease to exonuclease. *J Biol Chem* **287**: 2328–2341.
- Manthei KA, Keck JL. 2013. The BLM dissolvosome in DNA replication and repair. *Cell Mol Life Sci* **70**: 4067–4084.
- Manzan A, Pfeiffer G, Hefferin ML, Lang CE, Carney JP, Hopfner K-P. 2004. MlaA, a hexameric ATPase linked to the Mre11 complex in archaeal genomes. *EMBO Rep* **5**: 54–59.
- Maser RS, Zinkel R, Petrini JH. 2001. An alternative mode of translation permits production of a variant NBS1 protein

C.B. Schiller et al.

- from the common Nijmegen breakage syndrome allele. *Nat Genet* **27**: 417–421.
- Matsui E, Musti KV, Abe J, Yamasaki K, Matsui I, Harata K. 2002. Molecular structure and novel DNA binding sites located in loops of flap endonuclease-1 from *Pyrococcus horikoshii*. *J Biol Chem* **277**: 37840–37847.
- Matsumoto Y, Miyamoto T, Sakamoto H, Izumi H, Nakazawa Y, Ogi T, Tahara H, Oku S, Hiramoto A, Shiiki T, et al. 2011. Two unrelated patients with *MRE11A* mutations and Nijmegen breakage syndrome-like severe microcephaly. *DNA Repair (Amst)* **10**: 314–321.
- McKee AH, Kleckner N. 1997. A general method for identifying recessive diploid-specific mutations in *Saccharomyces cerevisiae*, its application to the isolation of mutants blocked at intermediate stages of meiotic prophase and characterization of a new gene *SAE2*. *Genetics* **146**: 797–816.
- * Mehta A, Haber JE. 2014. Sources of DNA double-strand breaks and models for recombinational DNA repair. *Cold Spring Harb Perspect Biol* doi: 10.1101/cshperspect.a016428.
- Melander F, Bekker-Jensen S, Falck J, Bartek J, Mailand N, Lukas J. 2008. Phosphorylation of SDT repeats in the MDC1 N terminus triggers retention of NBS1 at the DNA damage-modified chromatin. *J Cell Biol* **181**: 213–226.
- Mimitou EP, Symington LS. 2008. Sae2, Exo1 and Sgs1 collaborate in DNA double-strand break processing. *Nature* **455**: 770–774.
- Mimitou EP, Symington LS. 2010. Ku prevents Exo1 and Sgs1-dependent resection of DNA ends in the absence of a functional MRX complex or Sae2. *EMBO J* **29**: 3358–3369.
- Miyamoto R, Morino H, Yoshizawa A, Miyazaki Y, Maruyama H, Murakami N, Fukada K, Izumi Y, Matsuura S, Kaji R, et al. 2013. Exome sequencing reveals a novel *MRE11* mutation in a patient with progressive myoclonic ataxia. *J Neurol Sci* **337**: 219–223.
- Möckel C, Lammens K, Schele A, Hopfner KP. 2012. ATP driven structural changes of the bacterial Mre11:Rad50 catalytic head complex. *Nucleic Acids Res* **40**: 914–927.
- Moreno-Herrero F, de Jager M, Dekker NH, Kanaar R, Wyman C, Dekker C. 2005. Mesoscale conformational changes in the DNA-repair complex Rad50/Mre11/Nbs1 upon binding DNA. *Nature* **437**: 440–443.
- Mullen JR, Nallasetth FS, Lan YQ, Slagle CE, Brill SJ. 2005. Yeast Rmi1/Nce4 controls genome stability as a subunit of the Sgs1-Top3 complex. *Mol Cell Biol* **25**: 4476–4487.
- Myung K, Chen C, Kolodner RD. 2001a. Multiple pathways cooperate in the suppression of genome instability in *Saccharomyces cerevisiae*. *Nature* **411**: 1073–1076.
- Myung K, Datta A, Kolodner RD. 2001b. Suppression of spontaneous chromosomal rearrangements by S phase checkpoint functions in *Saccharomyces cerevisiae*. *Cell* **104**: 397–408.
- Nakada D, Matsumoto K, Sugimoto K. 2003. ATM-related Tel1 associates with double-strand breaks through an Xrs2-dependent mechanism. *Genes Dev* **17**: 1957–1962.
- Neale MJ, Pan J, Keeney S. 2005. Endonucleolytic processing of covalent protein-linked DNA double-strand breaks. *Nature* **436**: 1053–1057.
- Nicolette ML, Lee K, Guo Z, Rani M, Chow JM, Lee SE, Paull TT. 2010. Mre11-Rad50-Xrs2 and Sae2 promote 5' strand resection of DNA double-strand breaks. *Nat Struct Mol Biol* **17**: 1478–1485.
- Nimonkar AV, Özsoy AZ, Genschel J, Modrich P, Kowalczykowski SC. 2008. Human exonuclease 1 and BLM helicase interact to resect DNA and initiate DNA repair. *Proc Natl Acad Sci* **105**: 16906–16911.
- Nimonkar AV, Genschel J, Kinoshita E, Polaczek P, Campbell JL, Wyman C, Modrich P, Kowalczykowski SC. 2011. BLM-DNA2-RPA-MRN and EXO1-BLM-RPA-MRN constitute two DNA end resection machineries for human DNA break repair. *Genes Dev* **25**: 350–362.
- Niu H, Chung WH, Zhu Z, Kwon Y, Zhao W, Chi P, Prakash R, Seong C, Liu D, Lu L, et al. 2010. Mechanism of the ATP-dependent DNA end-resection machinery from *Saccharomyces cerevisiae*. *Nature* **467**: 108–111.
- Nowotny M, Gaidamakov SA, Crouch RJ, Yang W. 2005. Crystal structures of RNase H bound to an RNA/DNA hybrid: Substrate specificity and metal-dependent catalysis. *Cell* **121**: 1005–1016.
- Orans J, McSweeney EA, Iyer RR, Hast MA, Hellinga HW, Modrich P, Beese LS. 2011. Structures of human exonuclease 1 DNA complexes suggest a unified mechanism for nuclease family. *Cell* **145**: 212–223.
- Palmeri S, Rufa A, Pucci B, Santarnecchi E, Malandrini A, Stromillo ML, Mandala M, Rosini F, De Stefano N, Federico A. 2013. Clinical course of two Italian siblings with ataxia-telangiectasia-like disorder. *Cerebellum* **12**: 596–599.
- Park YB, Chae J, Kim YC, Cho Y. 2011. Crystal structure of human Mre11: Understanding tumorigenic mutations. *Structure* **19**: 1591–1602.
- Paull TT, Gellert M. 1998. The 3' to 5' exonuclease activity of Mre 11 facilitates repair of DNA double-strand breaks. *Mol Cell* **1**: 969–979.
- Paull TT, Gellert M. 1999. Nbs1 potentiates ATP-driven DNA unwinding and endonuclease cleavage by the Mre11/Rad50 complex. *Genes Dev* **13**: 1276–1288.
- Pellegrino S, Radzimanowski J, de Sanctis D, Boeri Erba E, McSweeney S, Timmins J. 2012. Structural and functional characterization of an SMC-like protein RecN: New insights into double-strand break repair. *Structure* **20**: 2076–2089.
- Pelletier H, Sawaya MR, Wolfle W, Wilson SH, Kraut J. 1996. Crystal structures of human DNA polymerase β complexed with DNA: Implications for catalytic mechanism, processivity, and fidelity. *Biochemistry* **35**: 12742–12761.
- Perry JJ, Yannone SM, Holden LG, Hitomi C, Asaithamby A, Han S, Cooper PM, Chen DJ, Tainer JA. 2006. WRN exonuclease structure and molecular mechanism imply an editing role in DNA end processing. *Nat Struct Mol Biol* **13**: 414–422.
- Pike AC, Shrestha B, Popuri V, Burgess-Brown N, Muzzolini L, Costantini S, Vindigni A, Gileadi O. 2009. Structure of the human RECQ1 helicase reveals a putative strand-separation pin. *Proc Natl Acad Sci* **106**: 1039–1044.
- Pitts SA, Kullar HS, Stankovic T, Stewart GS, Last JJ, Bedenham T, Armstrong SJ, Piane M, Chessa L, Taylor AM, et al. 2001. *hMRE11*: Genomic structure and a null mutation identified in a transcript protected from nonsense-mediated mRNA decay. *Hum Mol Genet* **10**: 1155–1162.

- Pokharel S, Campbell JL. 2012. Cross talk between the nuclease and helicase activities of Dna2: Role of an essential iron-sulfur cluster domain. *Nucleic Acids Res* **40**: 7821–7830.
- Prinz S, Amon A, Klein F. 1997. Isolation of *COM1*, a new gene required to complete meiotic double-strand break-induced recombination in *Saccharomyces cerevisiae*. *Genetics* **146**: 781–795.
- Quaiser A, Constantinesco F, White MF, Forterre P, Elie C. 2008. The Mre11 protein interacts with both Rad50 and the HerA bipolar helicase and is recruited to DNA following γ -irradiation in the archaeon *Sulfolobus acidocaldarius*. *BMC Mol Biol* **9**: 25.
- Reis CC, Batista S, Ferreira MG. 2012. The fission yeast MRN complex tethers dysfunctional telomeres for NHEJ repair. *EMBO J* **31**: 4576–4586.
- Sakurai S, Kitano K, Yamaguchi H, Hamada K, Okada K, Fukuda K, Uchida M, Ohtsuka E, Morioka H, Hakoishima T. 2005. Structural basis for recruitment of human flap endonuclease 1 to PCNA. *EMBO J* **24**: 683–693.
- Sartori AA, Lukas C, Coates J, Mistrik M, Fu S, Bartek J, Baer R, Lukas J, Jackson SP. 2007. Human CtIP promotes DNA end resection. *Nature* **450**: 509–514.
- Sato A, Mishima M, Nagai A, Kim SY, Ito Y, Hakoshima T, Jee JG, Kitano K. 2010. Solution structure of the HRDC domain of human Bloom syndrome protein BLM. *J Biochem* **148**: 517–525.
- Savitsky K, Bar-Shira A, Gilad S, Rotman G, Ziv Y, Vanagaite L, Tagle DA, Smith S, Uziel T, Sfez S, et al. 1995. A single ataxia telangiectasia gene with a product similar to PI-3 kinase. *Science* **268**: 1749–1753.
- Schaeper U, Subramanian T, Lim L, Boyd JM, Chinnadurai G. 1998. Interaction between a cellular protein that binds to the C-terminal region of adenovirus E1A (CtBP) and a novel cellular protein is disrupted by E1A through a conserved PLDLS motif. *J Biol Chem* **273**: 8549–8552.
- Schiller CB, Lammens K, Guerini I, Coords B, Feldmann H, Schlauderer F, Möckel C, Schele A, Strasser K, Jackson SP, et al. 2012. Structure of Mre11-Nbs1 complex yields insights into ataxia-telangiectasia-like disease mutations and DNA damage signaling. *Nat Struct Mol Biol* **19**: 693–700.
- Schmutte C, Marinescu RC, Sadoff MM, Guerrette S, Overhauser J, Fishel R. 1998. Human exonuclease I interacts with the mismatch repair protein hMSH2. *Cancer Res* **58**: 4537–4442.
- Shen B, Nolan JP, Sklar LA, Park MS. 1997. Functional analysis of point mutations in human flap endonuclease-1 active site. *Nucleic Acids Res* **25**: 3332–3338.
- Shibata A, Moiani D, Arvai AS, Perry J, Harding SM, Genois MM, Maity R, van Rossum-Fikkert S, Kertokallio A, Romoli F, et al. 2014. DNA double-strand break repair pathway choice is directed by distinct MRE11 nuclease activities. *Mol Cell* **53**: 7–18.
- Spycher C, Miller ES, Townsend K, Pavic L, Morrice NA, Jancsak P, Stewart GS, Stucki M. 2008. Constitutive phosphorylation of MDC1 physically links the MRE11-RAD50-NBS1 complex to damaged chromatin. *J Cell Biol* **181**: 227–240.
- Steitz TA, Steitz JA. 1993. A general two-metal-ion mechanism for catalytic RNA. *Proc Natl Acad Sci* **90**: 6498–6502.
- Stewart GS, Maser RS, Stankovic T, Bressan DA, Kaplan MI, Jaspers NG, Raams A, Byrd PJ, Petrini JH, Taylor AM. 1999. The DNA double-strand break repair gene *hMRE11* is mutated in individuals with an ataxia-telangiectasia-like disorder. *Cell* **99**: 577–587.
- Stracker TH, Morales M, Couto SS, Hussein H, Petrini JH. 2007. The carboxy terminus of NBS1 is required for induction of apoptosis by the MRE11 complex. *Nature* **447**: 218–221.
- Sutherland BM, Bennett PV, Sidorkina O, Laval J. 2000. Clustered DNA damages induced in isolated DNA and in human cells by low doses of ionizing radiation. *Proc Natl Acad Sci* **97**: 103–108.
- Swan MK, Legris V, Tanner A, Reaper M, Vial S, Bords R, Pollard JR, Charlton PA, Golec JMC, Bertrand A. 2014. Structure of human Bloom's syndrome helicase in complex with ADP and duplex DNA. *Acta Cryst* **70**: 1465–1475.
- * Symington LS. 2014. End resection at DNA double-strand breaks: Mechanism and regulation. *Cold Spring Harb Perspect Biol* doi: 10.1101/cshperspect.a016436.
- Szankasi P, Smith GR. 1992. A DNA exonuclease induced during meiosis of *Schizosaccharomyces pombe*. *J Biol Chem* **267**: 3014–3023.
- Szankasi P, Smith GR. 1995. A role for exonuclease I from *S. pombe* in mutation avoidance and mismatch correction. *Science* **267**: 1166–1169.
- Tauchi H, Kobayashi J, Morishima K, Matsuura S, Nakamura A, Shiraishi T, Ito E, Masnada D, Delia D, Komatsu K. 2001. The forkhead-associated domain of NBS1 is essential for nuclear foci formation after irradiation but not essential for hRAD50-hMRE11-NBS1 complex DNA repair activity. *J Biol Chem* **276**: 12–15.
- Thompson LH. 2012. Recognition, signaling, and repair of DNA double-strand breaks produced by ionizing radiation in mammalian cells: The molecular choreography. *Mutat Res* **751**: 158–246.
- Tishkoff DX, Boerger AL, Bertrand P, Filosi N, Gaida GM, Kane MF, Kolodner RD. 1997. Identification and characterization of *Saccharomyces cerevisiae* EXO1, a gene encoding an exonuclease that interacts with MSH2. *Proc Natl Acad Sci* **94**: 7487–7492.
- Tishkoff DX, Amin NS, Viars CS, Arden KC, Kolodner RD. 1998. Identification of a human gene encoding a homologue of *Saccharomyces cerevisiae* EXO1, an exonuclease implicated in mismatch repair and recombination. *Cancer Res* **58**: 5027–5031.
- Trenz K, Smith E, Smith S, Costanzo V. 2006. ATM and ATR promote Mre11 dependent restart of collapsed replication forks and prevent accumulation of DNA breaks. *EMBO J* **25**: 1764–1774.
- Trujillo KM, Sung P. 2001. DNA structure-specific nuclease activities in the *Saccharomyces cerevisiae* Rad50-Mre11 complex. *J Biol Chem* **276**: 35458–35464.
- Trujillo KM, Yuan SS, Lee EY, Sung P. 1998. Nuclease activities in a complex of human recombination and DNA repair factors Rad50, Mre11, and 95. *J Biol Chem* **273**: 21447–21450.
- Trujillo KM, Roh DH, Chen L, Van Komen S, Tomkinson A, Sung P. 2003. Yeast xrs2 binds DNA and helps target rad50 and mre11 to DNA ends. *J Biol Chem* **278**: 48957–48964.

C.B. Schiller et al.

- Truong LN, Li Y, Shi LZ, Hwang PY, He J, Wang H, Razavian N, Berns MW, Wu X. 2013. Microhomology-mediated end joining and homologous recombination share the initial end resection step to repair DNA double-strand breaks in mammalian cells. *Proc Natl Acad Sci* **110**: 7720–7725.
- Tsubouchi H, Ogawa H. 2000. Exo1 roles for repair of DNA double-strand breaks and meiotic crossing over in *Saccharomyces cerevisiae*. *Mol Biol Cell* **11**: 2221–2233.
- Tsukamoto Y, Mitsuoka C, Terasawa M, Ogawa H, Ogawa T. 2005. Xrs2p regulates Mre11p translocation to the nucleus and plays a role in telomere elongation and meiotic recombination. *Mol Biol Cell* **16**: 597–608.
- Tsutakawa SE, Tainer JA. 2012. Double strand binding-single strand incision mechanism for human flap endonuclease: Implications for the superfamily. *Mech Ageing Dev* **133**: 195–202.
- Tsutakawa SE, Classen S, Chapados BR, Arvai AS, Finger LD, Guenther G, Tomlinson CG, Thompson P, Sarker AH, Shen B, et al. 2011. Human flap endonuclease structures, DNA double-base flipping, and a unified understanding of the FEN1 superfamily. *Cell* **145**: 198–211.
- Uchisaka N, Takahashi N, Sato M, Kikuchi A, Mochizuki S, Imai K, Nonoyama S, Ohara O, Watanabe F, Mizutani S, et al. 2009. Two brothers with ataxia-telangiectasia-like disorder with lung adenocarcinoma. *J Pediatr* **155**: 435–438.
- Usui T, Ohta T, Oshiumi H, Tomizawa J, Ogawa H, Ogawa T. 1998. Complex formation and functional versatility of Mre11 of budding yeast in recombination. *Cell* **95**: 705–716.
- van Noort J, van Der Heijden T, de Jager M, Wyman C, Kanaar R, Dekker C. (2003). The coiled-coil of the human Rad50 DNA repair protein contains specific segments of increased flexibility. *Proc Natl Acad Sci* **100**: 7581–7586.
- Varon R, Vissinga C, Platzer M, Cerosaletti KM, Chrzanowska KH, Saar K, Beckmann G, Seemanova E, Cooper PR, Nowak NJ, et al. 1998. Nibrin, a novel DNA double-strand break repair protein, is mutated in Nijmegen breakage syndrome. *Cell* **93**: 467–476.
- Vindigni A, Hickson ID. 2009. RecQ helicases: Multiple structures for multiple functions? *HFSP J* **3**: 153–164.
- Vindigni A, Marino F, Gileadi O. 2010. Probing the structural basis of RecQ helicase function. *Biophys Chem* **149**: 67–77.
- Walker JR, Corpina RA, Goldberg J. 2001. Structure of the Ku heterodimer bound to DNA and its implications for double-strand break repair. *Nature* **412**: 607–614.
- Waltes R, Kalb R, Gatei M, Kijas AW, Stumm M, Sobeck A, Wieland B, Varon R, Lerenthal Y, Lavin MF, et al. 2009. Human RAD50 deficiency in a Nijmegen breakage syndrome-like disorder. *Am J Hum Genet* **84**: 605–616.
- Wang Y, Cortez D, Yazdi P, Neff N, Elledge SJ, Qin J. 2000. BASC, a super complex of BRCA1-associated proteins involved in the recognition and repair of aberrant DNA structures. *Genes Dev* **14**: 927–939.
- Wang Y, Juranek S, Li H, Sheng G, Wardle GS, Tuschl T, Patel DJ. 2009. Nucleation, propagation and cleavage of target RNAs in Ago silencing complexes. *Nature* **461**: 754–761.
- Wang H, Shao Z, Shi LZ, Hwang PY, Truong LN, Berns MW, Chen DJ, Wu X. 2012. CtIP protein dimerization is critical for its recruitment to chromosomal DNA double-stranded breaks. *J Biol Chem* **287**: 21471–21480.
- Wei T, Zhang S, Zhu S, Sheng D, Ni J, Shen Y. 2008. Physical and functional interaction between archaeal single-stranded DNA-binding protein and the 5′-3′ nuclease NurA. *Biochem Biophys Res Commun* **367**: 523–529.
- Wei T, Zhang S, Hou L, Ni J, Sheng D, Shen Y. 2011. The carboxyl terminal of the archaeal nuclease NurA is involved in the interaction with single-stranded DNA-binding protein and dimer formation. *Extremophiles* **15**: 227–234.
- Westmoreland JW, Resnick MA. 2013. Coincident resection at both ends of random, γ-induced double-strand breaks requires MRX (MRN), Sae2 (Ctp1), and Mre11-nuclease. *PLoS Genet* **9**: e1003420.
- Wigley DB. 2013. Bacterial DNA repair: Recent insights into the mechanism of RecBCD, AddAB and AdnAB. *Nat Rev Microbiol* **11**: 9–13.
- Williams RS, Moncalian G, Williams JS, Yamada Y, Limbo O, Shin DS, Grocock LM, Cahill D, Hitomi C, Guenther G, et al. 2008. Mre11 dimers coordinate DNA end bridging and nuclease processing in double-strand-break repair. *Cell* **135**: 97–109.
- Williams RS, Dodson GE, Limbo O, Yamada Y, Williams JS, Guenther G, Classen S, Glover JN, Iwasaki H, Russell P, et al. 2009. Nbs1 flexibly tethers Ctp1 and Mre11-Rad50 to coordinate DNA double-strand break processing and repair. *Cell* **139**: 87–99.
- Wilson DM III, Carney JP, Coleman MA, Adamson AW, Christensen M, Lamerdin JE. 1998. Hex1: A new human Rad2 nuclease family member with homology to yeast exonuclease 1. *Nucleic Acids Res* **26**: 3762–3768.
- Wiltzius JJ, Hohl M, Fleming JC, Petrini JH. 2005. The Rad50 hook domain is a critical determinant of Mre11 complex functions. *Nat Struct Mol Biol* **12**: 403–407.
- Wong AK, Ormonde PA, Pero R, Chen Y, Lian L, Salada G, Berry S, Lawrence Q, Dayananth P, Ha P, et al. 1998. Characterization of a carboxy-terminal BRCA1 interacting protein. *Oncogene* **17**: 2279–2285.
- Wu L, Luo K, Lou Z, Chen J. 2008. MDC1 regulates intra-S-phase checkpoint by targeting NBS1 to DNA double-strand breaks. *Proc Natl Acad Sci* **105**: 11200–11205.
- Wu P, Takai H, De Lange T. 2012. Telomeric 3′ overhangs derive from resection by Exo1 and apollo and fill-in by POT1b-associated CST. *Cell* **150**: 39–52.
- Xu YN, Bazeille N, Ding XY, Lu XM, Wang PY, Bugnard E, Grondin V, Dou SX, Xi XG. 2012a. Multimeric BLM is dissociated upon ATP hydrolysis and functions as monomers in resolving DNA structures. *Nucleic Acids Res* **40**: 9802–9814.
- Xu Z, Zan H, Pone EJ, Mai T, Casali P. 2012b. Immunoglobulin class-switch DNA recombination: Induction, targeting and beyond. *Nat Rev Immunol* **12**: 517–531.
- Xue Y, Ratcliff GC, Wang H, Davis-Searles PR, Gray MD, Erie DA, Redinbo MR. 2002. A minimal exonuclease

Structural Mechanisms of Recombination

- domain of WRN forms a hexamer on DNA and possesses both 3'-5' exonuclease and 5'-protruding strand endonuclease activities. *Biochemistry* **41**: 2901–2912.
- Yang W, Hendrickson WA, Crouch RJ, Satow Y. 1990. Structure of ribonuclease H phased at 2 Å resolution by MAD analysis of the selenomethionyl protein. *Science* **249**: 1398–1405.
- Yeeles JT, Cammack R, Dillingham MS. 2009. An iron-sulfur cluster is essential for the binding of broken DNA by AddAB-type helicase-nucleases. *J Biol Chem* **284**: 7746–7755.
- Yoshida T, Claverie JM, Ogata H. 2011. Mimivirus reveals Mre11/Rad50 fusion proteins with a sporadic distribution in eukaryotes, bacteria, viruses and plasmids. *Virol J* **8**: 427.
- You Z, Chahwan C, Bailis J, Hunter T, Russell P. 2005. ATM activation and its recruitment to damaged DNA require binding to the C terminus of Nbs1. *Mol Cell Biol* **25**: 5363–5379.
- Yu X, Wu LC, Bowcock AM, Aronheim A, Baer R. 1998. The C-terminal (BRCT) domains of BRCA1 interact in vivo with CtIP, a protein implicated in the CtBP pathway of transcriptional repression. *J Biol Chem* **273**: 25388–25392.
- Yu X, Chini CC, He M, Mer G, Chen J. 2003. The BRCT domain is a phospho-protein binding domain. *Science* **302**: 639–642.
- Yuan J, Chen J. 2009. N terminus of CtIP is critical for homologous recombination-mediated double-strand break repair. *J Biol Chem* **284**: 31746–31752.
- Zahra R, Blackwood JK, Sales J, Leach DR. 2007. Proofreading and secondary structure processing determine the orientation dependence of CAG-CTG trinucleotide repeat instability in *Escherichia coli*. *Genetics* **176**: 27–41.
- Zhang S, Wei T, Hou G, Zhang C, Liang P, Ni J, Sheng D, Shen Y. 2008. Archaeal DNA helicase HerA interacts with Mre11 homologue and unwinds blunt-ended double-stranded DNA and recombination intermediates. *DNA Repair* **7**: 380–391.
- Zhu J, Petersen S, Tessarollo L, Nussenzweig A. 2001. Targeted disruption of the Nijmegen breakage syndrome gene NBS1 leads to early embryonic lethality in mice. *Curr Biol* **11**: 105–109.
- Zhu Z, Chung WH, Shim EY, Lee SE, Ira G. 2008. Sgs1 helicase and two nucleases Dna2 and Exo1 resect DNA double-strand break ends. *Cell* **134**: 981–994.
- * Zickler D, Kleckner N. 2014. Recombination, pairing, and synapsis of homologs during meiosis. *Cold Spring Harb Perspect Biol* doi: 10.1101/cshperspect.a016626.

3. Discussion

All living organisms have developed mechanisms to protect their genome from DNA damage. During these repair pathways DNA lesions are recognized and repaired to ensure genome integrity. DNA double strand breaks (DSBs) are the most threatening DNA lesions by disrupting the whole DNA duplex. Un- or misrepaired DSBs can induce cell death, chromosomal rearrangements or mutations, which cause carcinogenesis in humans (Myung *et al.* 2001a, Myung *et al.* 2001b, Hanahan and Weinberg 2011). The major pathways to repair DSBs are canonical non-homologous end joining (c-NHEJ), alternative NHEJ (alt-NHEJ) or microhomology-mediated end joining (MMEJ) and homologous recombination (HR). The eukaryotic Mre11-Rad50-Nbs1 (MRN) complex plays an important role during these repair pathways. In MMEJ and HR, MRN senses DSBs and initiates the resection of the DNA end (Chiruvella *et al.* 2013). Further, MRN recruits other repair factors to DSB sites and stimulates the cell cycle checkpoint (Assenmacher and Hopfner 2004, Williams *et al.* 2010). When this work was started no crystal structure of eukaryotic Rad50 was available and little was known about its interaction with Mre11 or DNA. The aim of this project was to analyze the architecture and the function of the eukaryotic MR(N) complex on DNA binding.

In this work, different MRN subcomplexes from the eukaryotic organism *Chaetomium thermophilum* (Ct) were recombinantly expressed and purified. After crystallization, the structure of the dimeric CtMre11 catalytic domain (CtMre11^{CD}) and the dimerized CtRad50 nucleotide-binding domain (CtRad50^{NBD}) in complex with the C-terminal Rad50-binding domain of CtMre11 (CtMre11^{RBD}) were solved. Subsequently, the structure of dimeric CtRad50^{NBD} in complex with double stranded DNA (dsDNA) was determined. Based on these structural information biochemical experiments were performed. To investigate the function of MRN *in vivo*, the effects of budding yeast *Rad50* mutations were analyzed by plate survival assays under DNA damaging conditions.

3.1 Eukaryotic CtMre11^{CD} and CtMre11^{RBD}-CtRad50^{NBD} crystal structures

The presented results give new insights into the architecture of the eukaryotic MR(N) complex. The crystal structures of CtMre11^{CD} and CtMre11^{RBD}-CtRad50^{NBD} (CtM^{RBD}R^{NBD}) from *C. thermophilum* reveal new features of the eukaryotic MR(N) complex and explain the mode of binding between Mre11 and Rad50.

3.1.1 Crystal structure of the catalytic domain of CtMre11

For structural information about the *C. thermophilum* MR(N) complex, the structure of the catalytic domain of CtMre11 was determined. In the CtMre11^{CD} structure the complete eukaryotic insertion loops were modeled into the electron density (Chapter 2.1, Figure 1). The overall architecture is similar to the Nbs1-bound *Schizosaccharomyces pombe* Mre11^{CD} (SpMre11^{CD}-Nbs1) crystal structure. However, the CtMre11^{CD} structure is even more compact due to a slight movement of the capping domain towards the nuclease active site. Interestingly, the eukaryotic specific insertion loops are ordered in a similar fashion like in SpMre11^{CD}-Nbs1 (Seifert *et al.* 2015). In the SpMre11^{CD}-Nbs1 structure the Nbs1 peptide interacts with and stabilizes the eukaryotic insertion loops (Schiller *et al.* 2012). In the CtMre11^{CD} the Nbs1-binding site of the SpMre11^{CD}-Nbs1 structure is occupied by symmetry related molecules and the ordering of these insertion loops could additionally be stabilized by crystal packing. The dimer interface is characterized by mainly hydrophobic interactions between helices $\alpha 2$ and $\alpha 3$ of each protomer, hydrogen bonds with Arg66 as well as interactions between the eukaryotic insertion loops. The larger dimer interface, compared to archaeal Mre11, indicates a stronger interaction between the CtMre11 protomers (Seifert *et al.* 2015). The recently found *MRE11* mutation in a PMA (progressive myoclonic ataxia) patient leads to a substitution of Ala for Val at position 47, which could disturb the interaction between Nbs1 and Mre11 (Miyamoto *et al.* 2014). The amino acid (aa) substitution is located in helix $\alpha 1$ where in the SpMre11^{CD}-Nbs1 crystal structure an interaction between this helix and the Nbs1 fragment has been identified (PDB code 4FBK) (Schiller *et al.* 2012). However, the interacting Arg518 is replaced by Leu in human Nbs1. Additionally, cells from this PMA patient show decreased MRN expression levels (Miyamoto *et al.* 2014).

Interestingly, the human Mre11^{CD} crystal structure represents a different conformation of the dimer interface. Thereby, the helices $\alpha 2$ and $\alpha 3$ do not form the characteristic hydrophobic dimerization domain, but the dimer is stabilized by a disulfide bond between Cys146 of each protomer (Park *et al.* 2011). Further, the interaction between the eukaryotic insertion loops from each protomer is disturbed compared to the CtMre11^{CD} structure (Seifert *et al.* 2015). It is also unclear how Nbs1 is able to bridge the dimer interface in the conformation of the human Mre11^{CD} structure.

Very recently, it was reported that mutations in the *MRE11* yeast gene suppress the effect of CtIP (*Sae2*) deletion on DNA damage repair *in vivo*. One mutation is located in the eukaryotic specific insertion loop and probably decreases the interaction between Mre11 and Nbs1 (Xrs2) (Chen *et al.* 2015). Thereby, the mutated Pro110 corresponds to Pro110 in CtMre11 and Pro119 in SpMre11, which forms a hydrogen bond with Lys526 from SpNbs1 (Schiller *et al.* 2012). Since Nbs1 stimulates DNA unwinding and DNA binding of MRN, the reported mutation might suppress these effects (Paull and Gellert 1999, Trujillo *et al.* 2003). Interestingly, the mutation and the resulting suppression of the *sae2Δ* phenotype are independent of the Mre11 nuclease activity. Additional experiments indicate that independent of the Mre11 nuclease, CtIP is important for the removal of MRN (MRX) from DSBs (Chen *et al.* 2015). However, *in vitro* experiments showed that CtIP (*Sae2*) promotes the endonucleolytic cut by MRN (Cannavo and Cejka 2014). Together, these studies reveal two functions of the CtIP(*Sae2*)-MRN interaction. One is the initiation of resection and the other function is the removal of MRN from DSBs. Considering the fact that yeast CtIP (*Sae2*) itself shows endonuclease activity *in vitro*, more detailed research is needed to unravel this MRN-CtIP pathway (Lengsfeld *et al.* 2007).

3.1.2 Crystal structure of dimeric CtMre11^{RBD}-CtRad50^{NBD}

The crystal structure of ATP γ S bound CtMre11^{RBD}-CtRad50^{NBD} (CtM^{RBD}R^{NBD}) reveals interesting features of the eukaryotic MR(N) complex. The CtRad50^{NBD} structure represents the characteristic overall shape of Rad50^{NBD} known from other prokaryotic crystal structures (Hopfner *et al.* 2000b, Lammens *et al.* 2011, Williams *et al.* 2011). It is characterized by the globular domain, which consists of interacting Rad50 N- and C-terminus, and the truncated coiled-coil (CC) domain. The non-hydrolysable ATP analog

ATP γ S and the magnesium ion are bound between the conserved Walker A, Walker B and signature motifs (Chapter 2.2, Figure 1). Based on the crystal structure of the CtRad50^{NBD} dimer, six eukaryotic insertions are recognized in comparison to prokaryotic Rad50^{NBD} (Chapter 2.2, Figure 2).

Another interesting characteristic of the CtRad50^{NBD} structure is a very sulfur rich cluster in close proximity to the ATPase domain. This cluster contains four methionines (Met166, Met1194, Met1201 and Met1203) and one cysteine (Cys1207). Whether the oxidation state of these residues plays an important role for the DNA repair under oxidative stress conditions has to be investigated intensively. Since ATM gets activated by oxidative stress, the same could be true for the MRN complex (Paull 2015). From these five residues the Met1194, Met1203, Cys1207 are conserved in eukaryotes and in some eukaryotes Met166 and Met1201 are replaced by other hydrophobic amino acids. Thus, the cluster forms a very hydrophobic area, which also could play a more structural than a regulatory role.

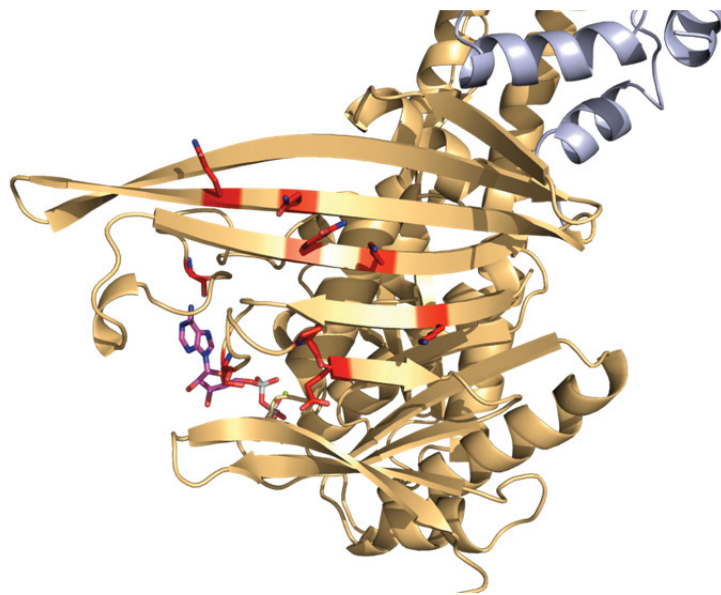


Figure 10: Crystal structure of CtM^{RBD}-R^{NBD} protomer (M^{RBD}: blue; R^{NBD}: light orange) with highlighted *rad50S* mutations (red). ATP γ S (magenta/gray) and the magnesium ion (green) are depicted.

Previously, the description of *rad50S* (separation-of-function) mutations in yeast revealed an impaired meiotic recombination phenotype but show no survival effect under DNA damaging conditions. The *rad50S* mutations are located in lobe I and are mostly found in

the surface exposed β -sheets β 1, β 2, β 4 and β 5. These mutations consist of Lys6Glu, Ser14Pro, Arg20Met, Glu21Lys, Val63Glu, Gln79Lys, Lys81Ile, Asn97Asp and Gln99Lys in yeast which correspond to residues Lys6, Ser14, P20, Glu21, Ala64, Gln80, Lys82, Asn98 and Gln100 in CtRad50 (Figure 10) (Alani *et al.* 1990). Whether the mutated residues are necessary for the interaction with meiotic recombination factors or whether they play a regulatory function in MRN, has to be investigated in future studies. Also the partly substitution of hydrophobic residues by polar or charged amino acids and vice versa, makes it more difficult to predict a structural function of the *rad50S* mutations.

3.1.3 Comparison between CtRad50^{NBD} and prokaryotic Rad50^{NBD} structures

Comparison with dimerized prokaryotic Rad50^{NBD} crystal structures reveals six insertions in the eukaryotic CtRad50^{NBD}. These insertions and the elongated C-terminus of CtRad50^{NBD} enlarge the surface exposed area of the protein. Insertion I is located in β -sheet β 1 and consists of amino acids 17–19. Insertion II is located near the CtRad50^{NBD} dimer interface. It is close to the ATP binding Walker A domain and its conformation might be regulated by the nucleotide state. Previous results from archaeal MR show that this region (Leu51–Arg67 in *Pyrococcus furiosus* Rad50; corresponding to Leu55–Lys75 in CtRad50) undergoes structural rearrangements upon ATP binding (Williams *et al.* 2011). Insertion III enlarges β -sheet β 6 and thereby especially residues Arg105, Lys108, Arg109 increase the positively charged area in the dimer groove. Insertion IV is the largest eukaryotic insertion. It forms a large hairpin structure that consists of β -sheets β 8 and β 9. It is located adjacent to the Rad50 CCs and contains a relatively conserved YNYR motif afterwards. Whether insertion IV plays a role in the CC orientation or the YNYR motif is functionally important, has to be analyzed. Additionally, insertion V elongates helix α J by five residues and is located in the same area like Insertion VI and the elongated Rad50 C-terminus.

3.1.4 The C-terminal CtMre11 Rad50-binding domain

At the beginning of this work the eukaryotic mode of binding between Mre11 and Rad50 was unclear. Prokaryotic structures of the Rad50^{NBD} bound to the Mre11^{RBD} reported an

interaction between the base of the Rad50 CCs and two or three helices in the Mre11 C-terminal region. The structure of CtM^{RBD}R^{NBD} revealed a large C-terminal Mre11^{RBD} consisting of five α -helices. This domain interacts with the CtRad50 CCs and the interactions are facilitated by mainly hydrophobic residues. The C-terminus of Mre11^{RBD} points towards the globular domain of the dimerized CtRad50^{NBD} (Chapter 2.2, Figure 1). Interestingly, a mutation in this Mre11^{RBD} has been found in an ATLD patient, which indicates functional importance of the RBD (Delia *et al.* 2004). The conformation of the Mre11^{RBD} might also be important for the function of MRN, since the Mre11 C-terminus is able to interact with DNA and is playing an important role in meiotic recombination (Furuse *et al.* 1998, Usui *et al.* 1998, Bhattacharyya *et al.* 2008). A sequence alignment of the Mre11^{RBD} reveals less conservation among eukaryotes, which makes it more difficult to predict functional important residues (Chapter 2.2, supplementary Figure S2). According to the Mre11^{RBD}-Rad50^{NBD} (M^{RBD}R^{NBD}) crystal structures from *P. furiosus* and *Methanocaldococcus jannaschii*, the first α -helix in the RBD is not present in *P. furiosus* M^{RBD}R^{NBD}. Additionally, in the *Thermotoga maritima* (Tm) and *M. jannaschii* (Mj) MR^{NBD} crystal structures the CCs are disturbed at the position where Mre11 interacts with Rad50 (Lim *et al.* 2011, Möckel *et al.* 2012). However, the *C. thermophilum* and *P. furiosus* M^{RBD}R^{NBD} structures reveal continuous α -helices in this region (Williams *et al.* 2011) (Chapter 2.2, Figure 2).

3.2 Eukaryotic MR(N) and ATP-dependent conformational changes

The presented results enable the modeling of a eukaryotic MR(N) complex in ATP-bound and ATP-free state.

3.2.1 Eukaryotic MR(N) model

The CtM^{RBD}R^{NBD} structure and the CtMre11^{CD} structure can be aligned onto the ATP γ S bound MR^{NBD} structure from *M. jannaschii* (Lim *et al.* 2011). In this model the CtRad50^{NBD} fits into the CtMre11^{CD} dimer active site. Also the close proximity of the capping domain C-terminus and the N-terminus of the CtMre11^{RBD} support this model and there is enough space for the 25 amino acid (aa) linker between the two domains. However, structural information about the very C-terminus of Mre11, which follows the

RBD, is missing so far. In the ATP-bound CtMre11^{CD;RBD}-Rad50^{NBD} (CtM^{CD;RBD}R^{NBD}) model the eukaryotic insertions V, VI and the elongated C-terminus are located close to the Mre11 subunit (Chapter 2.2, Figure 2, 3A). The functional importance of this enlarged interface has to be analyzed. In the ATP-bound CtM^{CD;RBD}R^{NBD} model, the C-terminus of the Mre11^{RBD} points towards the catalytic domain of CtMre11 (Figure 11). Since the C-terminal part of budding yeast Mre11 is important for meiotic recombination and DNA binding (Furuse *et al.* 1998, Usui *et al.* 1998, Bhattacharyya *et al.* 2008), the Mre11 C-terminus could be localized in the globular head module of MR(N). Thereby, the very C-terminus of Mre11 might play a structural as well as a functional role.

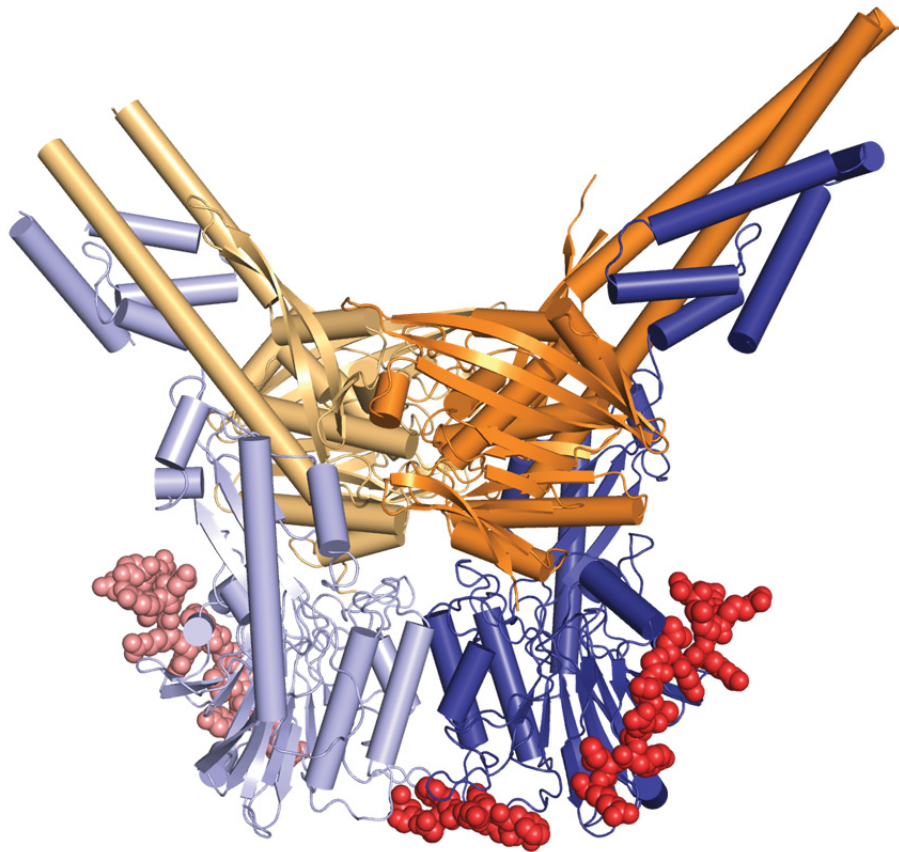


Figure 11: Docking model of MRN head complex in ATP-bound state. SpMre11^{CD}-Nbs1 (PDB: 4FBW) was aligned onto CtMre11 in the CtMre11^{CD;RBD}-Rad50^{NBD} model. CtMre11-Rad50^{NBD} (Mre11: light and dark blue; Rad50: light and dark orange) and SpNbs1 (red and light red) are depicted.

With the results from the SpMre11^{CD}-Nbs1 crystal structure we are able to predict the Nbs1 peptide in this ATP-bound conformation (Figure 11). However, since Rad50 is

absent in the SpMre11^{CD}-Nbs1 structure, it is unclear if the ATP state and the Rad50 conformation influence the binding of Nbs1 to Mre11.

3.2.2 ATP-dependent conformational changes of eukaryotic MR(N)

Based on studies with bacterial MR, it is possible to align the CtMre11^{CD} and CtRad50^{NBD} structures onto the “closed” ATP-bound MjMre11-Rad50^{NBD} and the “open” ATP-free TmMre11-Rad50^{NBD} structures (Figure 12) (Lammens *et al.* 2011, Lim *et al.* 2011).

SAXS (small angle X-ray scattering) data reveal that in the purified CtMR^{hc} (Mre11 aa 1–567; Rad50 aa 1–224-GGAGGAGG-1099–1315) complex, the maximum distance between the particles in the protein (D_{max}) decreases upon addition of ATPγS. The shape of the scattering curve and the particle distance (P(r)) distribution curve indicate a more globular protein, induced by ATPγS. Without ATP analog the shape of the curve is probably influenced by elongated and more globular complexes in the sample because for Rad50 dimerization and ATP binding the protomers have to be in close proximity as well.

Chemical cross-linking of the MRN head complex (Mre11 aa 1–567; Rad50 aa 1–214-GGAGGAGG-1109–1315; Nbs1 aa Met-565–714) with the lysine specific cross-linker DSS (disuccinimidyl suberate) in the presence of ATPγS resulted in one cross-linked protein band with the approximate molecular weight of the MRN head complex. Due to the specific length of DSS, identification of the cross-linked lysine residues by mass spectrometry enabled the localization of domains in close proximity. The Nbs1 peptide could not be localized in respect to the MR complex because of missing structural information but probably also because of high flexibility. However, from the data it could be concluded that the ATP-bound Rad50^{NBD} dimer is localized in the Mre11 nuclease active site (Chapter 2.2, Figure 3 and supplementary Figure S3).

The ATP-free state of TmMR^{NBD} (Lammens *et al.* 2011) indicates an extreme conformation of the complex and various flexible intermediate conformations are expected in solution (Figure 12). This ATP-dependent conformational rearrangement was shown for the bacterial and archaeal MR complex (Lammens *et al.* 2011, Williams *et al.* 2011, Möckel *et al.* 2012). Since the Mre11 binding domain of Nbs1 is accessible in the “open” and “closed” conformation, it is unclear how Nbs1 is able to stimulate the DNA

binding affinity as well as DNA unwinding on a structural level (Paull and Gellert 1999, Trujillo *et al.* 2003).

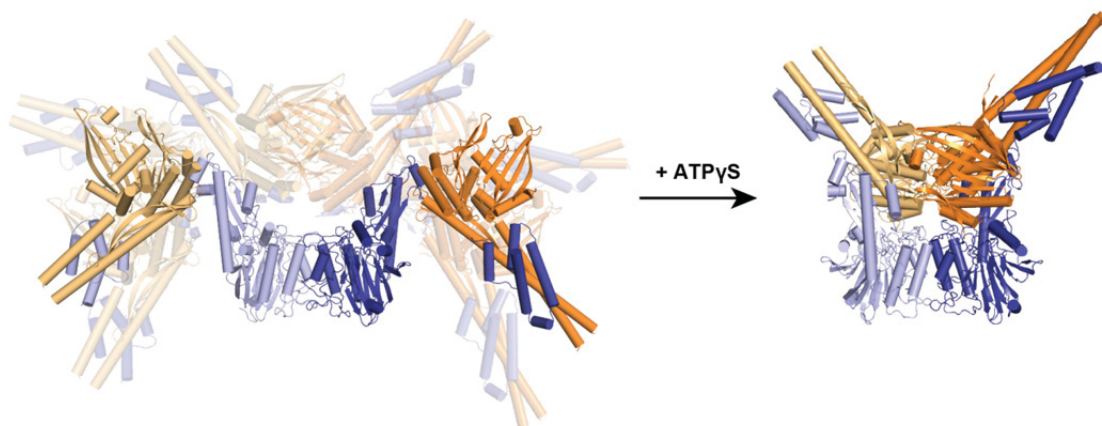


Figure 12: Models of the ATP-free “open” and ATP-bound “closed” CtMR^{NBD} complex. CtMre11^{CD} dimer was aligned onto the TmMre11 or MjMre11 crystal structures for the open and closed MR model, respectively. CtRad^{NBD} protomers were aligned onto each TmRad50 protomer in the open conformation and the dimeric CtRad50^{NBD} was aligned onto the archaeal MjRad50^{NBD} dimer in the ATPγS-bound MjMR^{NBD} structure (Lammens *et al.* 2011, Lim *et al.* 2011).

3.3 Structure of CtRad50^{NBD}-DNA and comparison with DNA-free CtRad50^{NBD} and TmRad50^{NBD}-DNA crystal structures

During this work the crystal structures of dimeric TmRad50^{NBD}-DNA and dimeric CtRad50^{NBD} with and without bound dsDNA were solved.

3.3.1 The CtRad50^{NBD}-DNA crystal structure

The presented crystal structure explains the mode of binding of dsDNA to CtRad50^{NBD} (CtRad50^{NBD}-DNA). In the crystal the dsDNA density builds a pseudo-continuous DNA helix, in which no clear DNA end is detectable. The DNA is located in the positively charged Rad50 dimer groove between the two CCs. The Rad50 dimer binds symmetrically to a DNA duplex with a length of approximately 18 base pairs (Chapter 2.2, Figure 4 and supplementary Figure S4). This structure explains the importance of ATP for the positioning of lobe I and II, the dimer conformation and the assembly of the four DNA binding motifs on each side of the Rad50 dimer (Chapter 2.2, Figure 5).

In the past, it was reported that in the presence of a non-hydrolysable ATP analog the human MR complex preferentially binds to DNA with a 3' overhang (de Jager *et al.* 2002). Under these conditions the Mre11 DNA binding groove is probably blocked by the dimerized Rad50^{NBD} and thus the DNA interacts with Rad50. The here presented results from *in vitro* DNA binding assays further confirm the preferred binding to 3' DNA overhangs by Rad50 (Chapter 2.2). With the CtRad50^{NBD}-DNA crystal structure it is now able to explain this interesting characteristic. By denoting the strand polarity as the direction from the center towards the outside, the protein interacts and stabilizes the 3'→5' DNA strand close to the center of the Rad50 dimer. But the 5'→3' strand makes only protein contacts with the β -sheet β 6 on the outer side of the Rad50 dimer. This DNA interaction in the center of the Rad50 dimer probably explains the increased affinity to DNA with 3' overhangs than for 5' overhangs. Using DNA with complementary 3' overhangs the stabilized overhangs are able to anneal in the center of the Rad50 dimer. This fact seems to result in a dissociation constant similar to continuous 35bp dsDNA, which bridges the whole Rad50 dimer. Consistent with this observation, it was reported that Rad50 facilitates DNA bridging to enable DNA end-joining *in vitro*. Thereby, DNA with complementary 3' overhangs was incubated with MR and the ligation efficiency was ATP-dependent (Deshpande *et al.* 2014).

Altogether, these experiments indicate an important function of Rad50 for DNA tethering and end-joining, but the role of Rad50 DNA binding during c-NHEJ or MMEJ *in vivo* has to be analyzed further.

3.3.2 Comparison between CtRad50^{NBD}-DNA and DNA-free CtRad50^{NBD}

Comparison of the DNA-free and DNA-bound CtRad50^{NBD} structures reveal minor changes in the protein conformation. The positively charged dimer groove between the CCs is also present when DNA is absent. This explains why ATP or non-hydrolysable ATP analogs increase the DNA affinity of Rad50 dramatically (Rojowska *et al.* 2014). Comparison of the CtRad50^{NBD} and the CtRad50^{NBD}-DNA structures reveals a structural rearrangement of the CCs (Chapter 2.2, supplementary Figure S4). Nevertheless, with *P. furiosus* Rad50 it has been shown that dependent on the crystal packing, the CCs can adopt different conformations within the same organism (Williams *et al.* 2011). In the DNA-free CtRad50^{NBD} structure the Mre11^{RBD} is bound to the CCs. However, it is

unclear whether the DNA or the absence of the Mre11^{RBD} in the CtRad50^{NBD}-DNA crystal structure influences the CC orientation.

3.3.3 Comparison with the TmRad50^{NBD}-DNA structure

In *T. maritima* Rad50^{NBD} (TmRad50^{NBD}), dsDNA also binds to the dimer groove. The crystal structure of DNA-bound TmRad50^{NBD} explains the binding mode of dsDNA to some parts of Rad50. Although *in vitro* experiments showed that ATP or non-hydrolysable ATP analogs increase the affinity to DNA and the positively charged groove spans the whole dimer, the DNA interacts with only one Rad50 protomer in the crystal structure. The DNA binding domain in the second protomer is occupied by symmetry related TmRad50^{NBD}-DNA molecules (Chapter 2.3) (Rojowska *et al.* 2014). The DNA conformation also might represent a transient state, in which DNA first binds to one lobe and then is guided towards the dimer groove to interact with the second protomer. Thereby, the CtRad50^{NBD}-DNA structure represents the state, in which both protomers interact with the DNA.

3.4 Plate survival assay with *Saccharomyces cerevisiae* Rad50 mutants

Different *S. cerevisiae* Rad50 mutants resulted in growth defects on genotoxic agents like the topoisomerase I inhibitor camptothecin (CPT), the ribonucleotide reductase inhibitor hydroxyurea (HU) or the DNA strand break inducer bleomycin (Bleo).

According to the crystal structure of CtRad50^{NBD}-DNA, the mutated residues K103^{ScE}, K104^{ScE} and N190^{ScD} (corresponding to Q104^{Ct}, R105^{Ct} and N191^{Ct}, respectively) do not make direct contacts with the DNA and show a similar growth phenotype like wild-type Rad50. These residues together with the major groove located R132^{Sc} (R131^{Ct}), which forms the DNA binding motif II, seem to play a minor role in DNA damage response (Chapter 2.2 and 2.3) (Rojowska *et al.* 2014). Additionally, the major DNA contacts in the DNA binding motif I are characterized by interactions with the protein main chain of β -sheet $\beta 6$ in CtRad50^{NBD}-DNA (Chapter 2.2, Figure 5). The mutations K60^{ScE} (R61^{Ct}) in the DNA binding motifs III and R1205^{ScE} (R1208^{Ct}) result in growth defects in the presence of camptothecin. Interestingly, inhibition of Rad50 dimerization by the

S1205^{Sc}R (S1208^{Ct}) mutation shows the same growth defect on genotoxic agents like the E1235^{Sc}Q (E1238^{Ct}) mutation, which inhibits ATP hydrolysis. These results highlight the importance of the properly assembled Rad50 dimer groove for DNA binding and damage repair.

Since newly replicated chromosome ends represent a blunt DNA end on the leading strand, this has to be processed to prevent genome instability. The presented telomere maintenance experiment reveals the effect of Rad50 mutants in budding yeast. By mutating residues, which are important for DNA binding in the TmRad50 dimer groove *in vitro*, the mutations K103^{Sc}E, K104^{Sc}E, R131^{Sc}E, K103^{Sc}E+R131^{Sc}E, K104^{Sc}E+R131^{Sc}E and R1201^{Sc}E reduce telomere lengths. Also the S1205^{Sc}R mutation, which disturbs Rad50 dimerization and thus decreases DNA binding, results in shorter telomeres. Interestingly, inhibition of ATP hydrolysis by the E1235^{Sc}Q mutation, which stabilizes the Rad50 dimer conformation, leads to the same telomere length like the wild-type strain. In contrast, this E1235^{Sc}Q mutant shows severe effects on DNA repair (Chapter 2.3, Figure 4) (Rojowska *et al.* 2014).

Taken together, these *in vivo* experiments with *S. cerevisiae rad50* mutants show that the ATPase activity of MR(N) is essential for DNA repair. Thereby, binding of DNA to the Rad50 dimer groove but also ATP hydrolysis, which enables access to the Mre11 active site or DNA unwinding, are important. In contrast, the closed ATP-bound MR(N) conformation seems to be sufficient for telomere maintenance.

3.5 Model of the ATP-dependent conformations of the eukaryotic MRN complex

Using the presented MR crystal structures from *C. thermophilum* together with previous structural information about MR(N), it is possible to generate a DNA binding model for the eukaryotic MR(N) complex in ATP-bound and ATP-free state. In the closed ATP-bound conformation the dimerized Rad50^{NBD} interacts with dsDNA and blocks the Mre11 active site (Figure 13A). Biochemical experiments showed that in the ATP-bound conformation MR is able to tether two DNA ends (Deshpande *et al.* 2014) with higher affinity towards 3' overhangs (de Jager *et al.* 2002) (Figure 13A). These results are consistent with the structural and biochemical results from this work. However, it is unclear, whether in the closed conformation, ssDNA reaches into the active site of Mre11

to be processed or whether ATP has to be hydrolyzed to make the nuclease accessible (Figure 13B). Upon ATP hydrolysis the nuclease active site of Mre11 becomes accessible for dsDNA to be processed. Interestingly, the ATP-bound conformation seems to be sufficient for ATM activation, DNA tethering and telomere maintenance, but ATP-dependent Rad50 dimerization and ATP hydrolysis are important for DNA repair (Lee *et al.* 2013, Deshpande *et al.* 2014, Rojowska *et al.* 2014).

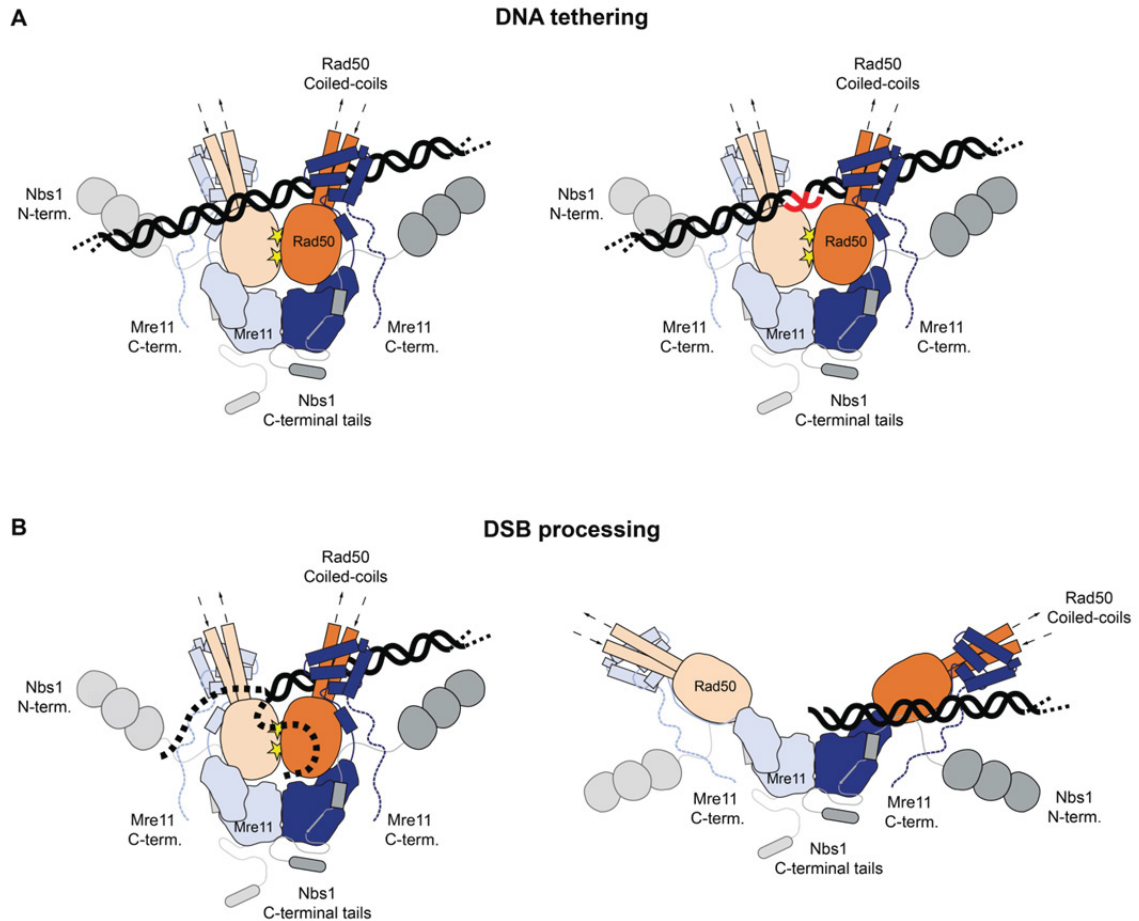


Figure 13: DNA binding models of MRN in ATP-bound and ATP-free conformation. (A) Model for the closed MRN complex during DNA tethering. MRN binds internal DNA (left) and DNA with cohesive end (right). (B) Models of the closed (left) and open (right) MRN complex during nucleolytic DNA processing.

3.6 Outlook

The presented work gives new insights into the structural architecture of the eukaryotic MRN complex. Since DNA can bind to the Mre11 as well as the Rad50 subunit, more research is needed to answer the interplay between these two DNA binding modes. Further, the regulation of these two modes has to be studied in future experiments. On a

structural level, it has to be analyzed how a DNA DSB is recognized by MRN and how the resection is initiated. Therefore, crystal or electron microscopy structures of MR(N) in different states and in complex with other DNA repair factors are required, and more structural information about the Nbs1 interaction will be useful. Based on the presented and future structural results more detailed biochemical and cell biology experiments can be performed to investigate the MRN functions on DNA DSB repair, meiosis or telomere maintenance. Thereby, so far structurally uncharacterized parts of the whole MRN complex have to be analyzed and the MRN functions in context of other genome maintenance factors have to be investigated intensively.

Recent publications revealed that CtIP (Sae2) plays an important role in DSB resection initiation and the removal of MRN from DSBs (Cannavo and Cejka 2014, Chen *et al.* 2015). It would be interesting how the MRN-CtIP interaction regulates this mechanism on a structural level. Structural studies showed the interaction between CtIP and Nbs1 via the FHA domain (Williams *et al.* 2009). But it is unclear, if this is the interaction that regulates the MRN endonuclease activity. Also the signal transduction onto ATM and the mode of binding to this kinase have to be investigated on a structural level. In general, to further understand the multiple functions of MRN, more intensive studies will be needed.

4. Appendix

4.1 References

- Aguilera, A. and B. Gomez-Gonzalez (2008). "Genome instability: a mechanistic view of its causes and consequences." *Nat Rev Genet* **9**(3): 204-217.
- Ajimura, M., S. H. Leem and H. Ogawa (1993). "Identification of new genes required for meiotic recombination in *Saccharomyces cerevisiae*." *Genetics* **133**(1): 51-66.
- Alani, E., R. Padmore and N. Kleckner (1990). "Analysis of wild-type and rad50 mutants of yeast suggests an intimate relationship between meiotic chromosome synapsis and recombination." *Cell* **61**(3): 419-436.
- Almond, J. R., B. A. Stohr, A. K. Panigrahi, D. W. Albrecht, S. W. Nelson and K. N. Kreuzer (2013). "Coordination and processing of DNA ends during double-strand break repair: the role of the bacteriophage T4 Mre11/Rad50 (MR) complex." *Genetics* **195**(3): 739-755.
- Anderson, D. E., K. M. Trujillo, P. Sung and H. P. Erickson (2001). "Structure of the Rad50-Mre11 DNA repair complex from *Saccharomyces cerevisiae* by electron microscopy." *J Biol Chem* **276**(40): 37027-37033.
- Arthur, L. M., K. Gustausson, K. P. Hopfner, C. T. Carson, T. H. Stracker, A. Karcher, D. Felton, M. D. Weitzman, J. Tainer and J. P. Carney (2004). "Structural and functional analysis of Mre11-3." *Nucleic Acids Res* **32**(6): 1886-1893.
- Assenmacher, N. and K. P. Hopfner (2004). "MRE11/RAD50/NBS1: complex activities." *Chromosoma* **113**(4): 157-166.
- Bennett, C. B., T. J. Westmoreland, J. R. Snipe and M. A. Resnick (1996). "A double-strand break within a yeast artificial chromosome (YAC) containing human DNA can result in YAC loss, deletion or cell lethality." *Mol Cell Biol* **16**(8): 4414-4425.
- Berkovich, E., R. J. Monnat, Jr. and M. B. Kastan (2007). "Roles of ATM and NBS1 in chromatin structure modulation and DNA double-strand break repair." *Nat Cell Biol* **9**(6): 683-690.
- Bhattacharyya, M. K., K. M. Matthews and A. J. Lustig (2008). "Mre11 nuclease and C-terminal tail-mediated DDR functions are required for initiating yeast telomere healing." *Chromosoma* **117**(4): 357-366.
- Blier, P. R., A. J. Griffith, J. Craft and J. A. Hardin (1993). "Binding of Ku protein to DNA. Measurement of affinity for ends and demonstration of binding to nicks." *J Biol Chem* **268**(10): 7594-7601.
- Bonetti, D., M. Clerici, N. Manfrini, G. Lucchini and M. P. Longhese (2010). "The MRX complex plays multiple functions in resection of Yku- and Rif2-protected DNA ends." *PLoS One* **5**(11): e14142.
- Bonetti, D., M. Martina, M. Clerici, G. Lucchini and M. P. Longhese (2009). "Multiple pathways regulate 3' overhang generation at *S. cerevisiae* telomeres." *Mol Cell* **35**(1): 70-81.
- Bonetti, D., M. Martina, M. Falcettoni and M. P. Longhese (2014). "Telomere-end processing: mechanisms and regulation." *Chromosoma* **123**(1): 57-66.
- Boulton, S. J. and S. P. Jackson (1998). "Components of the Ku-dependent non-homologous end-joining pathway are involved in telomeric length maintenance and telomeric silencing." *EMBO J* **17**(6): 1819-1828.
- Bromberg, K. D., A. B. Burgin and N. Osheroff (2003). "A two-drug model for etoposide action against human topoisomerase IIalpha." *J Biol Chem* **278**(9): 7406-7412.

- Buis, J., Y. Wu, Y. Deng, J. Leddon, G. Westfield, M. Eckersdorff, J. M. Sekiguchi, S. Chang and D. O. Ferguson (2008). "Mre11 nuclease activity has essential roles in DNA repair and genomic stability distinct from ATM activation." Cell **135**(1): 85-96.
- Cadet, J., J. L. Ravanat, M. TavernaPorro, H. Menoni and D. Angelov (2012). "Oxidatively generated complex DNA damage: tandem and clustered lesions." Cancer Lett **327**(1-2): 5-15.
- Caldecott, K. W. (2014). "DNA single-strand break repair." Exp Cell Res **329**(1): 2-8.
- Cannavo, E. and P. Cejka (2014). "Sae2 promotes dsDNA endonuclease activity within Mre11-Rad50-Xrs2 to resect DNA breaks." Nature **514**(7520): 122-125.
- Cannon, B., J. Kuhnlein, S. H. Yang, A. Cheng, D. Schindler, J. M. Stark, R. Russell and T. T. Paull (2013). "Visualization of local DNA unwinding by Mre11/Rad50/Nbs1 using single-molecule FRET." Proc Natl Acad Sci U S A **110**(47): 18868-18873.
- Carney, J. P., R. S. Maser, H. Olivares, E. M. Davis, M. Le Beau, J. R. Yates, 3rd, L. Hays, W. F. Morgan and J. H. Petrini (1998). "The hMre11/hRad50 protein complex and Nijmegen breakage syndrome: linkage of double-strand break repair to the cellular DNA damage response." Cell **93**(3): 477-486.
- Chapman, J. R. and S. P. Jackson (2008). "Phospho-dependent interactions between NBS1 and MDC1 mediate chromatin retention of the MRN complex at sites of DNA damage." EMBO Rep **9**(8): 795-801.
- Chen, H., R. A. Donnianni, N. Handa, S. K. Deng, J. Oh, L. A. Timashev, S. C. Kowalczykowski and L. S. Symington (2015). "Sae2 promotes DNA damage resistance by removing the Mre11-Rad50-Xrs2 complex from DNA and attenuating Rad53 signaling." Proc Natl Acad Sci U S A **112**(15): E1880-1887.
- Chen, L., C. J. Nievera, A. Y. Lee and X. Wu (2008). "Cell cycle-dependent complex formation of BRCA1-CtIP-MRN is important for DNA double-strand break repair." J Biol Chem **283**(12): 7713-7720.
- Chen, L., K. Trujillo, W. Ramos, P. Sung and A. E. Tomkinson (2001). "Promotion of Dnl4-catalyzed DNA end-joining by the Rad50/Mre11/Xrs2 and Hdf1/Hdf2 complexes." Mol Cell **8**(5): 1105-1115.
- Chiruvella, K. K., Z. Liang and T. E. Wilson (2013). "Repair of double-strand breaks by end joining." Cold Spring Harb Perspect Biol **5**(5): a012757.
- Ciccio, A. and S. J. Elledge (2010). "The DNA damage response: making it safe to play with knives." Mol Cell **40**(2): 179-204.
- Connelly, J. C., E. S. de Leau and D. R. Leach (1999). "DNA cleavage and degradation by the SbcCD protein complex from *Escherichia coli*." Nucleic Acids Res **27**(4): 1039-1046.
- Connelly, J. C., E. S. de Leau and D. R. Leach (2003). "Nucleolytic processing of a protein-bound DNA end by the *E. coli* SbcCD (MR) complex." DNA Repair (Amst) **2**(7): 795-807.
- Connelly, J. C., E. S. de Leau, E. A. Okely and D. R. Leach (1997). "Overexpression, purification, and characterization of the SbcCD protein from *Escherichia coli*." J Biol Chem **272**(32): 19819-19826.
- Connelly, J. C., L. A. Kirkham and D. R. Leach (1998). "The SbcCD nuclease of *Escherichia coli* is a structural maintenance of chromosomes (SMC) family protein that cleaves hairpin DNA." Proc Natl Acad Sci U S A **95**(14): 7969-7974.
- Connelly, J. C. and D. R. Leach (1996). "The sbcC and sbcD genes of *Escherichia coli* encode a nuclease involved in palindrome inviability and genetic recombination." Genes Cells **1**(3): 285-291.

- Costanzo, V., K. Robertson, M. Bibikova, E. Kim, D. Grieco, M. Gottesman, D. Carroll and J. Gautier (2001). "Mre11 protein complex prevents double-strand break accumulation during chromosomal DNA replication." Mol Cell **8**(1): 137-147.
- Darmon, E., J. K. Eykelenboom, F. Lincker, L. H. Jones, M. White, E. Okely, J. K. Blackwood and D. R. Leach (2010). "*E. coli* SbcCD and RecA control chromosomal rearrangement induced by an interrupted palindrome." Mol Cell **39**(1): 59-70.
- Das, D., D. Moiani, H. L. Axelrod, M. D. Miller, D. McMullan, K. K. Jin, P. Abdubek, T. Astakhova, P. Burra, D. Carlton, H. J. Chiu, T. Clayton, M. C. Deller, L. Duan, D. Ernst, J. Feuerhelm, J. C. Grant, A. Grzechnik, S. K. Grzechnik, G. W. Han, L. Jaroszewski, H. E. Klock, M. W. Knuth, P. Kozbial, S. S. Krishna, A. Kumar, D. Marciano, A. T. Morse, E. Nigoghossian, L. Okach, J. Paulsen, R. Reyes, C. L. Rife, N. Sefcovic, H. J. Tien, C. B. Trame, H. van den Bedem, D. Weekes, Q. Xu, K. O. Hodgson, J. Wooley, M. A. Elsliger, A. M. Deacon, A. Godzik, S. A. Lesley, J. A. Tainer and I. A. Wilson (2010). "Crystal structure of the first eubacterial Mre11 nuclease reveals novel features that may discriminate substrates during DNA repair." J Mol Biol **397**(3): 647-663.
- de Jager, M., J. van Noort, D. C. van Gent, C. Dekker, R. Kanaar and C. Wyman (2001). "Human Rad50/Mre11 is a flexible complex that can tether DNA ends." Mol Cell **8**(5): 1129-1135.
- de Jager, M., C. Wyman, D. C. van Gent and R. Kanaar (2002). "DNA end-binding specificity of human Rad50/Mre11 is influenced by ATP." Nucleic Acids Res **30**(20): 4425-4431.
- Degrassi, F., M. Fiore and F. Palitti (2004). "Chromosomal aberrations and genomic instability induced by topoisomerase-targeted antitumour drugs." Curr Med Chem Anticancer Agents **4**(4): 317-325.
- Delia, D., M. Piane, G. Buscemi, C. Savio, S. Palmeri, P. Lulli, L. Carlessi, E. Fontanella and L. Chessa (2004). "MRE11 mutations and impaired ATM-dependent responses in an Italian family with ataxia-telangiectasia-like disorder." Hum Mol Genet **13**(18): 2155-2163.
- Delmas, S., I. G. Duggin and T. Allers (2013). "DNA damage induces nucleoid compaction via the Mre11-Rad50 complex in the archaeon *Haloferax volcanii*." Mol Microbiol **87**(1): 168-179.
- Deng, Y., X. Guo, D. O. Ferguson and S. Chang (2009). "Multiple roles for MRE11 at uncapped telomeres." Nature **460**(7257): 914-918.
- Dery, U., Y. Coulombe, A. Rodrigue, A. Stasiak, S. Richard and J. Y. Masson (2008). "A glycine-arginine domain in control of the human MRE11 DNA repair protein." Mol Cell Biol **28**(9): 3058-3069.
- Desai-Mehta, A., K. M. Cerosaletti and P. Concannon (2001). "Distinct functional domains of nibrin mediate Mre11 binding, focus formation, and nuclear localization." Mol Cell Biol **21**(6): 2184-2191.
- Deshpande, R. A., G. J. Williams, O. Limbo, R. S. Williams, J. Kuhnlein, J. H. Lee, S. Classen, G. Guenther, P. Russell, J. A. Tainer and T. T. Paull (2014). "ATP-driven Rad50 conformations regulate DNA tethering, end resection, and ATM checkpoint signaling." EMBO J **33**(5): 482-500.
- Dexheimer, T. S. (2013). DNA Repair Pathways and Mechanisms. DNA Repair of Cancer Stem Cells. L. A. Mathews, S. M. Cabarcas and E. M. Hurt, Springer Netherlands: 19-32.

- Digweed, M. and K. Sperling (2004). "Nijmegen breakage syndrome: clinical manifestation of defective response to DNA double-strand breaks." DNA Repair (Amst) **3**(8-9): 1207-1217.
- Eker, A. P., C. Quayle, I. Chaves and G. T. van der Horst (2009). "DNA repair in mammalian cells: Direct DNA damage reversal: elegant solutions for nasty problems." Cell Mol Life Sci **66**(6): 968-980.
- Eykelenboom, J. K., J. K. Blackwood, E. Okely and D. R. Leach (2008). "SbcCD causes a double-strand break at a DNA palindrome in the *Escherichia coli* chromosome." Mol Cell **29**(5): 644-651.
- Falck, J., J. Coates and S. P. Jackson (2005). "Conserved modes of recruitment of ATM, ATR and DNA-PKcs to sites of DNA damage." Nature **434**(7033): 605-611.
- Faure, V., S. Coulon, J. Hardy and V. Geli (2010). "Cdc13 and telomerase bind through different mechanisms at the lagging- and leading-strand telomeres." Mol Cell **38**(6): 842-852.
- Ferretti, L. P., L. Lafranchi and A. A. Sartori (2013). "Controlling DNA-end resection: a new task for CDKs." Front Genet **4**: 99.
- Frols, S., P. M. Gordon, M. A. Panlilio, I. G. Duggin, S. D. Bell, C. W. Sensen and C. Schleper (2007). "Response of the hyperthermophilic archaeon *Sulfolobus solfataricus* to UV damage." J Bacteriol **189**(23): 8708-8718.
- Furuse, M., Y. Nagase, H. Tsubouchi, K. Murakami-Murofushi, T. Shibata and K. Ohta (1998). "Distinct roles of two separable in vitro activities of yeast Mre11 in mitotic and meiotic recombination." EMBO J **17**(21): 6412-6425.
- Game, J. C. and R. K. Mortimer (1974). "A genetic study of x-ray sensitive mutants in yeast." Mutat Res **24**(3): 281-292.
- Gapud, E. J. and B. P. Sleckman (2011). "Unique and redundant functions of ATM and DNA-PKcs during V(D)J recombination." Cell Cycle **10**(12): 1928-1935.
- Garcia, V., S. E. Phelps, S. Gray and M. J. Neale (2011). "Bidirectional resection of DNA double-strand breaks by Mre11 and Exo1." Nature **479**(7372): 241-244.
- Gatei, M., D. Young, K. M. Cerosaletti, A. Desai-Mehta, K. Spring, S. Kozlov, M. F. Lavin, R. A. Gatti, P. Concannon and K. Khanna (2000). "ATM-dependent phosphorylation of nibrin in response to radiation exposure." Nat Genet **25**(1): 115-119.
- Ghodke, I. and K. Muniyappa (2013). "Processing of DNA double-stranded breaks and intermediates of recombination and repair by *Saccharomyces cerevisiae* Mre11 and its stimulation by Rad50, Xrs2, and Sae2 proteins." J Biol Chem **288**(16): 11273-11286.
- Ghosal, G. and J. Chen (2013). "DNA damage tolerance: a double-edged sword guarding the genome." Transl Cancer Res **2**(3): 107-129.
- Goudsouzian, L. K., C. T. Tuzon and V. A. Zakian (2006). "*S. cerevisiae* Tel1p and Mre11p are required for normal levels of Est1p and Est2p telomere association." Mol Cell **24**(4): 603-610.
- Haber, J. E. (2012). "Mating-type genes and MAT switching in *Saccharomyces cerevisiae*." Genetics **191**(1): 33-64.
- Hanahan, D. and R. A. Weinberg (2011). "Hallmarks of cancer: the next generation." Cell **144**(5): 646-674.
- Hartsuiker, E., K. Mizuno, M. Molnar, J. Kohli, K. Ohta and A. M. Carr (2009). "Ctp1CtIP and Rad32Mre11 nuclease activity are required for Rec12Spo11 removal, but Rec12Spo11 removal is dispensable for other MRN-dependent meiotic functions." Mol Cell Biol **29**(7): 1671-1681.

- Hector, R. E., R. L. Shtofman, A. Ray, B. R. Chen, T. Nyun, K. L. Berkner and K. W. Runge (2007). "Tel1p preferentially associates with short telomeres to stimulate their elongation." Mol Cell **27**(5): 851-858.
- Herdendorf, T. J., D. W. Albrecht, S. J. Benkovic and S. W. Nelson (2011). "Biochemical characterization of bacteriophage T4 Mre11-Rad50 complex." J Biol Chem **286**(4): 2382-2392.
- Hirano, Y., K. Fukunaga and K. Sugimoto (2009). "Rif1 and rif2 inhibit localization of tel1 to DNA ends." Mol Cell **33**(3): 312-322.
- Hoeijmakers, J. H. (2001). "Genome maintenance mechanisms for preventing cancer." Nature **411**(6835): 366-374.
- Hopfner, K. P., L. Craig, G. Moncalian, R. A. Zinkel, T. Usui, B. A. Owen, A. Karcher, B. Henderson, J. L. Bodmer, C. T. McMurray, J. P. Carney, J. H. Petrini and J. A. Tainer (2002). "The Rad50 zinc-hook is a structure joining Mre11 complexes in DNA recombination and repair." Nature **418**(6897): 562-566.
- Hopfner, K. P., A. Karcher, L. Craig, T. T. Woo, J. P. Carney and J. A. Tainer (2001). "Structural biochemistry and interaction architecture of the DNA double-strand break repair Mre11 nuclease and Rad50-ATPase." Cell **105**(4): 473-485.
- Hopfner, K. P., A. Karcher, D. Shin, C. Fairley, J. A. Tainer and J. P. Carney (2000a). "Mre11 and Rad50 from *Pyrococcus furiosus*: cloning and biochemical characterization reveal an evolutionarily conserved multiprotein machine." J Bacteriol **182**(21): 6036-6041.
- Hopfner, K. P., A. Karcher, D. S. Shin, L. Craig, L. M. Arthur, J. P. Carney and J. A. Tainer (2000b). "Structural biology of Rad50 ATPase: ATP-driven conformational control in DNA double-strand break repair and the ABC-ATPase superfamily." Cell **101**(7): 789-800.
- Hopkins, B. B. and T. T. Paull (2008). "The *P. furiosus* mre11/rad50 complex promotes 5' strand resection at a DNA double-strand break." Cell **135**(2): 250-260.
- Huang, L. C., K. C. Clarkin and G. M. Wahl (1996). "Sensitivity and selectivity of the DNA damage sensor responsible for activating p53-dependent G1 arrest." Proc Natl Acad Sci U S A **93**(10): 4827-4832.
- Kim, Y. J. and D. M. Wilson, 3rd (2012). "Overview of base excision repair biochemistry." Curr Mol Pharmacol **5**(1): 3-13.
- Kironmai, K. M. and K. Muniyappa (1997). "Alteration of telomeric sequences and senescence caused by mutations in RAD50 of *Saccharomyces cerevisiae*." Genes Cells **2**(7): 443-455.
- Kobayashi, J., H. Tauchi, S. Sakamoto, A. Nakamura, K. Morishima, S. Matsuura, T. Kobayashi, K. Tamai, K. Tanimoto and K. Komatsu (2002). "NBS1 localizes to γ -H2AX foci through interaction with the FHA/BRCT domain." Curr Biol **12**(21): 1846-1851.
- Kreuzer, K. N. and J. R. Brister (2010). "Initiation of bacteriophage T4 DNA replication and replication fork dynamics: a review in the Virology Journal series on bacteriophage T4 and its relatives." Virology **7**: 358.
- Kunkel, T. A. (1999). "The high cost of living. American Association for Cancer Research Special Conference: endogenous sources of mutations, Fort Myers, Florida, USA, 11-15 November 1998." Trends Genet **15**(3): 93-94.
- Lam, I. and S. Keeney (2015). "Mechanism and regulation of meiotic recombination initiation." Cold Spring Harb Perspect Biol **7**(1): a016634.
- Lammens, K., D. J. Bemeleit, C. Möckel, E. Clausen, A. Schele, S. Hartung, C. B. Schiller, M. Lucas, C. Angermüller, J. Söding, K. Strasser and K. P. Hopfner

- (2011). "The Mre11:Rad50 structure shows an ATP-dependent molecular clamp in DNA double-strand break repair." *Cell* **145**(1): 54-66.
- Langerak, P., E. Mejia-Ramirez, O. Limbo and P. Russell (2011). "Release of Ku and MRN from DNA ends by Mre11 nuclease activity and Ctp1 is required for homologous recombination repair of double-strand breaks." *PLoS Genet* **7**(9): e1002271.
- Lee, J. H., R. Ghirlando, V. Bhaskara, M. R. Hoffmeyer, J. Gu and T. T. Paull (2003a). "Regulation of Mre11/Rad50 by Nbs1: effects on nucleotide-dependent DNA binding and association with ataxia-telangiectasia-like disorder mutant complexes." *J Biol Chem* **278**(46): 45171-45181.
- Lee, J. H., M. R. Mand, R. A. Deshpande, E. Kinoshita, S. H. Yang, C. Wyman and T. T. Paull (2013). "Ataxia telangiectasia-mutated (ATM) kinase activity is regulated by ATP-driven conformational changes in the Mre11/Rad50/Nbs1 (MRN) complex." *J Biol Chem* **288**(18): 12840-12851.
- Lee, J. H. and T. T. Paull (2004). "Direct activation of the ATM protein kinase by the Mre11/Rad50/Nbs1 complex." *Science* **304**(5667): 93-96.
- Lee, J. H. and T. T. Paull (2005). "ATM activation by DNA double-strand breaks through the Mre11-Rad50-Nbs1 complex." *Science* **308**(5721): 551-554.
- Lee, J. H., B. Xu, C. H. Lee, J. Y. Ahn, M. S. Song, H. Lee, C. E. Canman, J. S. Lee, M. B. Kastan and D. S. Lim (2003b). "Distinct functions of Nijmegen breakage syndrome in ataxia telangiectasia mutated-dependent responses to DNA damage." *Mol Cancer Res* **1**(9): 674-681.
- Lengsfeld, B. M., A. J. Rattray, V. Bhaskara, R. Ghirlando and T. T. Paull (2007). "Sae2 is an endonuclease that processes hairpin DNA cooperatively with the Mre11/Rad50/Xrs2 complex." *Mol Cell* **28**(4): 638-651.
- Lim, H. S., J. S. Kim, Y. B. Park, G. H. Gwon and Y. Cho (2011). "Crystal structure of the Mre11-Rad50-ATPγS complex: understanding the interplay between Mre11 and Rad50." *Genes Dev* **25**(10): 1091-1104.
- Limbo, O., D. Moiani, A. Kertokallio, C. Wyman, J. A. Tainer and P. Russell (2012). "Mre11 ATLD17/18 mutation retains Tel1/ATM activity but blocks DNA double-strand break repair." *Nucleic Acids Res* **40**(22): 11435-11449.
- Lisby, M., J. H. Barlow, R. C. Burgess and R. Rothstein (2004). "Choreography of the DNA damage response: spatiotemporal relationships among checkpoint and repair proteins." *Cell* **118**(6): 699-713.
- Liu, S., L. F. Tian, Y. P. Liu, X. M. An, Q. Tang, X. X. Yan and D. C. Liang (2014). "Structural basis for DNA recognition and nuclease processing by the Mre11 homologue SbcD in double-strand breaks repair." *Acta Crystallogr D Biol Crystallogr* **70**(Pt 2): 299-309.
- Liu, T. and J. Huang (2014). "Quality control of homologous recombination." *Cell Mol Life Sci* **71**(19): 3779-3797.
- Lloyd, J., J. R. Chapman, J. A. Clapperton, L. F. Haire, E. Hartsuiker, J. Li, A. M. Carr, S. P. Jackson and S. J. Smerdon (2009). "A supramodular FHA/BRCT-repeat architecture mediates Nbs1 adaptor function in response to DNA damage." *Cell* **139**(1): 100-111.
- Lobachev, K. S., D. A. Gordenin and M. A. Resnick (2002). "The Mre11 complex is required for repair of hairpin-capped double-strand breaks and prevention of chromosome rearrangements." *Cell* **108**(2): 183-193.
- Luo, G., M. S. Yao, C. F. Bender, M. Mills, A. R. Bladl, A. Bradley and J. H. Petrini (1999). "Disruption of *mRad50* causes embryonic stem cell lethality, abnormal

- embryonic development, and sensitivity to ionizing radiation." Proc Natl Acad Sci U S A **96**(13): 7376-7381.
- Mahaney, B. L., K. Meek and S. P. Lees-Miller (2009). "Repair of ionizing radiation-induced DNA double-strand breaks by non-homologous end-joining." Biochem J **417**(3): 639-650.
- Majka, J., B. Alford, J. Ausio, R. M. Finn and C. T. McMurray (2012). "ATP hydrolysis by RAD50 protein switches MRE11 enzyme from endonuclease to exonuclease." J Biol Chem **287**(4): 2328-2341.
- Marteijn, J. A., H. Lans, W. Vermeulen and J. H. Hoeijmakers (2014). "Understanding nucleotide excision repair and its roles in cancer and ageing." Nat Rev Mol Cell Biol **15**(7): 465-481.
- Maser, R. S., R. Zinkel and J. H. Petrini (2001). "An alternative mode of translation permits production of a variant NBS1 protein from the common Nijmegen breakage syndrome allele." Nat Genet **27**(4): 417-421.
- Matsumoto, Y., T. Miyamoto, H. Sakamoto, H. Izumi, Y. Nakazawa, T. Ogi, H. Tahara, S. Oku, A. Hiramoto, T. Shiiki, Y. Fujisawa, H. Ohashi, Y. Sakemi and S. Matsuura (2011). "Two unrelated patients with *MRE11A* mutations and Nijmegen breakage syndrome-like severe microcephaly." DNA Repair (Amst) **10**(3): 314-321.
- Mehta, A. and J. E. Haber (2014). "Sources of DNA double-strand breaks and models of recombinational DNA repair." Cold Spring Harb Perspect Biol **6**(9): a016428.
- Melander, F., S. Bekker-Jensen, J. Falck, J. Bartek, N. Mailand and J. Lukas (2008). "Phosphorylation of SDT repeats in the MDC1 N terminus triggers retention of NBS1 at the DNA damage-modified chromatin." J Cell Biol **181**(2): 213-226.
- Mimitou, E. P. and L. S. Symington (2009). "DNA end resection: many nucleases make light work." DNA Repair (Amst) **8**(9): 983-995.
- Mimitou, E. P. and L. S. Symington (2010). "Ku prevents Exo1 and Sgs1-dependent resection of DNA ends in the absence of a functional MRX complex or Sae2." EMBO J **29**(19): 3358-3369.
- Miyamoto, R., H. Morino, A. Yoshizawa, Y. Miyazaki, H. Maruyama, N. Murakami, K. Fukada, Y. Izumi, S. Matsuura, R. Kaji and H. Kawakami (2014). "Exome sequencing reveals a novel *MRE11* mutation in a patient with progressive myoclonic ataxia." J Neurol Sci **337**(1-2): 219-223.
- Möckel, C., K. Lammens, A. Schele and K. P. Hopfner (2012). "ATP driven structural changes of the bacterial Mre11:Rad50 catalytic head complex." Nucleic Acids Res **40**(2): 914-927.
- Moreno-Herrero, F., M. de Jager, N. H. Dekker, R. Kanaar, C. Wyman and C. Dekker (2005). "Mesoscale conformational changes in the DNA-repair complex Rad50/Mre11/Nbs1 upon binding DNA." Nature **437**(7057): 440-443.
- Myung, K., C. Chen and R. D. Kolodner (2001a). "Multiple pathways cooperate in the suppression of genome instability in *Saccharomyces cerevisiae*." Nature **411**(6841): 1073-1076.
- Myung, K., A. Datta and R. D. Kolodner (2001b). "Suppression of spontaneous chromosomal rearrangements by S phase checkpoint functions in *Saccharomyces cerevisiae*." Cell **104**(3): 397-408.
- Nakada, D., K. Matsumoto and K. Sugimoto (2003). "ATM-related Tel1 associates with double-strand breaks through an Xrs2-dependent mechanism." Genes Dev **17**(16): 1957-1962.
- Nakamura, J., V. E. Walker, P. B. Upton, S. Y. Chiang, Y. W. Kow and J. A. Swenberg (1998). "Highly sensitive apurinic/aprimidinic site assay can detect spontaneous

- and chemically induced depurination under physiological conditions." Cancer Res **58**(2): 222-225.
- Neale, M. J., J. Pan and S. Keeney (2005). "Endonucleolytic processing of covalent protein-linked DNA double-strand breaks." Nature **436**(7053): 1053-1057.
- Nimonkar, A. V., J. Genschel, E. Kinoshita, P. Polaczek, J. L. Campbell, C. Wyman, P. Modrich and S. C. Kowalczykowski (2011). "BLM-DNA2-RPA-MRN and EXO1-BLM-RPA-MRN constitute two DNA end resection machineries for human DNA break repair." Genes Dev **25**(4): 350-362.
- Pardo, B., B. Gomez-Gonzalez and A. Aguilera (2009). "DNA repair in mammalian cells: DNA double-strand break repair: how to fix a broken relationship." Cell Mol Life Sci **66**(6): 1039-1056.
- Park, Y. B., J. Chae, Y. C. Kim and Y. Cho (2011). "Crystal structure of human Mre11: understanding tumorigenic mutations." Structure **19**(11): 1591-1602.
- Paull, T. T. (2015). "Mechanisms of ATM Activation." Annu Rev Biochem.
- Paull, T. T. and M. Gellert (1998). "The 3' to 5' exonuclease activity of Mre 11 facilitates repair of DNA double-strand breaks." Mol Cell **1**(7): 969-979.
- Paull, T. T. and M. Gellert (1999). "Nbs1 potentiates ATP-driven DNA unwinding and endonuclease cleavage by the Mre11/Rad50 complex." Genes Dev **13**(10): 1276-1288.
- Pommier, Y., C. Redon, V. A. Rao, J. A. Seiler, O. Sordet, H. Takemura, S. Antony, L. Meng, Z. Liao, G. Kohlhagen, H. Zhang and K. W. Kohn (2003). "Repair of and checkpoint response to topoisomerase I-mediated DNA damage." Mutat Res **532**(1-2): 173-203.
- Quaiser, A., F. Constantinesco, M. F. White, P. Forterre and C. Elie (2008). "The Mre11 protein interacts with both Rad50 and the HerA bipolar helicase and is recruited to DNA following γ -irradiation in the archaeon *Sulfolobus acidocaldarius*." BMC Mol Biol **9**: 25.
- Rass, E., A. Grabarz, I. Plo, J. Gautier, P. Bertrand and B. S. Lopez (2009). "Role of Mre11 in chromosomal nonhomologous end joining in mammalian cells." Nat Struct Mol Biol **16**(8): 819-824.
- Reardon, J. T. and A. Sancar (2003). "Recognition and repair of the cyclobutane thymine dimer, a major cause of skin cancers, by the human excision nuclease." Genes Dev **17**(20): 2539-2551.
- Reis, C. C., S. Batista and M. G. Ferreira (2012). "The fission yeast MRN complex tethers dysfunctional telomeres for NHEJ repair." EMBO J **31**(24): 4576-4586.
- Reynolds, J. J. and G. S. Stewart (2013). "A nervous predisposition to unrepaired DNA double strand breaks." DNA Repair (Amst) **12**(8): 588-599.
- Rojowska, A., K. Lammens, F. U. Seifert, C. Drenth, H. Feldmann and K. P. Hopfner (2014). "Structure of the Rad50 DNA double-strand break repair protein in complex with DNA." EMBO J **33**(23): 2847-2859.
- Schiller, C. B., K. Lammens, I. Guerini, B. Coords, H. Feldmann, F. Schlauderer, C. Möckel, A. Schele, K. Strasser, S. P. Jackson and K. P. Hopfner (2012). "Structure of Mre11-Nbs1 complex yields insights into ataxia-telangiectasia-like disease mutations and DNA damage signaling." Nat Struct Mol Biol **19**(7): 693-700.
- Schiller, C. B., F. U. Seifert, C. Linke-Winnebeck and K. P. Hopfner (2014). "Structural studies of DNA end detection and resection in homologous recombination." Cold Spring Harb Perspect Biol **6**(10): a017962.

- Seifert, F. U., K. Lammens and K. P. Hopfner (2015). "Structure of the catalytic domain of Mre11 from *Chaetomium thermophilum*." Acta Crystallogr F Struct Biol Commun **71**(Pt 6): 752-757.
- Sharples, G. J. and D. R. Leach (1995). "Structural and functional similarities between the SbcCD proteins of *Escherichia coli* and the RAD50 and MRE11 (RAD32) recombination and repair proteins of yeast." Mol Microbiol **17**(6): 1215-1217.
- Shim, E. Y., W. H. Chung, M. L. Nicolette, Y. Zhang, M. Davis, Z. Zhu, T. T. Paull, G. Ira and S. E. Lee (2010). "Saccharomyces cerevisiae Mre11/Rad50/Xrs2 and Ku proteins regulate association of Exo1 and Dna2 with DNA breaks." EMBO J **29**(19): 3370-3380.
- Spycher, C., E. S. Miller, K. Townsend, L. Pavic, N. A. Morrice, P. Janscak, G. S. Stewart and M. Stucki (2008). "Constitutive phosphorylation of MDC1 physically links the MRE11-RAD50-NBS1 complex to damaged chromatin." J Cell Biol **181**(2): 227-240.
- Stracker, T. H., M. Morales, S. S. Couto, H. Hussein and J. H. Petrini (2007). "The carboxy terminus of NBS1 is required for induction of apoptosis by the MRE11 complex." Nature **447**(7141): 218-221.
- Stracker, T. H. and J. H. Petrini (2011). "The MRE11 complex: starting from the ends." Nat Rev Mol Cell Biol **12**(2): 90-103.
- Sutherland, B. M., P. V. Bennett, O. Sidorkina and J. Laval (2000). "Clustered DNA damages induced in isolated DNA and in human cells by low doses of ionizing radiation." Proc Natl Acad Sci U S A **97**(1): 103-108.
- Symington, L. S. (2014). "End resection at double-strand breaks: mechanism and regulation." Cold Spring Harb Perspect Biol **6**(8): a016436.
- Taylor, A. M., A. Groom and P. J. Byrd (2004). "Ataxia-telangiectasia-like disorder (ATLD)-its clinical presentation and molecular basis." DNA Repair (Amst) **3**(8-9): 1219-1225.
- Taylor, A. M., D. G. Harnden, C. F. Arlett, S. A. Harcourt, A. R. Lehmann, S. Stevens and B. A. Bridges (1975). "Ataxia telangiectasia: a human mutation with abnormal radiation sensitivity." Nature **258**(5534): 427-429.
- Thompson, L. H. (2012). "Recognition, signaling, and repair of DNA double-strand breaks produced by ionizing radiation in mammalian cells: the molecular choreography." Mutat Res **751**(2): 158-246.
- Trenz, K., E. Smith, S. Smith and V. Costanzo (2006). "ATM and ATR promote Mre11 dependent restart of collapsed replication forks and prevent accumulation of DNA breaks." EMBO J **25**(8): 1764-1774.
- Trujillo, K. M., D. H. Roh, L. Chen, S. Van Komen, A. Tomkinson and P. Sung (2003). "Yeast xrs2 binds DNA and helps target rad50 and mre11 to DNA ends." J Biol Chem **278**(49): 48957-48964.
- Trujillo, K. M. and P. Sung (2001). "DNA structure-specific nuclease activities in the *Saccharomyces cerevisiae* Rad50-Mre11 complex." J Biol Chem **276**(38): 35458-35464.
- Trujillo, K. M., S. S. Yuan, E. Y. Lee and P. Sung (1998). "Nuclease activities in a complex of human recombination and DNA repair factors Rad50, Mre11, and p95." J Biol Chem **273**(34): 21447-21450.
- Truong, L. N., Y. Li, L. Z. Shi, P. Y. Hwang, J. He, H. Wang, N. Razavian, M. W. Berns and X. Wu (2013). "Microhomology-mediated End Joining and Homologous Recombination share the initial end resection step to repair DNA double-strand breaks in mammalian cells." Proc Natl Acad Sci U S A **110**(19): 7720-7725.

- Tsukamoto, Y., C. Mitsuoka, M. Terasawa, H. Ogawa and T. Ogawa (2005). "Xrs2p regulates Mre11p translocation to the nucleus and plays a role in telomere elongation and meiotic recombination." *Mol Biol Cell* **16**(2): 597-608.
- Uchisaka, N., N. Takahashi, M. Sato, A. Kikuchi, S. Mochizuki, K. Imai, S. Nonoyama, O. Ohara, F. Watanabe, S. Mizutani, R. Hanada and T. Morio (2009). "Two brothers with ataxia-telangiectasia-like disorder with lung adenocarcinoma." *J Pediatr* **155**(3): 435-438.
- Usui, T., T. Ohta, H. Oshiumi, J. Tomizawa, H. Ogawa and T. Ogawa (1998). "Complex formation and functional versatility of Mre11 of budding yeast in recombination." *Cell* **95**(5): 705-716.
- Varon, R., C. Vissinga, M. Platzer, K. M. Cerosaletti, K. H. Chrzanowska, K. Saar, G. Beckmann, E. Seemanova, P. R. Cooper, N. J. Nowak, M. Stumm, C. M. Weemaes, R. A. Gatti, R. K. Wilson, M. Digweed, A. Rosenthal, K. Sperling, P. Concannon and A. Reis (1998). "Nibrin, a novel DNA double-strand break repair protein, is mutated in Nijmegen breakage syndrome." *Cell* **93**(3): 467-476.
- Walker, J. E., M. Saraste, M. J. Runswick and N. J. Gay (1982). "Distantly related sequences in the alpha- and beta-subunits of ATP synthase, myosin, kinases and other ATP-requiring enzymes and a common nucleotide binding fold." *EMBO J* **1**(8): 945-951.
- Walker, J. R., R. A. Corpina and J. Goldberg (2001). "Structure of the Ku heterodimer bound to DNA and its implications for double-strand break repair." *Nature* **412**(6847): 607-614.
- Waltes, R., R. Kalb, M. Gatei, A. W. Kijas, M. Stumm, A. Sobeck, B. Wieland, R. Varon, Y. Lerenthal, M. F. Lavin, D. Schindler and T. Dork (2009). "Human RAD50 deficiency in a Nijmegen breakage syndrome-like disorder." *Am J Hum Genet* **84**(5): 605-616.
- Wang, Y., D. Cortez, P. Yazdi, N. Neff, S. J. Elledge and J. Qin (2000). "BASC, a super complex of BRCA1-associated proteins involved in the recognition and repair of aberrant DNA structures." *Genes Dev* **14**(8): 927-939.
- Wawrousek, K. E., B. K. Fortini, P. Polaczek, L. Chen, Q. Liu, W. G. Dunphy and J. L. Campbell (2010). "Xenopus DNA2 is a helicase/nuclease that is found in complexes with replication proteins And-1/Ctf4 and Mcm10 and DSB response proteins Nbs1 and ATM." *Cell Cycle* **9**(6): 1156-1166.
- Williams, G. J., S. P. Lees-Miller and J. A. Tainer (2010). "Mre11-Rad50-Nbs1 conformations and the control of sensing, signaling, and effector responses at DNA double-strand breaks." *DNA Repair (Amst)* **9**(12): 1299-1306.
- Williams, G. J., R. S. Williams, J. S. Williams, G. Moncalian, A. S. Arvai, O. Limbo, G. Guenther, S. SilDas, M. Hammel, P. Russell and J. A. Tainer (2011). "ABC ATPase signature helices in Rad50 link nucleotide state to Mre11 interface for DNA repair." *Nat Struct Mol Biol* **18**(4): 423-431.
- Williams, R. S., G. E. Dodson, O. Limbo, Y. Yamada, J. S. Williams, G. Guenther, S. Classen, J. N. Glover, H. Iwasaki, P. Russell and J. A. Tainer (2009). "Nbs1 flexibly tethers Ctp1 and Mre11-Rad50 to coordinate DNA double-strand break processing and repair." *Cell* **139**(1): 87-99.
- Williams, R. S., G. Moncalian, J. S. Williams, Y. Yamada, O. Limbo, D. S. Shin, L. M. Grocock, D. Cahill, C. Hitomi, G. Guenther, D. Moiani, J. P. Carney, P. Russell and J. A. Tainer (2008). "Mre11 dimers coordinate DNA end bridging and nuclease processing in double-strand-break repair." *Cell* **135**(1): 97-109.

- Wu, L., K. Luo, Z. Lou and J. Chen (2008). "MDC1 regulates intra-S-phase checkpoint by targeting NBS1 to DNA double-strand breaks." Proc Natl Acad Sci U S A **105**(32): 11200-11205.
- Xiao, Y. and D. T. Weaver (1997). "Conditional gene targeted deletion by Cre recombinase demonstrates the requirement for the double-strand break repair Mre11 protein in murine embryonic stem cells." Nucleic Acids Res **25**(15): 2985-2991.
- Xie, A., A. Kwok and R. Scully (2009). "Role of mammalian Mre11 in classical and alternative nonhomologous end joining." Nat Struct Mol Biol **16**(8): 814-818.
- Xu, Z., H. Zan, E. J. Pone, T. Mai and P. Casali (2012). "Immunoglobulin class-switch DNA recombination: induction, targeting and beyond." Nat Rev Immunol **12**(7): 517-531.
- Yoshida, T., J. M. Claverie and H. Ogata (2011). "Mimivirus reveals Mre11/Rad50 fusion proteins with a sporadic distribution in eukaryotes, bacteria, viruses and plasmids." Virology **438**: 427.
- You, Z., C. Chahwan, J. Bailis, T. Hunter and P. Russell (2005). "ATM activation and its recruitment to damaged DNA require binding to the C terminus of Nbs1." Mol Cell Biol **25**(13): 5363-5379.
- Zahra, R., J. K. Blackwood, J. Sales and D. R. Leach (2007). "Proofreading and secondary structure processing determine the orientation dependence of CAG-CTG trinucleotide repeat instability in *Escherichia coli*." Genetics **176**(1): 27-41.
- Zeman, M. K. and K. A. Cimprich (2014). "Causes and consequences of replication stress." Nat Cell Biol **16**(1): 2-9.
- Zhang, X. and T. T. Paull (2005). "The Mre11/Rad50/Xrs2 complex and non-homologous end-joining of incompatible ends in *S. cerevisiae*." DNA Repair (Amst) **4**(11): 1281-1294.
- Zhu, J., S. Petersen, L. Tessarollo and A. Nussenzweig (2001). "Targeted disruption of the Nijmegen breakage syndrome gene NBS1 leads to early embryonic lethality in mice." Curr Biol **11**(2): 105-109.

4.2 Abbreviations

5/4 PO/OH	Pentaerythritol propoxylate
6-FAM	6-carboxyfluorescein
8-OxoG	8-oxo-7,8dihydroguanine
Å	Angstrom
A-T	ataxia-telangiectasia
aa	amino acid (residue)
ABC	ATP-binding cassette
ADP	adenosine diphosphate
AFM	atomic force microscopy
alt-NHEJ	alternative NHEJ
AMPPNP	Adenosine 5'-(β,γ -imido)triphosphate
ATLD	ataxia-telangiectasia like disorder
ATM	ataxia-telangiectasia mutated
ATP	adenosine triphosphate
ATP γ S	Adenosine 5'-(γ -thio)triphosphate
BER	base excision repair
BLM	Bloom syndrome mutated
BIR	break-induced replication
Bleo	bleomycin
bp	base pair
BRCA1	breast cancer 1
BRCT domain	BRCA1 C-terminal domain
°C	degree Celsius
CC	coiled-coil
c-NHEJ	canonical NHEJ
<i>C. thermophilum</i> ; Ct	<i>Chaetomium thermophilum</i>
CD	catalytic domain
CPT	camptothecin
CtIP	CtBP-interacting protein
CtMre11	Mre11 from <i>C. thermophilum</i>
CtMR	MR from <i>C. thermophilum</i>
CtMRN	MRN from <i>C. thermophilum</i>
CtM ^{RBD} R ^{NBD}	CtMre11 ^{RBD} -CtRad50 ^{NBD}
CtRad50	Rad50 from <i>C. thermophilum</i>
CV	column volumes
CXMS	chemical cross-linking and mass spectrometry
DDR	DNA damage reversal (Chapter 1.1)
DDR	DNA damage response (Chapter 2.3, 2.4)
DMF	dimethylformamide

4. Appendix

DNA	deoxyribonucleic acid
DSB	double-strand break
DSBR	double-strand break repair
dsDNA	double-stranded DNA
DSS	disuccinimidyl suberate
<i>E. coli</i>	<i>Escherichia coli</i>
EMSA	electrophoretic mobility shift assay
FEN-1	flap endonuclease 1
FHA	forkhead associated
FRET	Förster/fluorescence resonance energy transfer
g	gram
GAR	glycine/arginine-rich
GG-NER	global genomic NER
h	hour
H2TH	helix-two-turn-helix
HAS	HerA-ATP synthase
hc; HC	head complex
HR	homologous recombination
HDR	homology directed repair
HDRC	helicase and RNaseD carboxy-terminal
HLH	helix-loop-helix
HsMre11	Mre11 from <i>Homo sapiens</i>
HU	hydroxyurea
IPTG	Isopropyl- β -D-thiogalactopyranosid
IR	ionizing radiation
K	Kelvin
K _d	dissociation constant
kDa	kilo Dalton
L	liter
LB	Luria-Bertani
LC-MS/MS	liquid chromatography coupled to tandem mass spectrometry
<i>M. jannaschii</i> ; Mj	<i>Methanocaldococcus jannaschii</i>
M	molar
MDC1	mediator of DNA damage checkpoint protein 1
Mg	magnesium
min	minute
MIM	Mre11-interacting module
MMEJ	microhomology-mediated end joining
MMR	mismatch repair
Mn	manganese
MN	Mre11-Nbs1

MR	Mre11-Rad50
MRN	Mre11-Rad50-Nbs1
MRX	Mre11-Rad50-Xrs2 (<i>S. cerevisiae</i> complex)
n	nano
NBD	nucleotide-binding domain
NBS	Nijmegen breakage syndrome
Nbs1	Nijmegen breakage syndrome 1
NBSLD	NBS-like disorder
NER	nucleotide excision repair
NHEJ	non-homologous end joining
NLS	nuclear localization signal
nt	nucleotide
OD ₆₀₀	optical density at 600 nm
<i>P. furiosus</i> ; Pf	<i>Pyrococcus furiosus</i>
PAGE	polyacrylamide gel electrophoresis
PARP	poly (ADP-ribose) polymerase
PDB	protein data bank
PEG	polyethylene glycol
PfMre11	Mre11 from <i>P. furiosus</i>
pH	potential of hydrogen
PMA	progressive myoclonic ataxia
rad50S	rad50 separation-of-function
RBD	Rad50-binding domain
rCID	rapid collision-induced dissociation
RNA	ribonucleic acid
ROS	reactive oxygen species
RPA	replication protein A
rpm	rotation per minute
RQC	RecQ carboxy-terminal
RT	room temperature
<i>S. cerevisiae</i> ; Sc	<i>Saccharomyces cerevisiae</i>
<i>S. pombe</i> ; Sp	<i>Schizosaccharomyces pombe</i>
SAD	single-wavelength anomalous dispersion
SAXS	small angle X-ray scattering
ScMre11	Mre11 from <i>S. cerevisiae</i>
SDS	sodium dodecyl-sulphate
SDSA	synthesis-dependent strand annealing
sec; s	second
SFM	scanning force microscopy
SLH	strand-loop-helix
SpMre11	Mre11 from <i>S. pombe</i>

4. Appendix

SSA	single-strand annealing
SSB	single-strand break
ssDNA	single-stranded DNA
STR	Sgs1-Top3-Rmi1
TC-NER	transcription-coupled NER
TCEP	tris(2-carboxyethyl)phosphine
<i>T. maritima</i> ; Tm; tm	<i>Thermotoga maritima</i>
TopI	topoisomerase I
UV	ultraviolet
V(D)J	variable(-diversity)-joining
wt	wild-type
Zn	zinc

4.3 Contributions

Declaration of contributions to “Structure of the catalytic domain of Mre11 from Chaetomium thermophilum”

I conceived the project and designed the Mre11, Rad50, Nbs1 constructs together with Katja Lammens and Karl-Peter Hopfner. I cloned, expressed and purified the MRN head complex, and crystallized the CtMre11 catalytic domain (CtMre11^{CD}). I solved the crystal structure together with Katja Lammens and built the structure into the electron density. I prepared all figures and wrote the manuscript with revision by Katja Lammens and Karl-Peter Hopfner.

Declaration of contributions to “Structural mechanism of ATP-dependent DNA binding by eukaryotic Rad50”

I purified various constructs of Mre11-Rad50(-Nbs1) with the help of Brigitte Keßler. I crystallized and solved the structures of the CtMre11^{RBD}-Rad50^{NBD} and Rad50^{NBD}-DNA complexes by SAD and molecular replacement, respectively. I built the structures into the electron densities and performed *in vitro* DNA binding experiments by fluorescence anisotropy measurements. I prepared and measured SAXS samples at the DESY (Deutsches Elektronen Synchrotron, Hamburg) synchrotron, and analyzed the data together with Katja Lammens. I performed *in vivo* experiments in yeast together with Brigitte Keßler and Katja Lammens. I prepared all figures as well as all supplementary figures and wrote the preliminary manuscript together with Karl-Peter Hopfner.

Declaration of contributions to “Structure of the Rad50 DNA double-strand break repair protein in complex with DNA”

I conceived additional experiments together with Katja Lammens, Heidi Feldmann and Karl-Peter Hopfner. I prepared yeast Rad50 mutant strains, performed yeast survival experiments and quantified the electrophoretic mobility shift assays (EMSAs). I prepared Figures 3 and 4, and re-wrote parts of the manuscript.

Declaration of contributions to “Structural Studies of DNA End Detection and Resection in Homologous Recombination”

I prepared Figures 1, 2, 3 and 4A. I wrote this review together with Christian Bernd Schiller, Christian Linke-Winnebeck and Karl-Peter Hopfner. Parts of the manuscript were used for parts of the introduction in this work (Chapter 1).

4.4 Declaration

Eidesstattliche Erklärung

Ich versichere hiermit an Eides statt, dass die vorgelegte Dissertation von mir selbständig und ohne unerlaubte Hilfe angefertigt ist.

München, den
(Florian Ulrich Seifert)

Erklärung

Hiermit erkläre ich, dass die Dissertation nicht ganz oder in wesentlichen Teilen einer anderen Prüfungskommission vorgelegt worden ist. Weiterhin habe ich weder an einem anderen Ort eine Promotion angestrebt noch angemeldet oder versucht eine Doktorprüfung abzulegen.

München, den
(Florian Ulrich Seifert)

4.5 Acknowledgements

I want to thank everybody who has contributed to the work in this thesis. First of all, I would like to thank my supervisor Prof. Dr. Karl-Peter Hopfner who gave me the opportunity to join his group and to work on such an interesting project in the field of DNA repair. I am very grateful for all his support and guidance through all this time and that he was always approachable to discuss scientific questions.

I am also very thankful to Prof. Dr. Heinrich Leonhardt for representing my thesis in the biology faculty and for fruitful advices in meetings. Further, I want to thank the third member of my thesis advisory committee Prof. Dr. Heinrich Jung for the support and the help over the last years.

I also would like to thank the whole Hopfner lab for the very nice and inspiring working atmosphere and for the great support during experiments and for fruitful discussions. There was always a helping hand in the lab or during data processing and I am already missing the long synchrotron nights with you guys.

Special thanks go to the numerous members of the MRN group for helpful discussions and ideas during meetings. Thereby, I especially want to thank Katja Lammens who taught me everything about structure determination and always had useful advices for the project. I also want to thank Brigitte Keßler for great help in the lab and all the contributions to this project. I think working in such a team definitely increased the outcome of this thesis and was the base for a successful work.

I am also grateful to all my friends and especially to Marta for the great support over the last years. You were always there to talk to and to spend time when I needed some distraction from the lab.

Nicht zuletzt möchte ich mich noch bei meiner Familie bedanken, die immer für mich da ist und mich in den letzten Jahren so sehr unterstützt hat.

4.6 Curriculum vitae

Personal Details

Name Florian Ulrich Seifert
Date of birth June 28th, 1988
Place of birth Biberach an der Riss, Germany
Nationality German

Academic Training

11.2011–present	PhD thesis in the group of Prof. Dr. Karl-Peter Hopfner, Gene Center, Ludwig-Maximilians-Universität (LMU) Munich, Germany
01.2011–08.2011	Bachelor thesis in the group of Prof. Dr. Karl-Peter Hopfner, Gene Center, LMU Munich, Germany
03.2010–12.2010	Internship and Student Assistant in the group of Prof. Dr. Karl-Peter Hopfner; Gene Center, LMU Munich, Germany
08.2010–09.2010	Internship at the Cancer Research UK in South Mimms, Great Britain
10.2009–02.2010	Tutor: Exercise course genetic, Department of Genetic, LMU Munich, Germany

Education

11.2011–present	PhD thesis in the group of Prof. Dr. Karl-Peter Hopfner, Gene Center and Department of Biochemistry, LMU Munich, Germany
2007–2011	Bachelor of Science in Biology (240 ECTS) at the LMU Munich, Germany
1998–2007	Pestalozzi-Gymnasium in Biberach an der Riss, Germany

4.7 Publications

Seifert FU, Lammens K, Stoehr G, Keßler B, Hopfner KP.

“Structural mechanism of ATP-dependent DNA binding by eukaryotic Rad50.”

Manuscript in preparation

Seifert FU, Lammens K, Hopfner KP.

“Structure of the catalytic domain of Mre11 from *Chaetomium thermophilum*.”

Acta Cryst. 2015 Jun 1. F71, 752-757 doi:10.1107/S2053230X15007566

Rojowska A, Lammens K, Seifert FU, Drenth J, Feldmann H, Hopfner KP.

“Structure of the Rad50 DNA double-strand break repair protein in complex with DNA.”

EMBO J. 2014 Dec 1;33(23):2847-59.

doi: 10.15252/emboj.201488889. Epub 2014 Oct 27.

Schiller CB*, Seifert FU*, Linke-Winnebeck C*, Hopfner KP.

“Structural studies of DNA end detection and resection in homologous recombination.”

Cold Spring Harb Perspect Biol. 2014 Jul 31;6(10):a017962.

doi: 10.1101/cshperspect.a017962.

* These authors contributed equally to this work.

Gerhold CB, Winkler DD, Lakomek K, Seifert FU, Fenn S, Kessler B, Witte G, Luger K, Hopfner KP.

“Structure of the Actin-related protein 8 and its contribution to nucleosome binding”

Nucleic Acids Res. 2012 Sept 40 (21): 11036-11046 doi:10.1093/nar/gks842